2016-07-28

A Landscape and Systems Ecology Approach for Predicting Fish Concentration in Seasonally Pulsed and Spatially Heterogeneous Wetlands

Simeon Yurek
University of Miami, syurek@bio.miami.edu

UNIVERSITY OF MIAMI

A LANDSCAPE AND SYSTEMS ECOLOGY APPROACH FOR PREDICTING FISH CONCENTRATION IN SEASONALLY PULSED AND SPATIALLY HETEROGENEOUS WETLANDS

By

Simeon Yurek

A DISSERTATION

Submitted to the Faculty of the
University of Miami
in partial fulfillment of the requirements for the
degree of Doctor of Philosophy

Coral Gables, Florida

August 2016

UNIVERSITY OF MIAMI

A dissertation submitted in partial fulfillment of
the requirements for the degree of
Doctor of Philosophy

A LANDSCAPE AND SYSTEMS ECOLOGY APPROACH FOR PREDICTING FISH CONCENTRATION IN SEASONALLY PULSED AND SPATIALLY HETEROGENEOUS WETLANDS

Simeon Yurek

Approved:

_____
Donald L. DeAngelis, Ph.D.
Adjunct Associate Professor
of Biology

_____
Daniel DiResta, Ph.D.
Senior Lecturer of Biology

_____
J. David Van Dyken, Ph.D.
Assistant Professor of Biology

_____
Guillermo Prado, Ph.D.
Dean of the Graduate School

_____
Joseph E. Serafy, Ph.D.
Research Associate Professor
of Biology

YUREK, SIMEON (Ph.D., Biology)
A Landscape and Systems Ecology Approach for Predicting Fish Concentration in Seasonally Pulsed and Spatially Heterogeneous Wetlands (August 2016)

Abstract of a dissertation at the University of Miami.

Dissertation supervised by Adjunct Associate Professor Donald L. DeAngelis.
No. of pages in text: (224)

Seasonal pulsing of hydrology in the Greater Everglades watershed produces dynamic, annual cycles of wetland flooding and drying, and of environmental conditions. Biota have adapted to exploit these pulses through movement and foraging behaviors. A primary ecological concern, pertinent to Everglades restoration, is to understand how sufficient concentration of aquatic biomass, particularly that of small fish and invertebrates, is produced under nutrient limited conditions, to support diverse and abundant communities of piscivorous predators, such as wading birds and herpetofauna. This question is investigated through computer simulation modeling of small−bodied fishes in the freshwater Everglades, and analyses of empirical monitoring data of mangrove−associated fishes along the shoreline of southern Florida.

In the freshwater Everglades, concentration of biomass, through interactions between movement behaviors, spatial heterogeneity of the landscape, and declining water levels, has been hypothesized to be a key function for making biomass available in useable densities. Fish avoid drying conditions by moving to adjacent refugia, and in the process become highly concentrated in localized areas. Although this conceptual picture is well known, spatially explicit prediction of the timing, magnitude, and duration of fish concentration across the landscape has not been possible. Here, a computer modeling approach, aimed at complementing monitoring, is developed for simulating and analyzing

landscape and food web dynamics of pulsed wetland ecosystems, by explicitly tracking growth and concentration of fish biomass, and accounting for dynamic movement behaviors in response to spatiotemporally shifting environmental conditions.

In coastal mangrove habitats, fluctuating and extreme salinity conditions have been hypothesized to constrain fish populations, and avoidance of hypersaline areas through movement is possible. Fish densities were related to frequency of hypersalinity over defined periods preceding surveys. Complementary quantile regression techniques were applied to make inferences on behavioral, population, and predator−prey dynamics, which can be tested with modeling.

Ecological responses at multiples spatial and temporal scales were investigated in both the empirical and simulation studies. Spatially explicit maps of biomass concentrations, across these scales, were generated from simulation models, and effects of hydrology and landscape connectivity on fish biomass were shown. This methodology offers a new approach for using empirical analyses to generate hypotheses and theory which can be investigated with computer simulation modeling, and for using computer modeling to inform decisions on monitoring strategy and resource management.

ACKNOWLEDGEMENTS

I would like to thank present and past members of my dissertation committee, Bob Cowen, Dan DiResta, Joe Serafy, and David Van Dyken, for their patience and guidance while I was completing this Ph.D. dissertation.

I thank my advisor, Don DeAngelis, of the U.S. Geological Survey, whose vision, expertise, and occasional hidden tactics greatly influenced my research path of simulation modeling. I also thank fellow labmates Jiang Jiang and Bo Zhang.

Very special thanks to masters of logistics, Linda White and Brian Teare, without whom nothing could be accomplished. I especially thank Brian for his generosity in sharing expertise, insight, and countless boating knowledge, during many long hours of field monitoring.

I thank Vic Engel, Tom Doyle, and Bogdan Chiviou of the USGS, for their support and guidance in model development, and in its application to governmental work. I thank Diego Lirman, Rolando Santos, and Ian Zink of the RSMAS Department of Marine Biology and Fisheries, as well as Joan Browder and Gladys Liehr of NOAA, Southeast Fisheries Science Center, and Sarah Bellmund, Herve Jobert, and Caroline Herman of Biscayne National Park, for their cooperative and integrative efforts on Biscayne Bay research. I thank Erik Stabenau of Everglades National Park for instruction on the use of hydrodynamic models and analysis of environmental data. I would also like to thank co−authors Laurel Larsen, Joel Trexler, and Jessica Klassen, and reviewers Bill Loftus,

Bill Fagan, Michael Osland, and two Anonymous for their useful perspective and suggestions, and Dale Gawlik for guidance on interpretation of model output. I thank Steve Green for recommendations on statistical procedures, and also the University of Miami Center for Computational Science for generous use of computing resources.

I thank my family for their continued love and support while I was conducting the research during this dissertation.

Funding for this project was provided by the U.S. Government through the Greater Everglades Priority Ecosystem Science Program and the Future Impacts of Sea Level Rise on Coastal Habitats and Species project of the U.S. Geological Survey, and by the Restoration Coordination and Verification Program of the U.S. Army Corps of Engineers and South Florida Water Management District. Funding from the University of Miami was provided by the James W. McLamore Fellowship in Tropical Biology, the William H. Evoy Graduate Research Support Fund, and the Max and Peggy Kriloff and University of Miami GAFAC Student Funds.

All field research complied with the Guidelines for the Use of Animals in Research and was conducted under the required permits of the State of Florida and the National Park Service. Any use of trade, product, or firm names is for descriptive purposes only and does not imply endorsement by the U.S. Government.

TABLE OF CONTENTS

LIST OF FIGURES

Chapter 5

LIST OF TABLES

LIST OF ABBREVIATIONS

BNP	Biscayne National Park
CERP	Comprehensive Everglades Restoration Plan
CEPP	Central Everglades Planning Project
DCI	Directional Connectivity Index
DEM	Digital Elevation Model
EDEN	Everglades Depth Estimation Network
ENP	Everglades National Park
FDAL	Fish Dispersal on Aquatic Landscapes
GEFISH	Greater Everglades Fish Model
GIS	Geographic Information System
HAED	High Accuracy Elevation Data
NAVD	North American Vertical Datum
NOAA	National Oceanic and Atmospheric Administration
PSU	Primary Study Unit
RSL	Ridge−and−Slough Landscape
SFWMD	South Florida Water Management District
SOFIA	South Florida Information Access
TSF	Time Since Flooding
USACE	U.S. Army Corps of Engineers
USGS	U.S. Geological Survey
UTM	Universal Transverse Mercator

Chapter 1

"Nobody has ever noticed a place except at a time, or a time except at a place."

– H. Minkowski, 1908

Introduction

Freshwater flow is a key component of many aquatic ecosystems (Poff et al. 1997). Landscape geomorphology, water quality, habitat, biota, and food webs are all impacted by hydrologic processes. In lowland habitats, such as wetlands and river floodplains, small changes in hydrology can propagate across large areas of the relatively flat landscape, leading to changes in nutrient cycles, population dynamics, food web interactions, and landscape processes that transport and concentrate resources (Junk et al. 1989, Yang et al. 2008). These hydrological and biological processes interact to form complex dynamic aquatic systems.

Ecologists and managers are concerned with determining the proper flow regimes, or rates and volumes of flow, for an ecosystem, to ensure that habitats remain within suitable ranges for biota, and to conserve overall system dynamics and prevent catastrophic shifts (Hsieh et al. 2005). Identifying thresholds beyond which these shifts occur, and the hydrologic changes that lead up to them, is important for developing conservation and management policy (Martin et al. 2009).

In seasonally–pulsed wetlands, shifts in rainfall patterns over short time scales, of weeks to months, can lead to a rapid sequence of changes in hydrology and ecology. Small changes in water depth and flow, dispersed over low elevation gradients, result in large spatial expansion and contraction of flooded habitat, and of environmental

conditions that are impacted by freshwater flow, such as water chemistry, temperature, and, in coastal areas, salinity.

These conditions determine the quality and availability of habitat for species. On a basic level, habitat becomes available to aquatic species when areas of the landscape are inundated. At the same time, species are differentially adapted to flooding, and in general, to suites of environmental conditions (Nordlie 2006, Pease et al. 1989), and for that reason, availability can vary within different ranges of the flooded landscape on a species–specific basis.

Changes in habitat can impact availability of resources, such as nutrients and prey, to consumers. As the landscape floods, terrestrial resources are released into the aquatic system, and pulsed biological responses are initiated, such as increased primary productivity and reproduction. This phenomenon has been termed the "flood–pulse concept" for river floodplain systems (Junk et al. 1989, Tockner et al. 2000), and also "nature's pulsing paradigm" (Odum et al. 1995).

Landscape processes affect the spatial ecology of flood pulses. Wetland landscapes have spatially heterogeneity at regional and local spatial scales. Regional elevation gradients are generally determined through the geology of the underlying substrate. At the local scale, differences in elevation occur between water flow ways (e.g., rivers, creeks, sloughs) and vegetated marshes. Spatially heterogeneous landscape topographies are formed as peats accrete through feedbacks between hydrologic flows and vegetation that entrain soils (Larsen & Harvey 2010). This process maintains elevation differentials between marshes and flow ways, through consistent flows.

The spatial pattern of flow ways, and the overall geomorphology of wetland landscapes, can be complex. Patterns such as dendritic (Simenstad et al. 2002), fractal (Liu et al. 2001, Wickham & Norton 1994), braided (Bornette et al. 1998), and anisotropic (Larsen & Harvey 2011) are possible. This process of landscape engineering is widespread across wetland ecosystems, including salt marshes, mangrove forests, river flood plains, anabranching rivers, parallel–drainage wetlands, and geographically isolated wetlands (Dale 2000, DeAngelis 2012, Larsen et al. 2007, Tiner 2003, Tockner & Stanford 2002).

Interactions between landscape geomorphology and the various phases of hydrology (e.g., flooding and drying) affect the relative connectedness of wetland habitat through time. Different areas of the wetland become connected and disconnected as water levels rise and fall. The spatial configuration of these areas varies, spatially, according to wetland geomorphology, and temporally, according to the hydrologic cycle. These combine to determine wetland connectivity, which is spatiotemporally dynamic, and can be measured using hydrologic indices (Larsen et al. 2012).

Dynamic spatial patterns of connectivity can lead to the formation of complex, heterogeneous spatial distributions of nutrients and biota (DeAngelis et al. 1998). When wetlands are fully flooded, much of the habitat is connected and available to biota, and in this sense, connectivity is omnidirectional. When water levels recede to intermediate and low levels, areas of the landscape that are higher, such as pannes and pools, become disconnected and isolated, and local connectivity decreases. Shifts in connectivity across these various phases may be critical turning points wherein species distributions become rapidly reorganized, spatially. Movement behaviors of motile aquatic species interact

with the spatially dynamic wetland, across interconnected flooded areas, and through time. The density of individuals and biomass can build up in higher levels in localized areas as their movement becomes restricted or channeled by landscape features (Kuslan 1976a,b). For that reason, it is important to understand the spatially explicit context of how species distributions change along with dynamic connectivity.

In addition to drying of the landscape, connectivity can decline through the formation of exclusion zones, or areas of environmental conditions that negatively impact the physiology, life history, and fitness of a species. For example, shallow water depths, hypoxia, and extreme and/or rapidly fluctuating temperature and salinity can be excluding factors that make habitat unavailable. These factors represent limits on species populations, and can be termed ecosystem constraints.

Avoidance of exclusion zones, through movement behaviors, adds further complexity to patterns of habitat selection of species (Chapman & Mckenzie 2009, Mayor et al. 2009), particularly if exclusion areas are spatially dynamic. In the case of wetland drying, as the spatial extent of flooded wetlands contracts, a "drying front" propagates across the landscape, representing the boundary of a spatially expanding exclusion zone. Fish avoid drying areas through movement, and become concentrated in dry season refugia (Loftus & Kuslan 1987). Another example of a spatially expanding exclusion zone is hypoxia. In the Neuse River estuary, North Carolina (USA), fish densities were lower within hypoxic zones than in adjacent refugia, apparently due to avoidance behaviors (Campbell & Rice 2014, Eby & Crowder 2002). The authors suggested that habitat compression was a mechanism that concentrated the fish. Both of the above cases, wetland drying and hypoxia, result from reductions in freshwater flows.

These various landscape, trophic, and behavioral processes interact to form complex dynamic ecosystems. Impacts of the combinations of these processes on the population dynamics of aquatic fauna are not well understood, because direct transactions, indirect relations, and feedbacks between biota and the physical environment are all possible (DeAngelis & Mooij 2005, Patten 2014, Rose 2000). One approach to linking biological responses to shifts in hydrology and landscape conditions is to evaluate constraints of the ecosystem on populations, and track how populations respond within those limits (Cade & Noon 2003, Ulanowicz 2014). For seasonally pulsed wetlands, the primary constraint is fluctuating hydrology (Loftus & Kushlan 1987). Many ecosystems successfully support diverse populations of fauna despite drought and flood conditions, which can be both advantageous and deleterious, depending on how species are adapted. The pulsing mechanism may be important to the persistence of populations, by increasing and maintaining resource availability over seasons (Kahl 1964, Odum et al. 1995, Yang et al. 2008). At the same time, limits to the range of fluctuation may also exist for ecosystems. It is important to develop a technology for tracking and analyzing these processes, so that critical thresholds can be identified (DeAngelis et al. 1998).

Scope of dissertation

This dissertation applied a landscape and systems ecology approach to evaluating processes by which shifts in environmental conditions of seasonally pulsed wetlands lead to changes in habitat quality, availability, and selection by wetland fishes. The overarching hypothesis of the dissertation was that interactions between population dynamics and movement behaviors of small–bodied fishes, on seasonally pulsed

wetlands with heterogeneous landscape geomorphologies, produce localized high densities of fish. These high densities are thought to be important for channeling biomass energy up to top predators (Kahl 1964). This dissertation developed ecological theory, discussed by DeAngelis et al. (1998), of landscape and trophic mechanisms, represented by the spatial concentration of fish over the landscape, that are integral to ecosystem function. New approaches of spatially explicit computer simulation modeling, application of dynamic connectivity theory, and analysis of empirical monitoring data were developed in this dissertation.

The flood pulse concept (Junk et al. 1989), which describes a process of increased ecological interactivity (e.g., growth, foraging, reproduction) during the initial phases of hydrologic pulsing in flood plains, was further developed in this dissertation for the latter phases of water recession, and for scenarios when flood cycles are altered through reduction in water flows. During these periods, exclusion zones develop that channel and concentrate biomass, potentially resulting in increased trophic transfers. Here, the flood–pulse concept was extended to wetland ecosystems, namely, the Everglades and its adjacent coastal mangroves, that are not considered river flood plains, but have energy dynamics that are similarly driven by flood pulsing.

Study ecosystems

The freshwater wetlands of the Everglades and coastal mangroves of southern Florida (USA) are seasonally pulsed by precipitation, which is concentrated during the months of mid–May to October (Thomas 1974). These ecosystems were historically linked through overland freshwater flows from the Everglades to the coast, and through

the Biscayne and Florida aquifers belowground (Lohmann et al. 2012), but were compartmentalized, and effectively isolated from each other, through anthropogenic development. Southern Florida has a distinct dry season, which spans several months and a range of temperatures, from 17 to 29°C (Thomas 1974). Transitions from the dry to wet season have been altered through water management, which delays delivery of flows to the Everglades and the coast (Light & Dineen 1994).

In addition to hydrology, low nutrient availability is a driving factor of the ecology of southern Florida wetlands. The Everglades has been described as oligotrophic (Davis 1994), and in coastal wetlands, nutrients can be low and limiting (Odum et al. 1982). These ecosystems differ from the common characterization of wetlands as nutrient–rich and highly productive ecosystems. A primary ecological question, and management concern, is to determine how sufficient biomass energy is produced to support diverse and abundant biological communities that include top predators. The working hypothesis, for over 60 years, has been that relatively low levels of productivity across the landscape become concentrated in localized areas through a combination of habitat compression and movement and aggregation behaviors (Gunderson & Loftus 1993, Kahl 1964, Odum & Heald 1972, Robertson & Kushlan 1974). These concentrations are manifested in drying slough patches in the Everglades, and in prop root habitats along mangrove–lined creeks (Rehage & Loftus 2007), and the coast (Serafy et al. 2007).

The link between research supporting this hypothesis and restoration of historic populations has not been adequately made. Wading bird populations are still well below their highly abundant, historic levels (Frederick et al. 2009, Rutchey et al. 2009), and populations of piscivorous fishes, alligators, and crocodiles have declined along the coast

(Lorenz & Serafy 2006, Mazzotti & Brandt 1994). In both cases, reductions in hydrologic flows are implicated (USACE, 1999).

This dissertation addressed these management and conservation concerns by developing a methodology for analyzing two ecological questions: (1) How do fish become concentrated in high densities through spatially propagating, temporally dynamic, landscape processes? (2) How do fish populations respond within the limits of ecosystem constraints, when these constraints are applied as spatiotemporally dynamic environmental conditions? These inter–related questions are answered in the following chapters of this dissertation.

Chapter 2

Simulating mechanisms for dispersal, production, and stranding of small forage fish in temporary wetland habitats

Summary

Movement strategies of small forage fish (<8 cm total length) between temporary and permanent wetland habitats affect their overall population growth and biomass concentrations, i.e., availability to predators. These fish are often the key energy link between primary producers and top predators, such as wading birds, which require high concentrations of stranded fish in accessible depths. Expansion and contraction of seasonal wetlands induce a sequential alternation between rapid biomass growth and concentration, creating the conditions for local stranding of small fish as they move in response to varying water levels. To better understand how landscape topography, hydrology, and fish behavior interact to create high densities of stranded fish, I first simulated population dynamics of small fish, within a dynamic food web, with different traits for movement strategy and growth rate, across an artificial, spatially explicit, heterogeneous, two–dimensional marsh slough landscape, using hydrologic variability as the driver for movement. Model output showed that fish with the highest tendency to invade newly flooded marsh areas built up the largest populations over long time periods with stable hydrologic patterns. A higher probability to become stranded had negative effects on long–term population size, and offset the contribution of that species to stranded biomass. The model was next applied to the topography of a 10 km × 10 km area of Everglades landscape. The details of the topography were highly important in

channeling fish movements and creating spatiotemporal patterns of fish movement and stranding. This output provides data that can be compared in the future with observed locations of fish biomass concentrations, or such surrogates as phosphorus 'hotspots' in the marsh.

Background

Seasonal and ephemeral wetland habitats that emerge and recede with seasonal oscillations in precipitation directly impact the abundance and vulnerability of key forage fish species that migrate from permanent water bodies to colonize them (Alho 2008, Bayley 1991, Daufresne et al. 2007). Many small fishes (<8 cm) exploit temporarily flooded wetlands for emerging forage resources, facilitating their growth and reproduction, and use these shallow areas as refuges from predation from larger piscivorous fish (Cucherousset et al. 2007, Hohausova et al. 2010, Winemiller & Jepsen 1998). Small fishes are often a primary link between lower trophic food webs and higher order predators, since they are adapted to colonizing flooding areas and rapidly expanding their populations through short generation times and fast growth rates (Grether & Kolluru 2011, Pires et al. 2011; Winemiller 1996, Winemiller & Jepsen 1998). These populations change spatially and temporally throughout the year as fish move into and out of flooding and drying areas. Thus, the transmission of energy through a food web in a seasonally flooded wetland ecosystem is mediated by the expansion and contraction of flooded habitat, to which the fish are adapted through movement.

For top predators that forage on these fish, processes that concentrate prey items and make them more vulnerable to predation are essential. Small fish have morphological

adaptations and behavioral strategies for evading predators. When spread evenly across the landscape, their densities may be simply too low to detect, or may not constitute sufficient densities to justify the energy expenditure required to pursue and capture them (Bakun 2006). During the breeding seasons of predators like wading birds, a steady supply of easily obtainable prey is necessary to support their offspring. Therefore, a mechanism is needed to concentrate prey items in usable densities. In seasonal graminoid wetlands, the drying of the marsh during months with little rainfall provides this mechanism. As the marsh dries, some fish follow the receding water to permanently flooded water bodies. However, many are trapped in ephemeral pools that gradually or rapidly dry out, leaving them vulnerable to capture (Gunderson & Loftus 1993, Kobza et al. 2004, Sheaves 2005). Large amounts of energy can be passed to higher trophic levels during this drying process.

In addition to factors imposed by the physical environment, like topography and hydrology, biotic factors such as life strategies are also influential in determining patterns of fish availability, and these strategies vary among small fish species. Small fish differ in growth rates and reproduction cycles, (Pires et al. 2011, Nordlie 2000), and may differ in both their rates of migration into newly flooded areas, and their abilities to avoid stranding when water levels recede, although these latter two are much more difficult to measure, considering the size of the animals and tracking technologies available.

Our objective is to model fish concentration and stranding on a realistic landscape so that the amounts of fish biomass that are trapped in ephemeral pools, and the amounts that move down to permanent water bodies, can be estimated through time across the landscape. Previous models have been developed to describe changing spatial patterns of

biomass densities of small fish communities across the landscape, and how they vary with landscape topography and seasonal hydrology (DeAngelis et al. 1997, Gaff et al. 2000; 2004, Jopp et al. 2010). My approach is novel in explicitly modeling the food base of the fish, and in considering the sensitivity of stranding behavior in relation to fish movement strategies, the subject of recent empirical study (e.g., Obaza et al. 2011). The model includes different combinations of these strategies for different small fish functional groups.

To elaborate in more detail on the biological and hydrological interactions that occur in most seasonal wetlands, I focus on a paradigm study region, the Greater Everglades freshwater marsh system (Florida, USA). Small fish in the Everglades broadly colonize flooding marshes as water levels rise during the wet season (Gunderson & Loftus 1993, Trexler et al. 2002, Turner et al. 1999), and retreat into areas of permanent water, such as sloughs and mangrove creek headwaters, during the dry season (Magoulick & Kobza, 2003, Rehage & Loftus 2007, Rehage & Trexler 2006), though many become trapped in ephemeral isolated patches of shallow water (Kobza et al. 2004, Parkos et al. 2011) as water levels recede. These small fish community dynamics result from complex interactions and feedbacks between abiotic and biotic environmental variables (e.g., trophic dynamics, predator abundance, resource availability, and refuge quality) and the scale of fish movement (Bronmark et al. 1992, Chick et al. 2004, Yoder et al. 2004). In this study, I focus on one of these variables, seasonally varying hydrology, as a driver for fish movement, and evaluate patterns of movement and stranding along flooding and drying fronts that propagate seasonally across a landscape.

Methods

The Greater Everglades Fish model (GEFISH) is a spatially explicit simulation model of a simple freshwater marsh food web with select mobile groups that disperse across the landscape. GEFISH models two key ecosystem processes on a generalized freshwater Everglades marsh: (1) local scale biomass production of functional groups that are linked through predator/prey interactions and (2) dispersal of biomass in response to an abiotic impetus that induces a qualitative change in habitat. This impetus is the seasonal rise and fall of water levels, which determine if habitat is available (i.e., is flooded) or unavailable (is dry) to aquatic species throughout the year. The model simulates space on a grid of 100 × 100 cells, representing a heterogeneous topography, and simulates the food web over a defined number of years on time steps of 0.1 day. For all cells at all time steps, local biomass production and subsequent decay is calculated for each functional group through a set of differential equations, and movement between flooding and drying cells for functionally mobile groups is calculated according to a set of governing algorithms.

Study site

The Everglades landscape is characterized by a minimal elevation gradient extended across a large spatial domain, with some local scale ridge–and–slough patterned variability (Larsen & Harvey 2011, Larsen et al. 2011, Nungesser 2011). The flat topography amplifies the effects of rising and falling water levels, where a slight change in water depth propagates across a broad spatial area. Slight depressions in elevation (i.e., sloughs) provide extensive shallow water habitat sufficient to support communities of small fish, and at the same time tend to exclude larger piscivorous fish, limiting their

densities in the high marsh (Chick et al. 2004, Rehage & Trexler 2006, Trexler et al. 2002, Winemiller, 1996). The braided ridge–and–slough patterning provides a network for small fish to migrate freely. Thus, seasonally pulsed marshes in the Everglades offer both refuge from predation and an expanded foraging area. However, as rainfall decreases during the dry season and surface waters retreat back into the substrate, the braided slough network fragments into independently isolated pools and ditches where large numbers of fishes become stranded. Ambient environmental conditions often decline in these ephemeral pools, and prey resources become depleted, or the water body dries out completely, wherein these refuges quickly convert to sink habitats (Kushlan 1974). Thus, as water levels rise and fall annually, small fish habitat transitions from an expanded, contiguous, wet season foraging area with high productivity and low predation, to a set of contracted dry season *refugia* with low survival.

Trophic web structure

The focus of my study is on populations of small fish functional groups (a functional group could consist of one abundant species). I model these fish groups as part of a simplified trophic web, to place them within the context of their energy base, so that the dynamics of their prey base can influence their growth, death, and movement. The GEFISH trophic web contains six functional groups organized across three trophic levels (Figure 2.1). The bottom trophic level contains two groups, a periphyton primary production group and a detrital pool; the second level has one group, invertebrates; the third level contains the three experimental small fish groups. Each food web component is described below.

Differential equations are shown for the key components, with the full set given in online Supplement 2A, Table S2A.1. They are approximated as difference equations with a 0.1 day time step, and are calculated simultaneously for all of the cells that are flooded at a given time step. The model is simulated using *Matlab* (Mathworks 2010).

The biomass density (g dry wt. m^{-2}) variables for each functional group are defined: *Periphyton*, *P(t)* and *Detritus*, *D(t)*: The periphyton and detritus groups are generalized aggregates that provide a forage base for the other functional groups. In the greater Everglades watershed, periphyton mat communities are complex conglomerates of benthic, floating, epiphytic and filamentous algae and freshwater diatoms, and are inhabited by fungi, protozoans, cyanobacteria and macro–invertebrates (Browder et al. 1994, Chick et al. 2008, Gaiser 2009). These mats contain various proportions of living and dead matter, with internal microbial recycling. Distinct algal and detrital energy pathways have been identified linked to periphyton (Belicka et al. 2012). For my purposes, I separated this complex into a periphyton group composed of living algal primary producers, and a detrital pool built of non–assimilated, egested, dying or decaying biomass contributed by other groups.

Periphyton biomass grows according to a logistic function with defined maximum growth rate, $Growth_{peri}$, and a density–dependent coefficient, K_{peri}, which determines how growth is slowed down as periphyton biomass increases. Periphyton dies off at a fixed linear rate, m_{peri}, when the cell is flooded, and at a greater rate, $mdry_{peri}$, when the cell is dry. These losses contribute to the detrital pool. Additional biomass is removed through predation by higher groups. Nutrient dynamics are not included.

$$\frac{dP(t)}{dt} = Growth_{peri}\left(1-\frac{P(t)}{K_{peri}}\right)P(t) - m_{peri}P(t) - Cons_{peri-by-invert}P(t)I(t) - \sum_{i=1,3}\left(\frac{Cons_{peri\text{-}by\text{-}fish,i}P(t)F_i(t)}{1+h_{peri}Cons_{peri\text{-}by\text{-}fish,i}P(t)+h_{invert}Cons_{invert\text{-}by\text{-}fish}I(t)+w_{fish,i}F_i(t)}\right) \quad (1)$$

Note $Cons_i$ are consumption rates, h_i is handling time of prey, and w is a self–interference term for consumers.

The net detrital pool is built of biomass accumulations that originate from mortality and non–assimilated prey items among the five other groups. Mortality is calculated for each group as a percentage of biomass (as described above). Non–assimilated prey biomass (from egestion or incomplete digestion) is calculated for each group as a fraction $(1-\eta)$ complementary to what is ingested by a consumer, where η is a coefficient for assimilation of consumed matter (see Eqs. (2) and (3)). Losses to the detrital pool are calculated by terms representing daily decomposition and consumption by invertebrates. The equation of the detrital pool is shown in Supplement 2a.

Invertebrates, *I(t)*: The standing crop of invertebrates, the only second–tier trophic group, grows according to a prey–dependent function. They feed on periphyton and detritus. Additionally, invertebrates sustain losses through daily mortality and predation by all three small fish groups (*Fish 1*, *Fish 2*, and *Fish 3*).

$$\frac{dI(t)}{dt} = Cons_{detritus\text{-}by\text{-}inverts}D(t) + \eta_{invert}Cons_{peri\text{-}by\text{-}inverts}P(t)I(t) - m_{invert}I(t) - \sum_{i=1,3}\left(\frac{Cons_{invert\text{-}by\text{-}fish,i}I(t)F_i(t)}{1+h_{peri}Cons_{peri\text{-}by\text{-}fish,i}P(t)+h_{invert}Cons_{invert\text{-}by\text{-}fish}I(t)+w_{fish,i}F_i(t)}\right) \quad (2)$$

Fish 1, *Fish 2*, and *Fish 3*; *F1(t)*, *F2(t)* and *F3(t)*: All three small fish groups feed on invertebrates and periphyton, and their respective biomass values grow according to a Beddington–DeAngelis (BD) type function. This function assumes that foraging by a given functional group is limited by self–interference competition that increases with group size (Beddington 1975, DeAngelis et al. 1975). The BD functional response is more stable than Holling Type II, and reduces the possibility of oscillations. Losses in biomass are accrued through daily mortality.

$$\frac{dF_i}{dt} = \eta_{fish}\sum_{i=1,3}\left(\frac{Cons_{peri\text{-}by\text{-}fish,i}P(t)F_i(t)}{1+h_{fish}Cons_{peri\text{-}by\text{-}fish,i}P(t)+h_{fish}Cons_{invert\text{-}by\text{-}fish,i}I(t)+w_{fish,i}F_i(t)}\right) + \eta_{fish}\sum_{i=1,3}\left(\frac{Cons_{invert\text{-}by\text{-}fish,i}I(t)F_i(t)}{1+h_{fish}Cons_{peri\text{-}by\text{-}fish,i}P(t)+h_{fish}Cons_{invert\text{-}by\text{-}fish,i}I(t)+w_{fish}F_i(t)}\right) - m_{fish,i}F_i(t) \quad (3)$$

Parameterization of these equations is discussed below.

Landscape topography

Two landscapes are considered in this study, each consisting of a grid of cells (100 ×100). The first is an artificial landscape designed only for troubleshooting the model and conducting a sensitivity analysis (see below), but it is based on general, broad–scale characteristics of an area of Everglades watershed within the Shark Valley region of Everglades National Park. Each cell represents a square, 1–ha segment, with the entire grid encompassing 100 km^2. The landscape topography is described by a mathematical function that supplies elevation values for each of the cells (Figure 2.2a). The landscape is a generalized slough system, with the slough terminating in a canal at its lowest end. The elevation gradients of the slough are based on elevation data queried from the High Accuracy Elevation Data (HAED) internet database of the USGS South Florida

Information Access (SOFIA) network (Desmond 2007) (see Supplement 2C for internet links). The canal terminus is lower in elevation than any other part of the marsh, and is designed to remain flooded during all hydrologic stages. As such, it provides a dry season refuge that fish can enter when water levels fall below the marsh surface.

The second landscape used in the model is a nearest neighbor topographic interpolation of an actual area of Everglades landscape, a 100 km^2 area of upper Shark River Slough (Figure 2.2b). The source data for the interpolation were the USGS's 400 m resolution HAED elevation data. This landscape was developed for the primary application of GEFISH, to simulate with spatial resolution on a real landscape the spatiotemporal dynamics of fish populations, particularly their concentration and stranding during the dry season. This landscape generally slopes toward the southwest, and is much more heterogeneous than the first one, with inter–braided sloughs circumscribing ridges and tree islands.

Seasonally varying water level

Water level was generated by a cosine function calculated at each time step to simulate seasonal water level fluctuations. Water level rises and falls with defined amplitude (*wlamp*), mean water level (*wlevmn*), and a period of 1 year (Figure 2.3a). The water level amplitude (artificial = 0.348 m, HAED = 0.408 m) and mean (artificial = 0.448, HAED = 1.267 m) were chosen so that the marsh on either of the simulated landscapes would fully flood with the exception of a few buffer cells at the highest elevations, and would almost completely dry out. Some parts of each landscape (the canal in the artificial landscape) remained flooded throughout all time steps.

Movement of organisms

As the water level rises or falls, cells along the respective flooding or drying fronts undergo a qualitative habitat transition to either available (wet) or unavailable (dry). This transition is a key driver in the GEFISH model for transport of biomass among cells throughout the grid. Of the six functional groups considered here, only the three fish functional groups (*Fish 1*, *Fish 2*, and *Fish 3*) actively disperse in response to this abiotic stimulus. There are small amounts of diffusion for these groups as well. *Invertebrates* and *Periphyton* are locally resident within cells and are assumed to be non–migratory. Further details concerning movement rules are described in Supplement 2B.

Small fish movement strategies

Small fishes of the Everglades differ in their rates of colonization of new areas and their ability to escape stranding. For example, *Lucania goodei* (Bluefin Killifish) regularly dominate throw trap samples in wet season marsh habitats (Trexler, personal communication), while *Jordanella floridae* (Flagfish) and *Gambusia holbrooki* (Eastern Mosquitofish) are the first to appear in reflooding areas (Trexler et al. 2002). Analyses of fish collection data suggest that hydroperiod is the primary driver for redistribution of fish biomass (Trexler et al. 2002). Therefore, in this study I assume that active movement in response to an abiotic stimulus (escaping drying fronts and following flooding fronts) is the primary mechanism for producing spatial and temporal distributions of small fish populations, and I tested how changes in movement strategy affect these distributions.

Four basic parameters related to movement strategy are used in the model to describe movement either into cells that are newly flooded or out of cells that are drying out. The first parameter, $thresh\_inv_i$, is the minimum water depth at which a fish group can viably exist in a cell, and is defined for each functional group i. Water depth for each cell is

calculated as the overall water level (landscape–wide) minus the cell elevation. Note that a cell with a given water depth could be wet with respect to one group, and dry for another. When the water level crosses that threshold from below, the cell transitions from dry to wet, and fish from adjacent cells can move in to colonize. All eight cells (perpendicular and diagonal) surrounding that transitional cell are evaluated in the same time step for their respective wet or dry status. A second parameter, $frac\_inv_i$, specifies what fraction of fish will leave these adjacent flooded cells to move into the newly flooded cell. When two or more cells simultaneously become flooded in the same time step, the fish leaving an adjacent cell are evenly divided between the newly flooded cells. As the water level declines, the opposite process takes place. When water depth in a particular cell declines below a certain threshold, $thresh\_leave_i$ (the third parameter, different in general from $thresh\_inv_i$), a fraction of fish, $frac\_leave_i$ (fourth parameter), move to adjacent cells that are still flooded, again dividing equally among two or more such cells.

I assume that some fish fail to leave a drying cell, and consider them trapped or stranded. In a real landscape, some fish move to the nearest low areas rather than moving ahead of the drying front because they are seeking better conditions or possibly are stressed and disoriented. They do not move far enough to constitute leaving a cell. Consequently, fish biomass becomes highly concentrated within cells, and easily accessed by predators. These stranded biomass values are calculated as the complement to the $frac\_leave_i$ parameters.

I also assume that a small fraction of fish biomass survives in remnant pools of a formally ‘dry’ cell, since fish are commonly sampled in these pools during the dry season

(Kobza et al. 2004, Loftus & Eklund 1994). An additional parameter, $frac\_surv_i$, is used to calculate the fraction of fish that survive. The mortality rate of these remaining fish is elevated to account for poor conditions and increased competition for resources. To take into account the costs of fish that are more dispersal oriented, tradeoffs in lower consumption rate, $Cons_{peri-by-fish,i}$ and $Cons_{invert-by-fish,i}$ are assumed.

Parameterization of model

Parameterization of the food web model was performed to produce production rates and biomass reasonably close to what is estimated in the field (see Supplement 2A, Table S2A.2). Model parameters that govern biomass production (density–dependent coefficient, prey consumption/assimilation, etc.) and spatial movement (diffusion, invasion/escape thresholds, proportion invading/escaping) were calibrated according to empirically derived estimates, with the goal of producing realistic ash free dry mass (AFDM) biomass density values (g dry wt. m^{-2}) having spatial and temporal patterns consistent with those reported in the scientific literature. Model assumptions regarding population dynamics and trophic interactions agree with empirical findings on southern Florida aquatic food web communities: for periphyton (Chick et al. 2008, Gaiser 2009, Liston & Trexler 2005, Sargeant et al. 2011, Turner et al. 1999); for invertebrates (King & Richardson 2007, Liston 2006, Liston et al. 2008, Liston & Trexler 2005, Parkos et al. 2011); for small fish (Ruetz et al. 2005, Trexler et al. 2002, Williams & Trexler 2006).

Simulations

Two classes of simulations of GEFISH were implemented: (1) a preliminary analysis to test model sensitivity, and (2) a realistic scenario on an actual landscape. For all

simulations, biomass densities for living and stranded biomass (at all cells where a drying event occurred) were recorded at daily intervals on separate, two–dimensional surface matrices of 10,000 spatial cells, and also as total biomass summed across the entire grid at daily time steps. The model was iterated over multiple years (*nyears* = 12) to eliminate the effect of initial conditions, and model output data were generated in the twelfth year. A simple sinusoidal representation of water level was used for the entire landscape. Although actual variation in water levels across a landscape is more complex than this approximation (due to the confluence of surface and groundwater flows, evaporation, relocation of water parcels through management, etc.), I considered it sufficient for the purposes of illustrating the temporal and spatial variation that might be expected for living and stranded fish biomass.

Sensitivity analysis

I conducted a preliminary analysis to evaluate the sensitivity of biomass response variables across the landscape to certain model parameters that I assume, with the support of canonical theory from the fields of physiology and mathematical modeling, to have the most impact on my results. This analysis was conducted in two parts, targeting two separate test groups: (1a) *energetics*: the coefficients of maximum feeding rate on periphyton and invertebrates by small fish (*cons_peri* and *cons_invert*), and (1b) *movement*: the amounts of fish biomass that invade and leave cells when changing water levels prompt them (*frac_inv* and *frac_leave*) (see Table 2.1). By design, I varied one group's parameters incrementally, and left all other parameters constant. I realize that there is uncertainty in many of the other parameter values of the trophic web (e.g., handling times, h_{peri} and h_{invert}; self–interference, w_{fish}). However, my emphasis in this

study was to compare relative spatiotemporal fish biomass growth and stranding dynamics for different assumptions on fish movement strategies, not to make absolute quantitative predictions.

In this analysis, I used the artificial landscape and a simplified version of the GEFISH food web model comprised of *P(t)*, *D(t)*, *I(t)*, and with only one small fish group, *F1(t)*, present. In both tests, a set of response variables were output from the model: the means of living and stranded fish biomass averaged over both a year and the whole region, and the values of living and stranded biomass for the specific cell where they reached maxima.

The fish group (or species) was first assigned a sequence of test values for *cons_peri* and *cons_invert* (see Table 2.1, under ENERGETICS), and a fixed intermediate movement strategy (*frac_inv* = 0.4, *frac_leave* = 0.4). Then conversely, a total of twelve small fish movement strategies were characterized by setting the parameters for fraction of fish moving into newly flooding cells (*frac_inv*) and fraction of fish escaping drying cells (*frac_leave*) with fixed energetic parameters (see Table 2.1, under MOVEMENT). These strategies are based on empirical observations that suggest certain biological fish species or ecological functional groups differ in these traits (Kushlan 1976b, Loftus & Kushlan 1987, Trexler et al. 2002).

Simulations on a realistic landscape

GEFISH was simulated on the portion of Everglades landscape shown in Figure 2.2b for all three fish species together (complete GEFISH food web model), each utilizing its own distinct movement strategy (i.e., different values of *frac_inv*, *frac_leave*, *thresh_inv*

and *thresh_leave*). The interpolated topography derived from HAED elevation values was used.

Results

Sensitivity analysis

Water level was highest (0.836 m) on Day 335 with 9110 cells flooded, and lowest (0.14 m) on Day 153 with 50 cells (canal) flooded. See online Supplement 2D for video depiction (*.mp4* format) of water level fluctuating against the topography. Cell hydroperiod (length of time inundated in days) varied between 0 and 365 days, and decreased with increasing distance from the canal. For a set of cells on a transect along the longitudinal axis of the slough and originating in the canal, respective hydroperiods were: cell (1,50) = 365 d, cell (2,50) = 328 d, cell (25,50) = 240 d, cell (50,50) = 179 d, cell (75,50) = 117 d, and cell (100,50) = 0 d. Each of the fish biomass response variables measured was highly sensitive to the consumption rates simulated (see Table 2.1, ENERGETICS). Based on this sensitivity analysis and further simulations, values of *cons_peri* = 0.02 and *cons_invert* = 8.2 were chosen as best fits of the model to the real world based on (1) empirical observations that fish biomass densities seldom reach more than two grams dry weight per square meter (Trexler et al. 2002); (2) molecular and stable isotopic energy pathway analyses that reveal that consumption of living algal matter (periphyton) is relatively low compared to invertebrates (Belicka et al. 2012); (3) further sensitivity analysis (not reported). These values were used for all subsequent simulations.

Using the above values of *cons_peri* and *cons_invert*, one fish species was again modeled sequentially for each of the twelve movement strategies, *frac_inv* and *frac_leave*, listed in Table 2.1 under MOVEMENT. Biomass patterns over a 1–year cycle for all three groups had three basic modes: concentration during the drying phase, depletion during the low water phase, and production and expansion during the flooding phase. In general, biomass densities were higher along the deeper central longitudinal axis of the sloughs, and lower along the slough perimeters. Complete model output from these simulations can be obtained from the corresponding author as *Matlab* formatted binary (*.mat*) files. Here I summarize the key sensitivities.

The effects of the different movement strategies on daily total living biomass (DTLB) summed daily across the region are shown in Figure 2.3b. Several differences among the strategies are conspicuous. First, DTLB values were highly sensitive to differences in *frac_leave*, the fraction of fish escaping the drying front, with the highest values of living biomass being associated with the highest *frac_leave* value, 0.8. Furthermore, these values were clustered in groups with the same *frac_leave* value. Living biomass was much less sensitive to *frac_inv*, but within these clustered groups, relatively higher DTLB values were associated with higher *frac_inv* values. When *frac_leave* = 0.8, the separation between DTLB values was greater. A second difference, attributable to *frac_inv*, was the delay in the peak total fish biomass relative to the water level. The peak in water level occurred on day 335, while the peaks of fish biomass were clustered between day 50 and day 65 of the subsequent year. Fish with lower *frac_inv* tended to lag those with the higher invading fractions by 10–15 days.

The daily total stranded biomass (DTSB) of fish did not reach measurable levels until after day 340 of the prior year (Figure 2.3c), reaching peak values generally between days 85 and 100, and dropping to zero by day 130. The large time lag between the beginning of falling water level and measurable stranding of fish occurred because the cells at the higher elevations had very low living fish biomass densities when water levels started to drop. The largest differences in DTSB were attributable to differences in the *frac_inv* strategies, where the strategy with the greatest value, *frac_inv* = 0.8, left consistently higher stranded biomass during the first 110 days of stranding (days 335–80). During the period of peak stranding, days 80–100, the DTSB response values reversed, and the strategies with lower *frac_inv* began to produce higher stranding densities. As the water level approached the lowest point, from days 100 to 130, DTSB quickly declined, with lower *frac_inv* strategies producing slightly higher densities.

Simulations on a realistic landscape

GEFISH was simulated on the realistic landscape (Figure 2.2b) in order to determine its potential usefulness in helping to identify when during a drying phase and where on the landscape concentrations of stranded fish would occur. In these simulations, GEFISH was used with three cohabitating fish species, each with its own strategies (Fish 1: *frac_inv* = 0.4, *frac_leave* = 0.05; Fish 2: *frac_inv* = 0.3, *frac_leave* = 0.3; Fish 3: *frac_inv* = 0.2, *frac_leave* = 0.7). Because it is impossible to show all of the spatial and temporal details of the population dynamics, I present here only some main results and show detailed output, including MP4 video documentation, in online Supplement 2D.

Figure 2.4 shows a sequential history in 10−day increments of fish biomass becoming stranded across the landscape, starting with day 50. Figure 2.5 shows a map of cumulative stranding over 1 year (*nyear* = 12) for each of the three fish groups, with the topography added for comparison. Note that the stranded biomass concentrations were maximized in the deeper southwest end of the slough. Concentrations of fish were also trapped in depressions in the higher areas, such as the depression in the extreme northeast corner, and the amounts trapped in a given cell varied according to strategy. Fish 3 clearly had the highest single–cell stranded biomass (1.366 g dry wt. m^{-2}) in cell (10,21), with other large spikes scattered across the landscape, while Fish 1 produced the largest bulk of somewhat evenly distributed biomass in the southwest corner of the slough. In all three cases, the fish escaping the drying front were channeled down the main slough, which lies slightly above the northeast to southwest diagonal, and, in particular, aggregated along the interface between higher marsh points and the central slough. In the model it was assumed that the fish could not move farther toward the southwest, so many fish were trapped in the southwest corner as the water receded in that general direction. However, during periods of lowest water, there is a pool remaining in that corner that the fish can move to for refuge (see online Supplement 2D for water level fluctuations on this topography). A plot of DTSB over the whole region during the period of receding water is shown in Figure 2.6. The maximum DTSB produced by Fish 3, the fish with the smallest *frac_inv* and largest *frac_leave*, was approximately half that of Fish 1 and Fish 2, whose maxima were quite similar and alternated from days 50 to 75.

Additional daily comparison plots of living biomass for all six functional groups are presented in supplementary MP4 video files in online Supplement 2D, as well as

comparison plots of stranded and living biomass for the three fish groups. These videos demonstrate that fish movement follows not only the primary longitudinal NE/SW directional axis of the slough, but also propagates perpendicular to the slough, exploiting the winding inter–braided network. Smaller branching rivulets of biomass can be observed reconvening at slough confluences, and aggregating as virtual 'hotspots'. These phenomena have been the subject of much speculation and observation in empirical studies. The sites of these hotspots have associated UTM coordinates, and metrics such as phosphorus concentration (ostensibly left by decaying stranded fish) can be ground–truthed in the field.

Discussion

Conservation biologists and resource managers have been investigating patterns of isolation and concentration of stranded fish populations, as well as rates of consumption and depletion by wading bird colonies (Gawlik 2002, Kushlan 1986, Lantz et al. 2011). A goal of the Comprehensive Everglades Restoration Plan (CERP) is to improve the breeding success of wading birds, one aspect of which is to maximize local concentrations of fish biomass across the landscape during the breeding season (USACE 1999). Loss of breeding habitat and decline of forage base (i.e., less small fish productivity) have been implicated in the substantial decline of wading bird populations (Kushlan 1986, Ogden 1994) and increased incidence of alligator and crocodilian nest failure (Mazzotti & Brandt 1994). The spatial and temporal patterns of fish concentration and stranding are especially important to wading bird nesting colonies. For example, successful fledging of wood stork offspring starting from the hatchling stage takes 60–65

days (Kahl 1962), so wood stork adults must locate a continuous source of concentrated prey throughout that period. Because of their ability to soar, wood storks can exploit a large area of marsh, so continuous availability of prey somewhere on the landscape during the breeding period is at least feasible if water levels are managed appropriately.

GEFISH is designed to help scientists and managers understand the way prey fish are concentrated across real landscapes, and to provide useful information on how water management practices can improve the spatial and temporal patterns of fish concentration. The model also generates scientifically interesting behavioral data that can be used to strengthen studies of how forage fish behavioral ecology influences their population dynamics. These insights are now possible because these simulations have spatial and temporal resolution. If the output data were averaged over these scales, the behavior patterns would be lost.

There are known differences among species in both the ability to invade flooding areas and escape drying areas. These differences result in different patterns of biomass being generated and stranded across the landscape, and may provide alternative strategies for survival. For example, high values of fraction invading, *frac_inv*, lead to higher biomass values (Figure 2.3b) than other strategies. However, that comes at a cost of slower buildup of biomass over a period of a few years. It required at least 10 years for fish with *frac_inv* = 0.8, starting with a very small population, to build up to maximum biomass values, whereas fish with smaller values built up biomass much faster. The reason is that most fish with *frac_inv* = 0.8 moved quickly out of long hydroperiod areas of the marsh into short hydroperiod areas, and did not leave behind enough fish to fully utilize the opportunity for quick population growth in the longer hydroperiod areas. Such

a strategy may be at a disadvantage when populations are frequently knocked down to very low levels by disturbances. However, if seasonal rainfall patterns are stable over long time periods, higher biomass levels are obtainable with this more aggressive colonization strategy. High levels of fish stranding had a strong negative effect on the biomass density of a fish species. This trade–off raises the question of why some fish are empirically observed (Trexler, personal observation) to have higher stranding rates than others.

From the point of view of predators such as wading birds, the variety of different fish movement strategies has advantages. As can be seen in Figure 2.6 for the realistic landscape simulation, the length of time that high rates of fish stranding span is somewhat longer for the three groups combined than that for any individual species. Also, the spatial patterns of fish stranding differ, with Fish 3, for example, creating larger, scattered spikes in stranded biomass (Figures 2.4 and 2.5).

The model simplified reality in several ways. The function that generated water level was strictly mathematical and without a stochastic component. This approach was convenient for this first generation model, but it limits the reality of the model, since meteorological and biological processes are not so simple. Water level data in the Everglades Depth Estimation Network (EDEN) database (Palaseanu & Pearlstine, 2008) indicate that the general seasonal pattern is sinusoidal, yet independent rain events can directly impact flooding regimes on a small, localized scale, where tracts of dried prairie can rapidly re–flood in less than 24 h (Trexler et al. 2002). My model did not produce this type of rainfall–induced local variability, but instead reflected mean trends, as if rainfall data were averaged over weeks, and water level sources were primarily gradual

groundwater upwelling from the substrate. Additionally, this model run did not contain inter–annual variability. It was run for a 12–year period with homogeneous conditions for all years, and the results of the last year were presented here. However, the model can be adapted to incorporate variability on any temporal scale (monthly, seasonal, and annual) to examine these types of effects.

Chick et al. (2004) proposed that when water levels drop below 10 cm, accumulation of flocculent materials and detritus threaten respiration to the extent that ponds become no longer inhabitable. I set water level parameters in the model so that the marshes would completely dry out, with the exception of a small permanent refuge, and remain dry for approximately 25–30 days. It is not always the case that sloughs in the Everglades dry out completely; there is regional variability in water depth, and frequency and duration of flooding and drying periods. My model output projected a biomass production distribution for a theoretical year that experienced a severe drydown disturbance event, with the limitation that all prior years experienced the same conditions. Again, the model did not place this year within a context of more favorable, adjacent years. Adding annual variability to the hydrologic function, and running the model for several decades, could produce a different trend.

Final remarks

The GEFISH model was developed to help study the dynamics, particularly the stranding behavior, of small fishes in a seasonal marsh. Model output showed that fish with the highest tendency to invade newly flooded areas of marsh were able to build up the largest populations over periods exceeding a decade. A higher probability to become

stranded, however, did not necessarily mean that it would contribute most to stranded fish biomass, because stranding had negative effects on fish population size that offset its contribution to stranded biomass.

This study serves as a model description for GEFISH, and presents sample output data that can be retrieved from it. In the future, the model will be adapted for targeted applications to realistic wetlands management scenarios. Any set of elevation points can serve as the topography. The water level function could be replaced by a data set generated from a sophisticated hydrologic model projection. For example, two model runs could include the past decade of water level data in areas of the Everglades such as Taylor Slough, and an upcoming decade following restoration re–construction and operations.

Figures

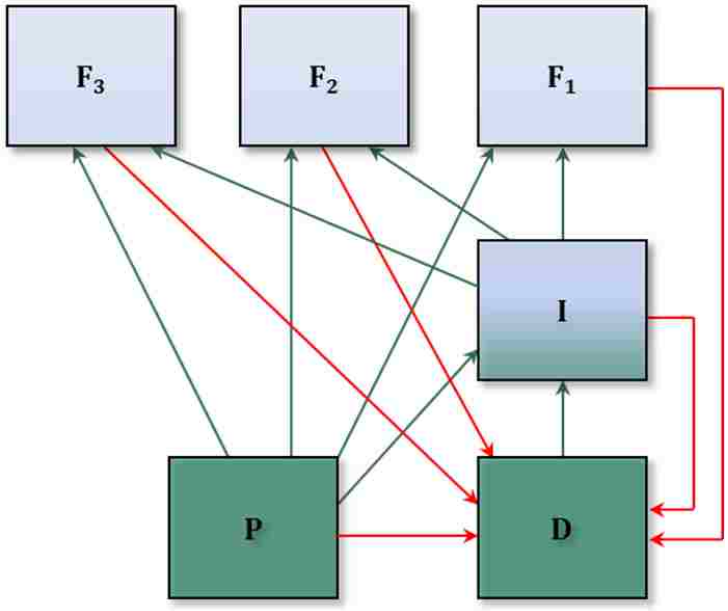

Figure 2.1. GEFISH model food web. Green arrows indicate consumption pathways; red arrows indicate contributions to detrital pool, accrued through mortality and incomplete prey assimilation. Functional groups are: P = Periphyton, D = Detritus, I = Invertebrates, and F_i = Small fish.

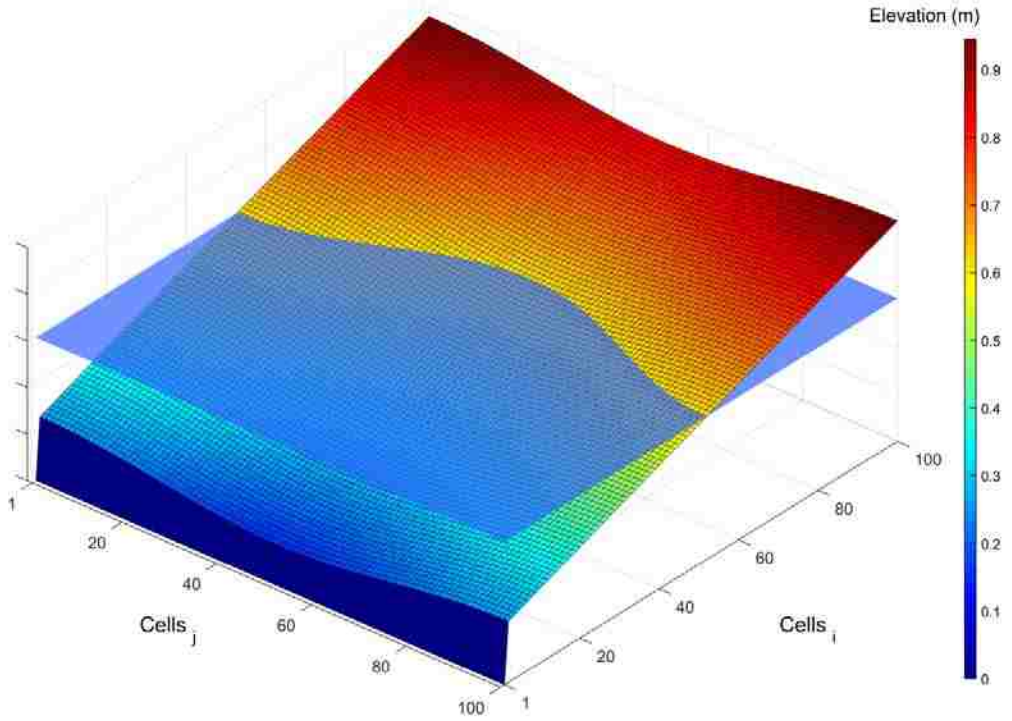

Figure 2.2a. Generalized artificial slough topography (color gradient) with water level (light blue) depicted at day 40; slough terminates in a canal at the lowest end.

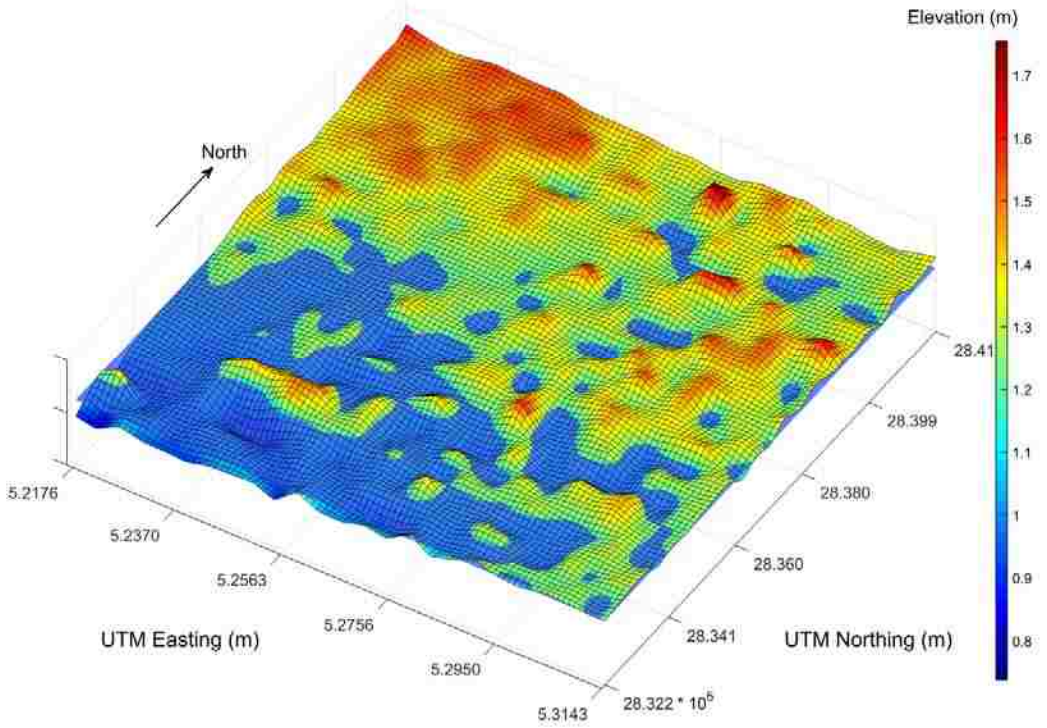

Figure 2.2b. HAED–interpolated real landscape with water level depicted at day 68. Axes are UTM easting and northing values in meters. Note values are at 1.0×10^5 scale.

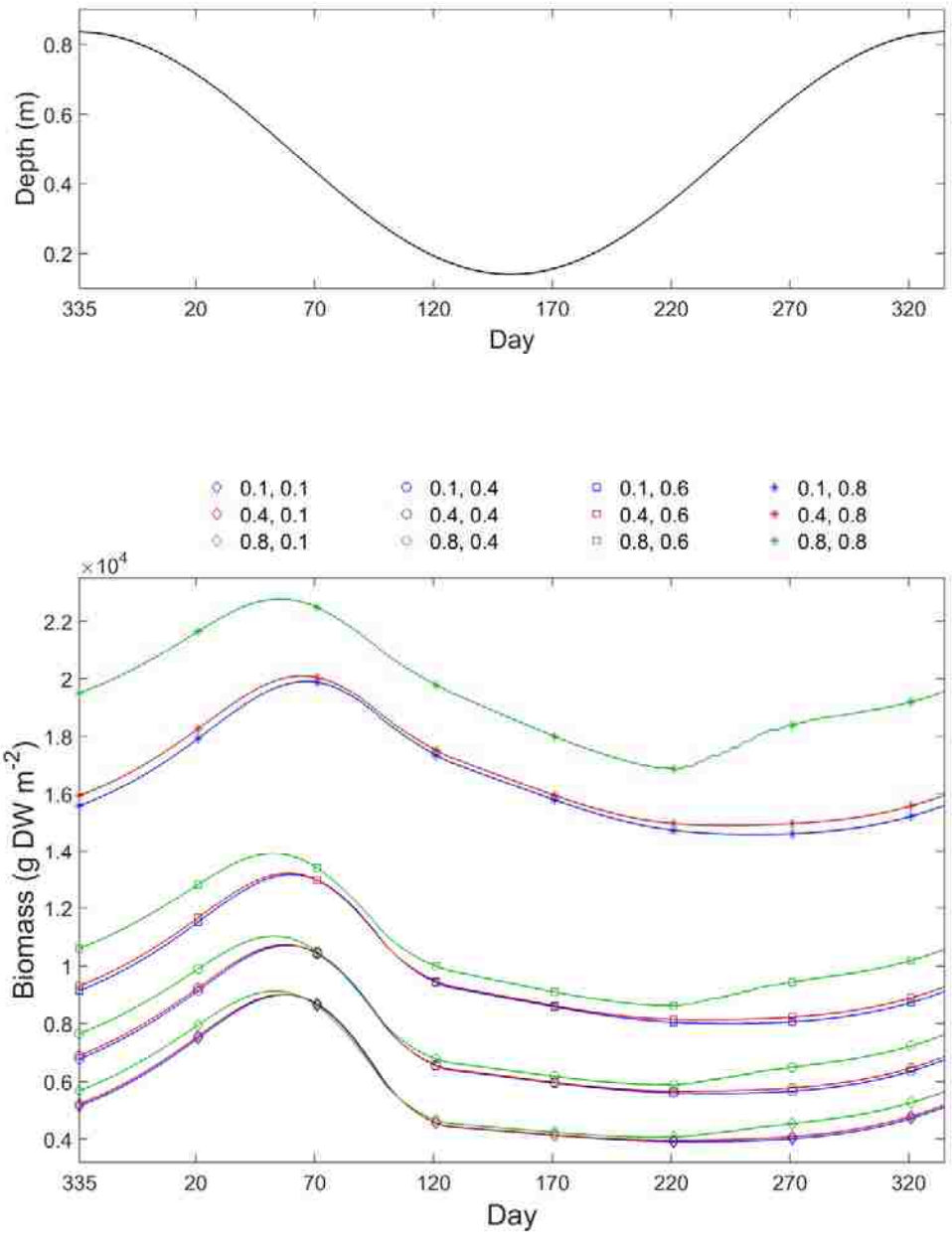

Figure 2.3. (a) Water level across the whole landscape. Depths in each cell are calculated by subtracting cell elevation from water level. (**b**) Daily living biomasses of fish summed across the whole landscape (DTLB). The biomass curves show four clusters, each cluster representing a different value of *frac_leave*, with the highest biomass cluster corresponding to the highest value, *frac_leave* = 0.8. Within each cluster, highest biomass (green lines) is associated with highest invasion value, *frac_inv* = 0.8.

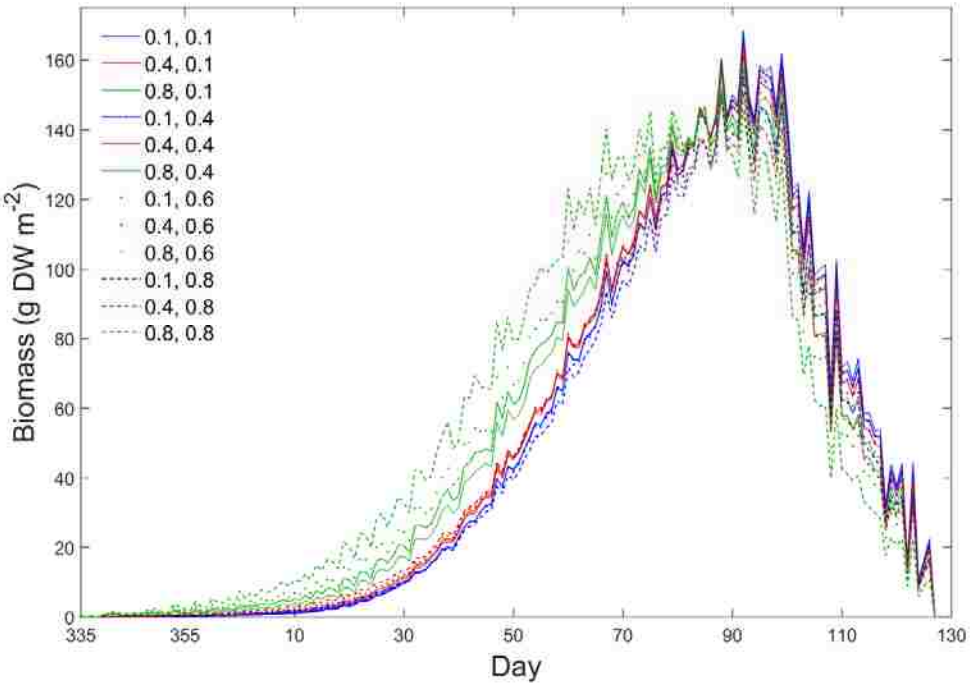

Figure 2.3. (c) Daily total stranded fish biomass summed across the whole landscape (DTSB). The early invaders (green lines) are the first to be stranded, as fish with high *frac_inv* reach higher elevations in greater numbers.

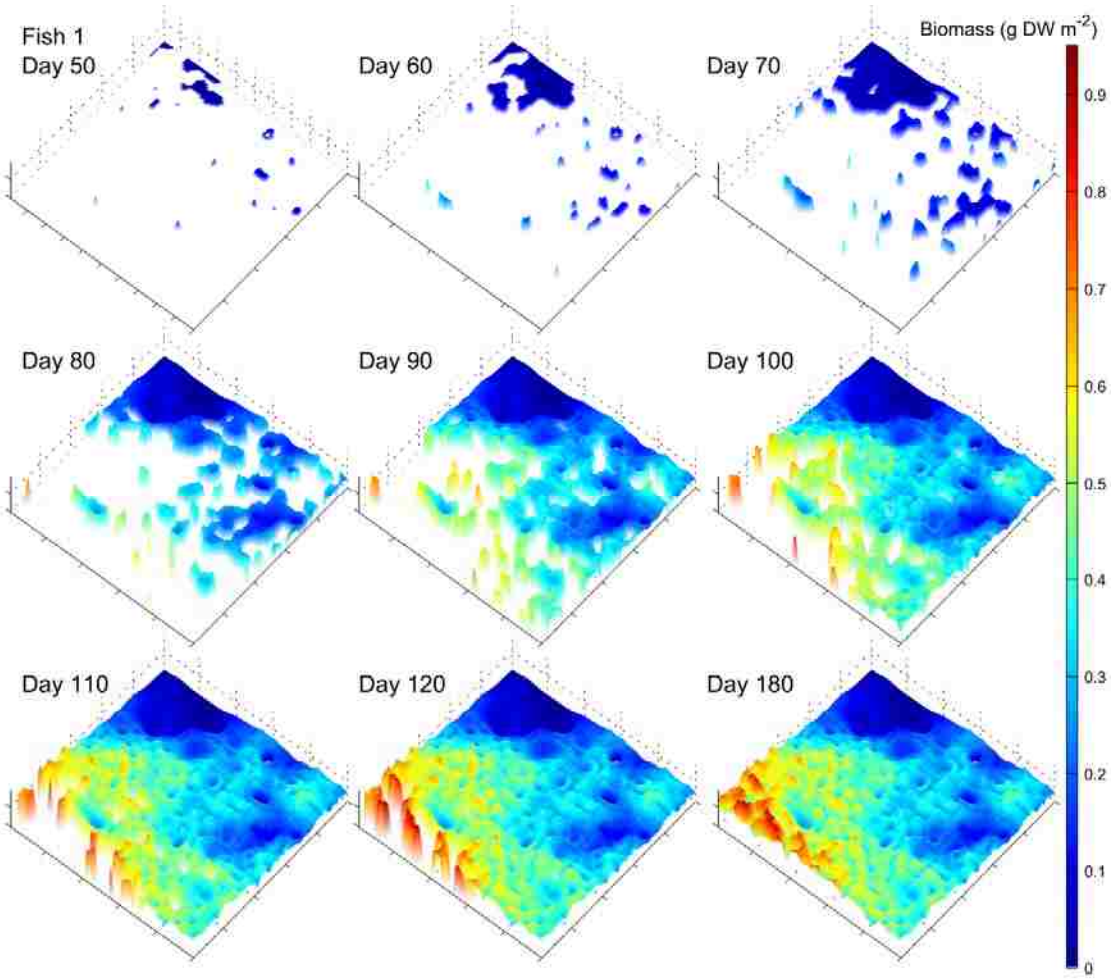

Figure 2.4. Sequential increments (10–day intervals, starting on day 50) of stranding of small fish biomass on realistic landscape as water levels fall. Color bar shows the stranded small fish biomass densities.

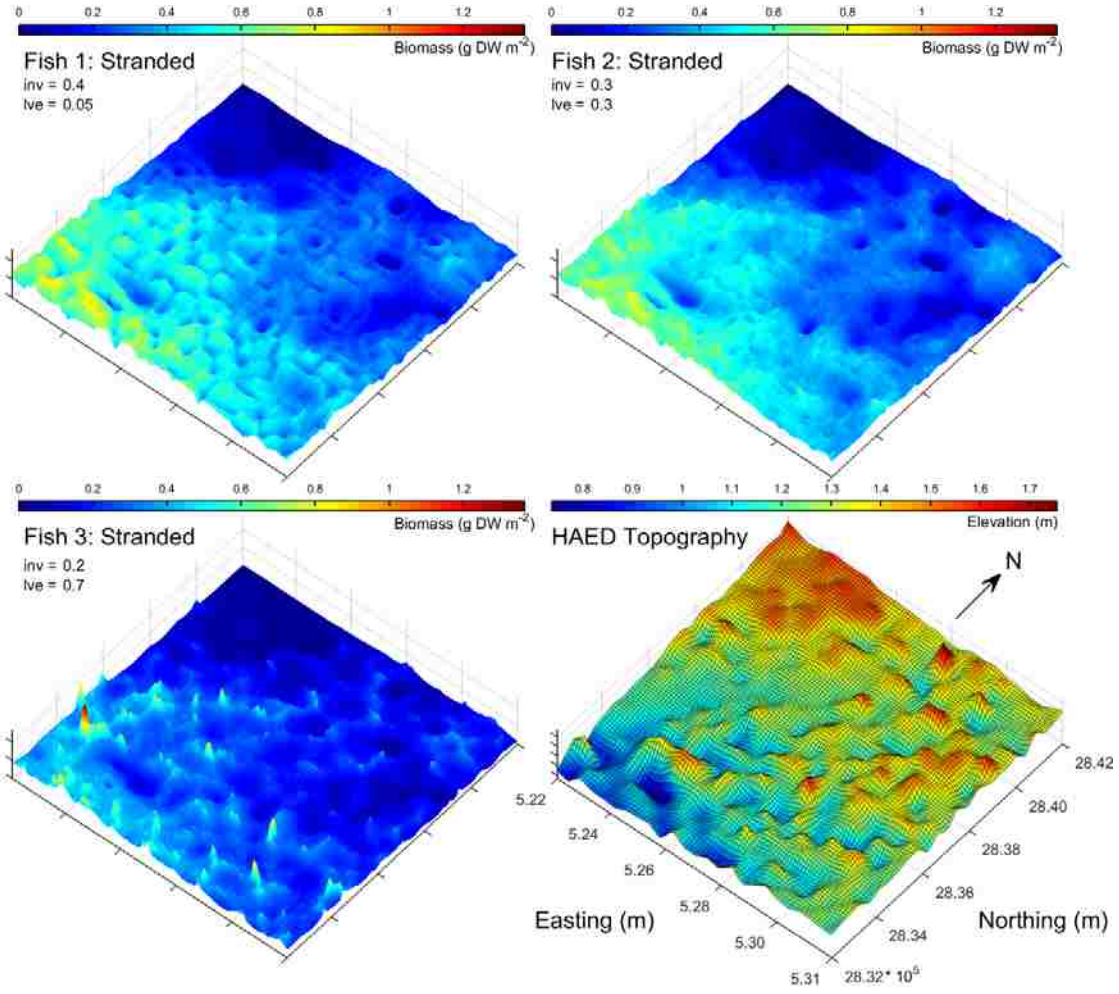

Figure 2.5. Total cumulative stranded biomass of each individual small fish species at the end of the dry season. Actual biomass densities may be locally higher, because the fish were probably concentrated in small depressions within the cells in which they were stranded. Fish 1: *frac_inv* = 0.4, *frac_leave* = 0.05; Fish 2: *frac_inv* = 0.3, *frac_leave* = 0.3; Fish 3: *frac_inv* = 0.2, *frac_leave* = 0.7.

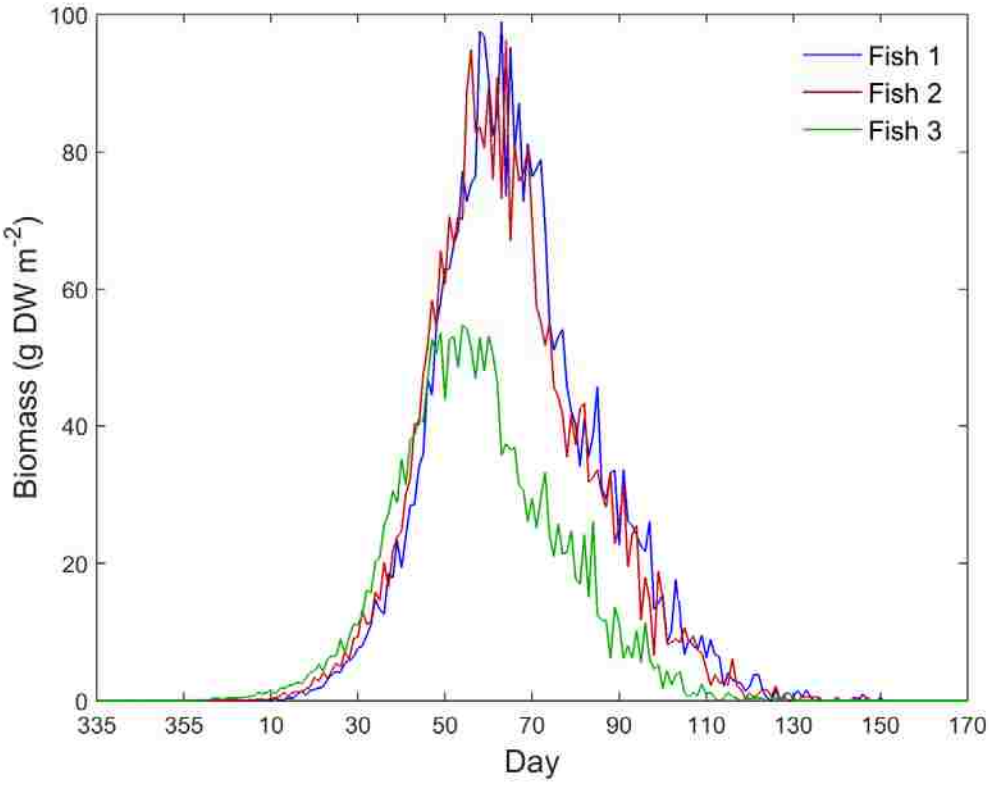

Figure 2.6. Plots of biomass stranded per day, summed over the whole landscape, for each of the three fish species. Fish 3, which had the smallest *frac_inv* and largest *frac_leave*, left the least stranded biomass.

Table 2.1. Values of parameters and biomass response variables for bioenergetics, *cons_peri* and *cons_invert*, and movement strategies, *frac_inv* and *frac_leave*, for sensitivity analysis. Units of biomass are g dry weight m^{-2}.

ENERGETICS

cons peri	*cons invert*	*frac inv*	*frac leave*	Mean living biomass	Max living biomass	Mean stranded biomass	Max stranded biomass
0.05	0.5	0.4	0.4	0.0436	0.5943	0.0482	0.1616
0.1	1	0.4	0.4	0.0871	1.1886	0.0964	0.3231
0.5	5	0.4	0.4	0.4350	5.9303	0.4810	1.6120
1	10	0.4	0.4	0.8678	11.8255	0.9596	3.2137
5	50	0.4	0.4	1.1695	13.4597	1.5410	4.1664
10	100	0.4	0.4	8.2972	112.1177	9.1603	30.3576
50	500	0.4	0.4	34.4472	450.3438	37.7893	120.0897

MOVEMENT

cons peri	*cons invert*	*frac inv*	*frac leave*	Mean living biomass	Max living biomass	Mean stranded biomass	Max stranded biomass
0.02	8.2	0.1	0.1	0.5377	4.1803	0.7908	2.8582
0.02	8.2	0.1	0.4	0.7117	6.1490	0.7842	2.7762
0.02	8.2	0.1	0.6	0.9628	9.0152	0.7724	2.6958
0.02	8.2	0.1	0.8	1.6488	16.4503	0.7308	2.5029
0.02	8.2	0.4	0.1	0.5414	6.9185	0.7981	2.7596
0.02	8.2	0.4	0.4	0.7176	9.7440	0.7939	2.6475
0.02	8.2	0.4	0.6	0.9725	13.6516	0.7852	2.5386
0.02	8.2	0.4	0.8	1.6747	23.6931	0.7508	2.3047
0.02	8.2	0.8	0.1	0.5647	46.7380	0.8339	2.5895
0.02	8.2	0.8	0.4	0.7600	68.8673	0.8463	2.7179
0.02	8.2	0.8	0.6	1.0546	104.1782	0.8626	2.9214
0.02	8.2	0.8	0.8	1.9517	220.6665	0.8983	3.6135

Supplement 2A.

Table S2A.1. Equations of the model.

Primary producer (periphyton), *P(t)*

$$\frac{dP(t)}{dt} = Growth_{peri}\left(1-\frac{P(t)}{K_{peri}}\right)P(t) - m_{peri}P(t)$$
$$- Cons_{peri-by-invert}P(t)I(t)$$
$$-\sum_{i=1,3}\left(\frac{Cons_{peri-by-fish,i}P(t)F_i(t)}{1+h_{peri}Cons_{peri-by-fish,i}P(t)+h_{invert}Cons_{invert-by-fish,i}I(t)+w_{fish,i}F_i(t)}\right)$$

Detritus, *D(t)*

$$\frac{dD}{dt} = m_{peri}P(t)+m_{inverti}I(t)+m_{fish1}F_1(t)+m_{fish2}F_2(t)+m_{fish3}F_3(t)$$

$$+(1-\eta_{invert})Cons_{peri-by-invert}P(t)I(t)$$
$$+(1-\eta_{fish})\sum_{i=1,3}\frac{Cons_{peri-by-fish,i}P(t)F_i(t)}{1+h_{peri}Cons_{peri-by-fish,i}P(t)+h_{inver}Cons_{invert-by-fish,i}I(t)+w_{fish,i}F_i(t)}$$
$$+(1-\eta_{fish})\sum_{i=1,3}\frac{Cons_{invert-by-fish,i}I(t)F_i(t)}{1+h_{peri}Cons_{peri-by-fish,i}P(t)+h_{invert}Cons_{inver-by-fish,i}I(t)+w_{fish,i}F_i(t)}$$

$$-Cons_{det\ ritus-by-inverts}D(t)I(t) - decomp_{det\ ritus}D(t)$$

Invertebrates, *I(t)*

$$\frac{dI(t)}{dt} = Cons_{\text{det } ritus-bv-inverts}D(t)I(t) - m_{invert}I(t)$$
$$+\eta_{invert}Cons_{peri-by-inverts}P(t)I(t)$$
$$-\sum_{i=1,3}\left(\frac{Cons_{invert-by-fish,i}I(t)F_i(t)}{1+h_{peri}Cons_{peri-by-fish,i}P(t)+h_{invert}Cons_{invert-by-fish,i}I(t)+w_{fish,i}F_i(t)}\right)$$

Small fish groups, $F_i(t)$ (i = 1,3)

$$\frac{dF_i}{dt} = \eta_{fish} \sum_{i=1,3} \left(\frac{Cons_{peri-by-fish,i} P(t) F_i(t)}{1 + h_{peri} Cons_{peri-by-fish,i} P(t) + h_{invert} Cons_{invert-by-fish,i} I(t) + w_{fish,i} F_i(t)} \right)$$

$$+ \eta_{fish} \sum_{i=1,3} \left(\frac{Cons_{invert-by-fish,i} I(t) F_i(t)}{1 + h_{peri} Cons_{peri-by-fish,i} P(t) + h_{invert} Cons_{invert-by-fish,i} I(t) + w_{fish} F_i(t)} \right) - m_{fish,i} F_i(t)$$

Table S2A.2. Variables and parameters of the model.

Variable	Units	Definition
P	g dW m^{-2}	Periphyton
D	g dW m^{-2}	Detritus
I	g dW m^{-2}	Invertebrates
F_i (i = 1,3)	g dW m^{-2}	Small fish species populations

Parameter	Value	Units	Definition
$Wlevmn_A$	0.488	m	Mean water level – artificial
$Wlevmn_H$	1.267	m	Mean water level – HAED
$Wlamp_A$	0.348	m	Water level amplitude – artificial
$Wlamp_H$	0.408	m	Water level amplitude – HAED
$Growth_{peri}$	0.15	g g^{-1} day^{-1}	Maximum periphyton growth
K_{peri}	110	g m^{-2}	Density dependent coefficient of periphyton growth
m_{peri}	0.01	day^{-1}	Mortality rate coefficients
m_{invert}	0.6	day^{-1}	"
m_{fish1}	0.019	day^{-1}	"
m_{fish2}	0.017	day^{-1}	"
m_{fish3}	0.015	day^{-1}	"
m_{peri_dry}	0.03	day^{-1}	Dry season mortality rate coefficients
m_{invert_dry}	0.005	day^{-1}	"
m_{fish1_dry}	0.002	day^{-1}	"
m_{fish2_dry}	0.002	day^{-1}	"

m_{fish3_dry}	0.002	day^{-1}	“
$Cons_{peri\text{-}by\text{-}invert}$	0.001	$g\ g^{-1}\ day^{-1}$	Consumption rate coefficients
$Cons_{detr\text{-}by\text{-}invert}$	0.4	$g\ g^{-1}\ day^{-1}$	Consumption rate coefficients
$Cons_{peri\text{-}by\text{-}fish1}$	0.02	$g\ g^{-1}\ day^{-1}$	“
$Cons_{peri\text{-}by\text{-}fish2}$	0.05	$g\ g^{-1}\ day^{-1}$	“
$Cons_{peri\text{-}by\text{-}fish3}$	0.07	$g\ g^{-1}\ day^{-1}$	“
$Cons_{invert\text{-}by\text{-}fish1}$	8.2	$g\ g^{-1}\ day^{-1}$	“
$Cons_{invert\text{-}by\text{-}fish2}$	8.6	$g\ g^{-1}\ day^{-1}$	“
$Cons_{invert\text{-}by\text{-}fish3}$	9.2	$g\ g^{-1}\ day^{-1}$	“
h_{peri}	0.16	day	Handling time of periphyton by fish
h_{invert}	0.16	day	Handling time of invertebrates by fish
η_{invert}	0.06		Assimilation coefficient
η_{fish}	0.35		“
w_{fish}	6000		Small fish self–interference coefficient
$decomp_{detritus}$	0.05	day^{-1}	Decomposition rate of detritus
$diff_{fish1}$	0.025		Diffusion coefficient
$diff_{fish2}$	0.025		“
$diff_{fish3}$	0.025		“
$threshinv_{fish1}$	0.02		Threshold for invading flooding cell
$threshinv_{fish2}$	0.04		“
$threshinv_{fish3}$	0.1		“
$fracinv_{fish1}$	0.4		Fraction invading a cell
$fracinv_{fish2}$	0.3		“
$fracinv_{fish3}$	0.2		“
$threshleave_{fish1}$	0.02		Threshold for leaving drying cell
$threshleave_{fish2}$	0.04		“

$threshleave_{fish3}$	0.10	“
$fracleave_{fish1}$	0.05	Fraction leaving drying cell
$fracleave_{fish2}$	0.3	“
$fracleave_{fish3}$	0.7	“
$fracsurv_{peri}$	0.2	Fraction that survives a cell drying
$fracsurv_{invert}$	0.2	“
$fracsurv_{fish1}$	0.12	“
$fracsurv_{fish2}$	0.12	“
$fracsurv_{fish3}$	0.12	“

Supplement 2B. Details on Movement Rules of Periphyton and Invertebrates

During cell dry down, periphyton and invertebrates sustain a loss to mortality associated with the drying bout. At the same time, a percentage is assumed to remain alive due to access to small ponds, solution holes or alligator trails. The percentage surviving is calculated according to a set of *frac_surv* parameters, and the complementary mortality value (*1-frac_surv*) contributes directly to the detrital pool. In subsequent time steps, these residual amounts that survived the drying bout (and persist in a qualitatively “dry” cell) are subjected to dry season mortality, via a set of parameters *m_dry*, to account for this transition in habitat. Dry season mortality is calculated in the set of differential equations described above.

During the rising water phase when a cell refloods, a small amount of periphyton and invertebrate biomass is assumed to be passively transported into flooding cells through hydrologic action along the flood front. This type of transport is not considered

an adaptive movement strategy based on a life history strategy, but rather, a passive, abiotic, advective transport mechanism. The result is to repopulate cells during the advent of the rainy season.

For each reflooding cell, all adjacent, available (wet) cells are identified according to the *Wmat* matrix. All four adjacent cells are evaluated for whether they are already flooded, such that they can contribute migrants to the newly flooded cells. They act as "donor" cells for the flooding cell, and a percentage of biomass is transferred from each.

Supplement 2C. USGS South Florida Information Access (SOFIA) High Accuracy Elevation Data (HAED) Internet links:

Measuring and Mapping the Topography of the Florida Everglades for Ecosystem Restoration
<<http://egsc.usgs.gov/isb/pubs/factsheets/fs02103.html>>

USGS HAED Elevation Data (download site)
<<http://sofia.usgs.gov/exchange/desmond/desmondelev.html#2>>

USGS HAED Electronic Atlas
<<http://sofia.usgs.gov/exchange/desmond/atlas/>>

HAED Overview: Investigators, Proposals, Work Plans, Summaries
<<http://sofia.usgs.gov/projects/index.php?project_url=elev_data>>

HAED Project Metadata
<<http://sofia.usgs.gov/metadata/sflwww/hi_accuracy_elev_collection_04.html>>

Supplement 2D.

Supplementary data associated with this chapter can be found, in the online version, at http://dx.doi.org/10.1016/j.ecolmodel.2012.11.001.

Chapter 3

Persistence and diversity of directional landscape connectivity improves biomass pulsing in simulations of expanding and contracting wetlands

Summary

Hydrology and landscape structure of flood−pulsed ecosystems mediate transfers of energy up the food chain by expanding and contracting in area, enabling spatial expansion and growth of fish populations during rising water levels, and subsequent concentration during the drying phase. Connectivity of flooded areas is dynamic as waters rise and fall, and is largely determined by landscape geomorphology and anisotropy. I developed a methodology for simulating fish dispersal and concentration on spatially−explicit, dynamic floodplain wetlands with pulsed food web dynamics to evaluate how changes in connectivity through time contribute to the concentration of fish biomass that is essential for higher trophic levels. The model also tracks a connectivity index (DCI) over different compass directions. I demonstrate the model, here, for a seasonally flood−pulsed, oligotrophic system, the Everglades, where flow regimes have been greatly altered. Three dispersing populations of functional fish groups were simulated with empirically−based dispersal rules on two landscapes, and two twelve−year time series of managed water levels for those areas. Simulation topographies represented intact and degraded ridge−and−slough landscapes (RSL). Simulation results showed large pulses of biomass concentration forming during the onset of the drying phase, when water levels were falling and fish began to converge into the sloughs. As water levels fell below the ridges, DCI declined over different directions, closing down

dispersal lanes, and fish density spiked. Persistence of intermediate levels of connectivity on the intact RSL enabled persistent concentration events throughout the drying phase. The intact landscape also buffered effects of wet season population growth . Water level reversals on both landscapes negatively affected fish densities by depleting fish populations without allowing enough time for them to regenerate. Testable, spatiotemporal predictions of the timing, location, duration, and magnitude of fish concentration pulses were produced by the model, and can be applied to restoration planning.

Background

Pulsed hydrologic flows play important roles in many aquatic ecosystems by creating pulses of resource production (e.g., fish and invertebrates) that are then concentrated in localized areas (Kahl 1964, Odum et al. 1995). Concentration occurs over a spatial domain, as these resources are channeled during falling water levels, at times forming large spikes in density (Yang 2008). Resource pulses may have long−term effects on ecosystems, possibly persisting within and sustaining the system (Holt 2008, Reigada et al. 2015). It is therefore important to understand how the spatial dynamics of resource pulse concentrations proceed over time.

In seasonally−pulsed wetlands, during the flooding phase, the wetland expands and terrestrial resources are released into the aquatic system, boosting primary and secondary biomass production. This biomass then becomes concentrated as waters recede and the wetland dries out and contracts. These ecosystem dynamics occur on river floodplains worldwide (Tockner & Stanford, 2002), and have been termed the ‘flood pulse concept’

for such systems (Junk et al. 1989, Tockner et al. 2000), but the concept is also potentially relevant for geographically isolated systems (Tiner 2003).

Many species have adaptive strategies of spreading across the landscape during the flooded phase, and of retreating to locate dry season refugia during periods of low water (Lytle & Poff 2004, Magoulick & Kobza, 2003). Movement strategies vary by species, and differ in the timing and rates of immigration and emigration (Goss et al. 2014), potentially resulting in successional community dynamics (Winemiller 1996). Monitoring of fish on floodplains has uncovered many details of movement strategy (Cucherousset et al. 2007, Dutterer et al. 2013, Saint−Paul et al. 2000, Zeug & Winemiller 2008), but further work is required to understand cumulative effects on the flood pulse at the ecosystem level, such as on trophic interactions (Chea et al. 2016, Winemiller & Jepsen 1998).

Connectivity of flooded areas changes throughout the various phases of rising and falling water levels. When the wetland is flooded, connectivity is considered high and populations can disperse in different directions. As the wetland dries out, connectivity decreases and movement becomes restricted, but a sufficient level of connectivity is needed for fish to continue to move towards refugia. These temporal dynamics of connectivity are thought to impact fish movement and assemblages (Burgess et al. 2013, Lasne et al. 2007). One potential explanation is that the overall flux of fish biomass across the landscape decreases as movement becomes restricted in localized areas, and large concentrations of biomass form that are isolated and removed from the population as areas dry out. Consideration of changes in the pattern of connectivity through time can help to understand the mechanisms of how small−bodied fishes (< 8 cm), which are prey

to higher trophic levels, are concentrated in short localized pulses over long periods of the drying season to maintain the higher trophic levels (Lake 2011).

Wetland connectivity is determined in large part by landscape geomorphology. Spatial heterogeneity of the landscape along slight elevation gradients can mediate large shifts in connectivity, as water levels rise and fall, because spatial conformation of the wetlands changes over time as different flooded areas become connected and disconnected (Mertes et al. 1995, Zeug & Winemiller 2008). Patterned landscapes, such as braided riverine networks or parallel drainage landscapes, can have complex connectivity, including directionally. For example, in anisotropic landscapes, connectance is strongly directional when the wetland is partially flooded and some of the topography is exposed, but omnidirectional when water levels rise above the landscape (Figure 3.1). These landscape effects, resulting in dynamic patterns of connectivity, have been studied primarily with regard to water flows (Larsen et al. 2012), but are relevant as well to motile biota.

Here, I present a general methodology for evaluating how species−specific movement behaviors interact with dynamic hydrology and heterogeneous landscape geomorphology to produce pulsed concentrations of fish. I combine empirically−characterized movement rules for flood−adapted fish with real landscape topographies and hydrologic data in a computer simulation model called FDAL (Fish Dispersal on Aquatic Landscapes). Fish movement is modeled with both directed and probabilistic elements, as short movements on a contiguous lattice that are based on the local environmental conditions where the fish occupy the landscape.

This model was developed to be broadly applicable to floodplain or transient wetland systems where hydrology, landscape geomorphology, fish movement strategies, and food web dynamics can be estimated. The model simulates and tracks dispersal and concentration of fish over spatially−explicit hydroscapes, and simultaneously tracks connectivity of the flooded wetland over different compass directions. The end product of the modeling is a set of two parallel time series: (1) fish biomass, and (2) directional landscape connectivity indices (DCI) defined over different directions for a given subregion of the wetland. These indices represent the likelihood that a population can traverse that area. The time series can be compared and used to make testable predictions of the timing, location, duration, and magnitude of fish concentration pulses, given landscape spatial structure and an annual hydrograph. The capability of the model for simulating fish movement fluxes across a landscape, with spatially varying and temporally dynamic hydrology, are demonstrated here by applying it to a seasonally−pulsed subtropical wetland, the Everglades, using hydrologic records, landscape topographies, and rules for fish movement taken from empirical studies.

Methods

Model description

FDAL simulates population growth, dispersal, and concentration of small−bodied fish in units of biomass (g dry weight m^{-2}). It combines a landscape topography layer, a time series record of hydrology, a generalized food web supporting the fish, and rules for their dispersal in response to dynamic habitat conditions. The model landscape is a spatially−explicit grid of contiguous cells with fixed elevations, and water depths that

change over time as hydrology interacts with topography. The size of the grid, scale of coverage, and landscape structure can be varied by the user. Here, the grid cell size is 20 × 20 m and the spatial extent is about 2 × 2 km. Variables of the model are assessed on discrete time steps, here 0.25 days.

Fish biomass is tabulated for each cell on the landscape, and recorded as time series. Biomass grows through consumption of lower trophic levels in the food web that have population dynamics that are strongly linked to hydrology. Modeling the fish by combining food web interactions and dispersal simulates the slow build−up of fish populations in newly flooded areas, which are rapidly concentrated as water levels recede. The food web contains six trophic functional groups: periphyton, detritus, invertebrates (periphyton−associated), and three fish groups. Biomass is conserved across groups. This food web structure and the differential equations governing trophic interactions were adapted from an earlier, site−specific model, GEFISH (Yurek et al. 2013), although these were the only features that were included in the new model. New algorithms were written that assign movement based on environmental conditions. Supplement 3A lists variables of the food web (Table S3A.1), differential equations for each variable, and parameters used in the Everglades example (Table S3A.2).

Transitions of fish biomass between cells are simulated to reflect rules of fish movement behavior based on empirical information. Three fish groups (F_i, i = 1, 2, 3) with qualitatively different adaptive movement strategies are used. Fish movement occurs in two overall modes, for wetland flooding and drying, and different movement behaviors are assumed for each mode. During periods of rising water, fish rapidly colonize newly flooding marshes to exploit the flood pulse. This behavior is simulated by assessing the

length of time, in days, that each cell on the landscape has been recently re−flooded (time since flooding, TSF), representing local resource abundance (DeAngelis et al. 2010, Goss et al. 2014). Fish biomass disperses in higher amounts into cells that have recently reflooded (low TSF), than into cells that have been flooded for longer (high TSF). If a cell dries out, TSF in that cell resets to zero. When water levels recede and the wetlands are drying, the second movement mode is engaged. Fish biomass disperses out of cells where water levels are approaching very shallow depths, and movement is further increased with higher water level recession rates.

Four spatially−explicit movement rules were assumed: (1) movement is possible between all adjacent wet cells at any time, but probability of movement is based on local environmental conditions, (2) interactions between fish movement behaviors and landscape structure determine the flux (biomass $cell^{-1}$ t^{-1}) of movement, (3) choice of movement direction is possible when water levels are rising (based on TSF), but not when falling (movement is equal between all wet cells), and (4) during the drying phase, fish biomass becomes stranded in cells that dry out with no adjacent wet cells.

Inter−cell movement occurs in FDAL in three parts, for both flooding and drying phases: (1) a cell is selected for movement, (2) a proportion of biomass is removed from that cell, and (3) that amount is divided between adjacent wet cells. Fish biomass moves only one cell at each time step (no multi−cell leaps), but rapid movement is possible since time steps are short and movement can occur simultaneously in multiple cells. Steps 1 and 2 are determined by two parameters, *p_move* and *frac_move*, the probability and fraction of movement, respectively, and Step 3 by an algorithm, *split_biomass*, that weights neighboring cells according to their habitat conditions. The probability, fraction,

and directional amounts of biomass that move are tabulated from qualitative scaling curves that relate biomass movement to environmental conditions in a cell (Figure S3B.2, Supplement 3B). These rules and algorithms were coded and annotated in *Matlab* (Mathworks Inc. 2015) and are available upon request from the corresponding author. The combination of activating a cell for movement, scaling the amount of fish biomass that moves, and splitting it in different directions is a new approach that has a net function of accelerating and decelerating directional fluxes according to a combination of local habitat conditions, fish movement behaviors, and the biomass densities of the fish. Convergences and divergences of movements within localized areas lead to nonlinear fluctuations in density.

Directional connectivity of flooded habitat

FDAL tracks wetland connectivity over different directions of the landscape, recursively at each time step, using an index (DCI) developed by Larsen et al. (2012), generating a time series of spatial information. This index quantifies connectivity of a subregion of landscape by measuring the relative length of a path through flooded habitat in a given direction. Briefly, the index estimates connectivity at the landscape scale by summing ratios of the shortest path along flooded cells to the direct distance, in a straight line, between every wet cell on the grid and all other rows. It varies between zero and one, with one representing landscapes with linear connected flow−paths along the direction of interest and lower values representing disconnected and/or tortuous flow paths along that direction. FDAL was programmed to calculate DCI for the eight principal compass rose directions (0°, 45°, 90°, 135°, 180°, 225°, 270°, 315°).

Application to the Everglades

To demonstrate model capability, I simulated movement behaviors of small−bodied Everglades fishes. The Everglades (Florida, USA) is a seasonally pulsed, spatially dynamic, subtropical karst wetland in which the amount of flooded area expands and contracts, similar to a river flood plain, but having lower flow velocities (0−1 cm s^{-1}, Gunderson & Loftus 1993). The landscape structure of the Everglades is a parallel drainage system described as ridge−and−slough landscape (RSL) (Larsen et al. 2007, McVoy et al. 2011, Ogden 2005; Figure S3B.1; Supplement 3B). The RSL comprises a network of parallel sloughs and intervening peat ridges that have accreted to slightly higher elevations, sustaining an elevation differential of ~10−20 cm (Harvey et al. 2009, Watts et al. 2010). The RSL is anisotropic in the north−south direction, with some east−west connectivity at gaps in the ridges. Fish in the Everglades use this slough network to navigate the flooding and drying wetland. Complex movements are possible, as functions of both the strong north−south orientation of the RSL and the east−west pattern of flooding and drying of the landscape.

The Everglades is characterized at the macroscale (200 km) by a low elevation gradient of 2.8 cm/km from north to south (Gunderson & Loftus 1993), at the mesoscale (20−100 m) by RSL structure and tree islands, and at the microscale (< 20 m) by peat and marl substrate (Craighead 1971). The landscape also rises slightly (~1m) in an east−west direction. Everglades hydrology is a composite of overland flows and groundwater (Gunderson & Loftus 1993, Parker 1955, Rosendahl & Rose 1892). During the wet season, the water table rises above ridges of the RSL, and connectivity is high and omnidirectional. When water levels recede, the ridges dry first, followed by the sloughs,

which become disconnected. Connectivity rapidly shifts to anisotropic and is limited to the slough flow−ways. This RSL−scale flooding−drying pattern occurs at different times on different parts of the greater regional landscape of the Everglades. For details of RSL process dynamics, see Davis et al. (1994), Ogden (2005), Larsen et al. (2007), and Larsen & Harvey (2010).

Water flows in the Everglades have been greatly reduced through the engineering and operation of an extensive canal and levee system, impounding much of the Everglades. Current flows are not sufficient to maintain historic ridge−slough elevation differentials. Many areas of slough have infilled and become vegetated (Davis et al. 1994, McVoy et al. 2011), and the RSL structure in these areas has degraded to patchy, isolated remnant pools. The intact and degraded RSL habitats occupy large sub−basins of the Everglades which are separated by levees and have distinct hydrological regimes. Small areas of the intact and degraded RSL were simulated in this study, by combining geospatial information at the three scales described above to generate the topographic structure (Figure 3.2). Each of these areas is approximately 4 km^2. The degraded area has lost its RSL topography, with only patches of flooded area left. See Supplement 3B and Chapter 4 for details.

Water stage data for each landscape were retrieved from the EDEN Water Surfaces database for 2001−2012 (sofia.usgs.gov/eden/models/watersurfacemod.php). A single hydrograph was produced for each landscape by averaging water level data over the landscape at each time point, and interpolating to time steps of 0.25d (Figure 3.2, top panel). Dashed lines represent maximum ridge elevation. There were 17,532 total time steps, including three leap years.

Everglades fishes adapted for simulation

The Everglades fish community is strongly size−structured, with the majority of biomass comprising short−lived cyprinodontiform species and juveniles of long−lived families, notably centrarchids (Trexler et al. 2002). These fish must disperse seasonally to avoid desiccation (Loftus & Kushlan, 1987). Species−specific dispersal dynamics were inferred from empirical sampling events, where evidence was found of directed movement and/or seasonally changing patterns of activity that vary by species (Obaza et al. 2011; Hoch et al. 2015).

Three functional fish groups ($Fish_{1–3}$) were used on both intact and degraded RSL simulation scenarios. These were based on real species: $Fish_1$ = *Gambusia holbrooki* (*G.h.*), $Fish_2$ = *Jordanella floridae* (*J.f.*), and $Fish_3$ = *Lucania goodei* (*L.g.*) (Hoch et al. 2015). Model life history traits of the simulated species match those of the real species as closely as possible. Species−specific tradeoffs between movement and population growth parameters were assumed.

The biomass fluxes between cells reflected fish movement behaviors, which differed between species and seasons. $Fish_1$ has the overall highest movement rates and directional bias of the three groups, rapidly colonizes temporarily flooding marshes, is the last to leave, and has highest movement activity during water level recession. $Fish_2$ is an intermediate movement type and has higher activity and directional bias when marshes are flooding than when drying. $Fish_3$ is relatively sedentary, is more active and abundant in long−hydroperiod sloughs, enters flooding areas slowly, and is slightly more active during the flood phase.

Analysis of model output

I first analyzed the physical dynamics of the model, then fish biomass relationships with these dynamics, over the drying phase when water levels were falling and fish move from higher to lower elevations. Shifts in connectivity impact dispersal at this time. The drying phase was defined as a period beginning when the water stage fell below a threshold of 20 cm above the highest ridge, which is also when fish began to move toward the deeper sloughs, and ending at the time when seasonal flooding began again.

Physical connectivity dynamics were summarized over the drying phase by comparing DCI and area of flooded habitat to water stage for each landscape. Flooded area represents the amount of wet cells available for concentrating fish.

Fish biomass was then related to DCI, inter−annually, using the drying phase of each year to proxy different scenarios of hydrological management. I was primarily interested in how the temporal patterns of hydrology over the drying phase produced high densities of fish biomass within the sloughs, representing the likely source of food for top predators. The timing, location, duration, and magnitude of these densities were of particular interest. Spatial distributions of fish biomass within the sloughs, at each time step, were tested for agreement with several theoretical distributions, using Lilliefors and χ^2 goodness−of−fit tests (Mathworks Inc. 2015). This provided an estimate of how the biomass was shifting over space.

Temporal distributions of high densities of fish biomass were evaluated at the time scale of the drying phase (several months). Biomass and DCI were compared temporally, by converting their respective time series to measures of persistence as follows: Continued maintenance of high fish densities over time, termed ‘persistence’ here, was

calculated as the frequency, in days, that biomass in a cell exceeded defined thresholds (10, 12, and 15 g m^{-2}) over the drying phase, and summing these frequencies over all slough cells. This produced a biomass metric, termed cell−days, for each cell, which can be predicted spatially in maps, summarizing concentration dynamics over the drying phase. These biomass thresholds were chosen as markers of super−concentrations, approximating the 0.999, 0.9995, and 0.9999 quantiles of biomass over the entire 12 years of simulations. Since connectivity varies directionally, and over time, continuation of connectivity was summarized as a measure of diversity across directions, by calculating the variance in DCI over the eight compass directions at each time step, and summing over the drying period. Fish biomass persistence was related to DCI persistence, and r−squared values of linear and logistic model fits were taken for qualitative comparison. Intact and degraded landscapes were analyzed independently.

The drying phase represents the time when fish populations transition from wet season growth mode to dry season concentration. To test if growth of biomass during the wet season impacted concentrations of biomass in single cells during the subsequent drying phase, fish biomass was summed over the entire landscape (all 10,000 cells) at Day 1 of the drying phase for each year, and was compared to select quantiles of biomass (0.1, 0.5, 0.75, 0.9, 0.99, 0.995, 0.999) taken over the full drying phase of that year.

Results

Landscape hydrology

Slough habitat area varied between landscapes; the intact and degraded RSLs had 4,181 and 1,251 total slough cells, respectively. The length of the drying phases also

varied between landscapes and years (Table S3C.1, Supplement 3C), ranging from 119 (2003) to 284 (2011) days on the intact RSL (mean = 194), and from 84 (2003) to 297 (2010) days on the degraded (mean = 200). The drying phases generally began earlier in the year for degraded (Oct−Nov) than for intact (Nov−Jan), and were generally longer, whereas, the length of time that the water was fully below the ridges was generally longer for intact (not shown). Complete drying, or drydown, occurred on the degraded RSL in 2001, 2006, 2007, 2009, 2011, but in no years for intact. In 2010, the water level did not fall below the marsh surface on intact, and fell below by only a few centimeters on degraded RSL.

The twelve year time series of simulations of water level and DCI, over eight directions, are shown in Figure 3.3 (top panel) for the intact RSL. The dashed line represents maximum ridge elevation. Peaks and troughs in water depths occurred near the end of the wet season and dry season, respectively. All eight DCI values remained near 1 for 2003, 2005, and 2010, when the water level did not fall far below the ridges. During the other nine dry seasons, DCI values diverged over different directions, for varying durations of time, after water levels fell below the ridge tops. During these periods, freedom of movement for fish was directionally restricted. Changes in DCI are much sharper than changes in water level, showing that movement can rapidly become restricted in all or some directions. Relationships between water level, DCI, and number of flooded cells are shown in Supplement 3C for intact and degraded RSLs.

Fish biomass

Twelve years of simulated fish populations are shown in Figure 3 (panel 2), for each of the three fish functional types. These represent all fish biomass summed over the

landscape. Note that in the three years when DCI remained near 1, total fish biomass remained constant, for about 1.5 years, due, in part, to the model assumption of continuous fish reproduction. Videos of fish movement simulations for a representative year (2002) on intact and degraded RSL are shown in Supplement 3E.

The distribution of fish biomass across the cells on the intact RSL followed a normal distribution for < 0.5% of time steps yr^{-1} (taken each year), a gamma distribution for 0.7–40% of time steps, an extreme value distribution for 0.5–60% of steps, and a lognormal distribution for 14–86% of steps. Biomass distributions were positive−skewed for all years (excepting some time steps in 2012), with mean skewness = 0.85. Overall, biomass values below the mean were similar among slough cells over time, while the right tail of the distribution, representing the highest accumulations of biomass, fluctuated the most.

The twelve years of single−cell fish density shown in Figure 3.3 (bottom three panels) are summarized as quantiles $\tau = 0.5$, 0.9, and 0.999. Each quantile represents the amount of biomass above which a percentage of cell densities are higher. For example, of the 4,181 slough cells on the intact RSL, biomass of 418 cells (10%) are higher and 3,763 (90%) are lower than the 0.9 quantile. Viewed as parallel time series, changes in single−cell density relative to the whole landscape can be tracked over time, for each species. Variation across levels of τ shows redistribution of fish biomass among cells, explicitly for each species. Median population densities are shown in the $\tau = 0.5$ graph (Figure 3.3, bottom). These stay roughly between 0.5 and 2.0 g m^{-2}, with the simulated $Fish_3$ (*L.g.*) consistently highest, and $Fish_1$ (*G.h.*) lowest. The $\tau = 0.9$ graph (middle) shows peaks in biomass density, particularly for *G.h.*, that coincide closely with when DCI began to deviate sharply from 1, as water stage fell below the ridges (dashed line).

G.h. exceeds 3.0 g m^{-2} at times, while falling to 0.5 g m^{-2} at others. This quantile notably shows interspecies variation in the timing of concentration, for example, peaks in *L.g.* follow *G.h.* Fish continued to be concentrated as water level fell, with some attenuation (see also Supplement 3F). When the water stage fell below the bottom of the slough, the landscape dried out (2011) and very few fish were left for concentration. Finally, the τ = 0.999 graph (Figure 3.3, third panel) shows much higher concentration of *G.h.* than the other two fish species. Pooled biomass of the three fish species at the 0.999 quantile (black line) exceeds 15 g m^{-2} at times, indicating these high fish biomass densities for some spatial cells, and *G.h.* comprises the majority of these amounts. Each year of simulations is shown at finer temporal scale in Supplement 3F.

Fish biomass persistence (frequency of exceedance of biomass threshold θ =10 g dry wt. m^{-2}) is mapped for each cell on the intact landscape for 2001 (Figure 3.4a; bottom panel), and 2011 (b). The period of diverse levels of DCI (top panel) was only slightly shorter for 2011 than for 2001, although the frequency of high biomass greatly exceeded that of 2001, which had two intervals of strong water level reversals that limited concentration later in the drying phase (Figure S3F.1A, Supplement F). The dotted line represents when water level first fell below ridges.

Fish biomass persistence related to intermediate DCI persistence (Σ *variance*) is shown in Figure 3.5. Each year is indicated by a single digit. A positive correlation (r−squared = 0.413, 0.406, and 0.401) occurred for all three thresholds (10, 12, and 15 g m^{-2}) of the intact RSL (black dotted line). Years 2001 and 2007 greatly altered the linear fit because of reversals. Excluding those years, the logistic model had the best fit (gray dotted lines; r−squared = 0.803, 0.872, 0.93). No correlation occurred for degraded RSL

(r−squared = 6.59e−04, 5.21e−04, and 0.006). *Σvariance* of degraded was an order of magnitude lower than intact RSL.

Wet season biomass growth impacted fish biomass accumulation over the drying phase differently for the intact and degraded RSL (Figure 3.6). Total biomass on Day 1 of the drying phase varied from $1.99 – 4.19\times10^4$ (g dry wt. m^{-2}) for the intact landscape, and from $2.03–4.2\times10^4$ (g dry wt. m^{-2}) for degraded (Table S3D.1, Supplement D). Slopes of the relationships of quantiles to Day 1 biomass were lowest, and varied the least, for many quantiles (0.1–0.9) of the intact RSL, while the 0.99–0.999 quantiles rose slightly. All quantile slopes of degraded were higher than intact, with highest slopes at the upper quantiles (0.99–0.999). Day 1 biomass on the degraded RSL was generally lower than on intact.

Discussion

I developed a methodology, based on work of Yurek et al. (2013), for simulating fish biomass spatial movement flux, using estimated adaptive movement strategies of small−bodied fish in response to seasonal flood pulses, to track how movement behaviors interact with hydrology to produce pulses of fish biomass concentration. I demonstrated the model using empirically−derived dispersal rules for fishes on hydrologically dynamic, spatially explicit, ridge−and−slough wetlands of the Everglades. Intact and degraded RSL landscapes were simulated, and empirical hydrological data for 2001−2012 were applied. Time series of fish biomass and connectivity of landscape subregions (DCI), measured over eight directions, were compared over the wetland drying phase. DCI was nonlinearly related to wetland flooded area, and was highly

variable during the intermediate phases of drying, when directionality became a key factor in determining connectivity of dispersal corridors. This intermediate period is a critical time when high biomass pulses form (Figure 3.3). Spatial diversity of connectivity was quantified over the drying phase as the summed variance of DCI over eight directions. Persistence of a large range of DCI variance produced the largest successive concentrations for the intact landscape. Tracking DCI and biomass in time series in this way provided simple summaries of the highly complex nonlinear interactions between hydrology, landscape structure, fish population dynamics, and movement behaviors that result in fish biomass pulses.

Videos of simulations (Supplement 3E) showed fish being channeled by falling water during the drying phase, first into the sloughs, and then down the sloughs as they dry. Some fish are concentrated and trapped in local depressions or cul−de−sacs (Figure S3G.3A, Supplement G), making them available to higher trophic levels. Others escape to permanent water and repopulate the landscape the next year.

Examination of trends of water stage, DCI, and fish biomass at high concentration levels in Figure 3 reveals some general relationships. There is a sequence of the effects of the landscape variables, water stage and DCI: water stage activates the fish to move when conditions become shallow, then the fish become aligned when DCI begins to decline and dispersal options become limited. It is essential that water stage falls below the ridge for directed channeling of fish biomass to occur and for high concentrations to form (see Supplement 3E). High levels of fish biomass can form even before the eight DCI indices decrease below 1. However, the period of time when the DCI indices begin to diverge from each other, such that connectivity decreased in some directions but remained high in

others, appears to be associated with especially high biomass concentrations, and divergence of DCI values over a long period of time, as in 2006, 2009, and 2011 on the intact RSL, is associated with prolonged high concentrations of fish, even though water levels are not receding much further during that time. I attribute this to fish being channeled into narrow ribbons of slough during these periods, and thus maintained at high concentrations for periods of months, as shown in videos in Supplement 3E.

DCI patterns may also provide some insight into water level reversals. Reversals that occurred before DCI divergence (intact RSL; 2004, 2009; Figure 3.3a) had little or no effect on subsequent fish concentration (Figure 3.3b), because there were minimal losses of living fish biomass up to that point. Reversals that occurred after DCI values diverged (2001, 2007) greatly reduced the chance of further concentrations, because large amounts of fish biomass had already been lost through stranding, and the reversal re−flooding time was not sufficient to produce enough biomass for further pulses of concentration. For that reason, 2001 and 2007 deviated from the linear relationship of biomass to $\Sigma variance$ (Figure 3.5), achieving lower levels of cell days despite DCI variance being maintained after the reversals. Excluding these years (Figure 3.5, dotted gray line), $\Sigma variance$ appears to be a good indicator of the persistence of high concentrations of fish biomass (r−squared = 0.8−0.93), although after some time, the cell−days value saturates, since biomass is gradually being lost to stranding.

Although water stage and DCI together explained some mechanisms that caused biomass to concentrate in high peaks, there were other hidden effects of the RSL shape and structure that were not captured by the DCI metric. For example, in 2003 and 2005 on the intact RSL (Figure 3.3), spikes in concentration occurred from May – July,

although DCI was effectively stable, and the water stage declined only slightly. Figures S3G.3A, S3G.5A (Supplement 3G) and videos from Supplement 3E suggest that sinks, where fish can be trapped, along the ridge−slough interface are responsible for these concentrations. Analyzing spatial configurations of these sinks, such as with Fourier descriptor spectra (Lloyd & Allen 2015), may be useful for complementing DCI. One interesting landscape effect was found in the comparison of wet season biomass to dry season concentration (Figure 3.6). The intermediate quantiles of biomass (drying phase) on the intact landscape were not very sensitive, suggesting that the intact RSL can buffer variations in wet season growth. This provides support for conserving RSL habitat.

FDAL was designed to incorporate basic assumptions about fish movement and trophic interactions. Movement patterns emerge in the model on short time steps through the interaction of dispersal rules and landscape hydrology. However, some limitations were present. The scale of the landscape was very small (2 × 2 km), and dispersal was confined to that area, with no emigration. This resulted in biomass accumulating at the lowest elevations along the southeast corner of the landscapes (Figure S3G.7B, S3G.9B, Supplement G). These accumulations were informative, though, because the effect was higher on the degraded RSL, suggesting landscape geomorphology may impact dispersal flux or speed at the scale of the landscape. Trexler et al. (2002) found a relationship of fish densities to a hydroperiod index, representing the number of days a wetland is flooded and available for population growth. The landscape scale of this study was not large enough to detect these effects, because only a small range of hydroperiods was considered over the limited spatial domain of the model. By increasing the size of

landscape domain, interactions between hydroperiod and dispersal can be simulated on larger scales.

Many ecosystems worldwide possess some or all of the qualities of pulsed precipitation, cyclical expansion and contraction of area, dynamic hydrology, structural topography engineered by water flows, and inhabitants with life history characteristics that are adapted to these conditions at varying degrees. Critically, the spatial phenomenon of wetland expansion and contraction, a physical energy subsidy, facilitates formation of biological energy pulses, through the interaction of dispersal and population growth across a dynamic landscape. Conservation of these ecosystems and their services requires management of the natural processes of flood pulses to ensure that high concentrations of biomass prey are produced and sustained to support top predators. My methodology provides a simulation platform for making testable spatial and temporal predictions of these processes, leading to a better understanding of flood−pulsed ecosystems and support for management decisions.

Figures

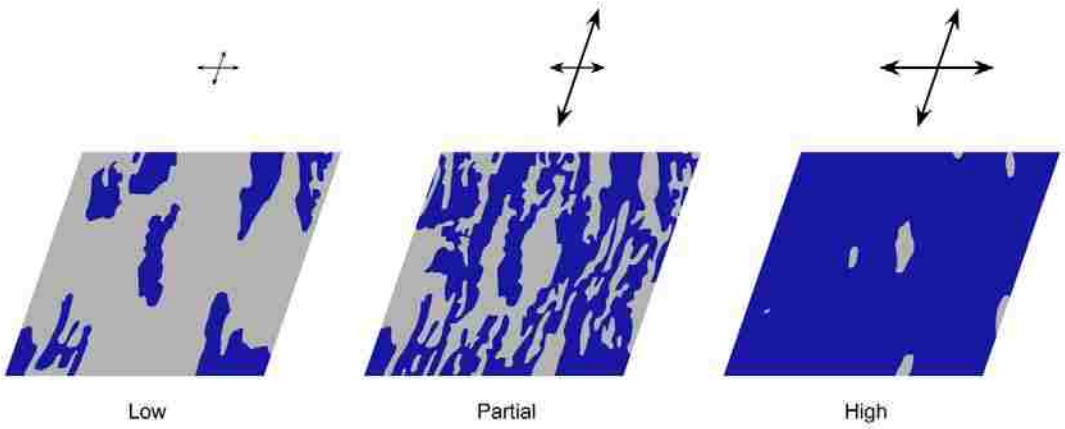

Figure 3.1. Dynamic connectivity of a conceptual, anisotropically−patterned landscape over three phases of flooding (blue): low, partial, and high. Gray indicates dry land. Arrow sizes and widths represent relative levels of connectivity over two example directions.

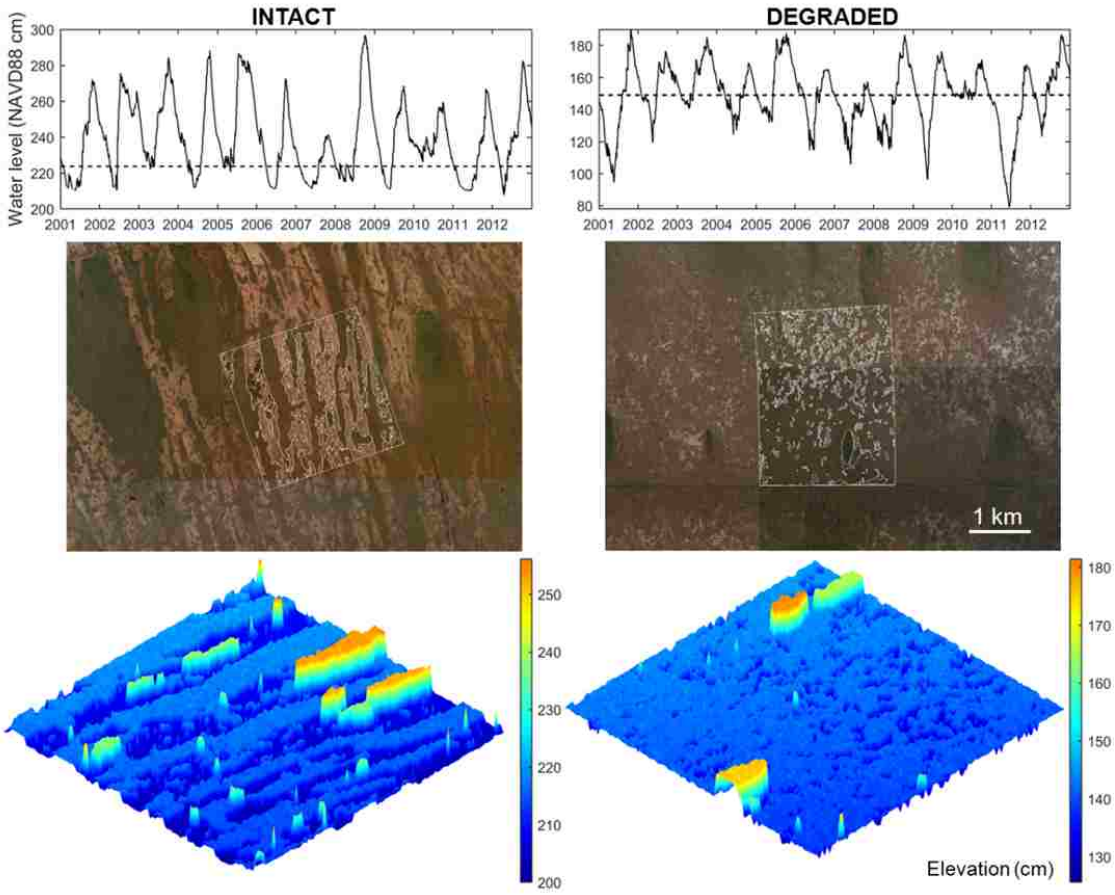

Figure 3.2. Intact (left panels) and degraded (right panels) Everglades RSL used in simulations. Top panels show water stage hydrographs over 12 years for each landscape. Dotted lines indicate maximum sawgrass ridge elevation. Middle panels show shapefiles of study areas (white) on aerial imagery. Bottom panels show the simulated three dimensional topographies. Note: green−yellow−orange features are tree islands.

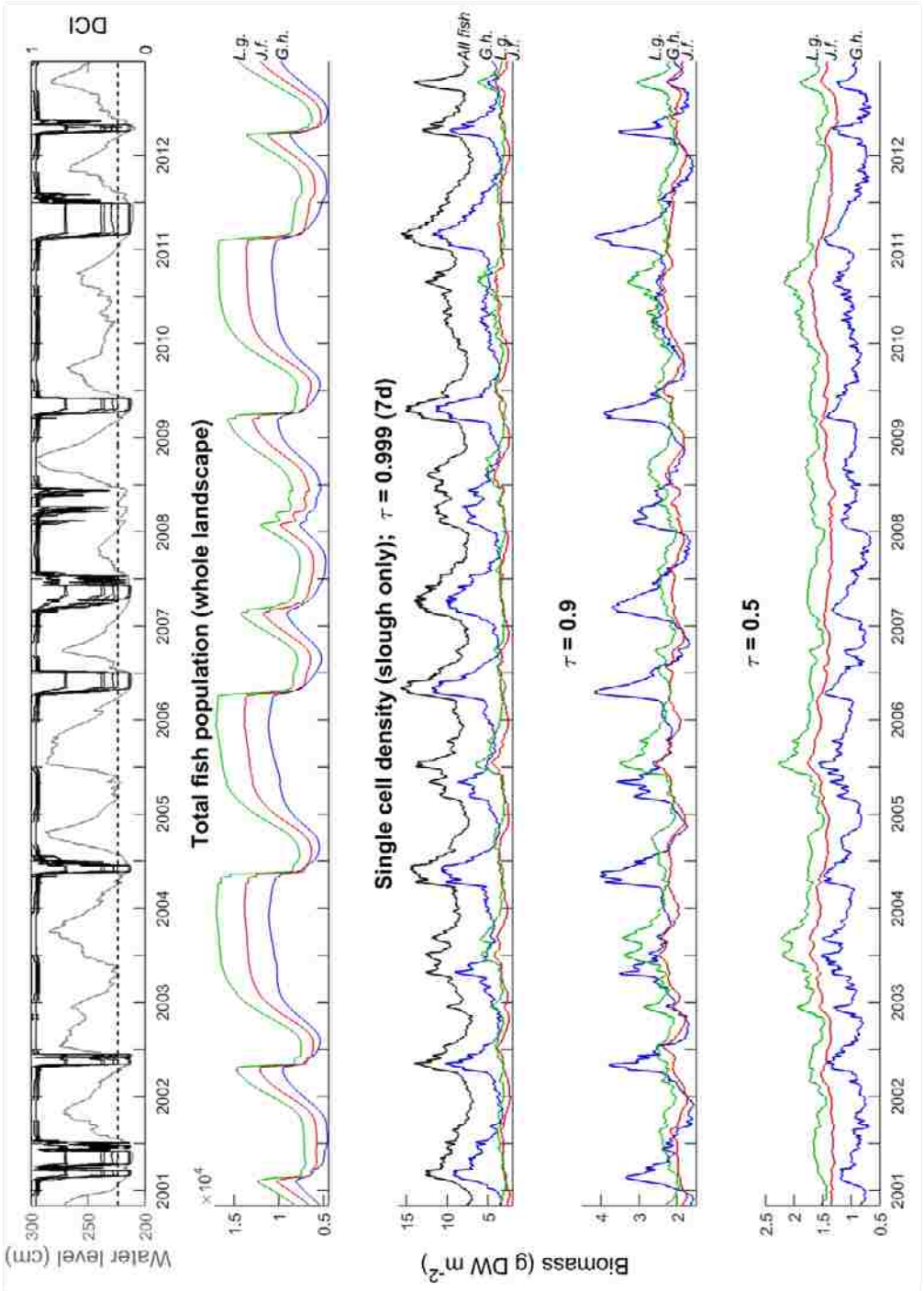

Figure 3.3. (Panel 1) Water level and 8 DCI values over 12−year simulation period. Dotted line indicates maximum sawgrass ridge elevation, referenced to water level. (Panel 2) Total fish biomasses summed over the whole landscape for three fish groups. L.g. = *Lucania goodie*, J.f. = *Jordanella floridae*, and G.h. = *Gambusia holbrooki*. (Panels 3−5) Single cell densities at three quantile levels (τ).

(a)

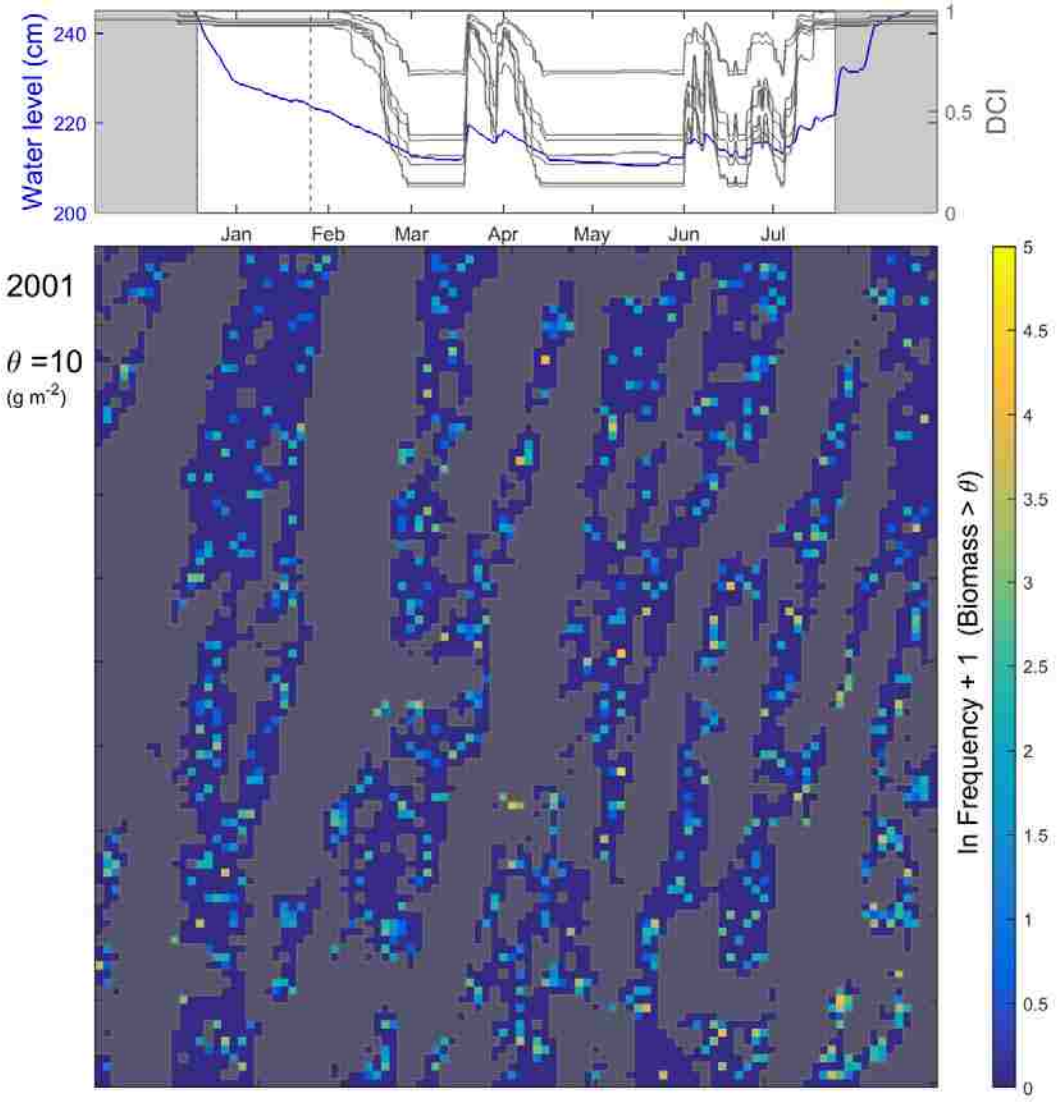

Figure 3.4a,b. Water stage (blue line; top panel) and DCI graphs (gray lines) over 8 compass rose directions, and spatially−explicit map of biomass persistence (bottom panel), for 2001(4a) and 2011(4b), on intact RSL. Biomass persistence was calculated as the frequency during the drying phase that biomass in a slough cell exceeded a defined threshold of 10 g dry wt. m^{-2}.

(b)

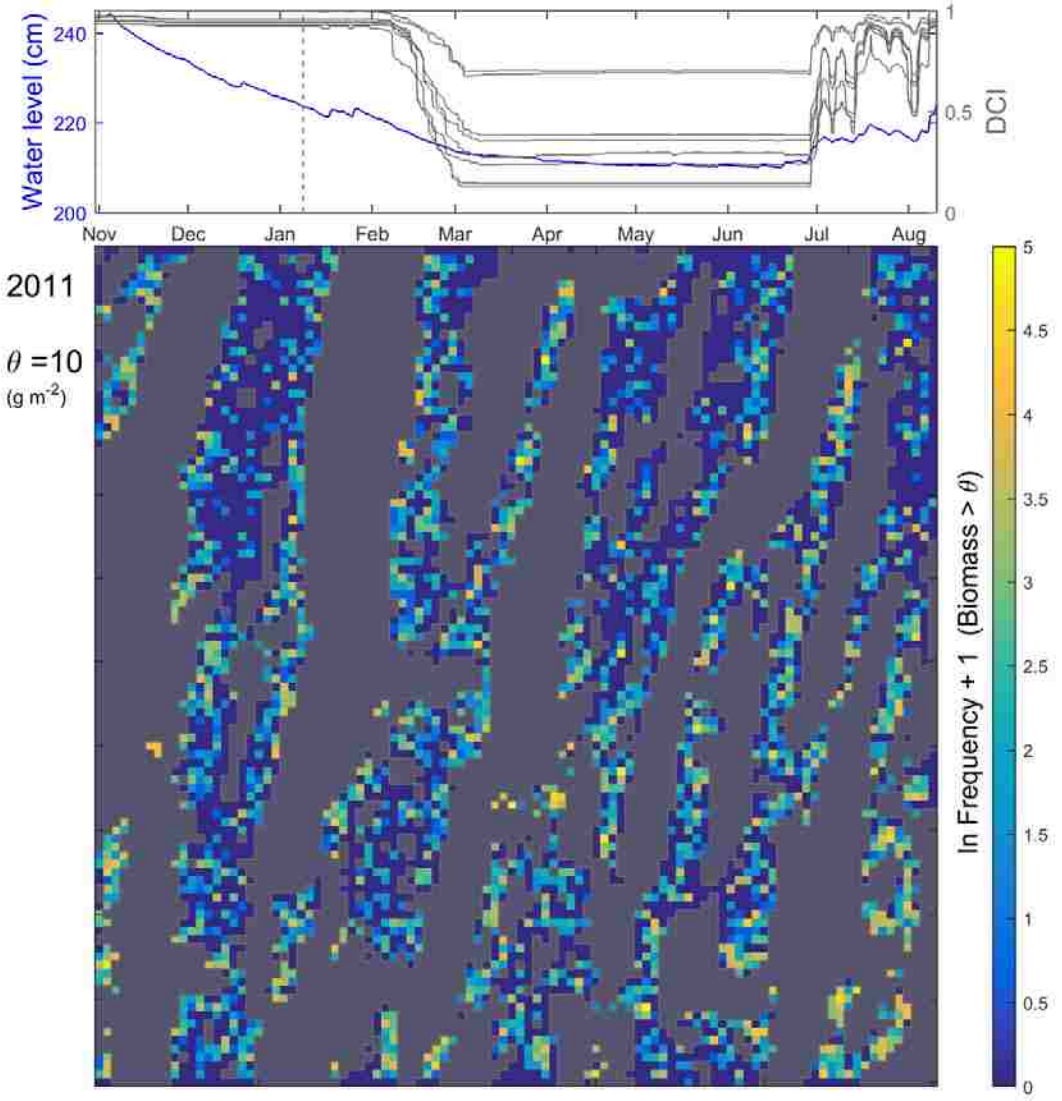
Water level (cm)
240
220
200
1
0.5
0
DCI
Nov
Dec
Jan
Feb
Mar
Apr
May
Jun
Jul
Aug
2011
θ =10
(g m-2)
5
4.5
4
3.5
3
2.5
2
1.5
1
0.5
0
ln Frequency + 1 (Biomass > θ)

Figure 3.4b.

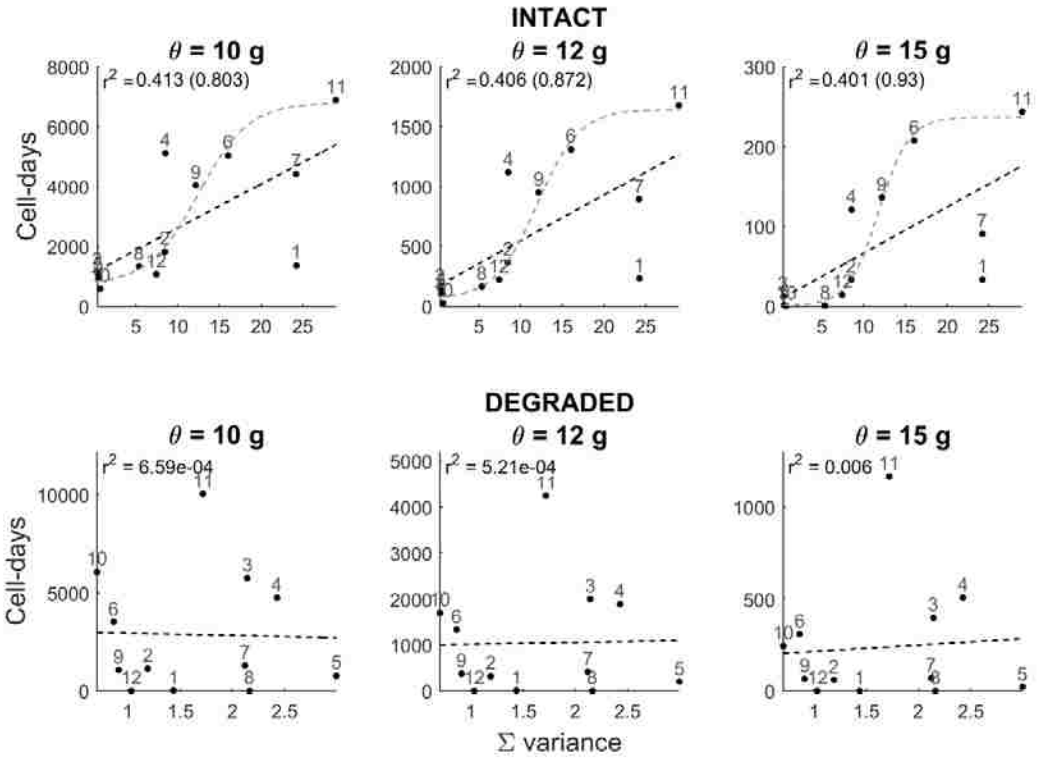

Figure 3.5. Biomass persistence (cell−days) related to summed DCI variance for intact (top) and degraded (bottom) RSL, for three biomass thresholds (left to right panels). DCI variance over eight compass directions was taken at each time step of the drying phase, and summed. Years are indicated by numbers 1−12. Linear model fit (all 12 years), and logistic model fit (2001, 2007 removed) indicated by black and gray dotted lines, respectively, with r−squared values (logistic fit in parentheses).

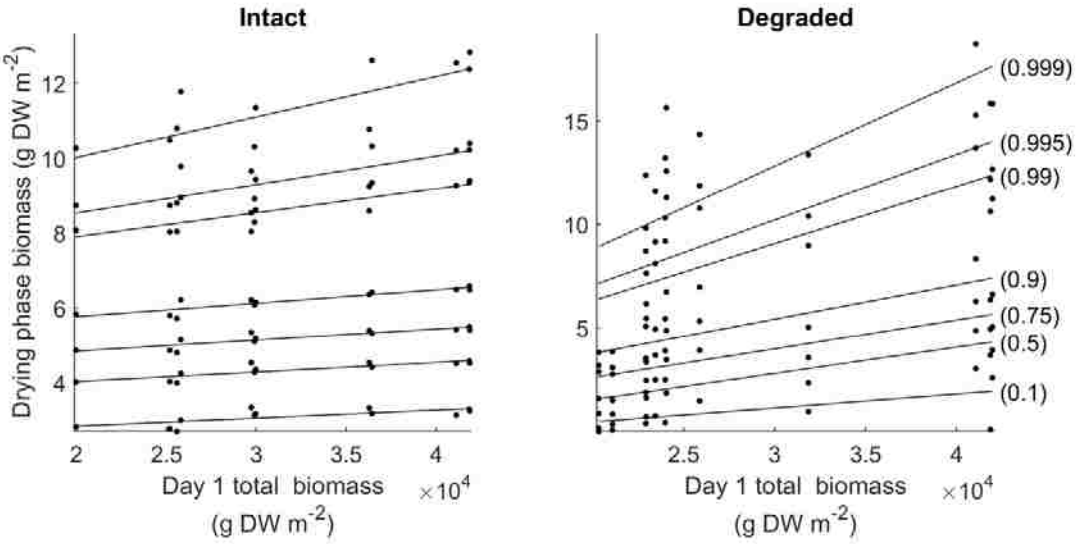

Figure 3.6. Quantiles of fish biomass over the drying phase of each year related to wet season biomass summed on Day 1 of the drying phase, for slough cells only. Quantile levels are indicated in parentheses. Day 1 biomass was taken at one time step, while drying phase quantiles were taken from biomass pooled over the entire drying period.

Supplement 3A.

Table S3A.1. Food web differential equations.

Primary producer (periphyton), *P(t)*

$$\frac{dP(t)}{dt} = Growth_{peri}\left(1-\frac{P(t)}{K_{peri}}\right)P(t) - m_{peri}P(t)$$
$$- Cons_{peri-by-invert}P(t)I(t)$$
$$-\sum_{i=1,3}\left(\frac{Cons_{peri-by-fish,i}P(t)F_i(t)}{1+h_{peri}Cons_{peri-by-fish,i}P(t)+h_{invert}Cons_{invert-by-fish,i}I(t)+w_{fish,i}F_i(t)}\right)$$

Detritus, *D(t)*

$$\frac{dD}{dt} = m_{peri}P(t)+m_{inverti}I(t)+m_{fish1}F_1(t)+m_{fish2}F_2(t)+m_{fish3}F_3(t)$$

$$+(1-\eta_{invert})Cons_{peri-by-invert}P(t)I(t)$$
$$+(1-\eta_{fish})\sum_{i=1,3}\frac{Cons_{peri-by-fish,i}P(t)F_i(t)}{1+h_{peri}Cons_{peri-by-fish,i}P(t)+h_{inver}Cons_{invert-by-fish,i}I(t)+w_{fish,i}F_i(t)}$$
$$+(1-\eta_{fish})\sum_{i=1,3}\frac{Cons_{invert-by-fish,i}I(t)F_i(t)}{1+h_{peri}Cons_{peri-by-fish,i}P(t)+h_{invert}Cons_{inver-by-fish,i}I(t)+w_{fish,i}F_i(t)}$$

$$-Cons_{det\ ritus-by-inverts}D(t)I(t)-decomp_{det\ ritus}D(t)$$

Invertebrates, *I(t)*

$$\frac{dI(t)}{dt} = Cons_{\text{det }ritus-bv-inverts}D(t)I(t)-m_{invert}I(t)$$
$$+\eta_{invert}Cons_{peri-by-inverts}P(t)I(t)$$
$$-\sum_{i=1,3}\left(\frac{Cons_{invert-by-fish,i}I(t)F_i(t)}{1+h_{peri}Cons_{peri-by-fish,i}P(t)+h_{invert}Cons_{invert-by-fish,i}I(t)+w_{fish,i}F_i(t)}\right)$$

Small fish groups, $F_i(t)$ (i = 1,3)

$$\frac{dF_i}{dt} = \eta_{fish} \sum_{i=1,3} \left(\frac{Cons_{peri-by-fish,i} P(t) F_i(t)}{1 + h_{peri} Cons_{peri-by-fish,i} P(t) + h_{invert} Cons_{invert-by-fish,i} I(t) + w_{fish,i} F_i(t)} \right)$$
$$+ \eta_{fish} \sum_{i=1,3} \left(\frac{Cons_{invert-by-fish,i} I(t) F_i(t)}{1 + h_{peri} Cons_{peri-by-fish,i} P(t) + h_{invert} Cons_{invert-by-fish,i} I(t) + w_{fish} F_i(t)} \right) - m_{fish,i} F_i(t)$$

Table S3A.2. Variables of the model

Variable	Units	Definition
P	g dry wt. m^{-2}	Periphyton
D	g dry wt. m^{-2}	Detritus
I	g dry wt. m^{-2}	Invertebrates
F_i (i = 1,3)	g dry wt. m^{-2}	Small fish species populations

Table S3A.3. Parameters used in the Everglades example.

Parameter	Value	Units	Definition
nj	100		# of columns in grid
ni	100		# of rows in grid
delt	0.25	day	time step; fraction of one day
indelt	4	day	# number of time steps per day
nyears	12	years	total number of years in simulation
nsteps	17,532	day	# of time steps in simulation
$Growth_{peri}$	0.15	g g^{-1} day^{-1}	maximum daily rate of growth of periphyton
K_{peri}	110	g m^{-2}	density dependent constant
$decomp_{detritus}$	0.05	day^{-1}	decomposition rate of detritus
$cons_{peri.invert}$	0.001	g g^{-1} day^{-1}	consumption rate of detritus by invertebrates
$cons_{detr.invert}$	0.4	g g^{-1} day^{-1}	consumption rate of detritus by invertebrates
η_{invert}	0.06		Assimilation coefficient for invertebrates
$cons_{peri.fish1}$	0.02	g g^{-1} day^{-1}	rate of consumption of periphyton by fish
$cons_{peri.fish2}$	0.05	g g^{-1} day^{-1}	"
$cons_{peri.fish3}$	0.07	g g^{-1} day^{-1}	"

$cons_{invert.fish1}$	8.2	g g^{-1} day^{-1}	Rate of consumption of invertebrates by fish
$cons_{invert.fish2}$	8.6	g g^{-1} day^{-1}	“
$cons_{invert.fish3}$	9.2	g g^{-1} day^{-1}	“
$h_{peri.fish}$	2.0	day	Time required to consume prey item
$h_{invert.fish}$	2.0	day	“
w_{fish1}	6000		Self−interference coefficient
w_{fish2}	6000		“
w_{fish3}	6000		“
η_{fish}	0.35		Assimilation coefficient for fish
m_{peri}	0.01	day^{-1}	Wet season mortality of periphyton
m_{invert}	0.6	day^{-1}	Wet season mortality of invertebrates
m_{fish1}	0.019	day^{-1}	Wet season mortality of fish
m_{fish2}	0.017	day^{-1}	“
m_{fish3}	0.015	day^{-1}	“
$m_{peri.dry}$	0.03	day^{-1}	Dry season mortality of periphyton (post drydown)
$m_{invert.dry}$	0.005	day^{-1}	Dry season mortality of invertebrates
$m_{fish1.dry}$	0.002	day^{-1}	Dry season mortality of fish
$m_{fish2.dry}$	0.002	day^{-1}	“
$m_{fish3.dry}$	0.002	day^{-1}	“
$frac.enter_{peri}$	0		Fraction moving into flooding neighbor cell
$frac.enter_{invert}$	0.1		“
$frac.enter_{fish1}$	0.6		“
$frac.enter_{fish2}$	0.35		“
$frac.enter_{fish3}$	0.2		“
$frac.leave_{peri}$	0		Fraction moving from drying cell
$frac.leave_{invert}$	0		“

$frac.leave_{fish1}$	0.9	“
$frac.leave_{fish2}$	0.2	“
$frac.leave_{fish3}$	0.2	“
$frac.surv_{peri}$	0.2	Fraction of periphyton surviving in dried cell
$frac.surv_{invert}$	0.8	Fraction of invertebrates surviving in dried cell
$frac.surv_{fish1}$	0.12	Fraction of fish surviving in dried cell
$frac.surv_{fish2}$	0.12	“
$frac.surv_{fish3}$	0.12	“

Supplement 3B. Everglades supporting documentation

Figure S3B.1. Everglades ridge−and−slough landscape (RSL). Photo by Bryan Botson.

Model topography and hydrographs for Everglades simulations

Two landscape topographies representing intact and degraded RSL were simulated from detailed maps created by the South Florida Water Management District (Watts et al. 2010). Figure 3.2 shows aerial imagery and the digitized topographies. Elevation data from the Everglades Depth Estimation Network (EDEN) Digital Elevation Model (DEM) (Liu et al. 2009), georeferenced shapefiles of vegetation communities, and empirical measurements of water depth differentials for each vegetation type (Givnish et al. 2008) were used to create the topographies. Landscapes were spatially−explicit on grids of 100 × 100 cells, with each cell 20 × 20 m. This scale was selected to capture the topography of the ridges (~20−100 m wide). Elevation pitch and RSL differentials were standardized for both landscapes, and random roughness was applied to elevations (mean = 0; S.D. = 1 cm).

Everglades fishes adapted for simulation

Fish "functional types" have been described and modeled for the Everglades (Gaff et al. 2000). Life histories for the three fish used in these simulations were developed from numerous empirical studies conducted over the past 40 years that have quantified relationships between fish density, community structure, and different spatiotemporal habitat metrics such as hydroperiod, drought frequency, wetland flooding, and benthic cover. (Goss et al. 2014, Hoch et al. 2015, Loftus & Kushlan 1987, Loftus & Eklund 1994, Obaza et al. 2011, Ruetz et al. 2005, Trexler et al. 2002).

Rules for fish movement were updated to reflect new information reported in recent empirical work by Goss et al. (2014), and Hoch et al. (2015). These studies quantified encounter rates (see Obaza et al. 2011) and throw trap densities of small fishes in long and short−hydroperiod marshes during the flooding and drying phase of the short−hydroperiod wetlands. Pulses of fish movement were found that varied in encounter rate between species, between long and short−hydroperiod marshes, and between periods of rising and falling water levels, suggesting species−specific differences in habitat selection and dispersal rate into ephemeral wetlands. The immigration patterns (Goss et al. 2014) and behavioral patterns (Hoch et al. 2015) timed with changing hydrologic conditions were used to support the assumptions and rules for fish movement in these simulations.

(a)

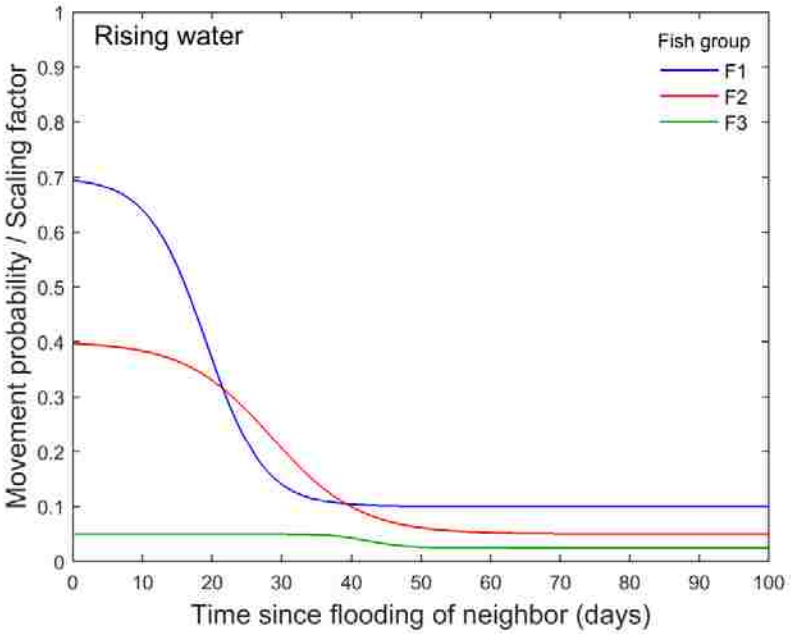
Rising water
Fish group
F1
F2
F3
Movement probability / Scaling factor
Time since flooding of neighbor (days)

(b)

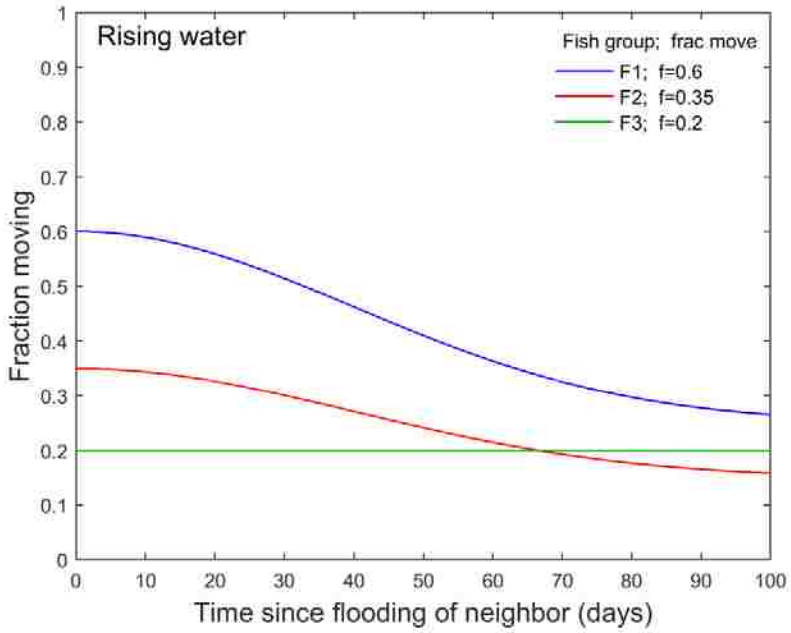
Rising water
Fish group; frac move
F1; f=0.6
F2; f=0.35
F3; f=0.2
Fraction moving
Time since flooding of neighbor (days)

(c)

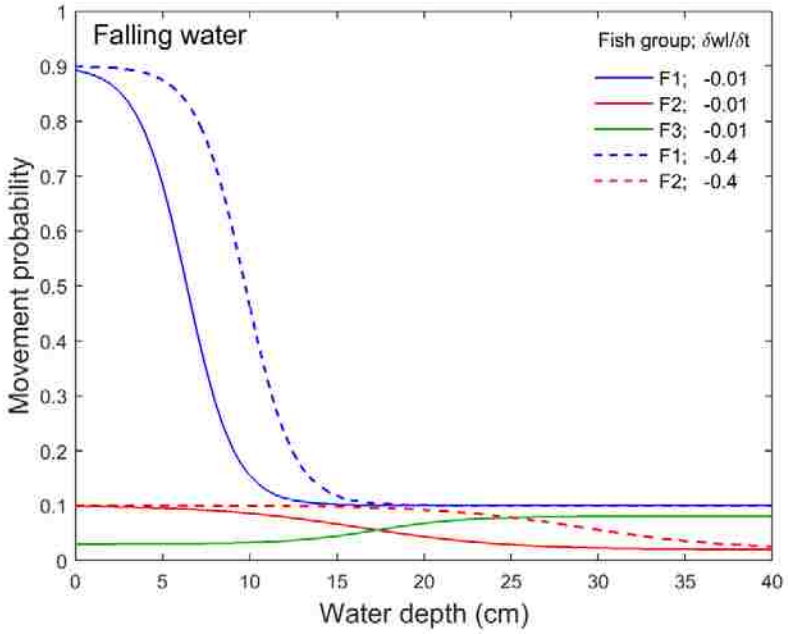

(d)

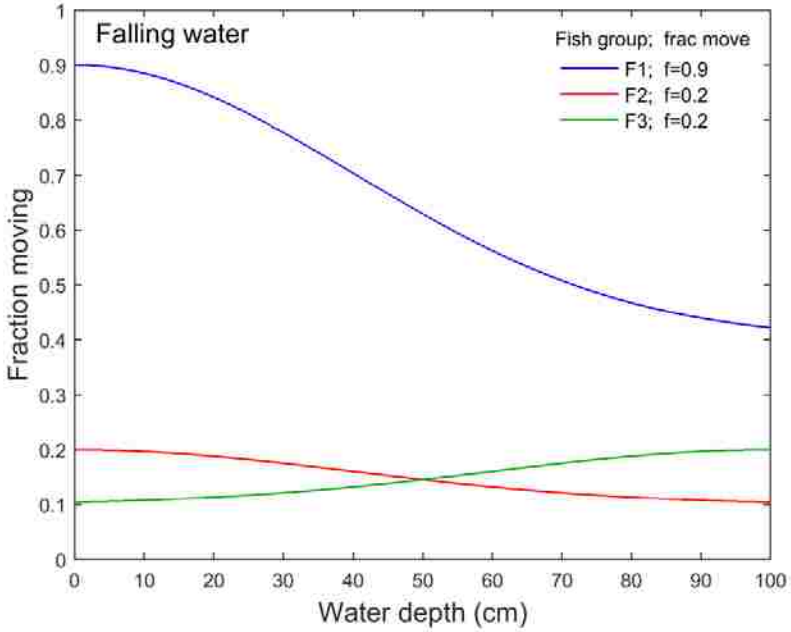

Figure S3B.2. Scaling functions of FDAL relating fish biomass movement to landscape environmental conditions for the flooding phases (panels a,b) and drying phase (panels c,d). Probability (panel a) and fraction (panel b) of biomass moving between cells is a function of the time since flooding of neighbor cells during the flood phase. Biomass is

scaled and split between neighbor cells with curves in panel *a*. During the drying phase, probability and fraction of movement are functions of water depth. Probability is additionally scaled by water level recession rate, for example, dotted line indicates faster recession (c).

Supplement 3C. Comparison of water level, DCI, and numbers of flooded cells.

The graphs of DCI and flooded area related to water level (Figure S3C.1a−c), had similar slopes, as water stage increased from the lowest part of the marsh (Intact = 200 cm, Degraded = 125.5 cm) to that of the highest sawgrass ridge (Intact = 223.7 cm, Degraded = 149 cm), above which they were asymptotic. However, the curves diverged in the intervening middle range of marsh elevations. Flooded area showed brief asymptotes for rising water stage for both intact and degraded, but the shift for degraded was much lower on the water stage axis than for intact, since it had fewer total slough cells (Figure S3C.1a). DCI for intact had a broader range of values across directions (0−315°) in the middle of the curve than degraded (Figure S3C.1b,c). For example, between water levels of 205 and 215 cm, intact maintained a diversity of DCI values (0.2−0.7) (Figure S3C.1b), while those for degraded, from 140 to 145cm, did not differ greatly from each other, and had steeper slopes (Figure S3C.1c). The primary difference between intact and degraded was that DCI for degraded declined sharply to near zero over all directions, while on intact, some of the directions maintained high levels as others fell. Also, some DCI levels fluctuated in a sawtooth pattern. Thus, DCI and flooded area were both correlated with water stage, but in qualitatively different ways. DCI and flooded habitat were also correlated with each other (Figure S3C.1d,e), but their relationship was nonlinear throughout most of the intermediate water levels for both landscapes.

Table S3C.1. Start dates and number of days within the drying phase for each simulated year (2001−2012) in the intact and degraded RSL. Note: Periods with Oct, Nov, or Dec start dates began in the previous calendar year.

	INTACT		DEGRADED	
Year	**Day 1**	**# days**	**Day 1**	**# days**
2001	Dec 18	215.5	Nov 30	84
2002	Jan 24	140.75	Nov 30	202.75
2003	Jan 24	119	Oct 6	232.25
2004	Jan 7	203	Nov 28	281.25
2005	Dec 17	163.75	Oct 25	225.5
2006	Jan 9	184	Dec 3	153.5
2007	Nov 18	253.5	Nov 3	170.25
2008	Oct 27	238	Nov 1	266.25
2009	Jan 12	152.75	Nov 18	140.5
2010	Nov 10	234.25	Oct 10	297.25
2011	Oct 30	283.5	Oct 5	163
2012	Jan 4	138.25	Nov 23	181.25

(a)

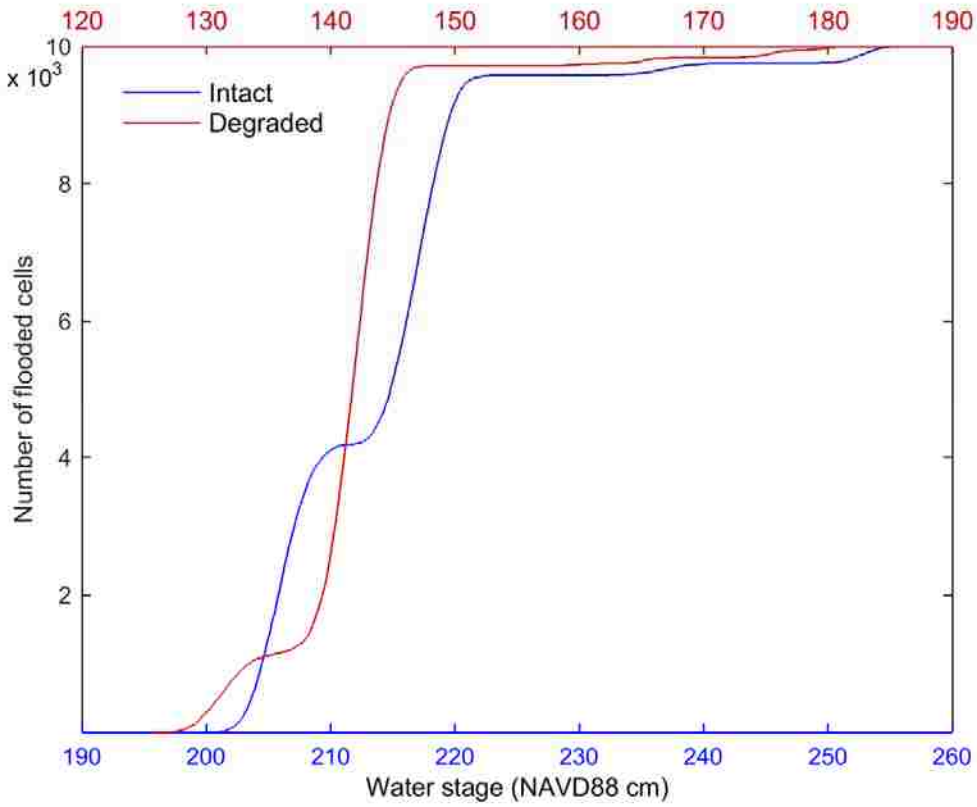

Figure S3C.1. (a) Number of flooded slough cells for each water level (cm), rising from low to high. Water stage is referenced to the North American Vertical Datum of 1988 (NAVD88) in centimeters. (b,c) Profile of directional connectivity index (DCI) over the range of water stages for the intact and degraded landscapes. DCI was calculated for the 8 compass rose directions (0, 45, 90, 135, 180, 225, 270, 315 degrees). (d,e) Profile of directional connectivity index (DCI) as landscape floods from dry (low number of flooded cells) to wet (high number of flooded cells) for each simulated topography, intact and degraded. The horizontal axis sorts cells from low to high elevation. DCI was also calculated over 8 directions here.

(b)

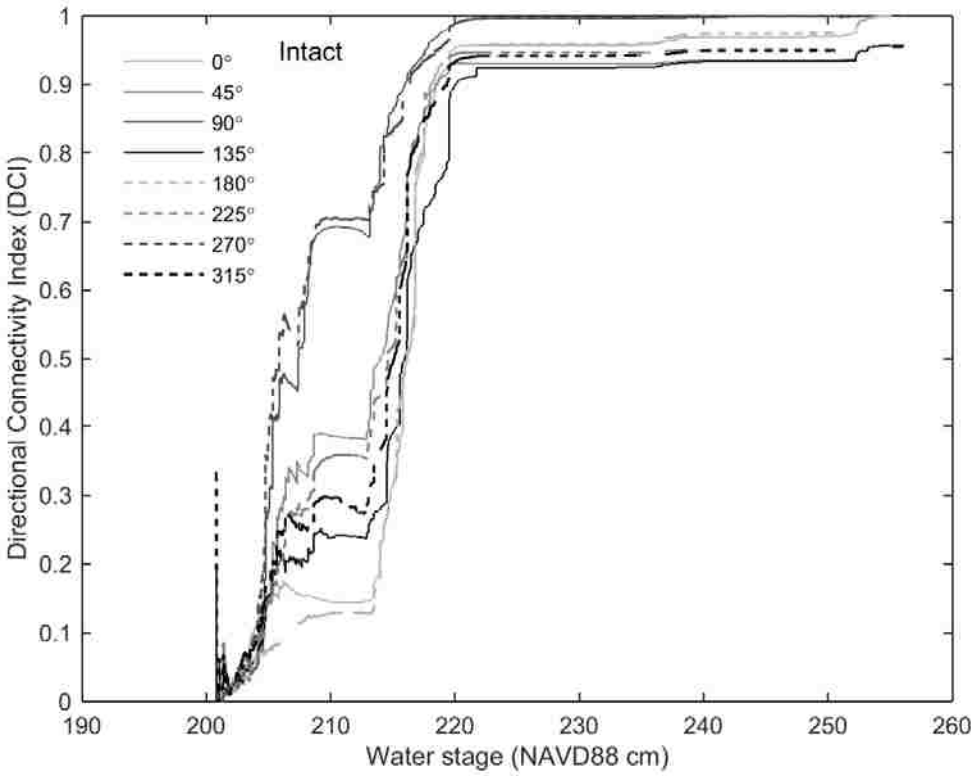
Intact
0°
45°
90°
135°
180°
225°
270°
315°
Directional Connectivity Index (DCI)
Water stage (NAVD88 cm)
0
0.1
0.2
0.3
0.4
0.5
0.6
0.7
0.8
0.9
1
190
200
210
220
230
240
250
260

(c)

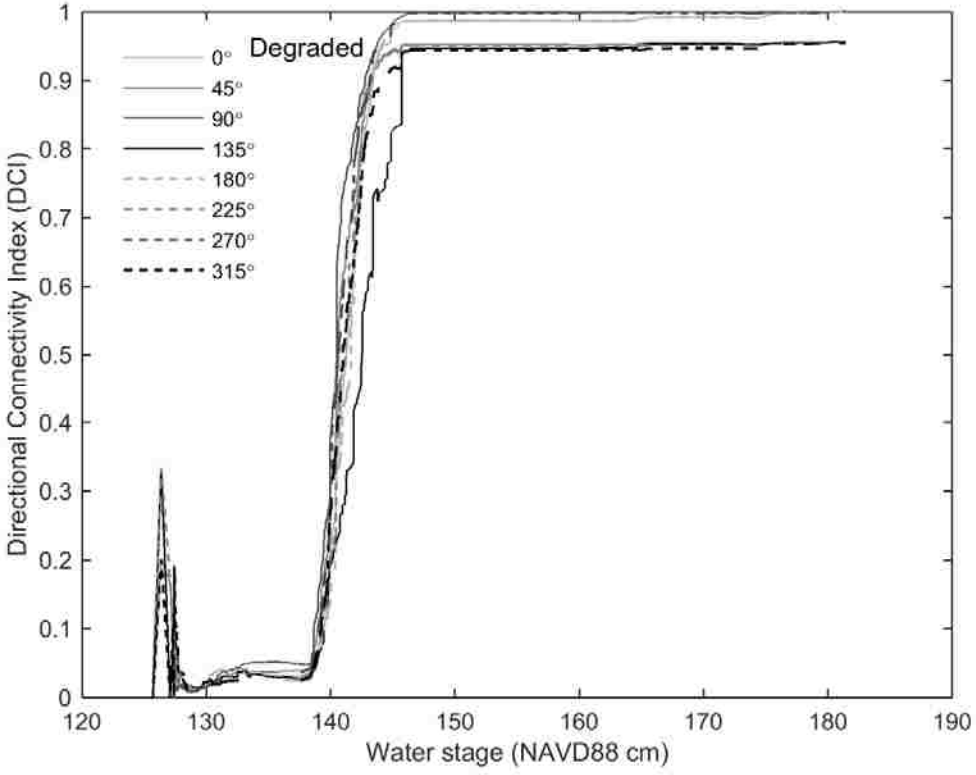
Degraded
0°
45°
90°
135°
180°
225°
270°
315°
Directional Connectivity Index (DCI)
Water stage (NAVD88 cm)
0
0.1
0.2
0.3
0.4
0.5
0.6
0.7
0.8
0.9
1
120
130
140
150
160
170
180
190

(d)

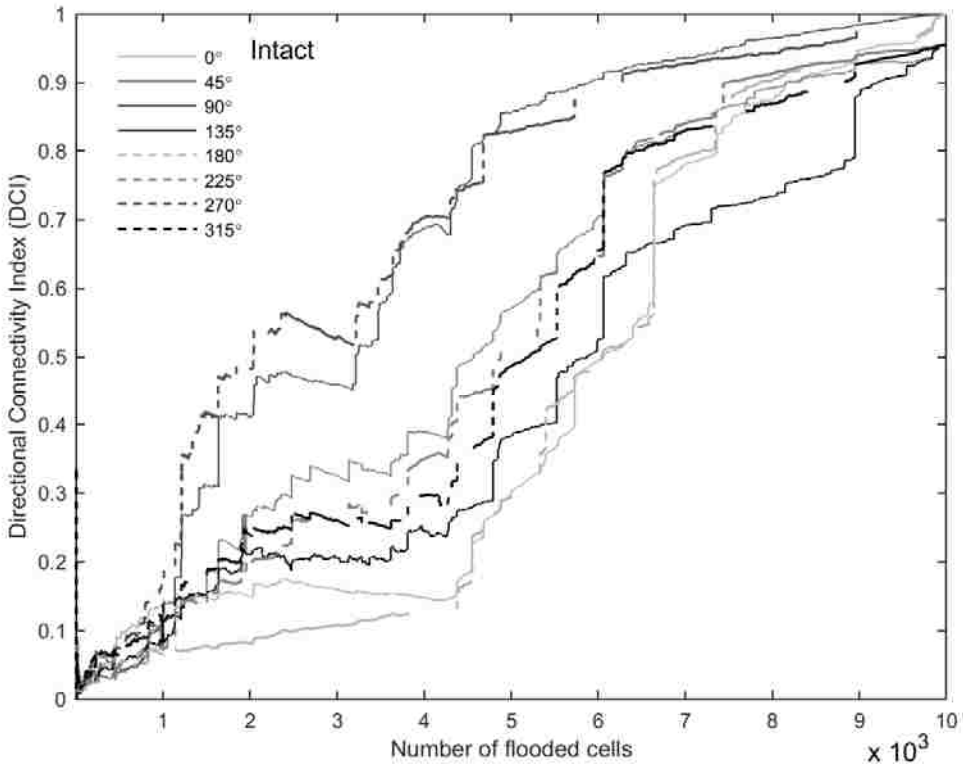
Intact
0°
45°
90°
135°
180°
225°
270°
315°
Directional Connectivity Index (DCI)
Number of flooded cells
x 10^3

(e)

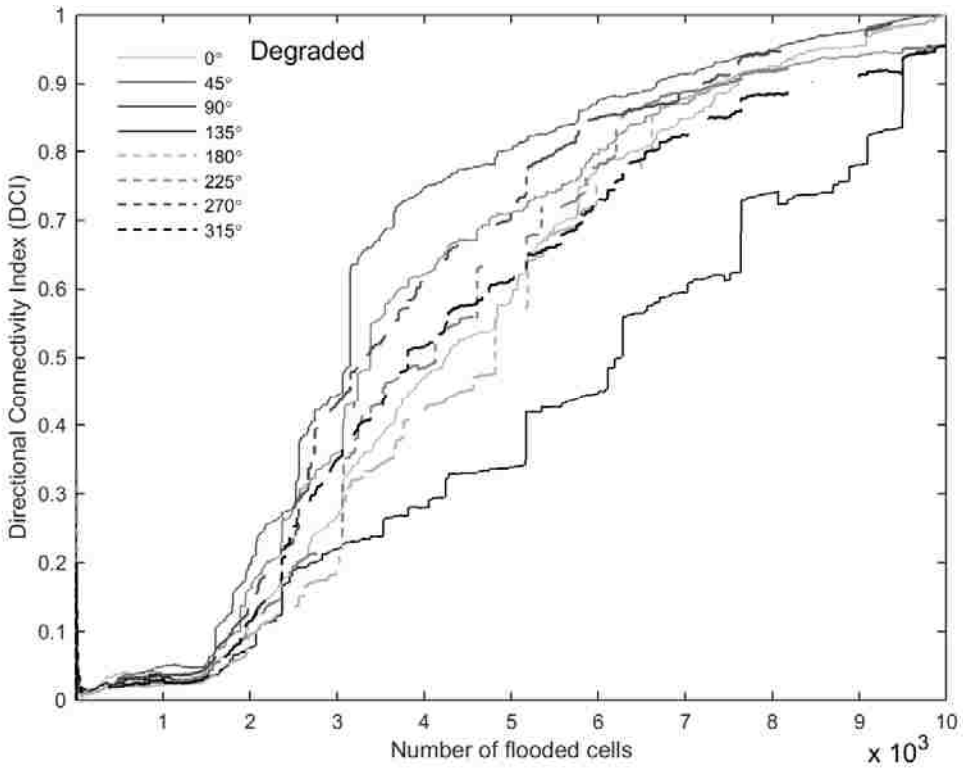
Degraded
0°
45°
90°
135°
180°
225°
270°
315°
Directional Connectivity Index (DCI)
Number of flooded cells
x 10^3

Supplement 3D. Wet season biomass at start of dry season.

Table S3D.1. Total fish biomass (g × 10^4 dry wt. m^{-2}) on the starting day of the drying phase for each year and landscape. Biomass was summed across the three fish groups. 'All cells' represents all living fish on the entire landscape, while 'Slough' represents only fish that were alive in slough cells. Mean (μ) ± Standard Error (S.E.) of biomass are summarized in the last line.

	INTACT		**DEGRADED**	
Year	**All cells**	**Slough**	**All cells**	**Slough (g×10^4 dry wt. m^{-2})**
2001	2.519	1.565	2.294	0.284
2002	2.998	1.667	2.292	0.284
2003	3.629	1.833	2.405	0.300
2004	4.184	1.903	4.187	0.505
2005	2.990	1.633	2.344	0.290
2006	4.186	1.885	4.197	0.519
2007	2.582	1.631	2.399	0.298
2008	1.998	1.679	2.033	0.253
2009	3.644	1.745	3.185	0.387
2010	2.973	1.688	2.589	0.321
2011	4.111	1.982	4.105	0.498
2012	2.559	1.558	2.110	0.262
μ(±S.E.)	3.198 (±0.21)	1.731 (±0.04)	2.845 (±0.24)	0.350 (±0.03)

Supplement 3E. Video of representative model output of fish channeling in the sloughs.

INTACT

<http://zorki.bio.miami.edu/~syurek/RSL_2016/Drying_Intact_2002.gif>>

DEGRADED

<http://zorki.bio.miami.edu/~syurek/RSL_2016/Drying_Degraded_2002.gif>

Figure S3E. Video (GIF format) of movement pulse formation.

These Graphics Information Format (GIF) animations show an overhead view of model output for Fish 1 over select wetland drying periods for intact (~140 days), and degraded (~200 days), as the landscape is drying from the northwest corner to the southeast. The top panel shows water level and DCI values (over 8 windrose directions) over this interval. For intact, receding water level results in complete drying of all of the sawgrass ridges on the landscape, and drying of the western−most slough. For degraded, water level falls completely below the sloughs and dries out the landscape completely. Note: these examples reflect only one year of simulation, and are not intended to reflect differences between landscapes.

For intact, as the ridges dry in the northwest corner (steps 250−400), fish move off of them into the sloughs, and aggregate along the ridge−slough edge. Since each slough is bordered by two ridges, there is a convergence of fish movement into the slough, from either side (steps 300−350). The RSL landscape is pitched in elevation from the NW to SE, and thus the sloughs run downhill from N to S, leading the fish in that direction. This

combination of perpendicular, convergent movement into the slough from the ridges, and longitudinal movement parallel to the slough, results in a slow accumulation of a concentrated pulse of moving biomass (steps 350−450). This pulse is further concentrated as it passes through a bottleneck of sawgrass ridges halfway down the slough (steps 450−500). In this way, the spatial structure of the landscape channels fish as they respond behaviorally to changes in hydrology. This visualization confirms the above application of DCI for quantifying a landscape's ability to concentrate fish.

For degraded, concentration occurs in isolated patches (steps 300−550), when the water level first begins to recede. Then, as DCI rapidly falls from 1 (highly connected) to near 0 (low connectivity), fish become quickly concentrated in the same patches, but can not move any further throughout the landscape (steps 550−575). In the center of the landscape, fish can be seen circulating within larger patches, but routes are not available for them to exit the patch and continue moving along the landscape. Following the shift in DCI, the landscape then dries out completely, and most of the fish die, with some remnant population left in the patchy sloughs.

Supplement 3F.

Figure S3F.1−12. Surface plots of the 500 largest biomass values, sorted at each time step (bottom panel), and corresponding time series of water level (red) and DCI over 8 compass rose directions (black) (top panel). Intact RSL had 4,181 total slough cells while degraded had 1,251 cells. Ranks are in order from lowest to highest (for example, intact, the highest biomass of intact is ranked 4,181). Gray dotted line (top panel) indicates maximum elevation of sawgrass ridges for each landscape. Time axes for each figure are scaled to the length of the drying phase, and vary in length by year.

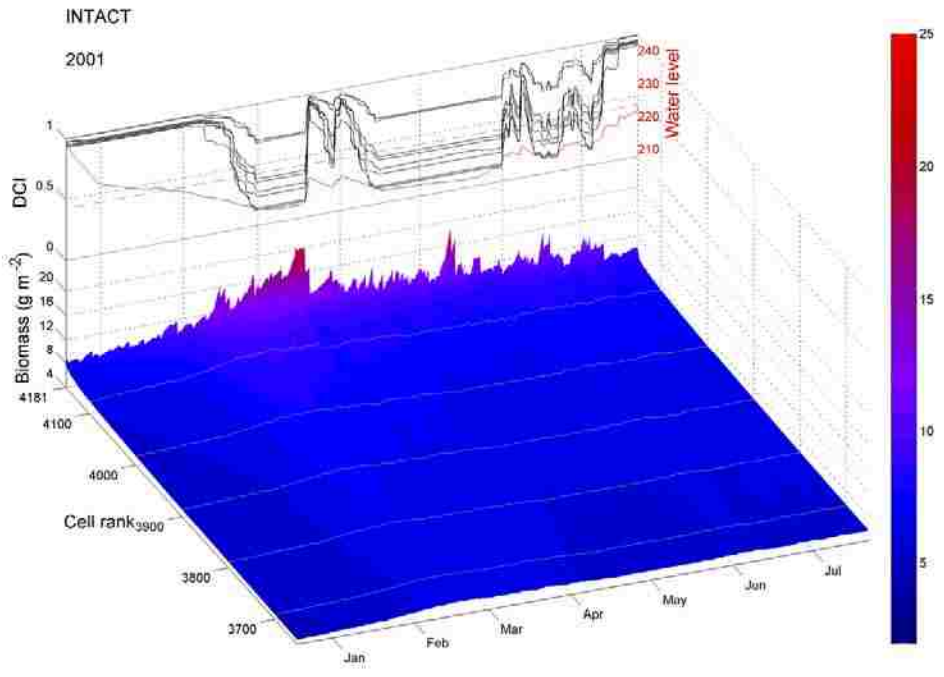

Figure S3F.1A.

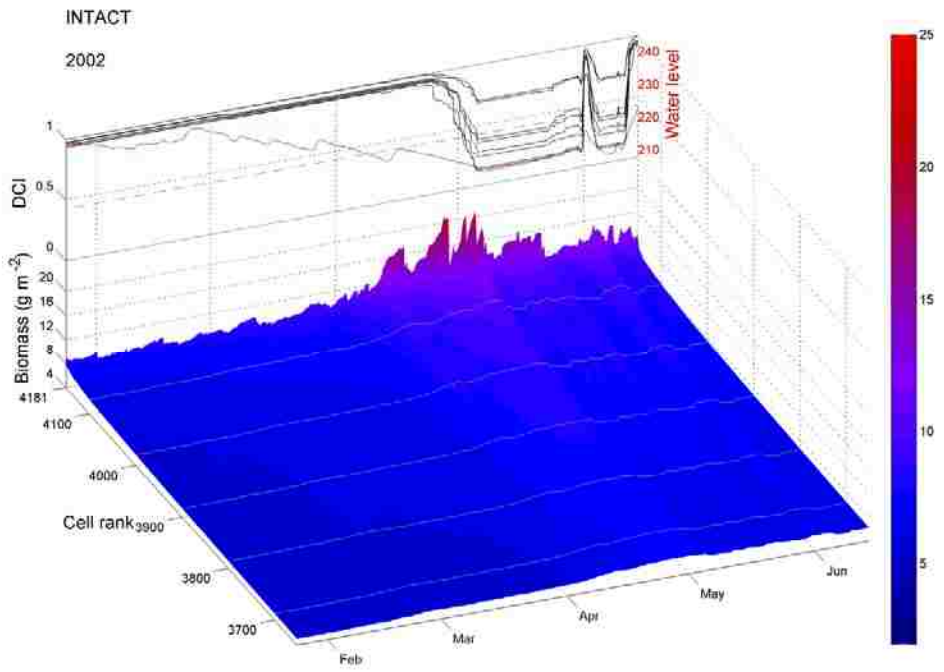

Figure S3F.2A.

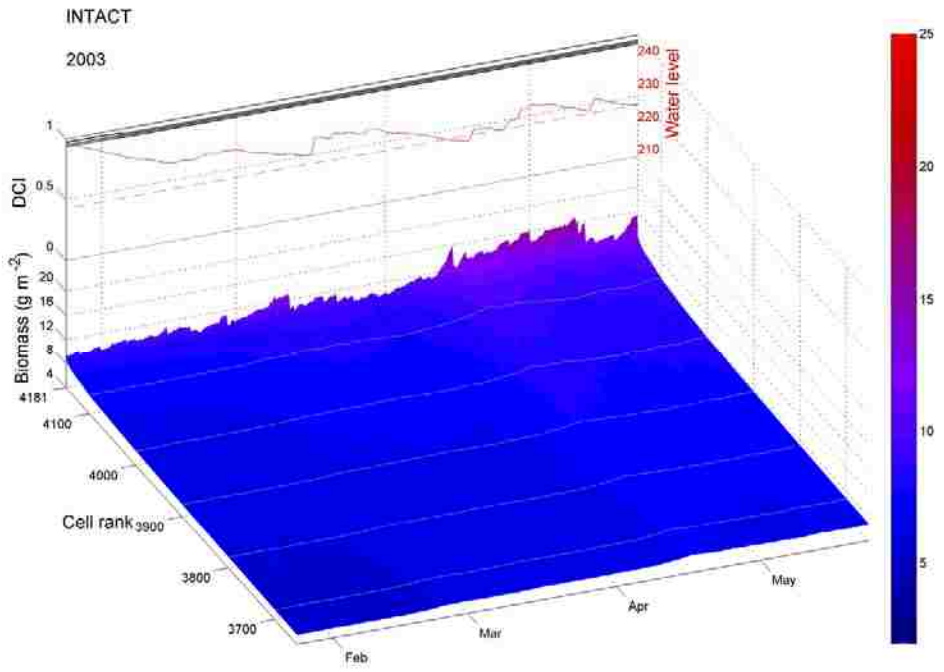

Figure S3F.3A.

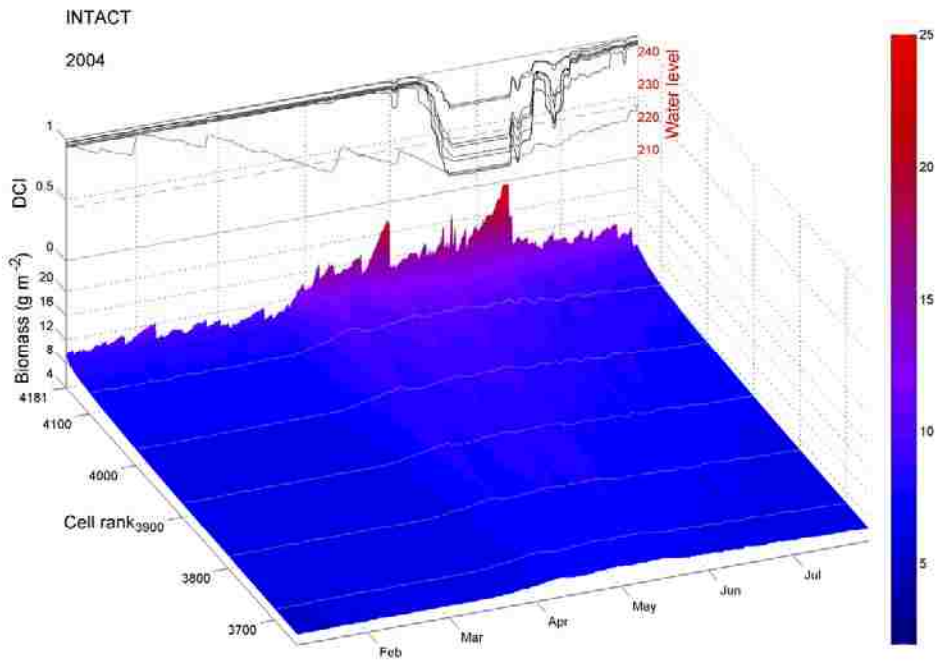

Figure S3F.4A.

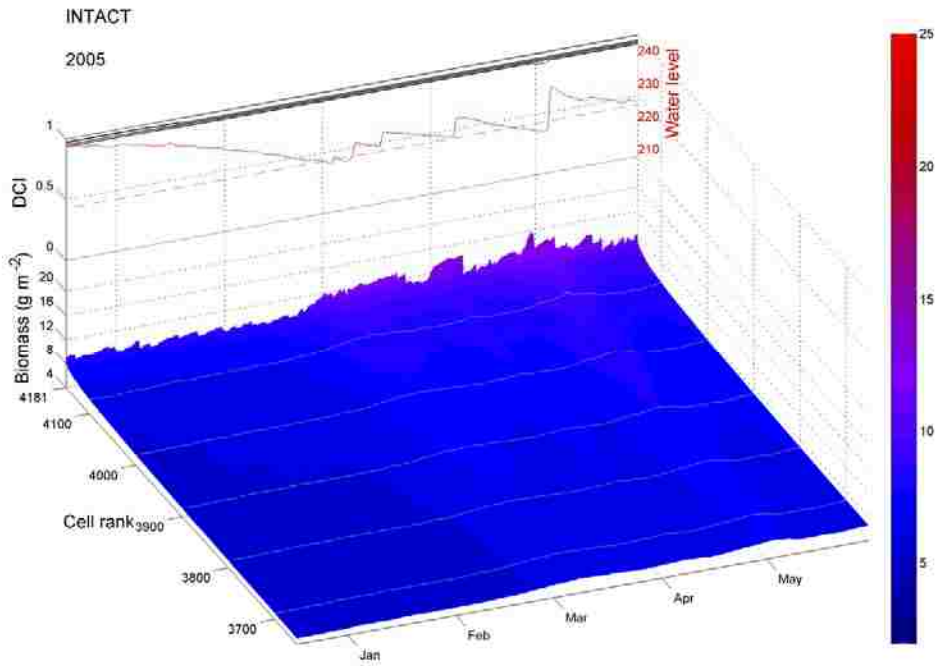

Figure S3F.5A.

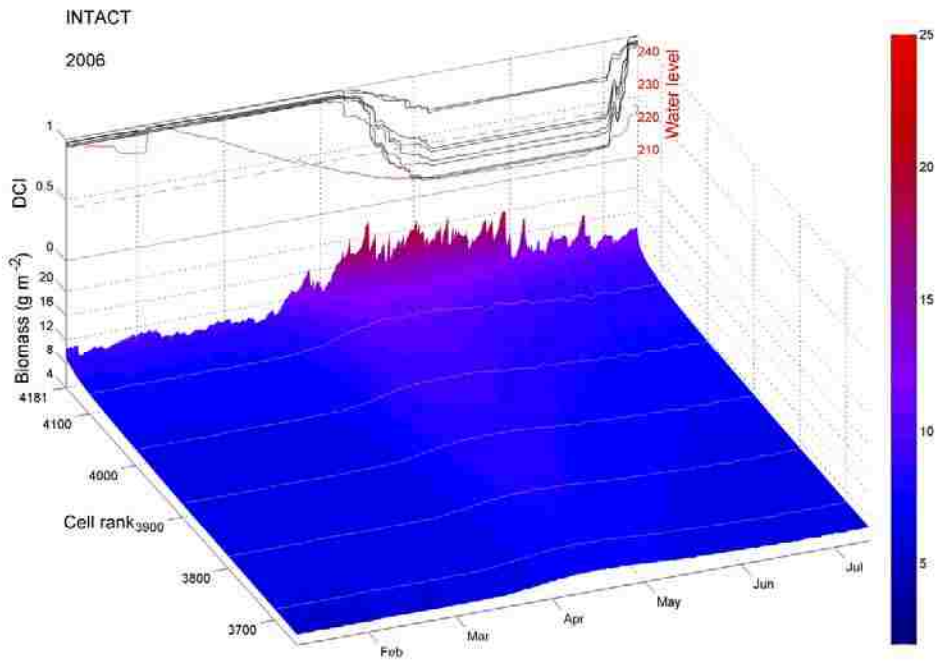

Figure S3F.6A.

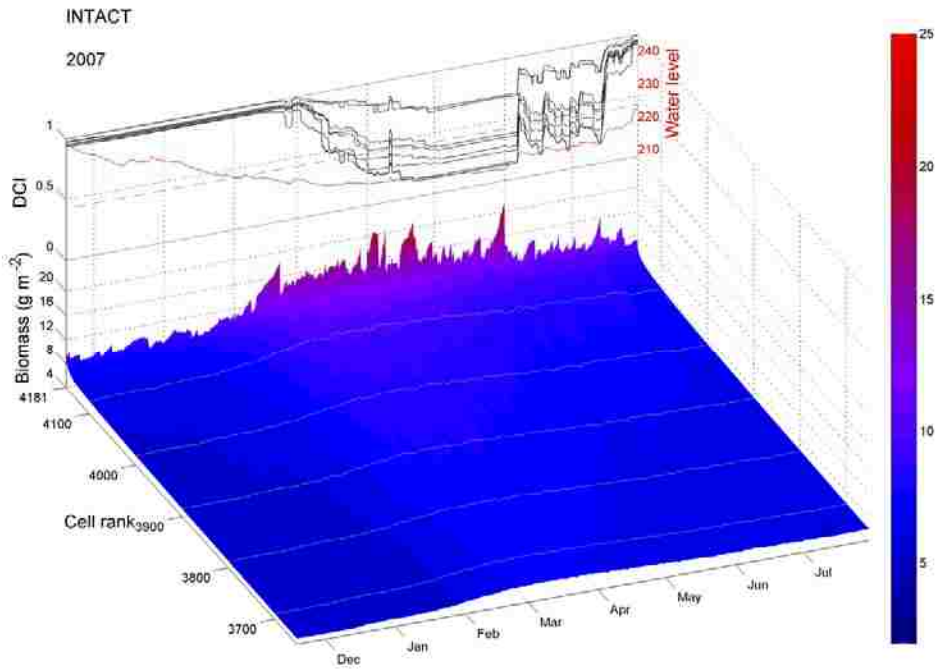

Figure S3F.7A.

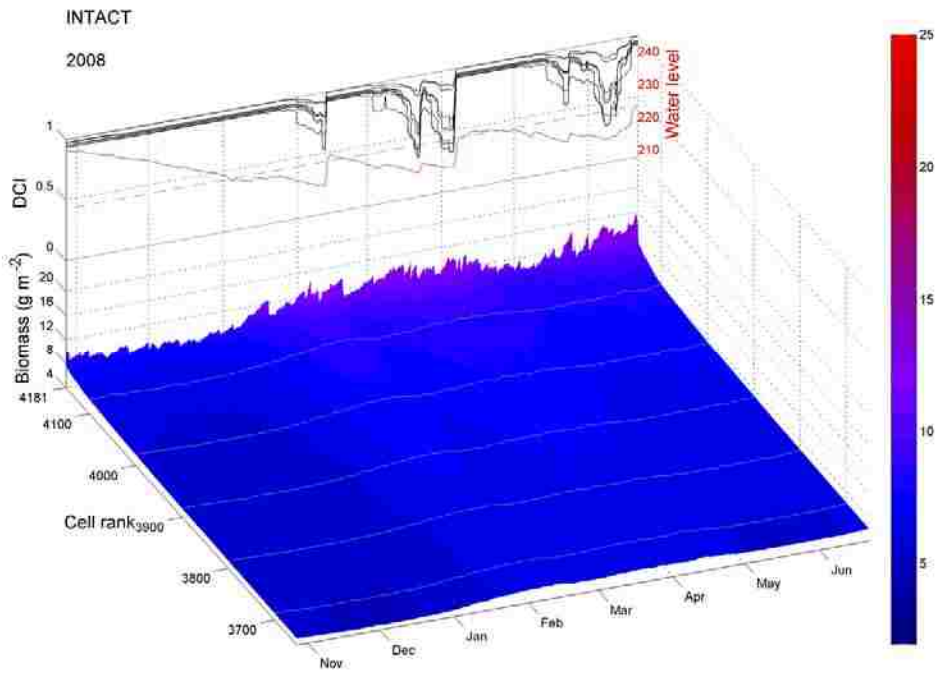

Figure S3F.8A.

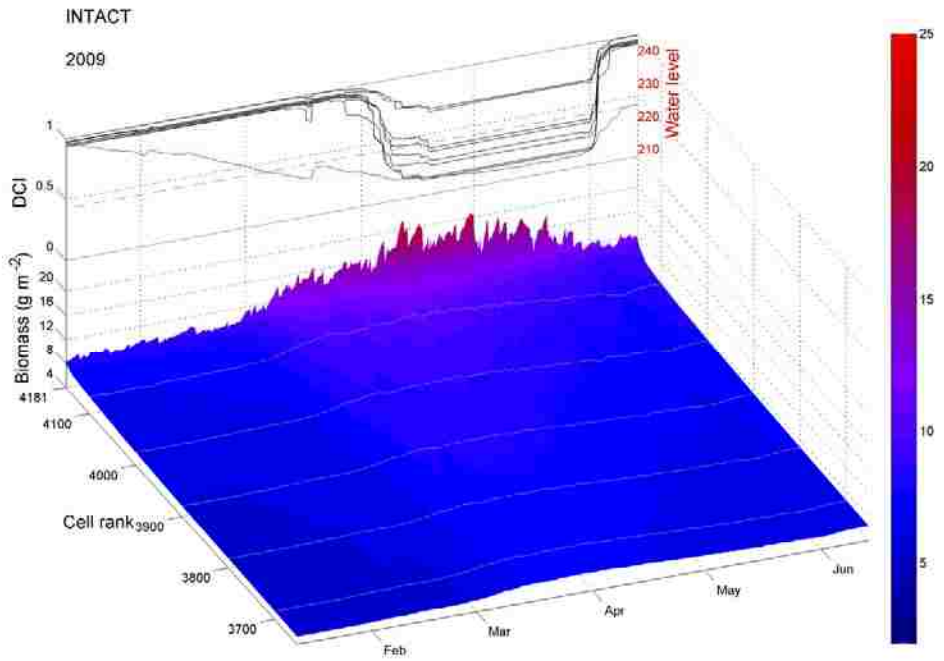

Figure S3F.9A.

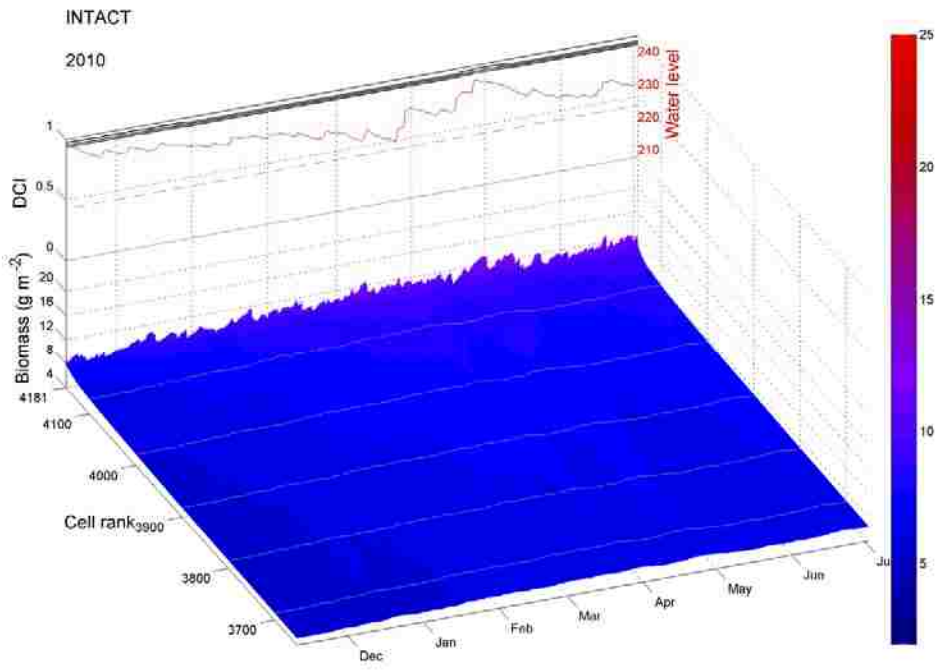

Figure S3F.10A.

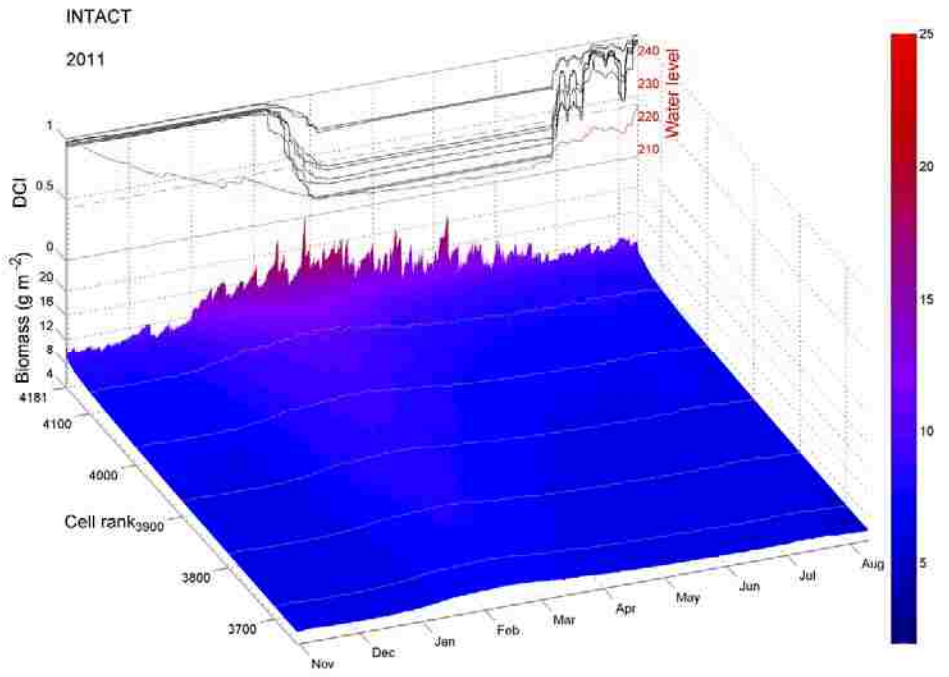

Figure S3F.11A.

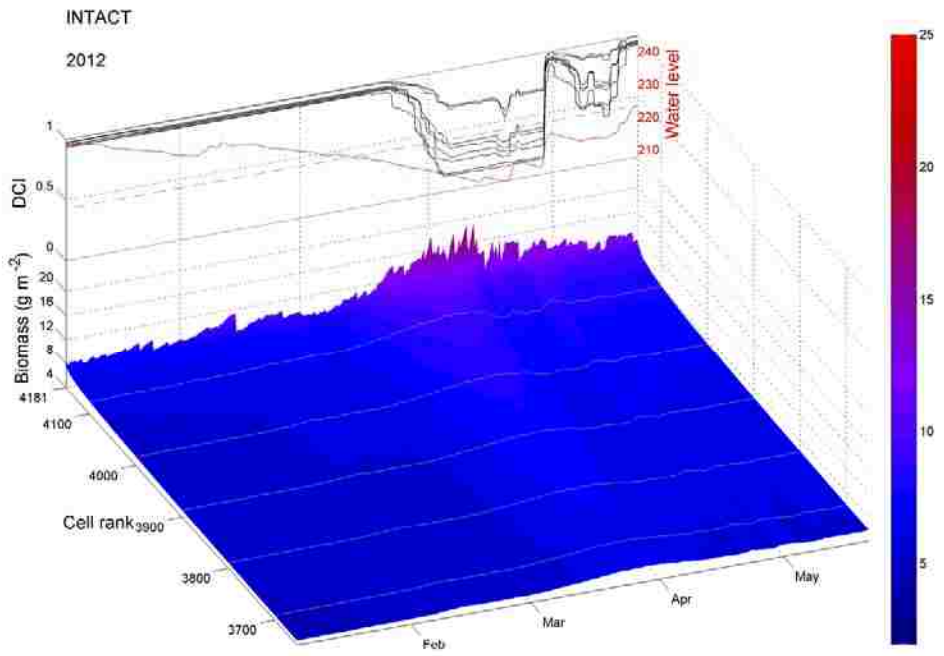

Figure S3F.12A.

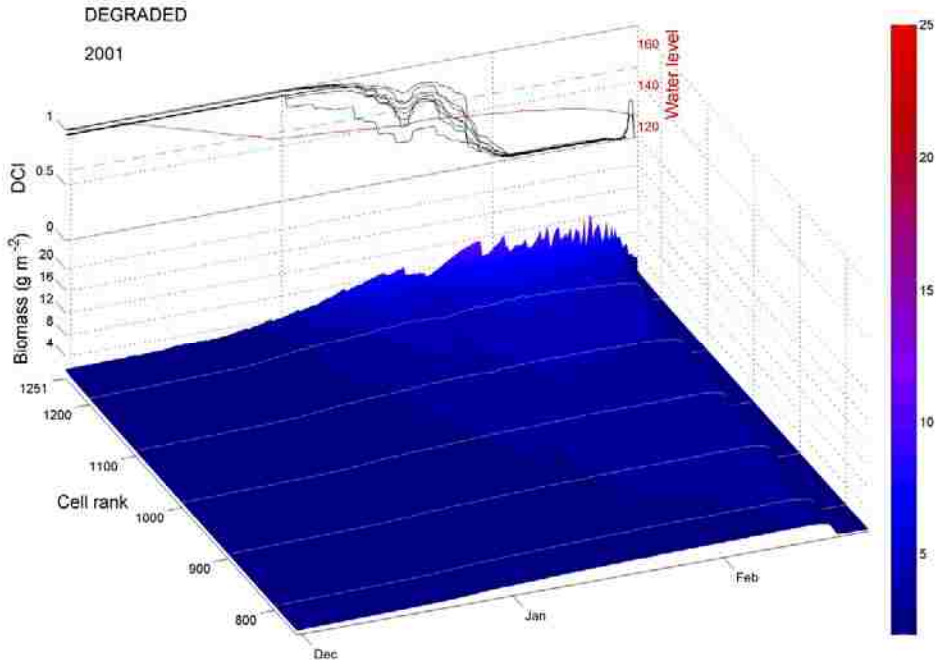

Figure S3F.1B.

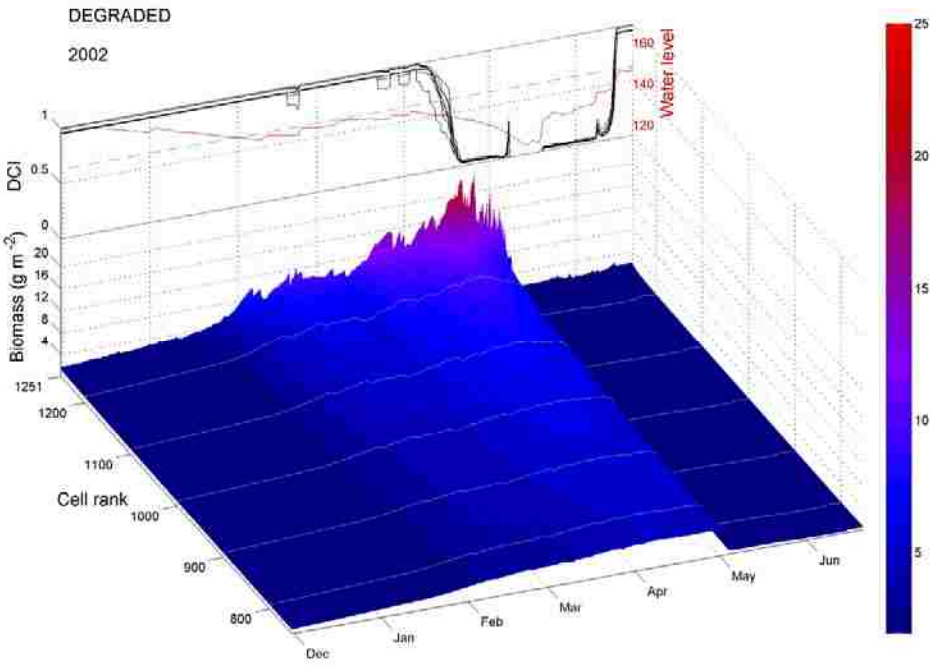

Figure S3F.2B.

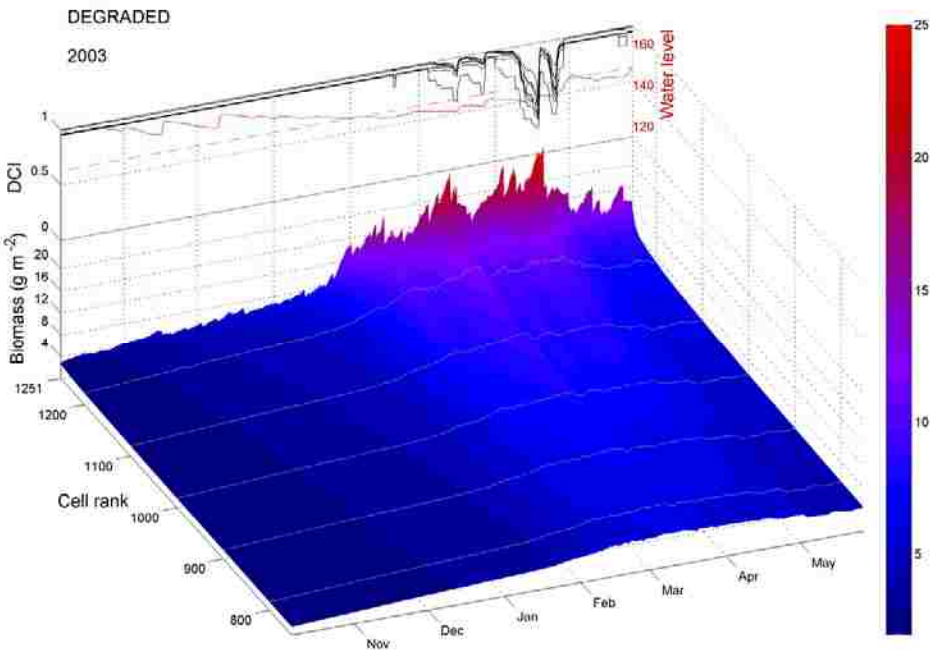

Figure S3F.3B.

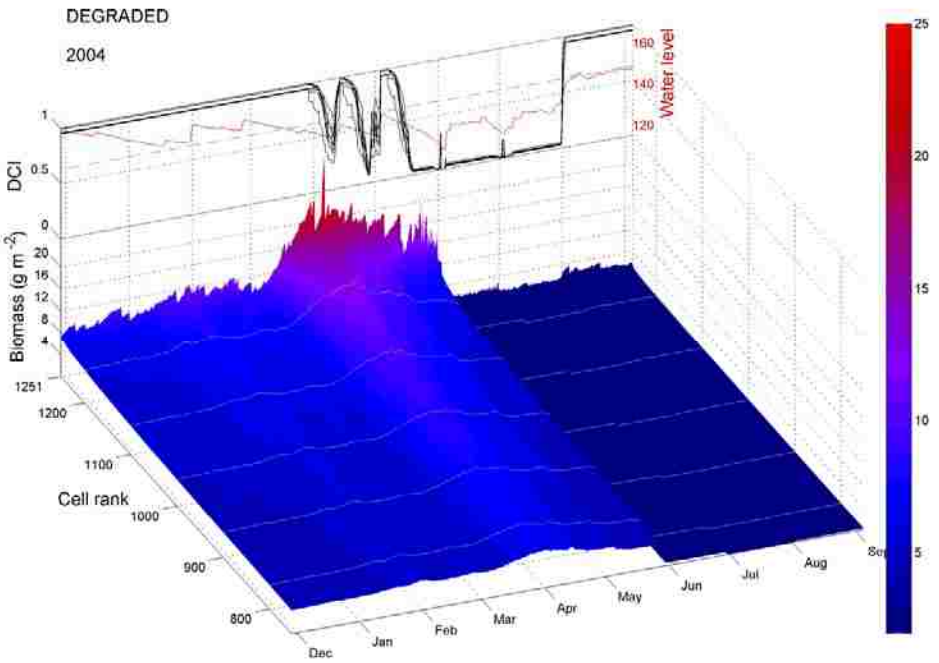

Figure S3F.4B.

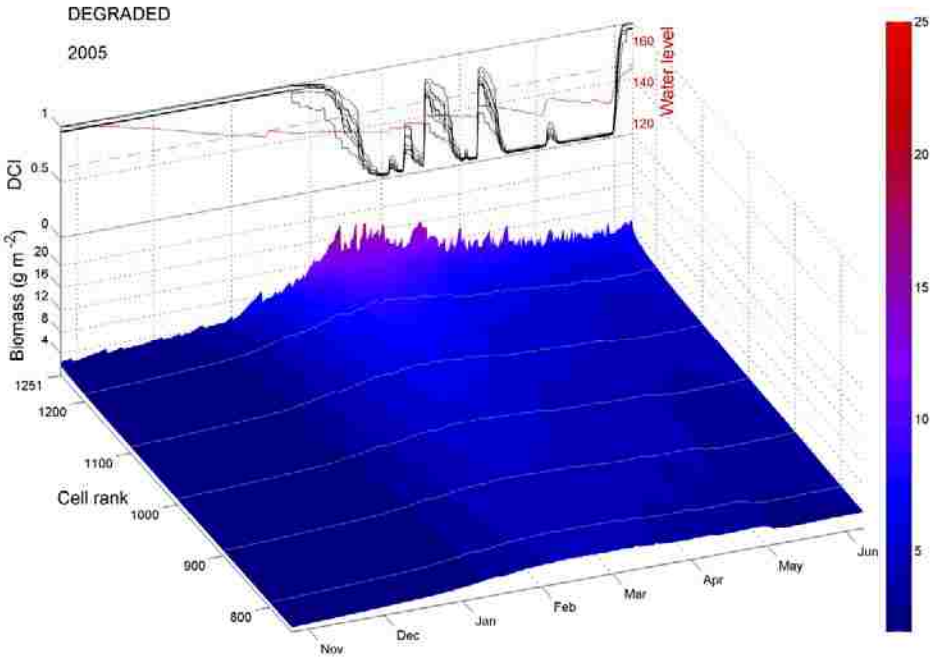

Figure S3F.5B.

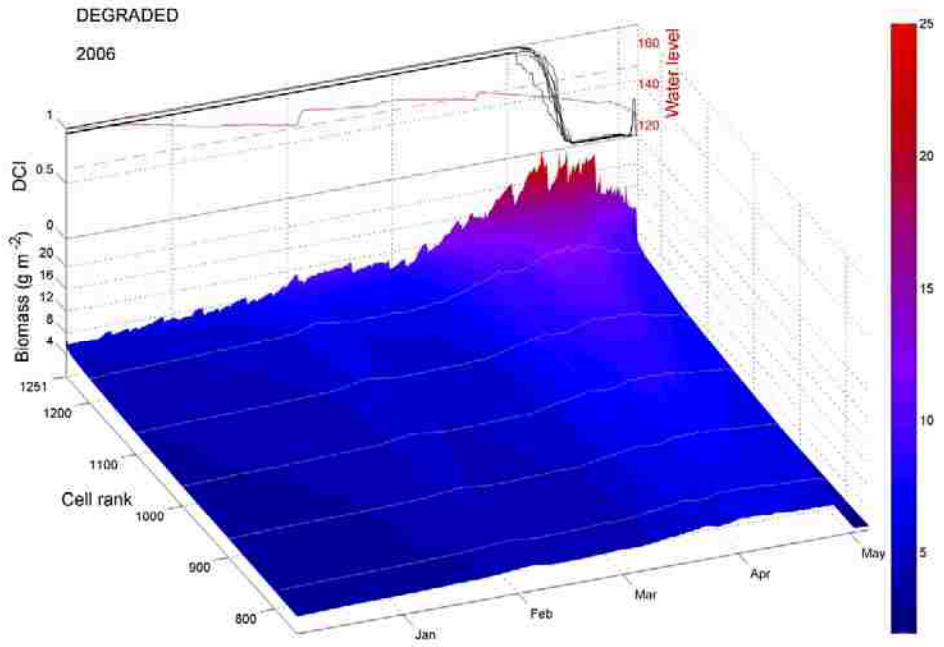

Figure S3F.6B.

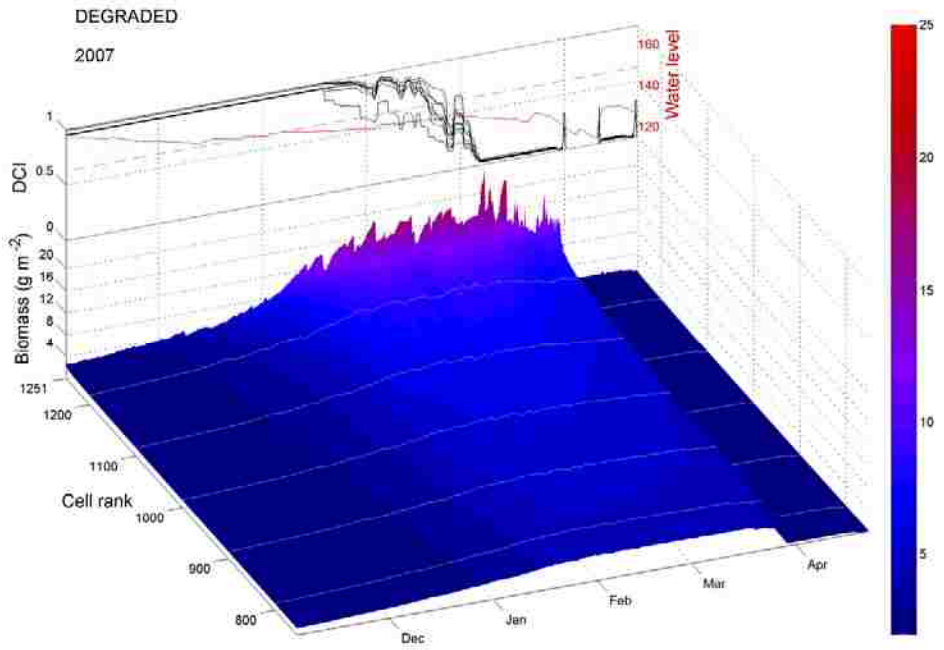

Figure S3F.7B.

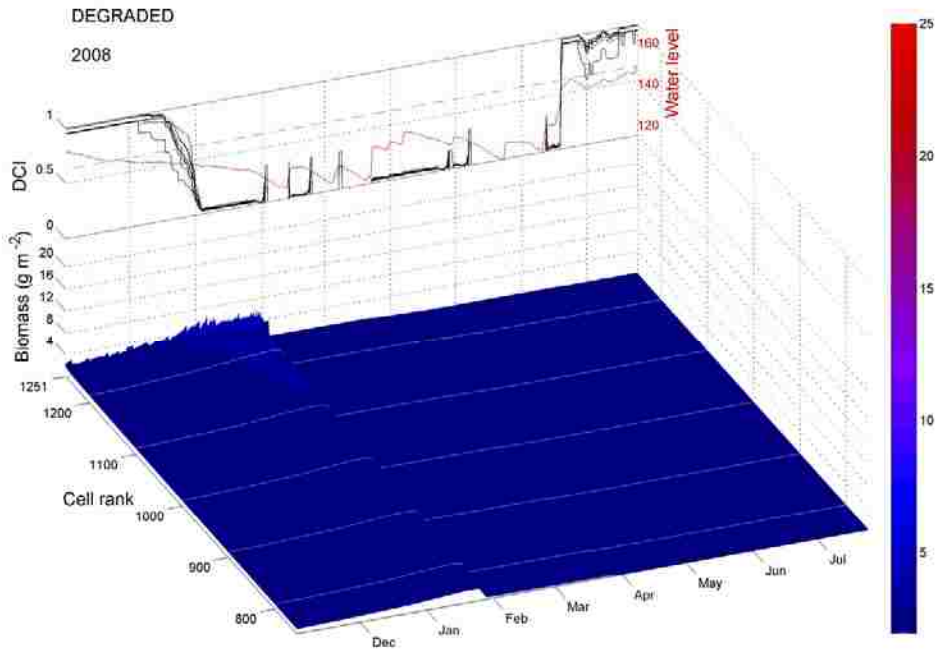

Figure S3F.8B.

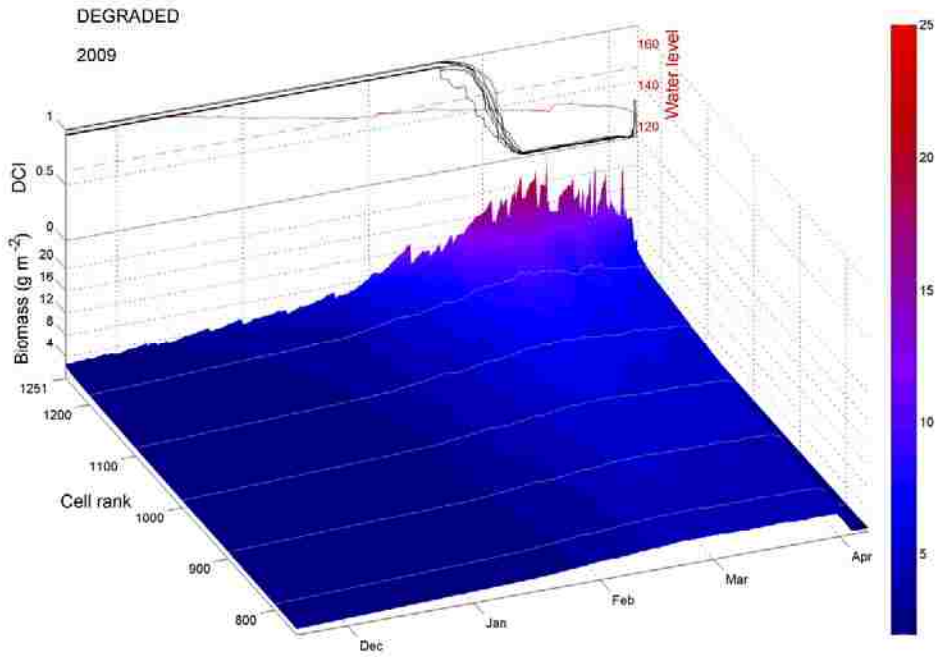

Figure S3F.9B.

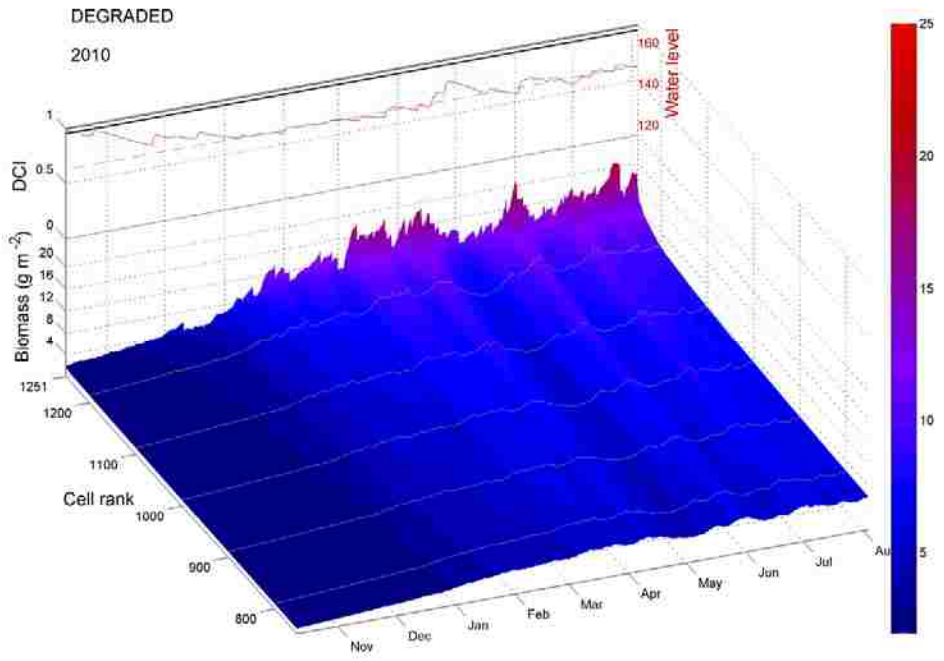

Figure S3F.10B.

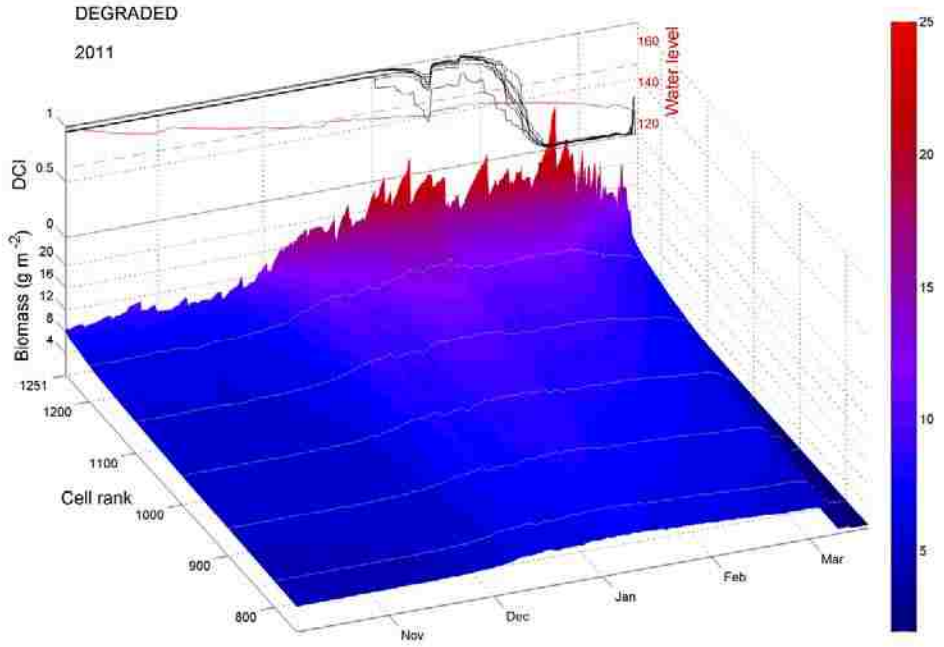

Figure S3F.11B.

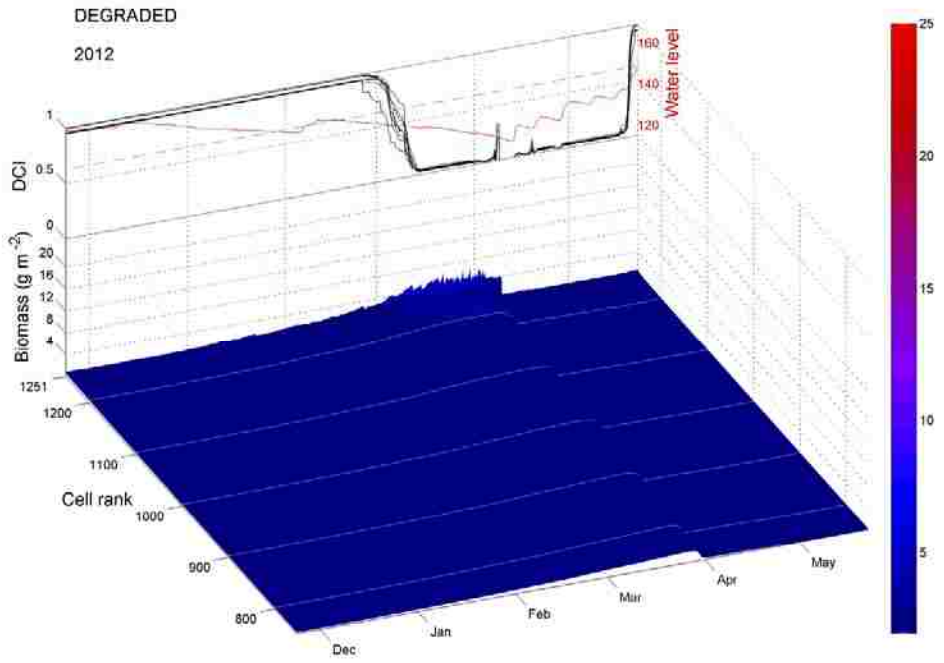

Figure S3F.12B

Supplement 3G. Spatial maps of frequency of single cell exceedance of biomass threshold of θ = 10 g dry wt. m^{-2}.

Figure S3G.1−12. Water stage (blue line; top panel) and DCI graphs (gray lines) over 8 compass rose directions, and spatially−explicit map of biomass persistence (bottom panel), on intact and degraded RSL. Biomass persistence was calculated as the frequency during the drying phase that biomass in a slough cell exceeded a defined threshold of 10 g dry wt. m^{-2}, and summed over cells as a metric of cell−days.

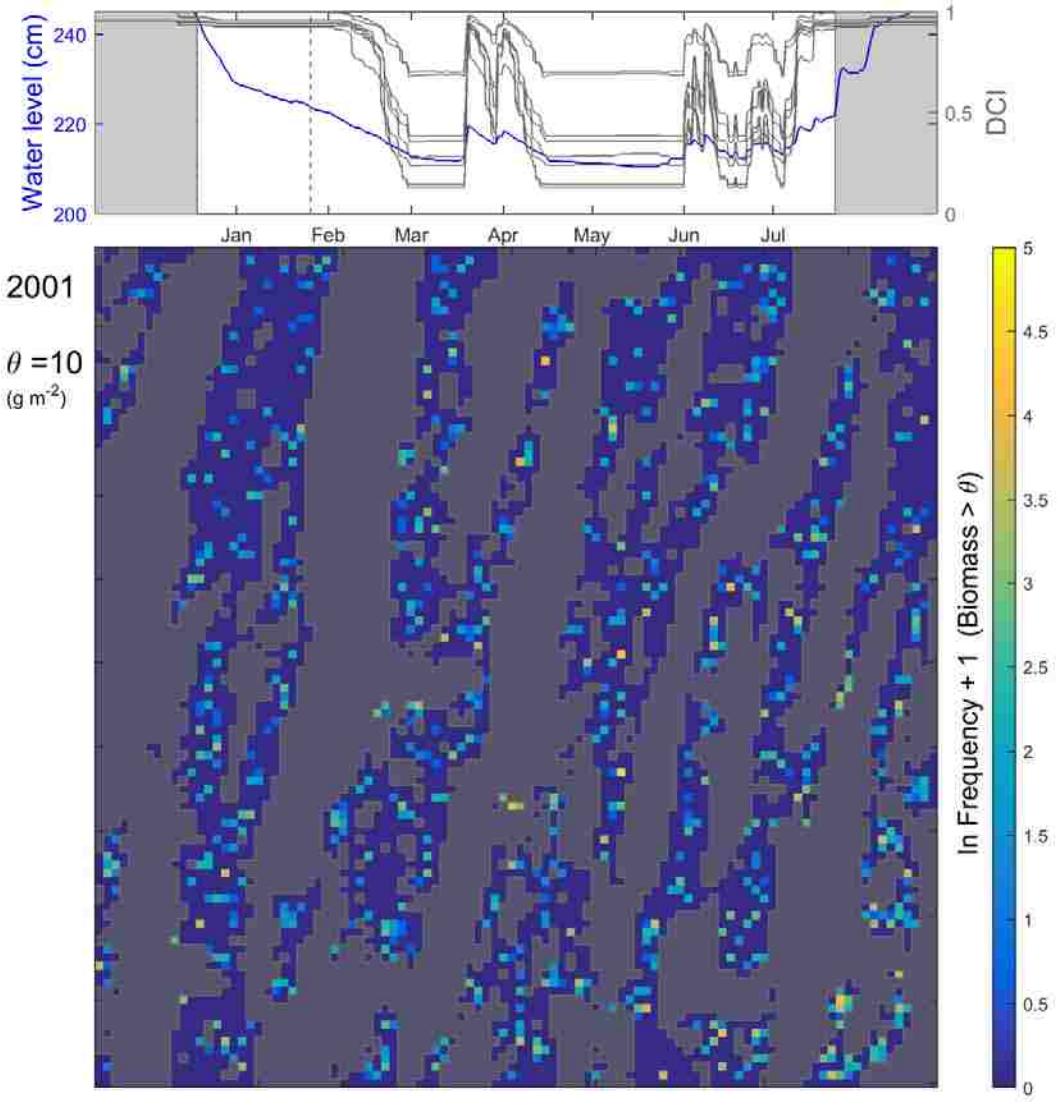

Figure S3G.1A.

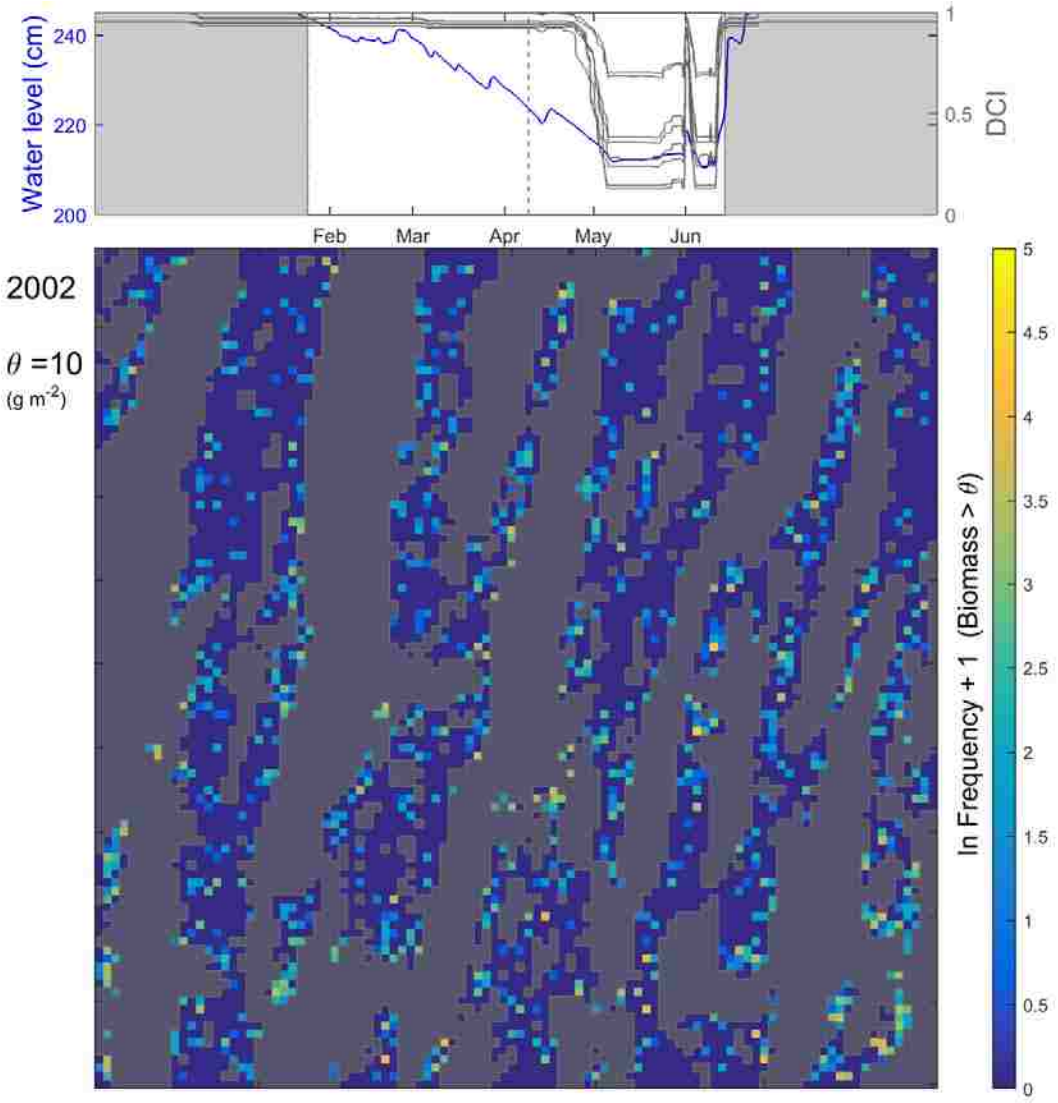

Figure S3G.2A.

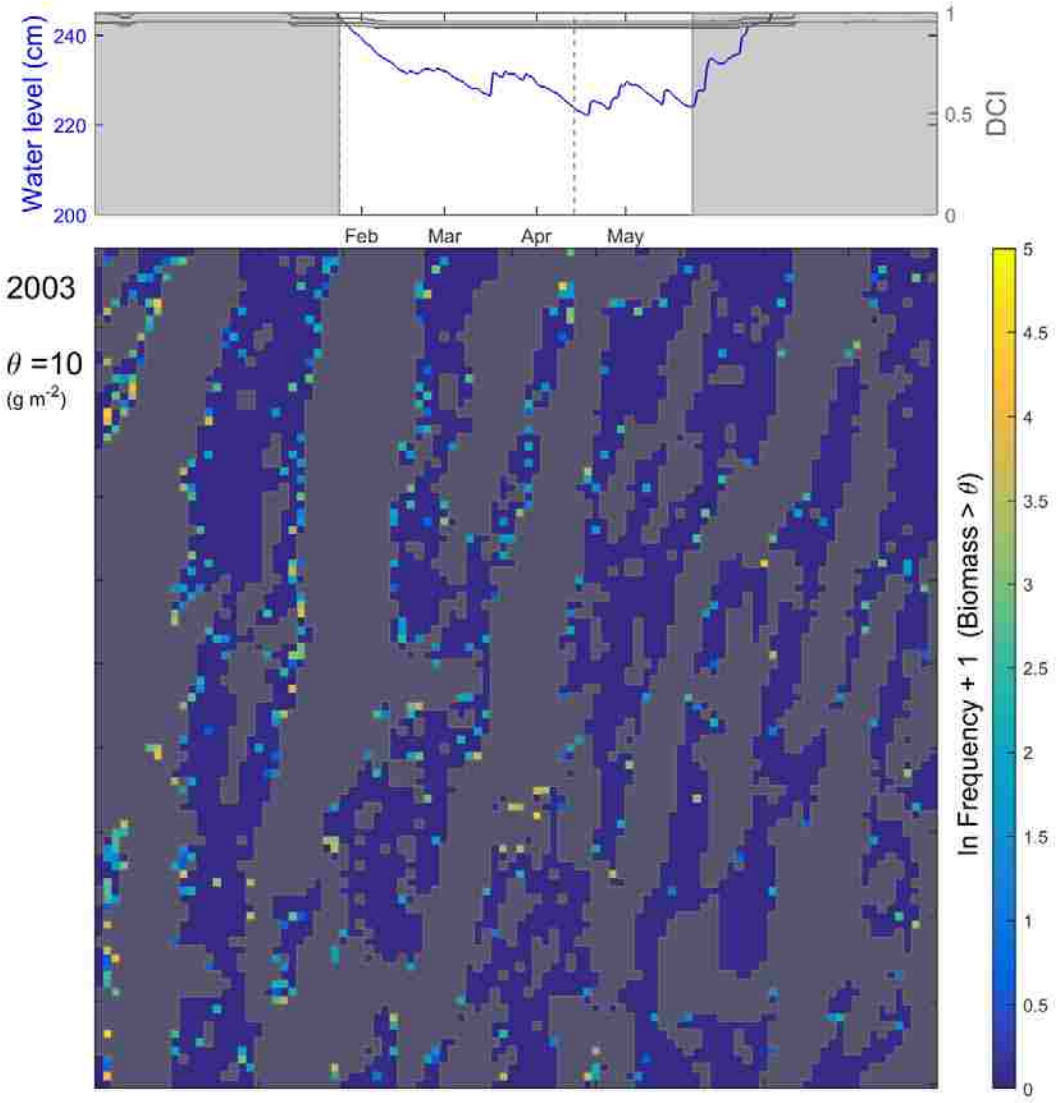

Figure S3G.3A.

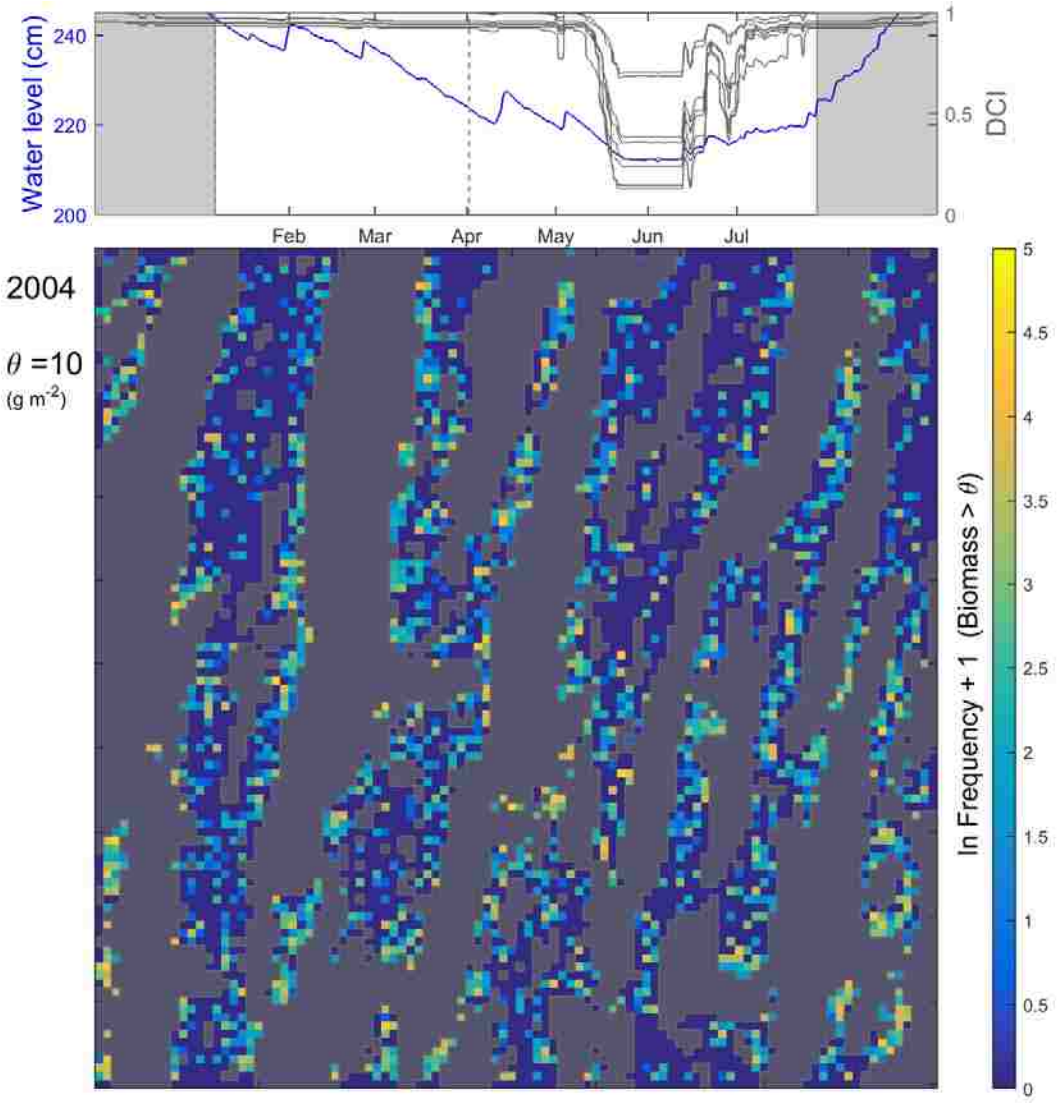

Figure S3G.4A.

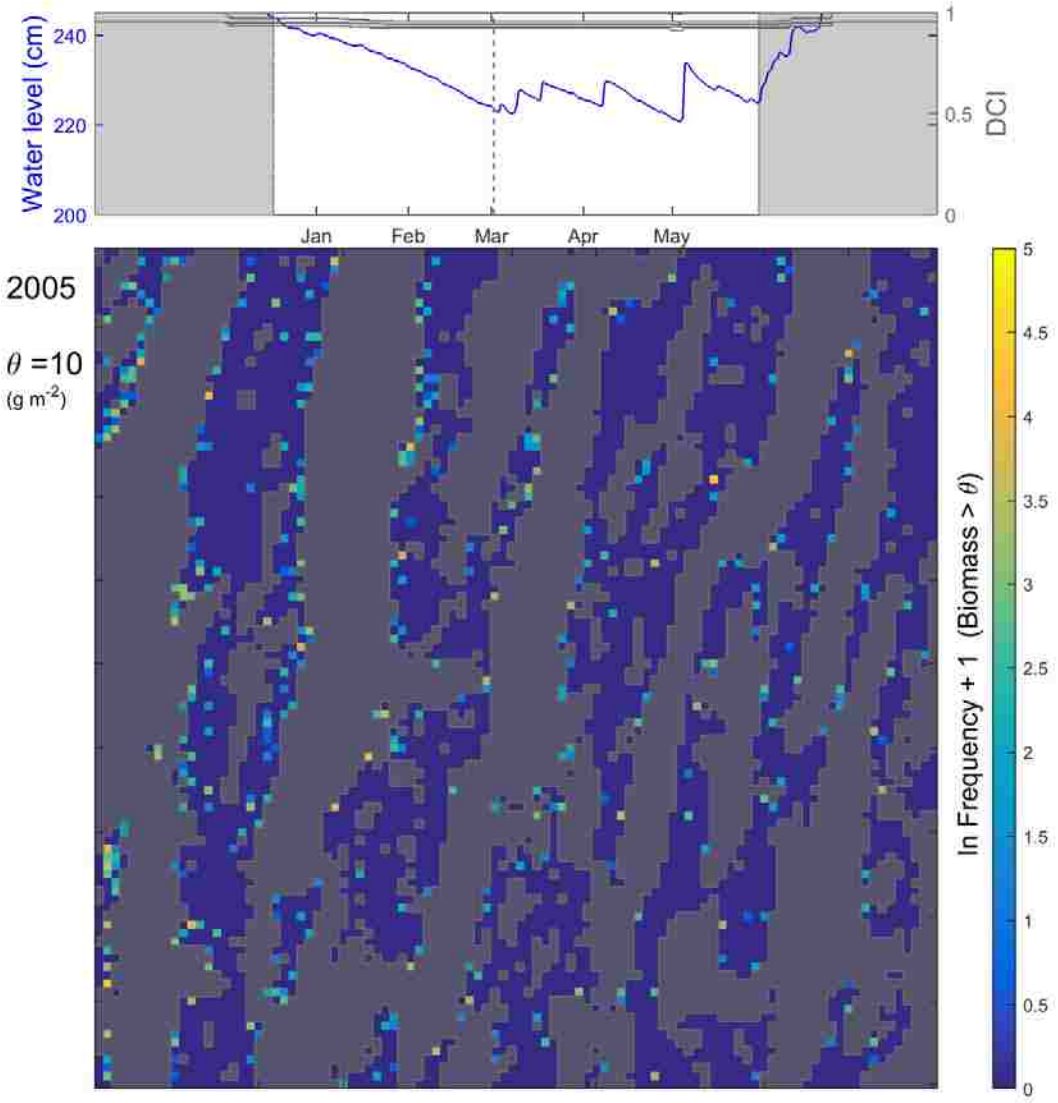

Figure S3G.5A.

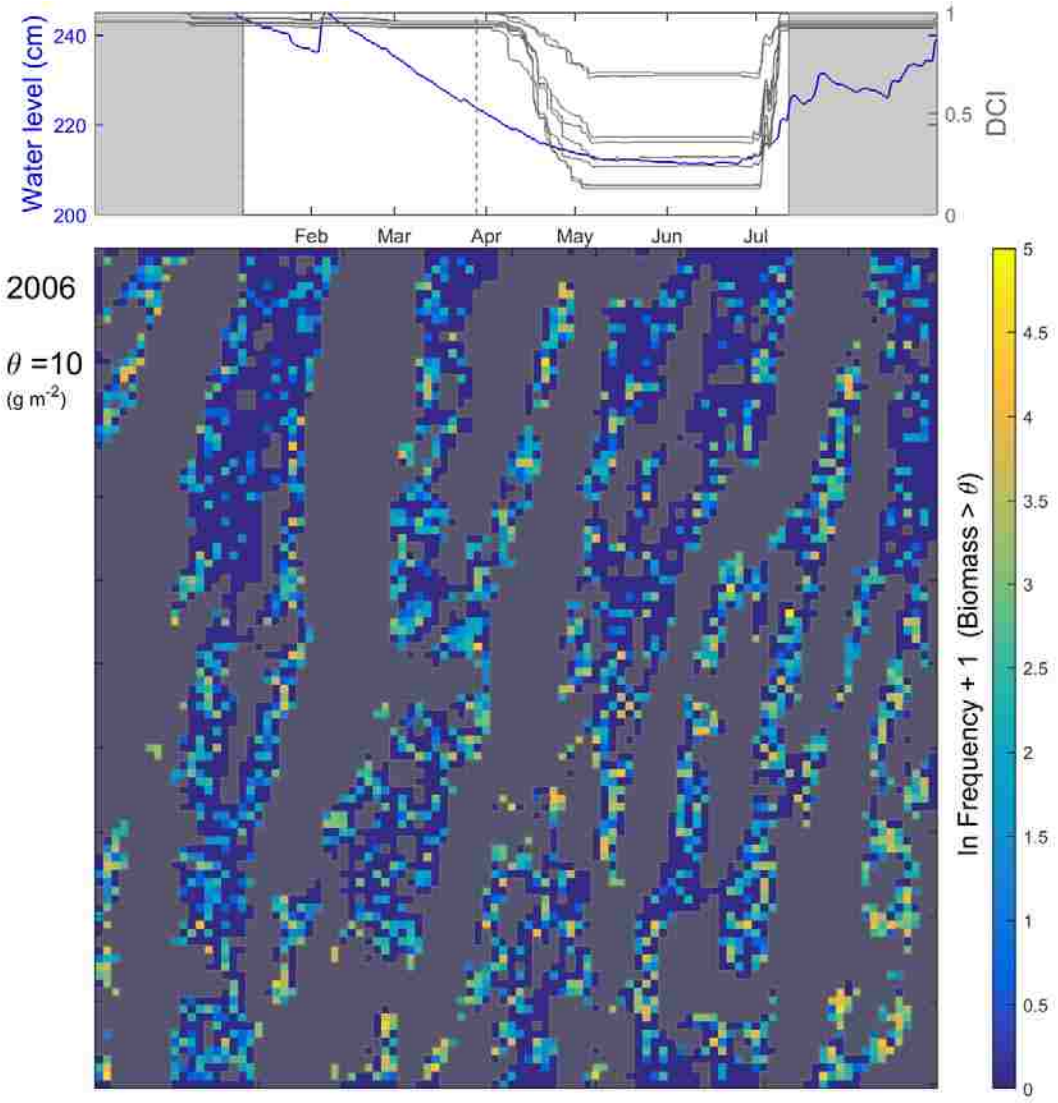

Figure S3G.6A.

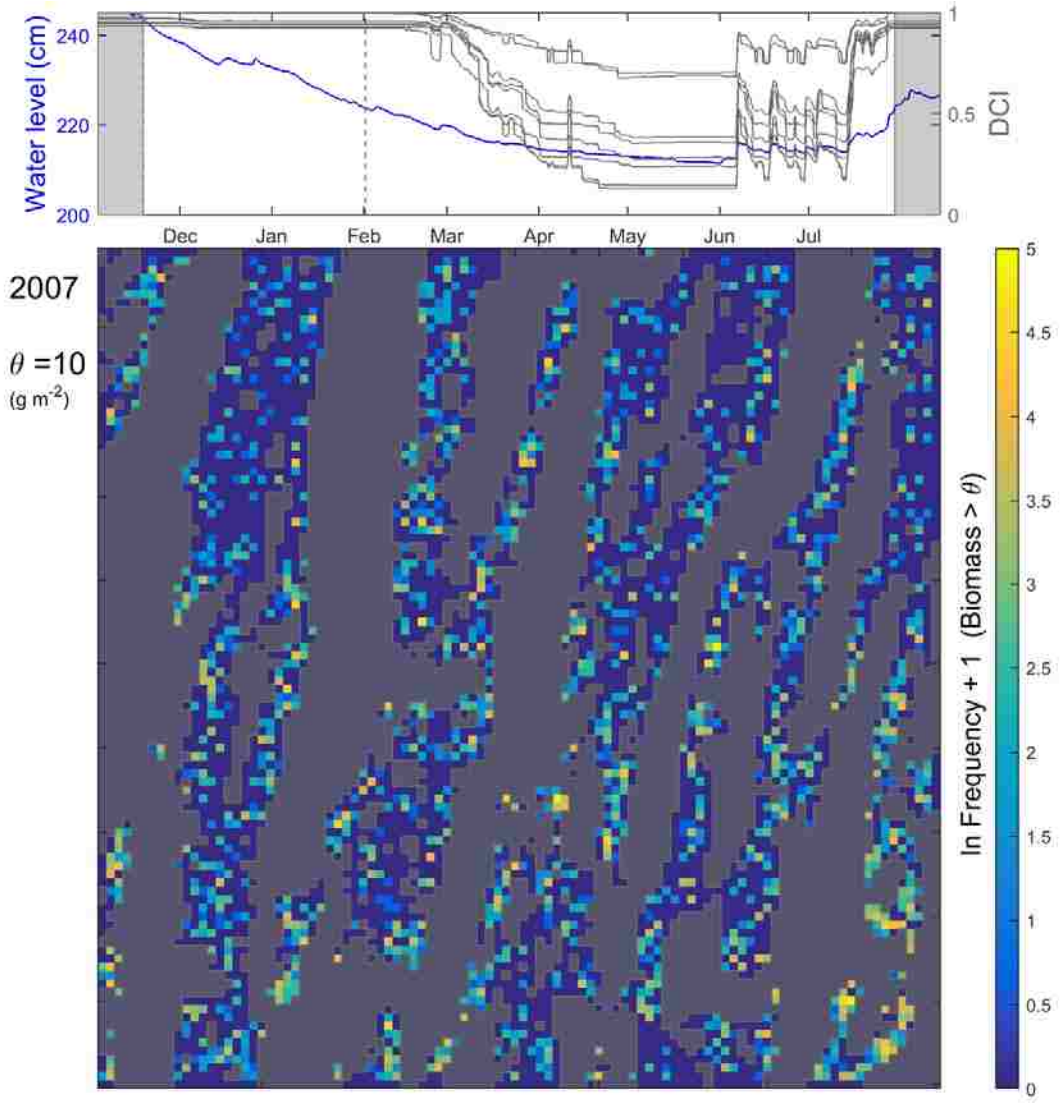

Figure S3G.7A.

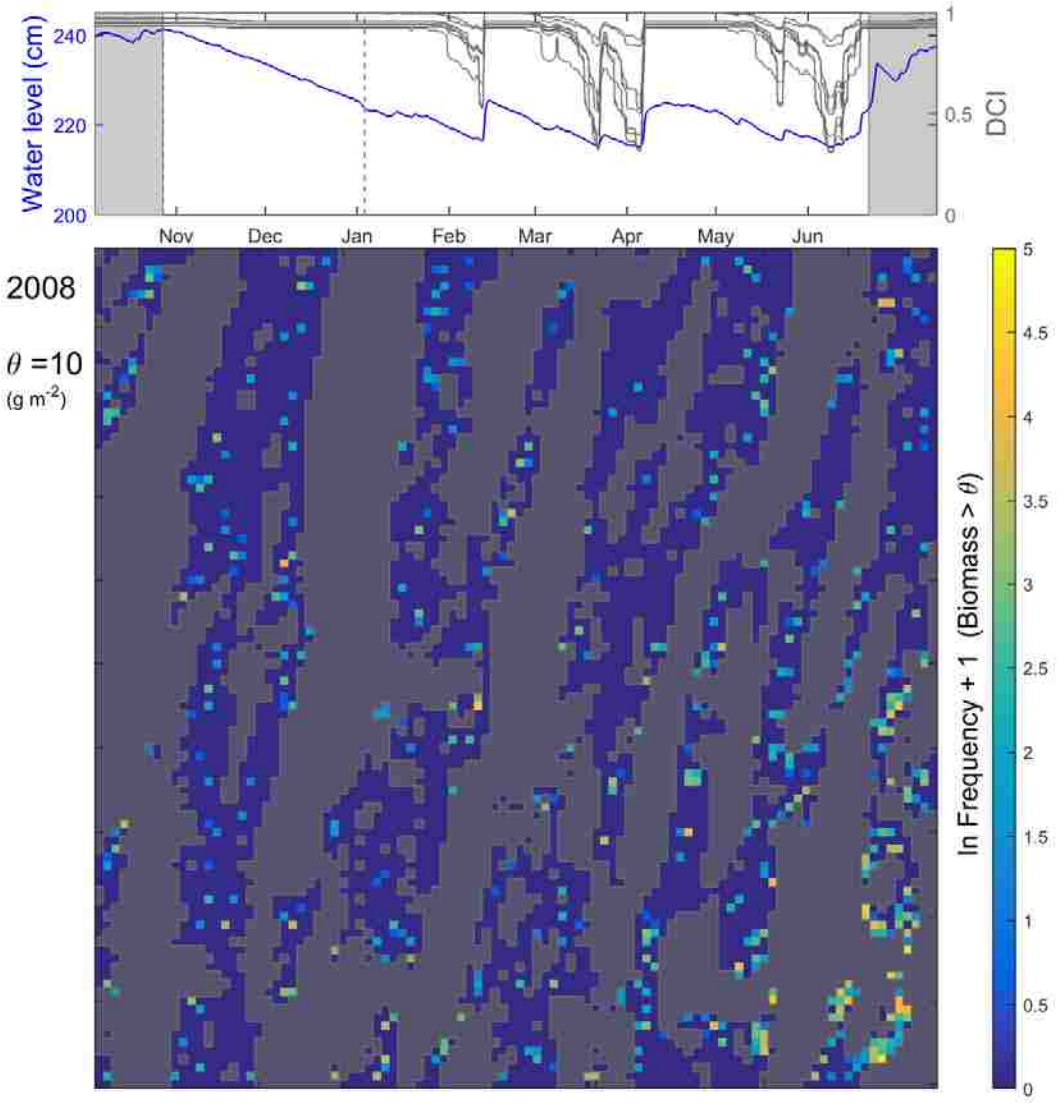

Figure S3G.8A.

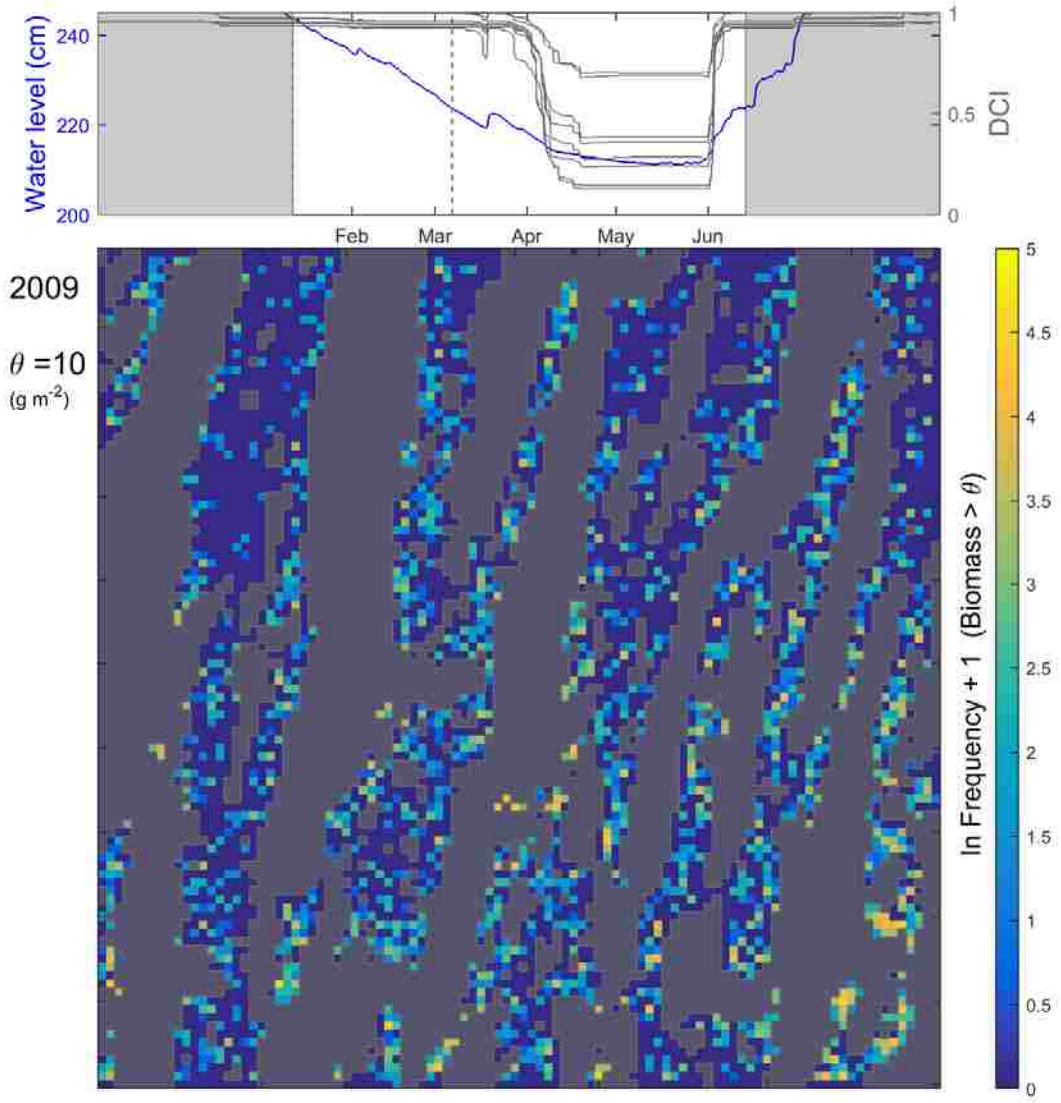

Figure S3G.9A.

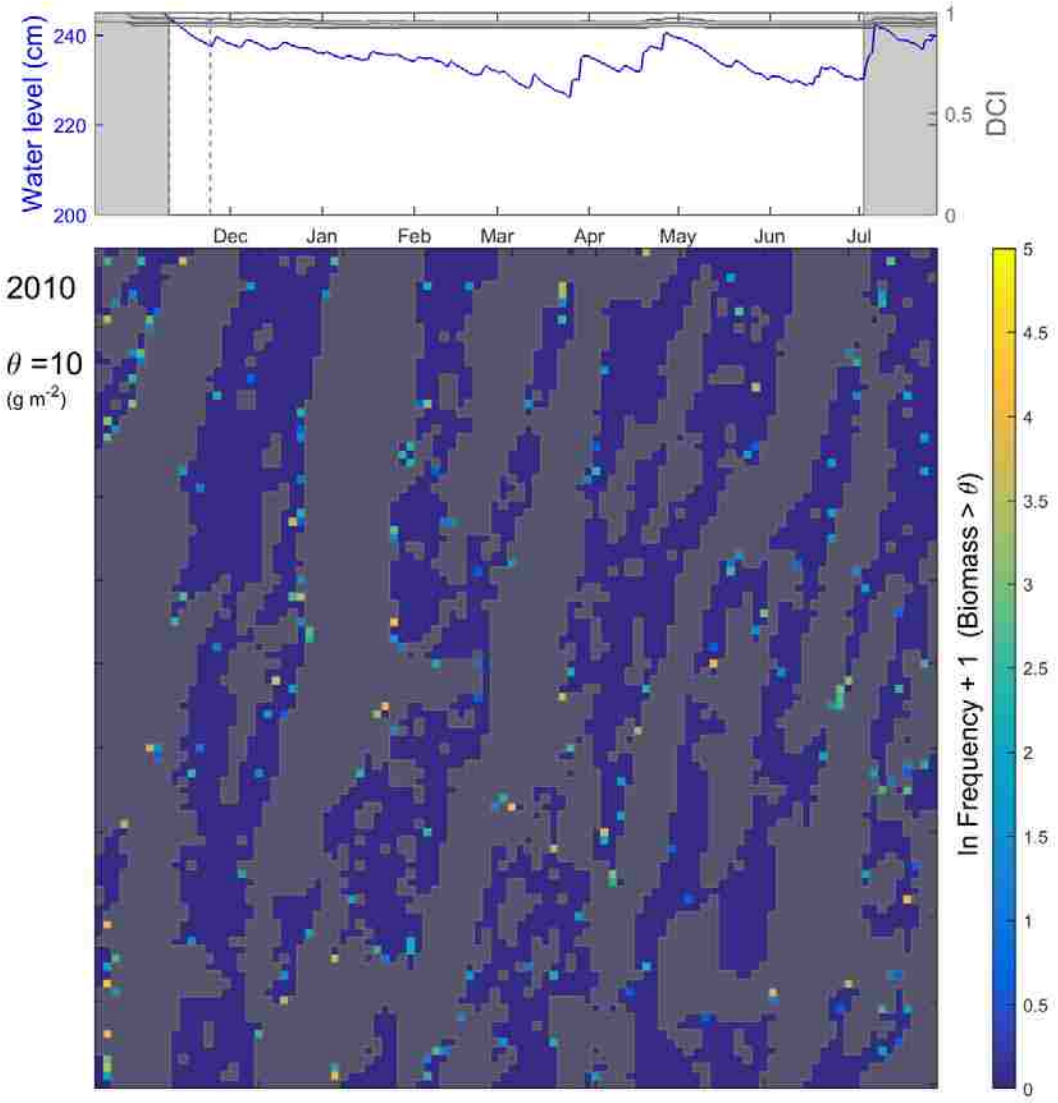

Figure S3G.10A.

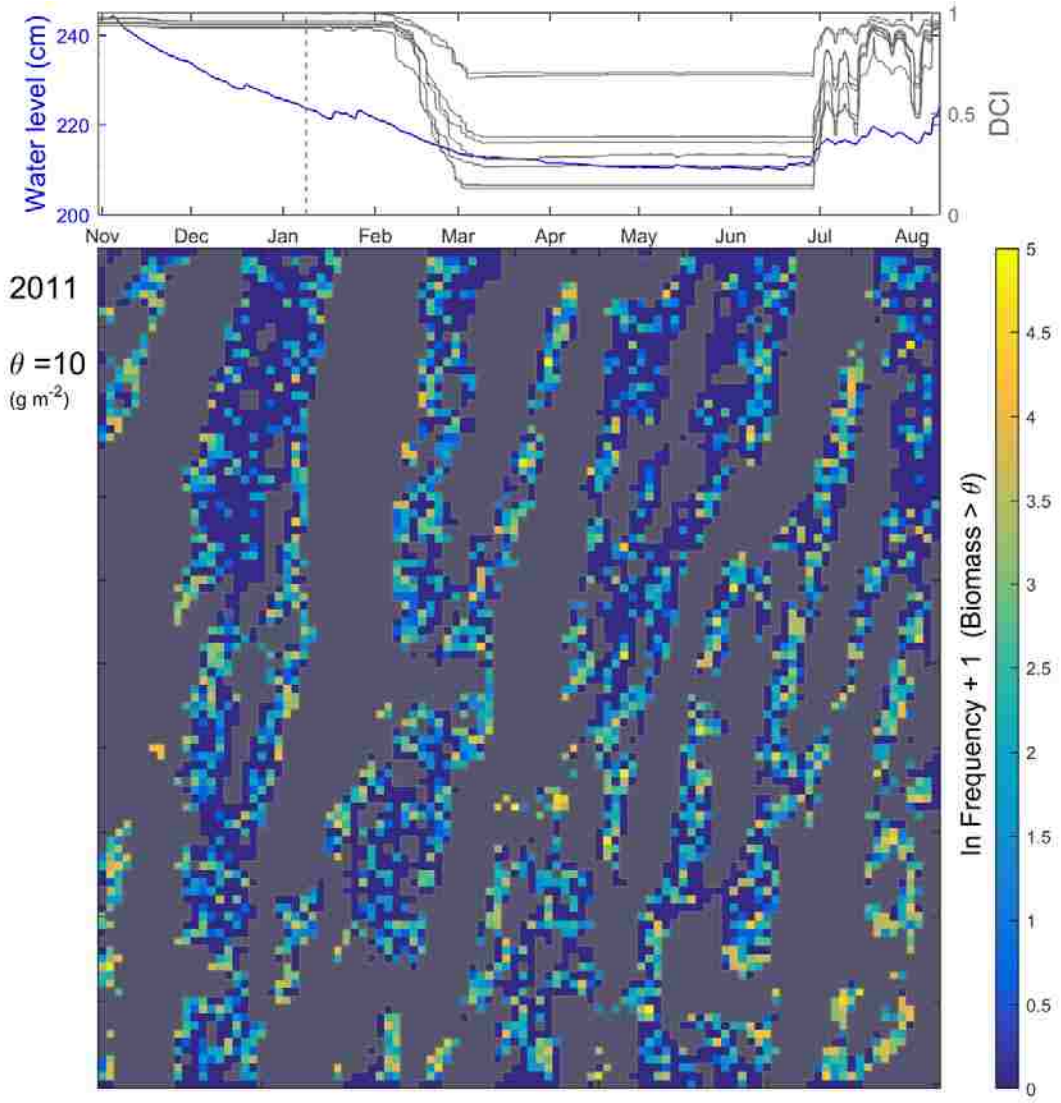

Figure S3G.11A.

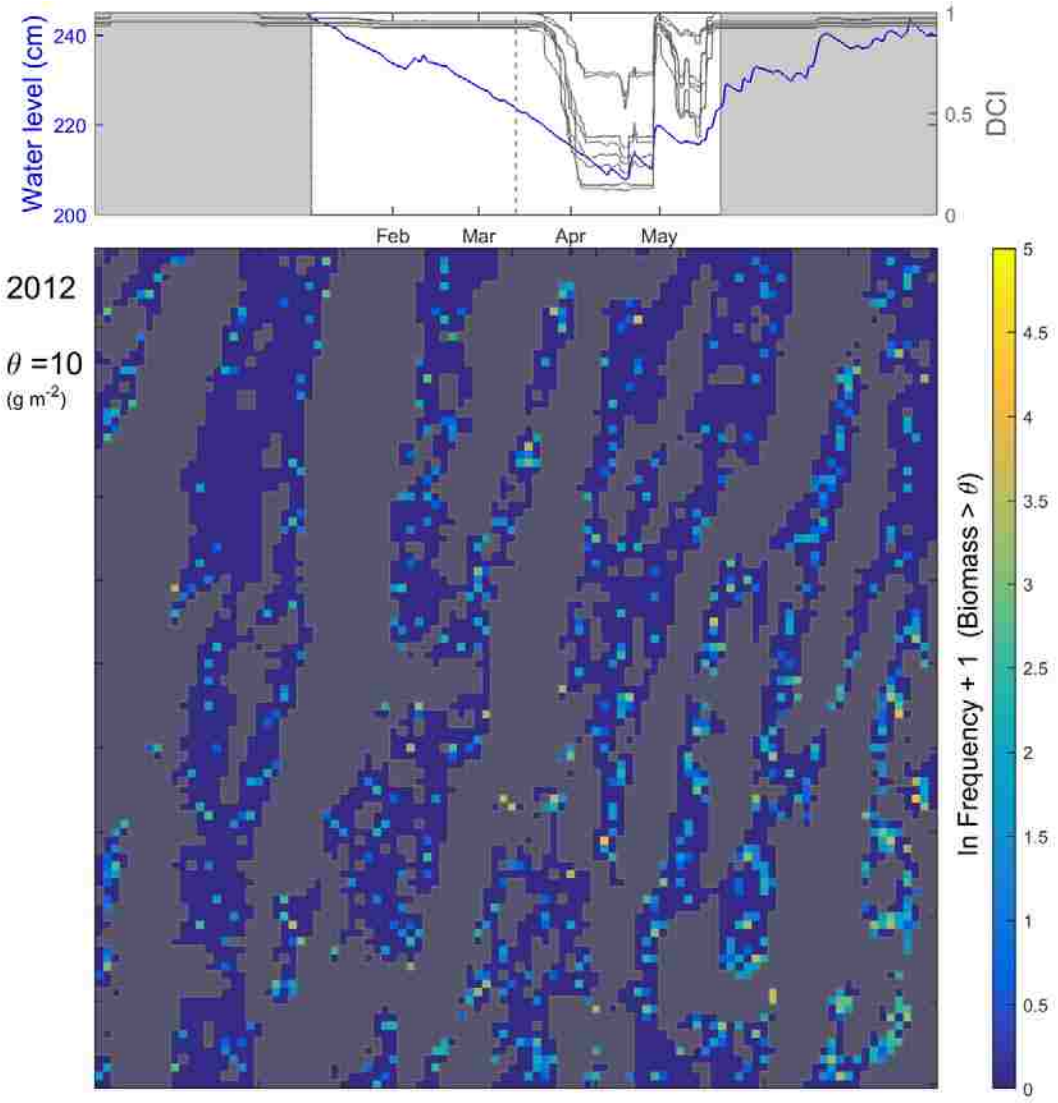

Figure S3G.12A.

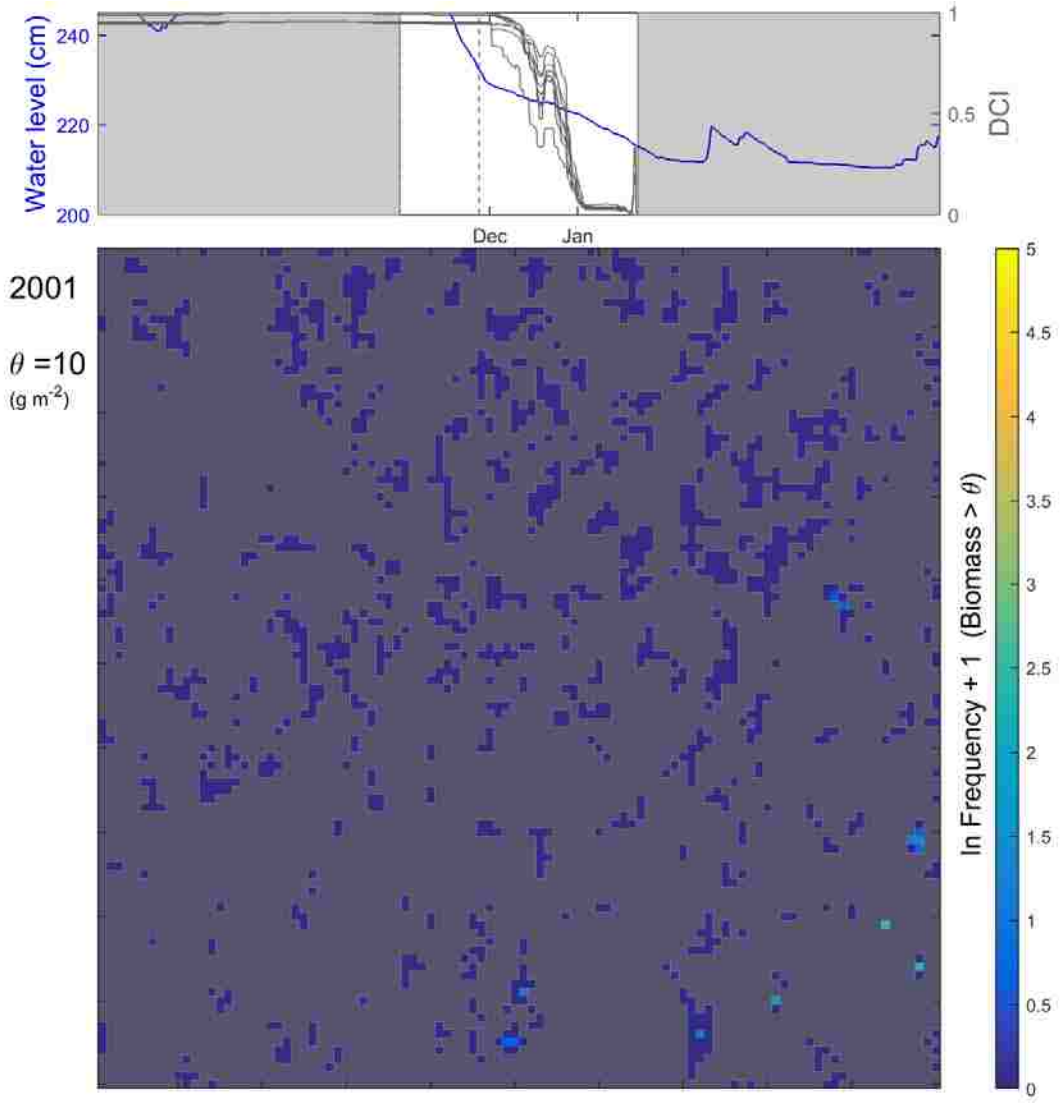

Figure S3G.1B.

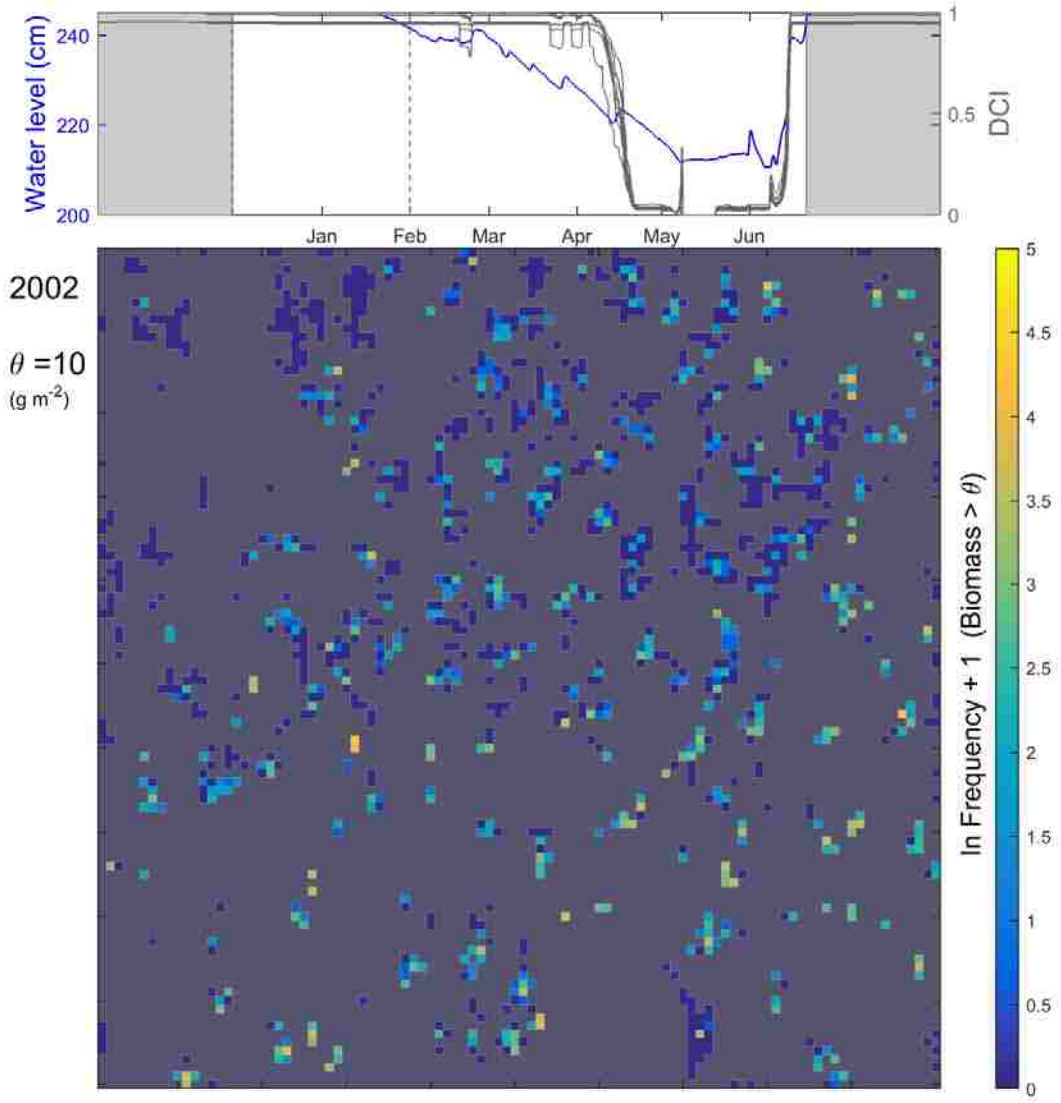

Figure S3G.2B.

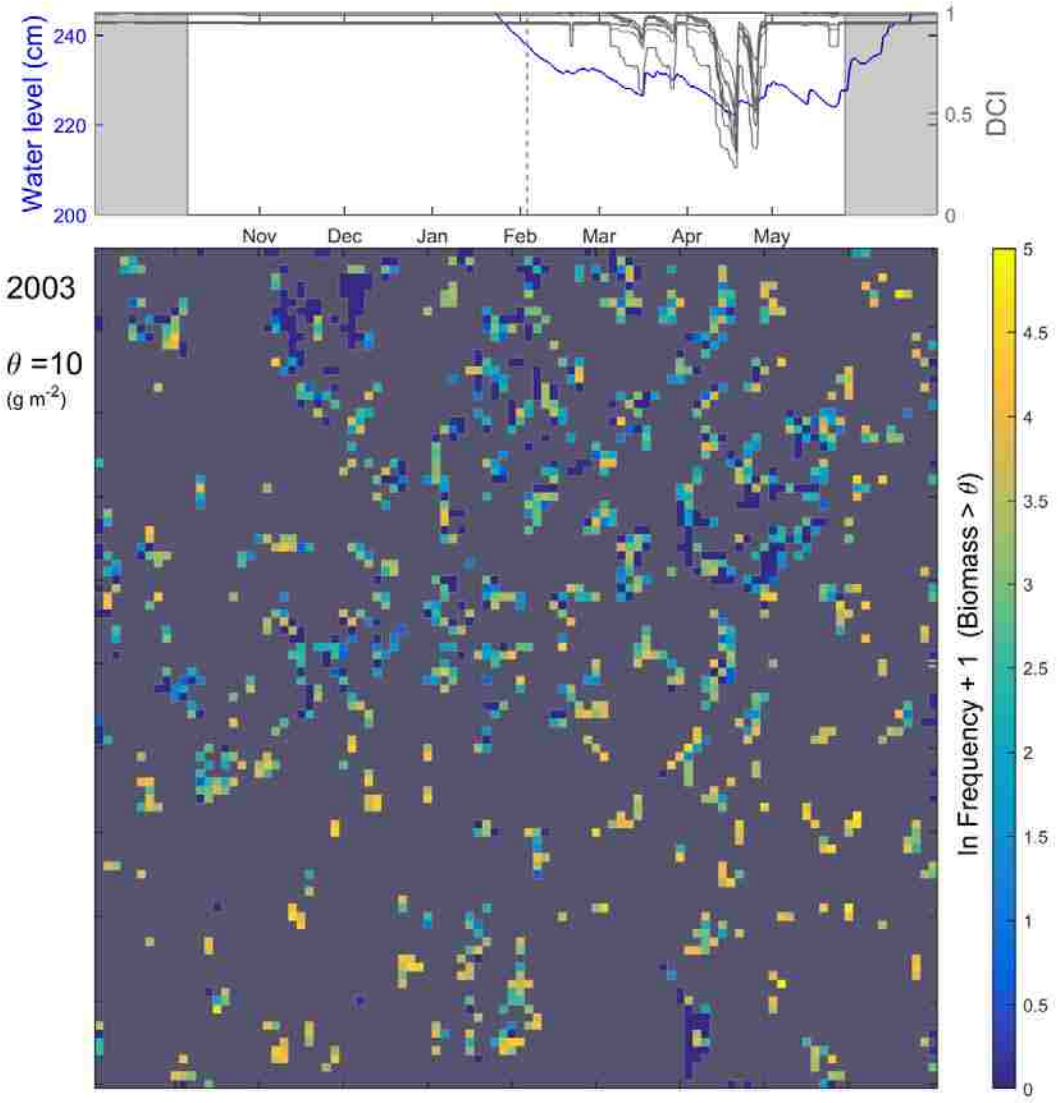

Figure S3G.3B.

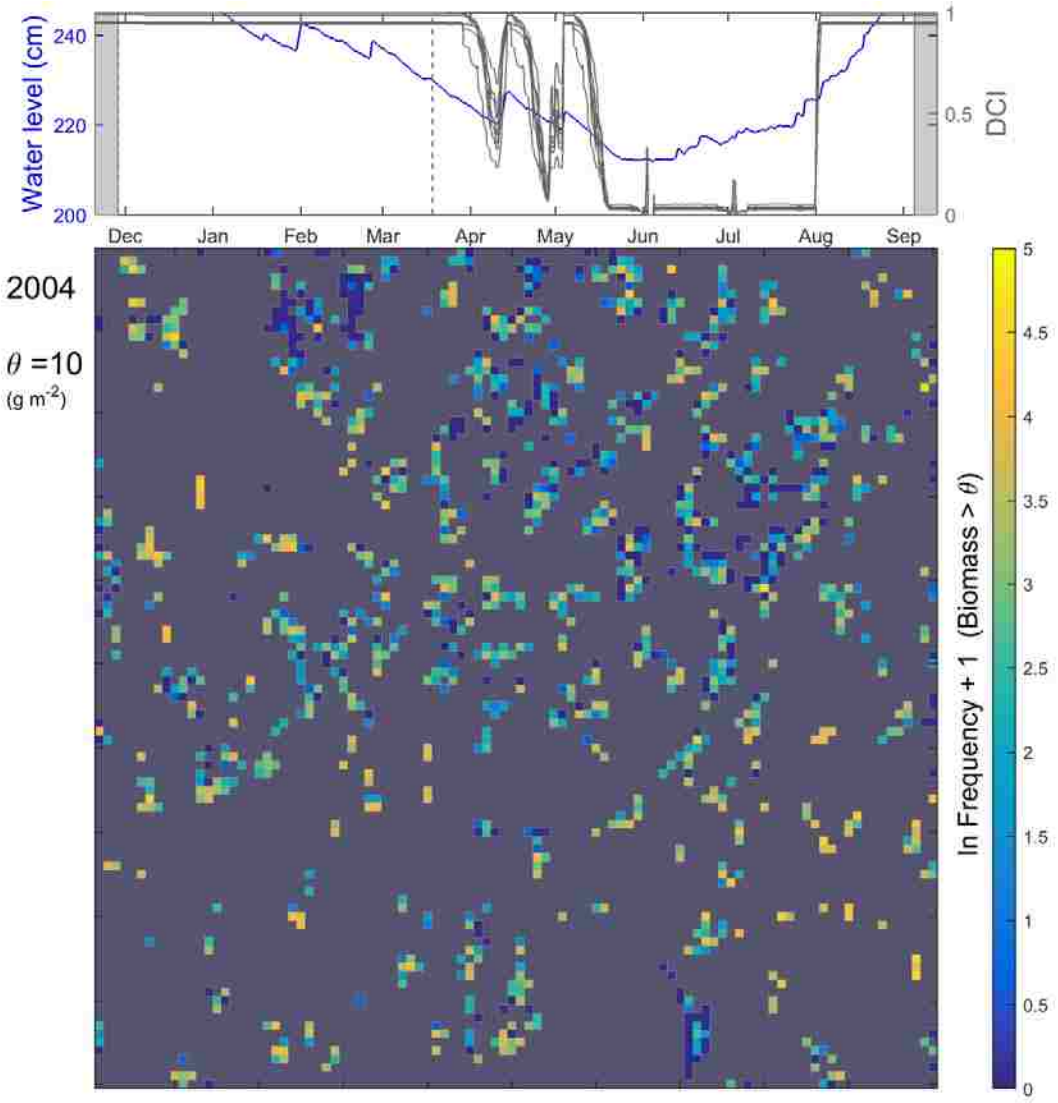

Figure S3G.4B.

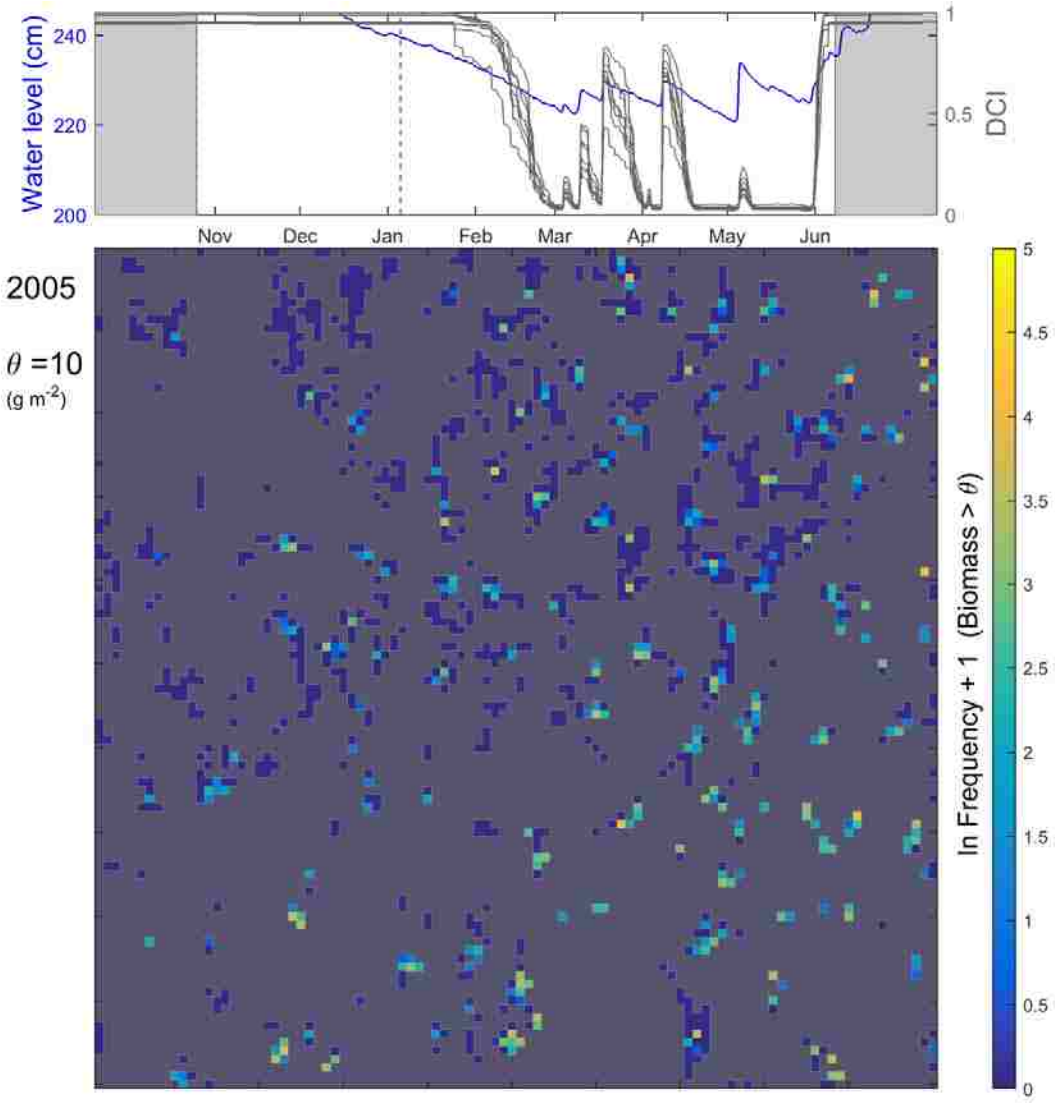

Figure S3G.5B.

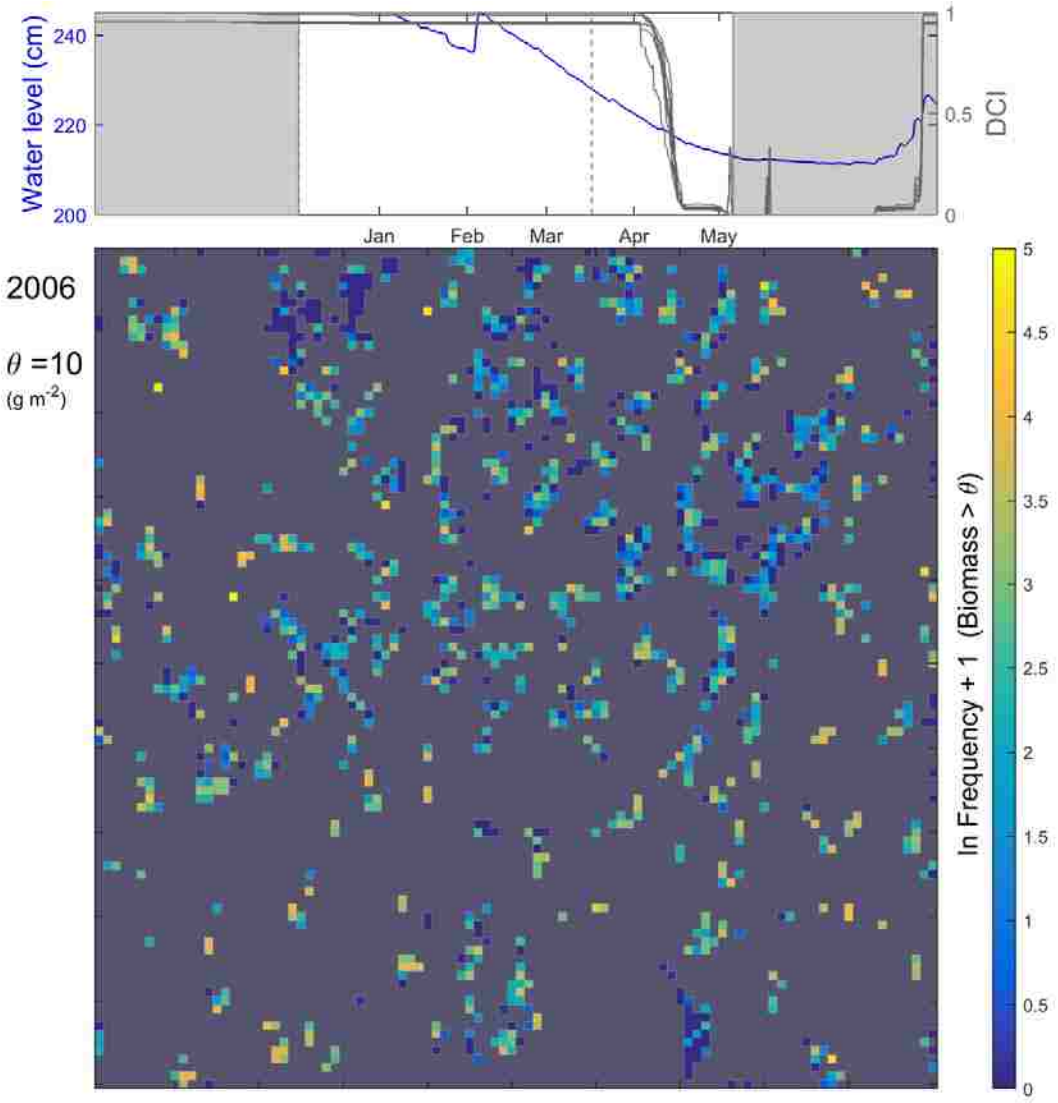

Figure S3G.6B.

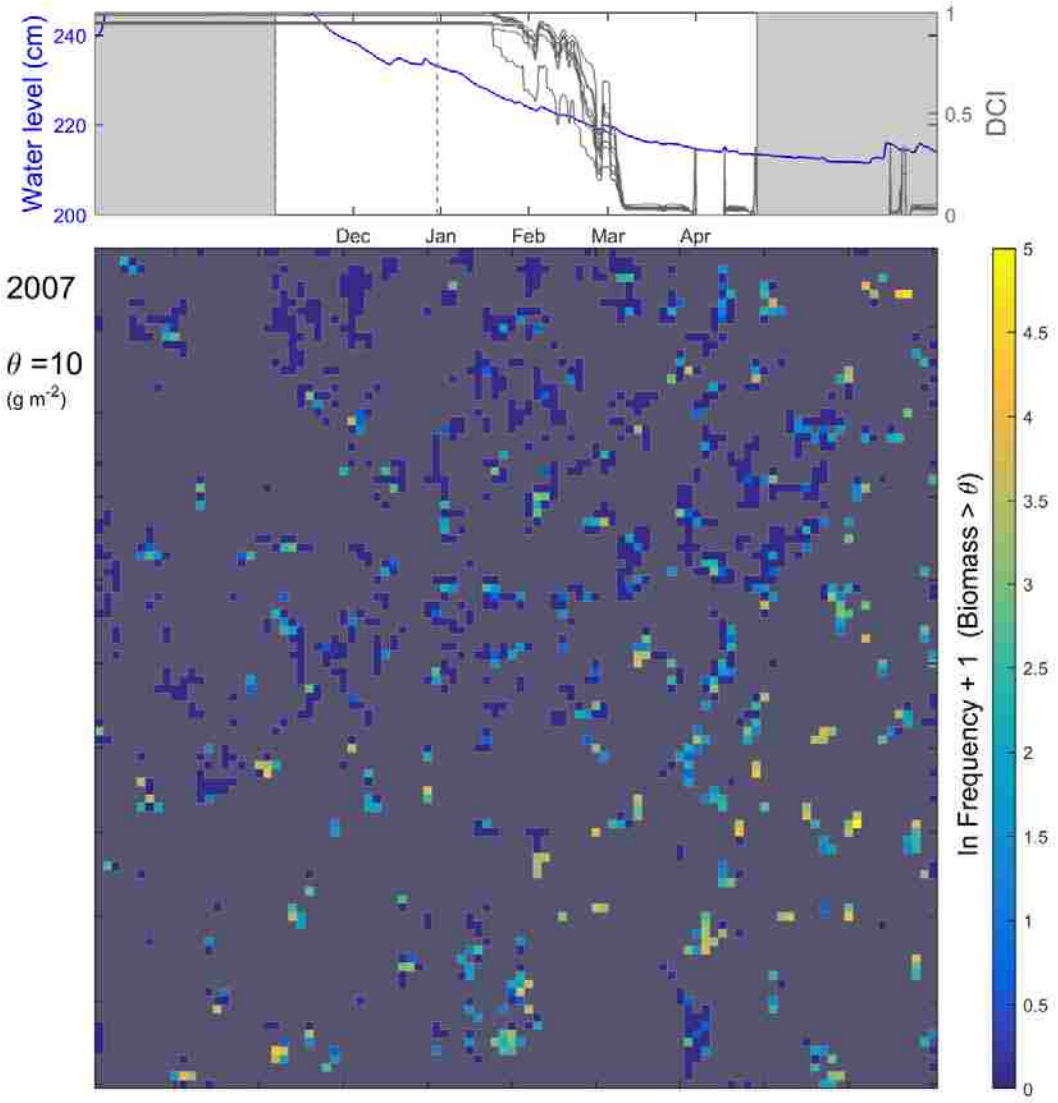

Figure S3G.7B.

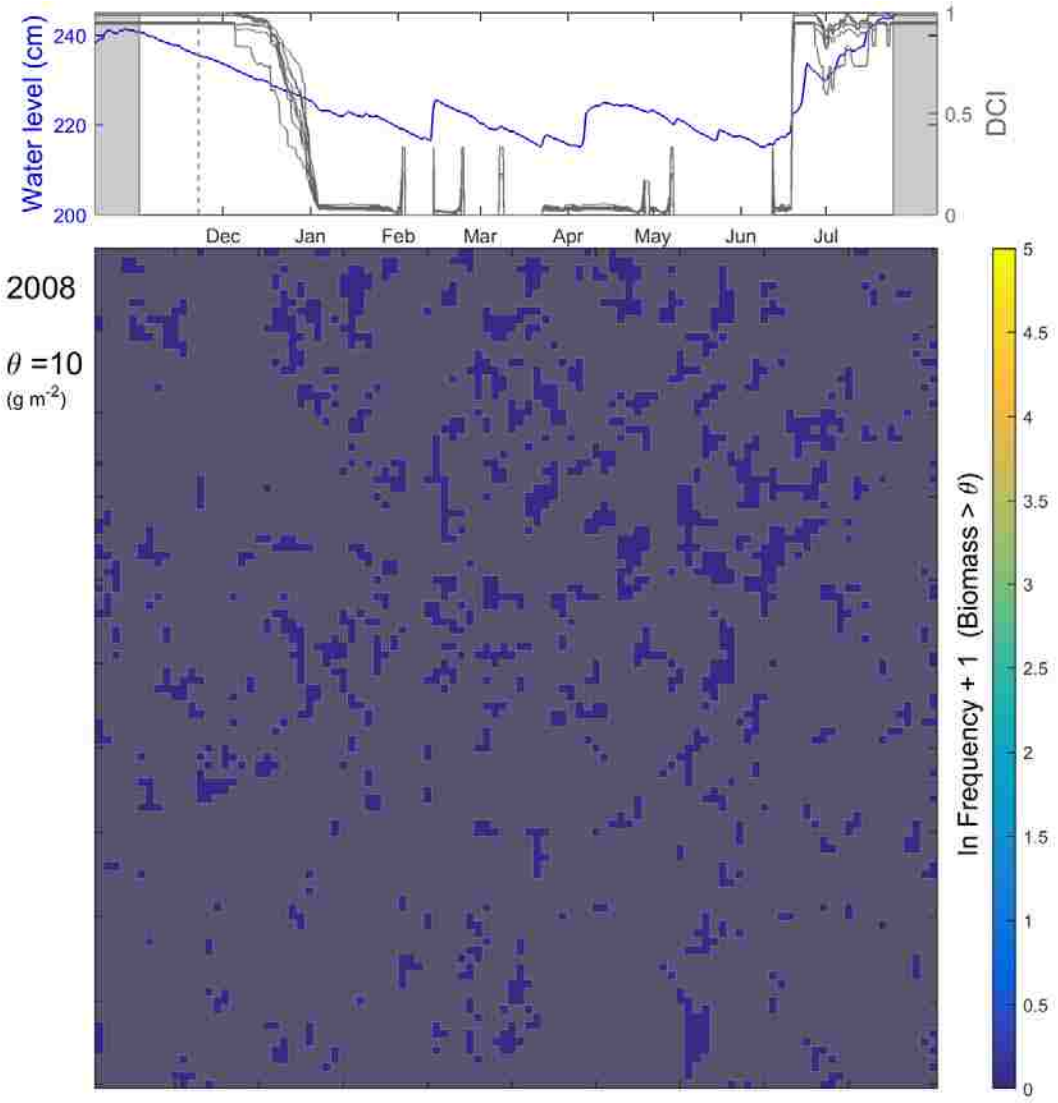

Figure S3G.8B.

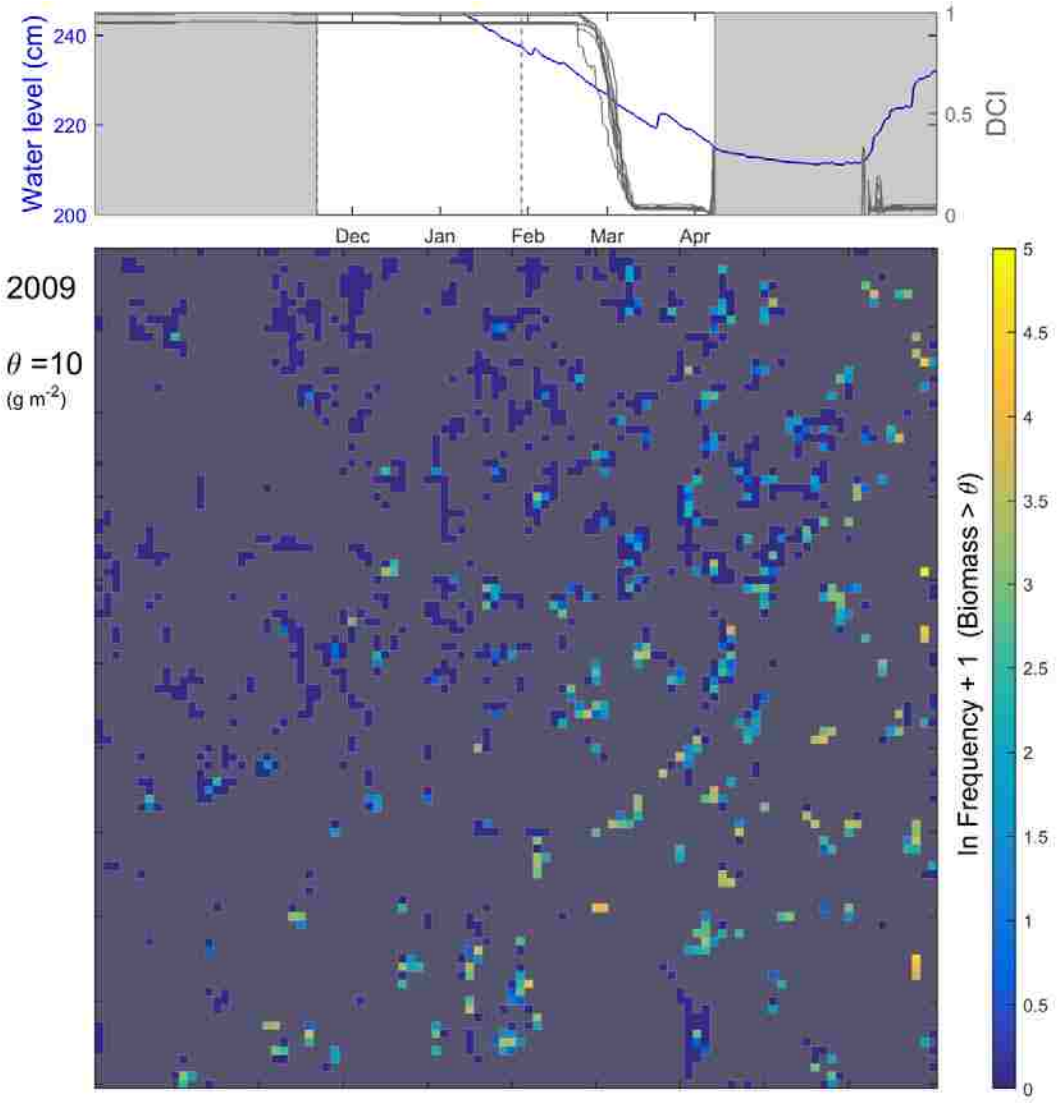

Figure S3G.9B.

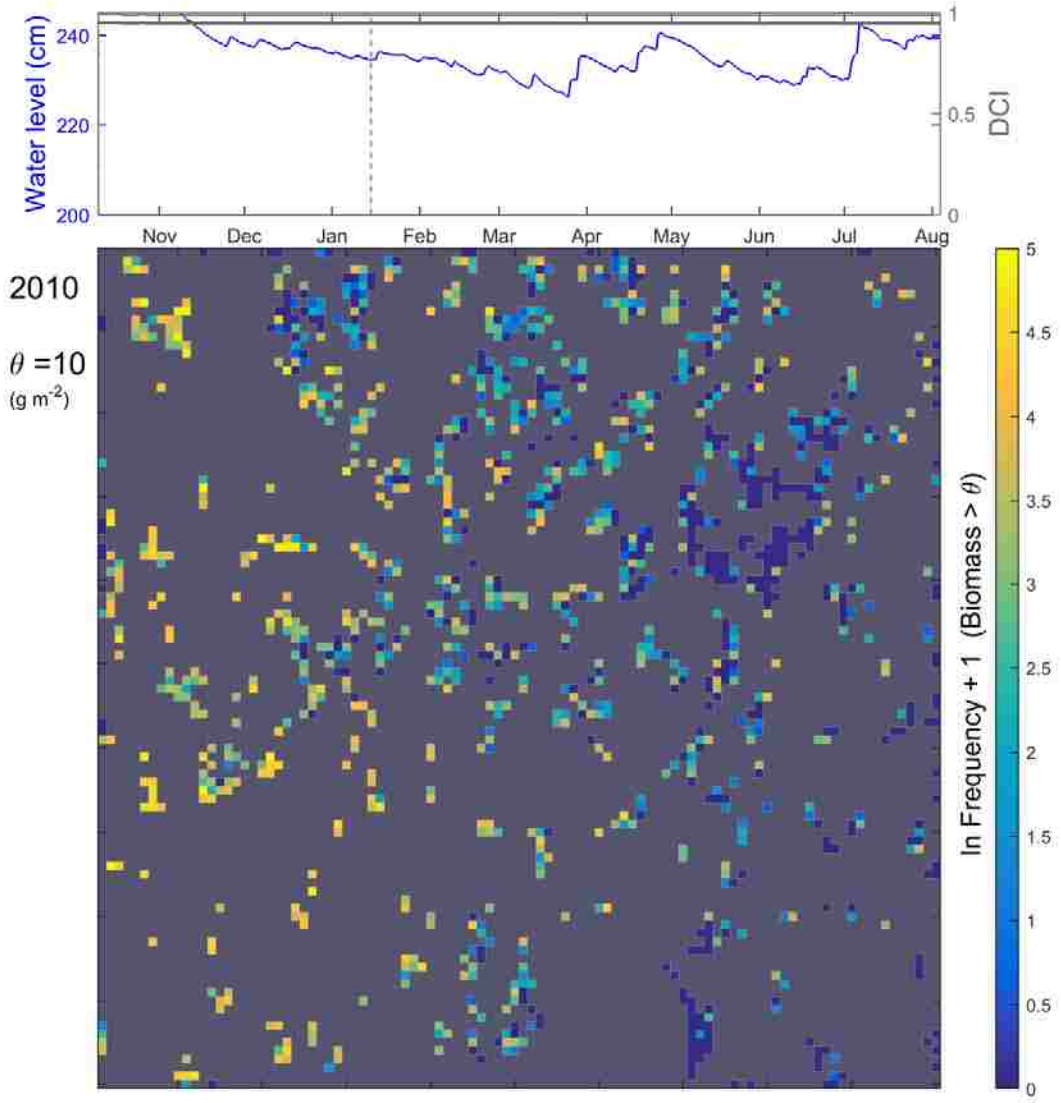

Figure S3G.10B.

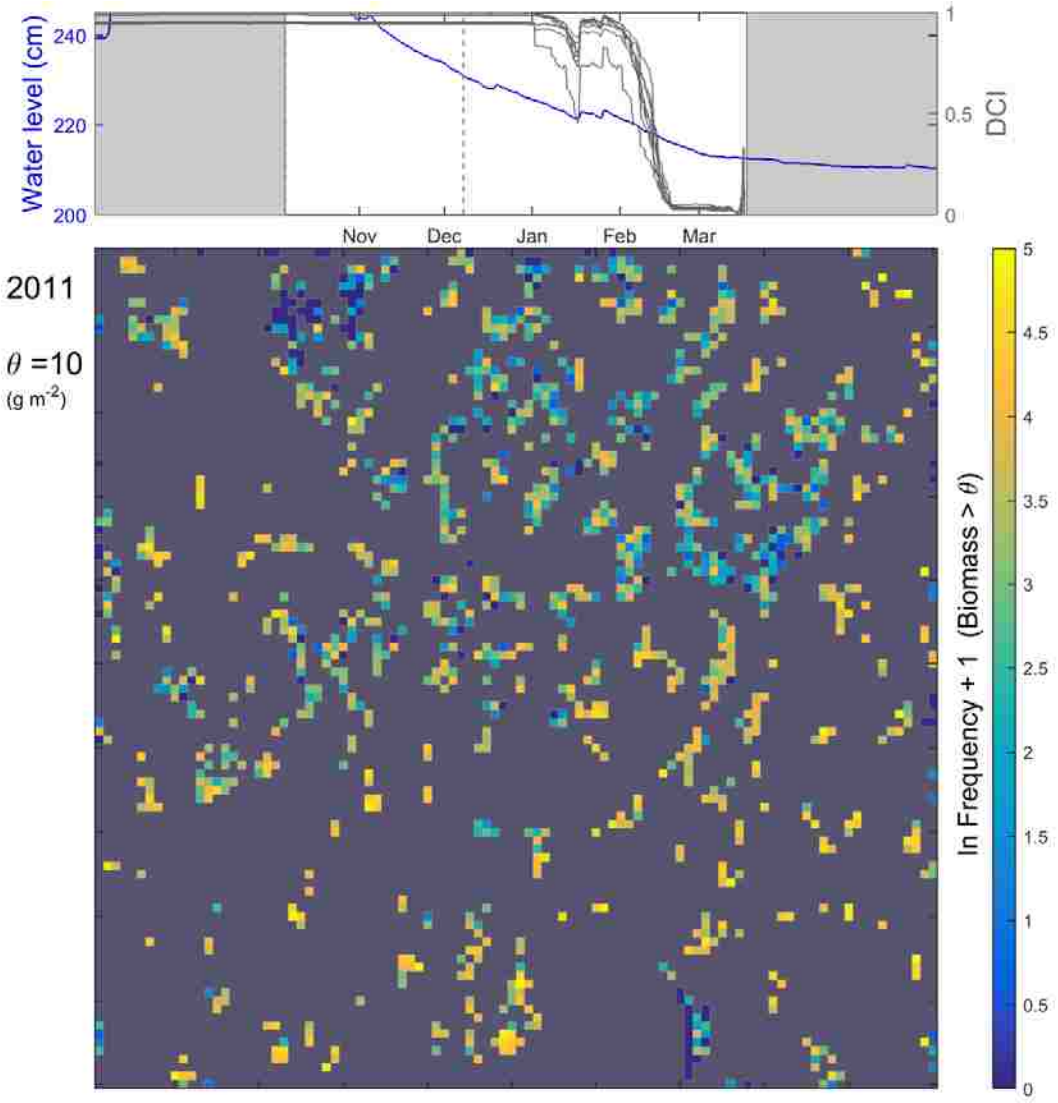

Figure S3G.11B.

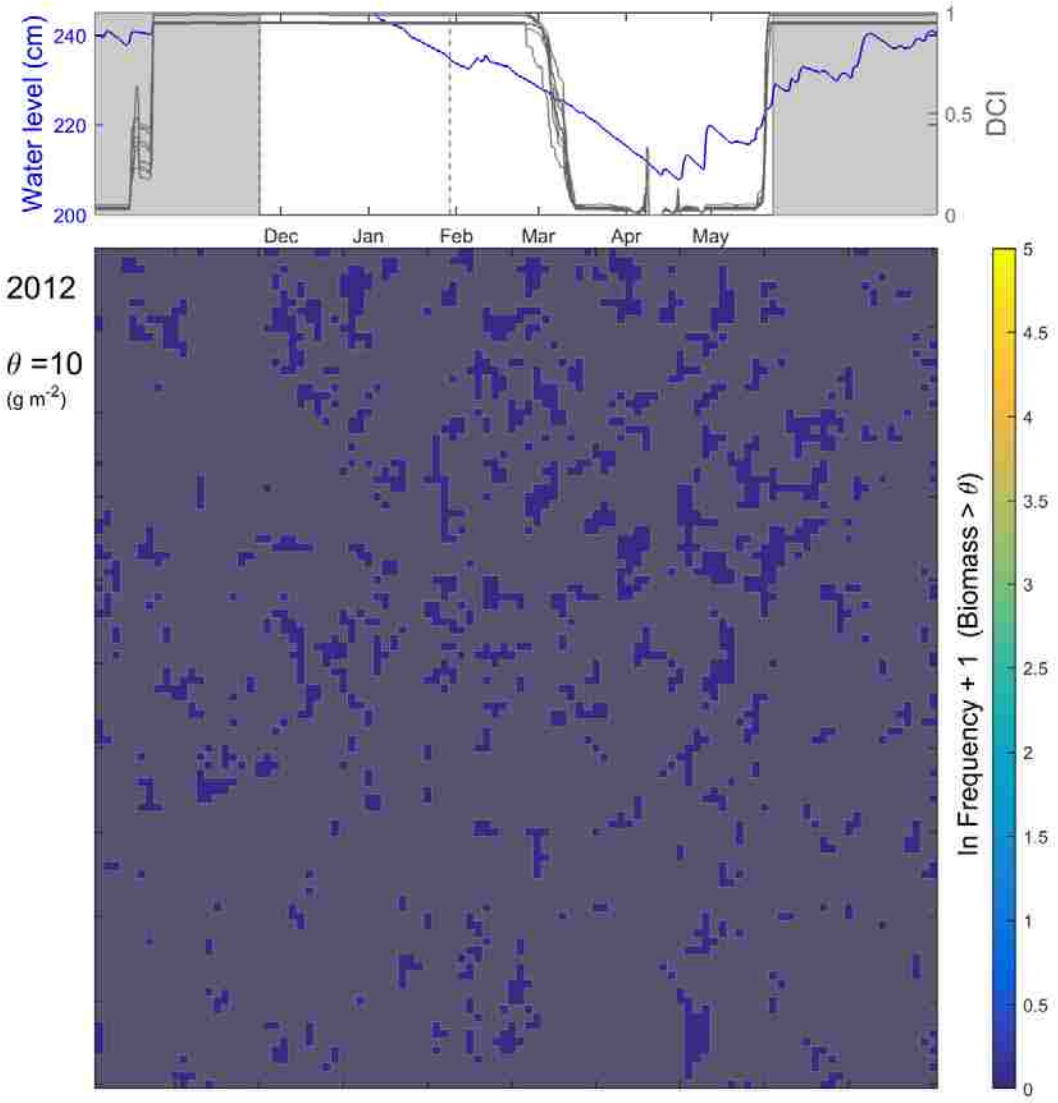

Figure S3G.12B.

Chapter 4

Generation of ridge−and−slough landscape topographies for use in the simulation model Fish Dispersal on Aquatic Landscapes (FDAL)

Summary

Two areas of Everglades ridge−and−slough landscape (RSL), one intact and one degraded, were modeled as three dimensional topographies for use in FDAL, a simulation model of food web interactions and dispersal and concentration of small−bodied fish (< 8 cm) on hydrologically pulsed, freshwater wetlands. Seasonal drying of the Everglades wetlands over RSL structure is hypothesized to be a critical process that spatially concentrates fish in high densities, making them available to top predators. FDAL was developed to test this hypothesis by simulating concentration phenomena on spatiotemporally dynamic hydroscapes. However, it was not known if the geodetic elevation data available for the Everglades are appropriate for modeling RSL, because they are not resolved at the scale of its structure (20−100 m). Thus, elevation data of the Digital Elevation Model (DEM) of the Everglades Depth Estimation Network (EDEN) were tested for differences between ridges and sloughs, which was expected to be ~15 cm. The DEM data were not sensitive to RSL structure, and instead described topographic relief at a macro−spatial scale of > 1 km. A methodology was then developed for post−calibrating the DEM data with other empirical and geodetic datasets. RSL topographies were manually constructed by combining two landscape layers: (1) a baseline layer that was derived from the DEM elevation data, that represented the regional gradient at a scale of kilometers, and (2) a layer that described elevation

differentials between RSL plant communities (i.e., ridges, sloughs, and tree islands), derived from maps of Primary Study Units (PSUs), and an empirical study that classified water depths for these communities. Two topographies were developed that simulated intact and degraded RSL habitat, and were compared to the DEM data. The complete process of generating these landscapes is presented here.

Background

Landscape structure mediates the timing and directional patterns of movement of many species of biota (Ovaskainen et al. 2008). Habitats that are used for movement are often part of larger mosaics that connect them. The relative connectedness of these habitats can change over time, as landscape structure changes, and as habitat quality varies with different environmental conditions (Tischendorf & Fahrig 2000b). Movement on dynamic landscapes can be complex, because movement behaviors interact with changes in landscape structure and habitat quality, which varies according to species' adaptations and life history strategies. Spatial heterogeneity of the landscape can further alter species movement patterns, for example, by channeling and concentrating movements in localized areas (Goodwin & Fahrig 2002).

To better understand these complex movement patterns, ecologists have endeavored to distinguish between effects on movement due to the physical landscape, and due to the biological movement strategies themselves (Calabrese & Fagan 2004). Different types of connectivity have been defined: 'structural connectivity', which refers to the physical connections between parts of the landscape, and 'functional connectivity', which refers to a species' ability to navigate these connections (Larsen et al. 2012, Ovaskainen et al.

2008, Tischendorf & Fahrig 2000a). Some debate has ensued over the definition of these terms, because they are interrelated, and also over which metrics best describe landscape effects on movement (Goodwin 2003).

Some insight into how structural and functional connectivity contribute to complex movement patterns can be gained by simulating different landscape topographies, and the ecosystem dynamics and behavioral movements that occur on them. Individual− and agent− based models (I/ABM) are often used in this way to isolate the effects of the landscape from biological processes, by varying movement strategies over different types of landscapes (DeAngelis et al. 1998). Results and interpretation of model simulations can vary greatly with different levels of realism, particularly when landscapes are modeled with spatially explicit precision (DeAngelis & Yurek 2016). Accurate geodetic data are therefore required to develop the simulated topographies.

One important consideration in modeling landscapes is to ensure that the ecological scale at which habitat selection and ecosystem processes are thought to occur is appropriately represented. Multiple scales can be possible (Levin 1992, Mayor et al. 2009). Landscape data are not always available at the required scale, because measurement at fine spatial scales in the field may not be logistically feasible, or the relevant scales may not be known. These deficiencies can be compensated for by combining, in layers, information from data sets at different spatial scales, to produce simulated topographies. Guidelines have been developed for ensuring that the simulated environment is relevant to the processes being studied, agrees with model assumptions, and does not introduce extraneous complexity (Grimm et al. 2010, Rose et al. 2015).

Here, I describe a methodology for modeling complex wetland topographies from elevation data and parameters that describe vegetation and hydrology. To demonstrate this application, ridge−and−slough landscapes (RSL) of the Everglades (FL, USA) were simulated. The RSL is a parallel drainage wetland geomorphology that is formed through heterogeneous spatial patterns of vegetation growth and peat accretion (Bernhardt et al. 2004, Larsen et al. 2007, Larsen & Harvey 2010). Changes in the overland freshwater flow regime in the Everglades has led to infilling of sloughs in some areas, loss of slough habitat, and encroachment by sawgrass (Davis et al. 1994, Ogden 2005). To examine effects of these habitat shifts on fish movement, intact and degraded RSL topographies were generated for use in FDAL, a simulation model of fish movement in response to changing hydrologic conditions (Yurek et al. 2016). These landscapes were based on maps of two study areas of the Everglades called Primary Study Units (PSU), 23 and 108, representing intact and degraded RSL structure, respectively (Figure 4.1).

Elevation data were needed to construct the RSL topographies, although it was not clear if the Digital Elevation Model (DEM) of the Everglades Depth Estimation Network (EDEN, Jones et al. 2012) was able to describe the fine scale of the RSL. Thus, the available elevation data were tested for differences between ridges and sloughs by selecting the DEM data that correspond with the PSU maps, and assigning vegetation types for each DEM point. When the DEM data were unable to reflect RSL patterns, the vegetation maps of PSUs 23 and 108 were converted to topographies using a combination of data representing macroscale (1−20 km) elevations supplied by the DEM, mesoscale (20−100m) height differentials relevant to the RSL, and randomized microscale (1−20m) "roughness" representing variations in the underlying geology.

Methods: Testing the DEM data

Overview

Elevation data of the DEM were modeled by Jones et al. (2012) on a grid (400 × 400 m) that is broader in scale than the structure of the ridges and sloughs, which are generally 20−100 m wide. Elevations were interpolated to the DEM scale from empirical measurements, and the model was calibrated to ensure high accuracy (±15 cm). This model was designed primarily for application to hydrodynamic modeling at the regional scale (Jones et al. (2012). It was therefore of interest, to applications of fish modeling, to see if the DEM points at the 400 m scale actually correctly indicated ridges and sloughs, when superimposed on a fine scale map.

The DEM data were tested by manually assigning habitat identifiers (e.g., slough, ridge, bayhead, etc.), based on Geographic Information System (GIS) maps of PSUs 23 and 108, and then comparing elevation differentials between habitat types. First, all DEM points were found within the two PSUs, and were associated with a GIS polygon that represented a vegetation patch. Because the polygons specified only common names of plant taxa (e.g., sawgrass, spikerush), and not an explicit RSL habitat type (e.g., slough), an empirical study by Givnish et al. (2008) was used as an intermediary to convert the plant identifier to an RSL habitat type. This study defined eight vegetation community categories and their respective dominant taxa (see below). Elevation data were then tested for differences across habitat type with basic nonparametric statistics.

PSU locations and characteristics

PSUs 23 and 108 are located in southern Florida (USA), in northern Water Control Area (WCA) 3A and southern WCA−3B, respectively (Figure 4.1). PSU 23 is 2 × 2 km, while PSU 108 is also 2 km wide, but is 2.5 km from north to south. PSU 23 is 27 km northwest of PSU 108, and is 71 cm higher in elevation. The mean elevations of PSUs 23 and 108 are 214.8 cm and 143.9 cm (relative to the North American Vertical datum; NAVD88), respectively. These distances and heights are approximate, and can differ from on−the−ground measurements.

The DEM elevation data show that the locale of PSU 23 has more topographic relief than that of PSU 108 (Figure 4.2), and the two PSUs are also oriented in different compass directions. PSU 23 is located in a depression on the landscape and slopes downward to the north, and is angled 0.336 radians west of north, while PSU 108 is in a generally flat area and slopes upward to the north−northwest, and is angled 0.035 radians. Elevations taken at DEM coordinates within an area surrounding PSU23 of radius of 3.2 km (arbitrarily chosen) differ by as much as 27.5 cm from each other, while similar elevations for PSU 108 differ by only 11.9 cm.

PSU vegetation maps

Vegetation communities of the PSUs were described by Graphic Information System (GIS) shapefiles (Watts et al. 2010, Figure 4.3). The boundaries of each community were delineated by vertices with coordinates in Universal Transverse Mercator (UTM) units. Each polygon had a plant cover category identifier (e.g., Sawgrass Marsh, Spikerush−Waterlily Marsh, etc.). PSU 23 had 209 polygons, while PSU 108 had 392. Elevation data were not available for these maps.

Assigning habitat type

The eight categories from Givnish et al. (2008) were reduced to six for this study for practical reasons, and because some distinctions could not be made with the PSU data. The two sawgrass categories, short and tall, were combined into one, and 'ridge−tree island transition' was not used. Givnish et al. (2008) listed the following taxa for each category: **flooded slough** had water lily (*Nymphaea*), bladderworts (*Utricularia*), and periphyton; **emergent slough** had spikerush (*Eleocharis*); **sawgrass** had (*Cladium jamaicense*); **low tree island** (fringes and tails of tree island) had pond apple (*Annona glabra*), button bush (*Cephalanthus occidentalis*), and coastal plain willow (*Salix caroliniana*); and **tall tree island** (raised cores and bayheads) had cocoplum (*Chrysobalanus icaco*), Florida strangler fig (*Ficus aurea*), southern wax myrtle (*Myrica cerifera*), and swamp bay (*Persea palustris*). No taxa were listed for **slough−ridge transition**. Following these assignments, I defined six FDAL habitat types (bold italic) to include the following PSU common name identifiers:

- ***Tall tree island***: Bayhead Shrubland, Bayhead Swamp Scrub, Bayhead Forest.
- ***Low tree island***: Willow Scrub, Willow Scrub−Cattail Marsh, Willow Shrubland−Sawgrass/Cattail Marsh, Willow Scrub−Sawgrass Marsh, Willow Shrubland.
- ***Sawgrass***: Sawgrass Marsh.
- ***Slough−ridge***: Panicgrass−Spikerush Marsh, Sawgrass−Waterlily Marsh, Sawgrass−Cattail Marsh, Spikerush−Sawgrass Marsh.
- ***Emergent slough***: Cattail Marsh, Spikerush Marsh, Spikerush−Cattail Marsh.
- ***Flooded slough***: Spikerush−Waterlily Marsh, Water (Gator Hole), Waterlily Marsh.

Analysis of ridge−and−slough elevations in DEM data

Givnish et al. (2008) reported an elevation difference of ~15 cm between sloughs and ridges, which is similar the 10−20 cm described by Harvey et al. (2009), and Watts et al. (2010). I hypothesized that the DEM elevation data points would reflect a similar range of differentials when compared to known ridges and sloughs within the boundaries of the PSU. To test this hypothesis, each DEM point was associated with the polygon containing it (Figure 4.3), and one of six habitat types was assigned (per above). Statistical differences between ridge−and−slough elevations were tested by a Wilcoxon rank sum test at $\alpha = 0.05$ under the null hypothesis: $\mu_{ridge} = \mu_{slough}$.

The macroscale features of the DEM topography, described above in *PSU locations and characteristics*, appeared to reflect patterns at the 1 to 2 km scale. It was therefore of interest to estimate this spatial scale of relief, because it may describe a topographic pattern that was specific to the local area of the landscape where the PSUs occur, and not necessarily to RSL topography. This was done by fitting polynomial surfaces to the UTM coordinates (x,y) of each PSU using the function *fit* in Matlab, including up to third order terms, following the model: $DEM = Intercept + x + x^2 + x^3 + y + y^2 + y^3 + \varepsilon$.
For each PSU, the residuals of the fit, the coefficient of determination adjusted by degrees of freedom (CD), and the mean squared error (MSE) were calculated.

Results: Testing the DEM data

No differences between ridge and slough elevations were found for both PSU 23 ($U = 109$; $p > /z/ = 0.67$), and PSU 108 ($U = 116$; $p > /z/ = 0.17$), suggesting that the DEM data are not sensitive to elevation differences at the horizontal mesoscale (Figure 4.4).

The mean elevation for DEM data points for PSU 23 increased slightly from slough to ridge, but only by 0.65 cm. The mean elevations of PSU 108 did not show any trend, and decreased from slough to ridge.

The fitted polynomial surfaces generally described increases in elevation over a scale of ~2 km (Figure 4.5). The surfaces fit the data well, with maximum deviation of the DEM elevations from the surfaces being ~1.25 cm for both landscapes (PSU 23 CD = 0.986, MSE = 0.874; PSU 108 CD = 0.899, MSE = 0.619). These surfaces are likely representative of the interpolation procedures by Jones et al. (2012). The results of the elevation tests and the surface fits lead me to conclude that the DEM data alone were not adequate for modeling RSL topographic structure, and that supplementary information was required. The topographic variability in Figure 4.5 was deemed to represent local features that could potentially create landscape effects that were not intended in the fish modeling, and also obscure those of the RSL. It was therefore removed (see below).

Construction of topography

Overview

The general methodology for creating the three dimensional topographies was to superimpose a grid of 100 × 100 cells, also used in FDAL, onto each of the PSU maps, so that an area of approximately 2 × 2 km was captured within the PSUs (Figure 4.6), and then assign elevations to each grid point. The elevations were calculated as the summation of: (1) a baseline regional elevation that was derived from the DEM (macroscale, 1−20 km), (2) an elevation differential relevant to the ridge−and−slough

(mesoscale, 20−100 m), and (3) additional randomized variability for each grid cell (microscale, 1−20 m).

FDAL grids

FDAL topographies were built on grids of 100 × 100 square cells that were 20 × 20 m each. This resolution was chosen to represent RSL topographic structure at a spatial scale that allowed fishes to move between and among ridges and sloughs (see Kahl 1964, Kushlan 1976b). Ridges and sloughs in the Everglades are generally 20−50 m wide, although in some places they can exceed 100 m in width. With a grid cell resolution of 20 m, the simulated ridges and sloughs in the FDAL model were 2−5 cells wide (or more), allowing elevation variability within ridges and sloughs. This relief was necessary to give the fish options to disperse in different directions, within ridges and sloughs, so that they can accumulate within a habitat type, simulating behaviors and spatial heterogeneity of fish distributions that are observed in the field (Trexler et al. 2002). In Chapter 3, simulation of movements that implicitly represent both horizontal and vertical movements was required. If the grid cells were wider, movement such as entrainment in local embayments or cul−de−sacs would not be possible, and the spatial movement patterns would be dominated by vertical ridge−slough movements.

The UTM coordinates of the FDAL grid cells were determined by finding the centroids of each PSU and building vertices outward from them at 20 m increments (Figure 4.6). Since square grids were desired, some of PSU 108 was clipped off by manually adjusting the centroid 200 m to the north, and selecting the northern part of the PSU. Both grids were rotated anti−clockwise (0.336 radians for PSU 23, and 0.035 radians for PSU 108) to align with the orientation at which the PSUs were mapped.

Assigning macroscale baseline elevations using DEM data

The primary landscape variables of interest for FDAL were annual hydrology and RSL structure. The topographic variability that was present in the modeled DEM elevations, at the scale of 2 km, and described above (Results and Figure 4.5), was deemed to conflict with this focus, so the orientation and pitch of PSUs 23 and 108 were standardized. Both landscapes were rotated clockwise so that the ridge−and−slough structure was aligned in the same direction for both grids, to the north, and the pitch of the landscapes was from northwest to southeast. The pitch and local topography were standardized by fitting a flat surface to the DEM elevation points, shown in Figure 4.2, using the function *fit* in *Matlab*. The fit object, *f*(DEM), was evaluated at each FDAL grid coordinate to create the baseline macroscale topography (Figure 4.7).

Assigning mesoscale RSL elevations

RSL structure was built onto the baseline landscapes by applying elevation differentials, derived from Table 4 of Givnish et al. (2008), for each of the six FDAL habitat types defined above. First, each FDAL grid cell was assigned a habitat type using the same methodology as for the DEM analysis (see section *Assigning habitat type*), producing gridded zones representing one of the possible habitat categories (Figure 4.8).

Then, elevations were assigned for each category. This required converting the water depths from Givnish et al. (2008) to proxy elevation differentials as follows. Table 4 of Givnish et al. lists the maximum, minimum, and average water depths of each habitat type for northern WCA−3A and southern WCA−3B, corresponding to PSUs 23 and 108, respectively. Elevation differentials were inferred by subtracting the water depths from an arbitrarily selected zero−point that was defined as the mean of the short and tall sawgrass

categories (Figure 4.9). These water depth differentials are shown in Figure 4.9 for all eight categories, and from here on are assumed to represent elevation differentials. For both landscapes, flooded sloughs (FS) were ~11 cm below sawgrass height, and emergent sloughs (ES) were ~10 cm below. These two categories, along with sawgrass ridges, comprised most of the FDAL grid cells for both PSUs (Figure 4.8). The other categories differed between landscapes (Figure 4.9), and ridge−tree island (R−T) for PSU 23 was below sawgrass elevation, possibly because it represents unvegetated areas under trees that become scoured out by water flows.

The differences in the tree island communities between PSUs were not relevant to the fish modeling, and also comprised a small area of the landscape (Figure 4.8). Tree islands were generalized by taking rounded estimates across PSUs. Including these simplifications, the following differentials were applied to both landscapes: Tall tree island (+35 cm), Low tree island (+20 cm), Sawgrass (+0 cm), Slough−ridge (-7 cm), Emergent slough (-10 cm), Flooded slough (-11 cm).

Assigning microscale randomly applied variability

The composite baseline (macroscale) and RSL (mesoscale) topography were given additional random elevations to simulate microscale variability due to the underlying geology, such as solution holes, or soil substrate dynamics, such as vertical expansion and contraction of peat (Chambers et al. 2015, Jones et al. 2012, Gleason & Stone 1994, Whelan et al. 2005). These elevation differences were determined by randomly drawing numbers from a normal distribution with mean = 0 and S.D. = 1 cm, using function *randn* in Matlab. The goal of adding microtopography was to vary the elevation difference between ridge and slough on a single cell basis, to create elevation differences within

habitat types, and to vary the heights of neighboring cells with respect to each other. This spatial variation is essential for simulating a variety of habitat conditions available to the fish for selection, leading to spatially heterogeneous patterns of fish movement.

Final landscapes

Figure 4.10 shows the final topographies that were developed to represent PSUs 23 and 108. Both of the landscapes are oriented north−south, and the elevations are pitched downward to the southeast. PSU 23 shows much more RSL relief than PSU 108, which more closely resembles a flat plane. The total area of slough habitat, which is important for concentrating fish (Kahl 1964), varies between PSUs. The total number of slough cells for PSU 23 is 4,181, and is 1,251 for PSU 108. Tree islands and bayhead transition habitats occur on both landscapes, but comprise a small area of the total landscape. Nonetheless, they are important and realistic barriers to dispersal, and affect the directional connectivity over the entire 2 km of the landscape, as well as the calculations of this metric (Larsen et al. 2012).

Final remarks

This study tested high accuracy elevation data of the Everglades landscape (DEM) for RSL patterning, and described a methodology for manually constructing RSL topographies. The DEM elevation data were modeled on a grid at 400 x 400 m resolution. At this scale, the macrotopography of regional elevation gradients, and other variation at a 1 to 2 km scale, can be detected. However, the scale of the RSL is finer (20−100 m). The DEM did not reflect RSL structure at the mesoscale, so topographies for PSUs 23 and 108 were manually constructed using a combination of DEM data, mapped empirical

study units (PSUs), empirical estimates from Givnish et al. (2008), and randomly applied roughness.

These three elevation layers represented topographic variability across macro−, meso−, and microscales. Ecological processes of movement behaviors of small−bodied fishes, and trophic interactions that result from their concentration and availability to top predators, are likely to vary qualitatively across these scales. All three of these scale levels could potentially impact the spatiotemporal patterns of fish concentration during the drying phase of the Everglades. Although, variables representing these scales are generally not available to be combined in one analytical platform. One practical reason is that quantifying this variation with on−the−ground measurements is not feasible over such a large expanse of wetlands.

This study demonstrated that computer modeling can be used to overcome limitations of empirical data collection, and of computer generated landscape DEMs, by combining targeted empirical measurements with layered GIS products, in a way that is ecologically relevant. It can be applied to larger scale projects, such as the Decompartmentalization Physical Model (USACE & USDOI 2015), so that areas of the Everglades are modeled with realistic boundary conditions, such as canals and levees, or to the RSL in Loxahatchee National Wildlife Refuge (Bernhardt & Williard 2009).

Figures

Figure 4.1. Location of PSUs 23 and 108 in southern Florida, USA. PSU 23 is located in the northern part of Water Control Area 3A (WCA). PSU 108 is in the southern part of WCA−3B.

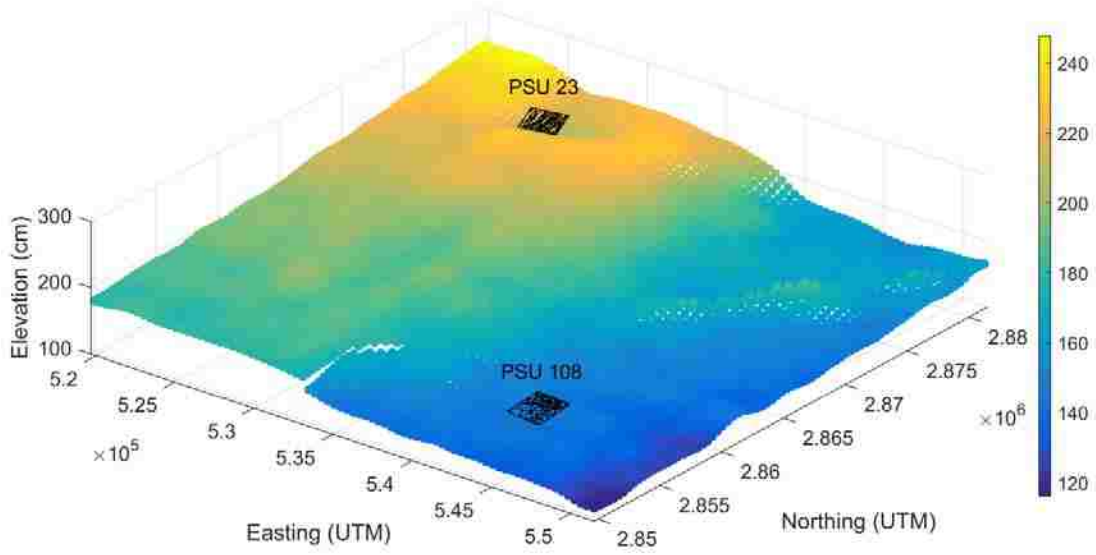

Figure 4.2. Topography of the region of the Everglades containing PSU 23 in northern WCA−3A, and PSU 108 in southern WCA−3B. Colored points are EDEN DEM elevations (NAVD88 cm). Shapefiles for PSUs 23 and 108 are mapped in black lines. PSU 23 is approximately 71 cm higher than PSU 108.

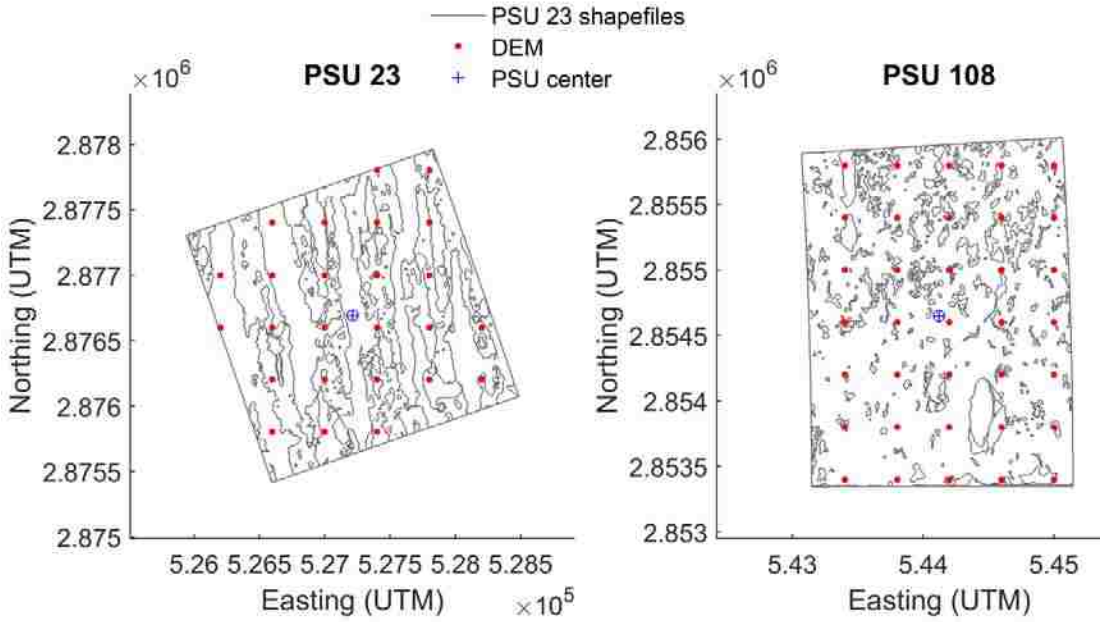

Figure 4.3. EDEN DEM elevations (NAVD88 cm) within the mapped areas of PSU 23 (left) and PSU 108 (right). Blue cross/circle represents the centroids of the PSUs.

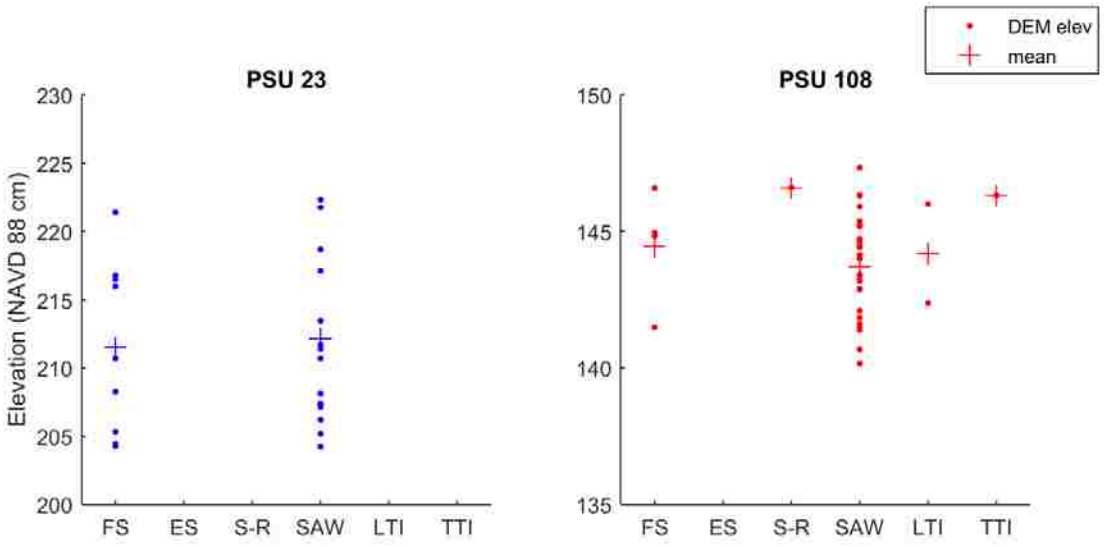

Figure 4.4. EDEN DEM elevations (NAVD88 cm) plotted by vegetation category for PSU 23 (blue) and PSU 108 (red). The six categories are: flooded slough (FS), emergent slough (ES), sawgrass−ridge (S−R), sawgrass (SAW), low tree island (LTI), and tall tree island (TTI). Mean elevations for each category are indicated by cross (+). Note: Some categories did not have DEM points that fell within them.

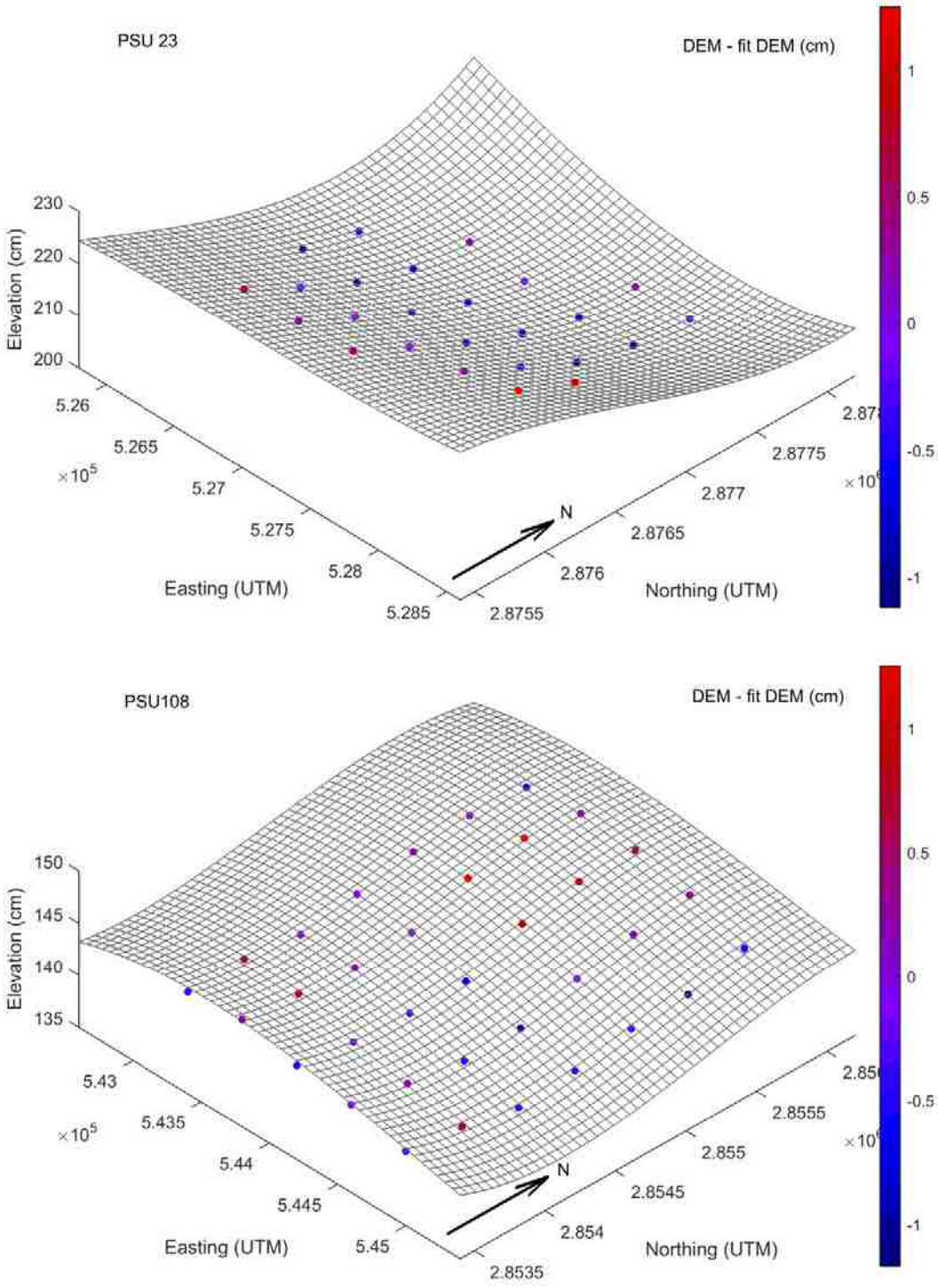

Figure 4.5. DEM elevation points (colored) and fitted polynomial surface (gray mesh) for PSUs 23 and 108. Colors of points indicate the difference between each DEM elevation and the corresponding value on the fitted surface. Arrow indicates north.

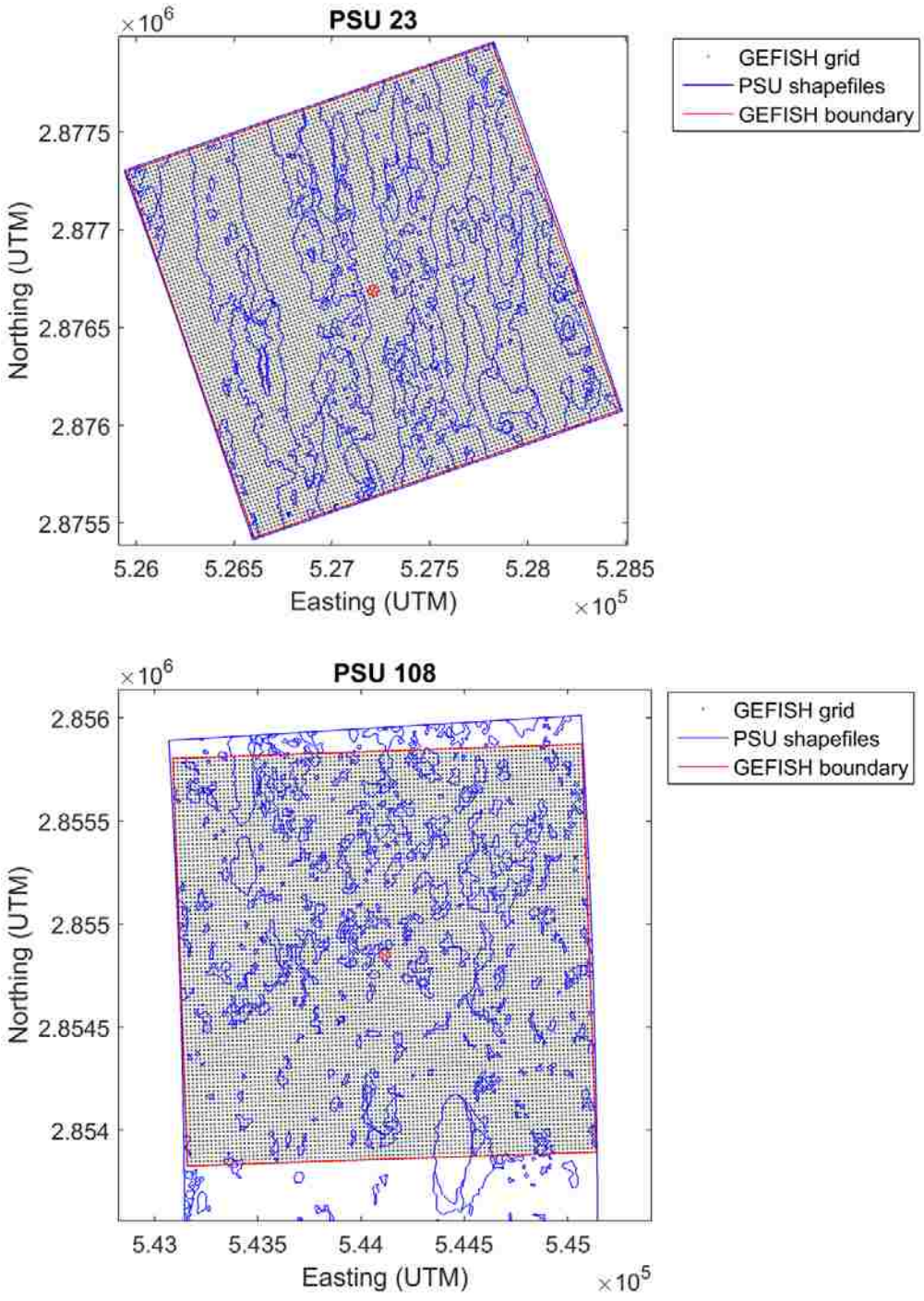

Figure 4.6. Shapefiles (blue lines) detailing vegetation communities of PSU 23 (top panel) and PSU 108 (bottom panel), with FDAL grids (gray dots) rotated to align with PSU orientation. Red circles represent shapefile centroids. Note: PSU 108 centroid was manually adjusted 200 m to the north since the PSU was mapped as a rectangle.

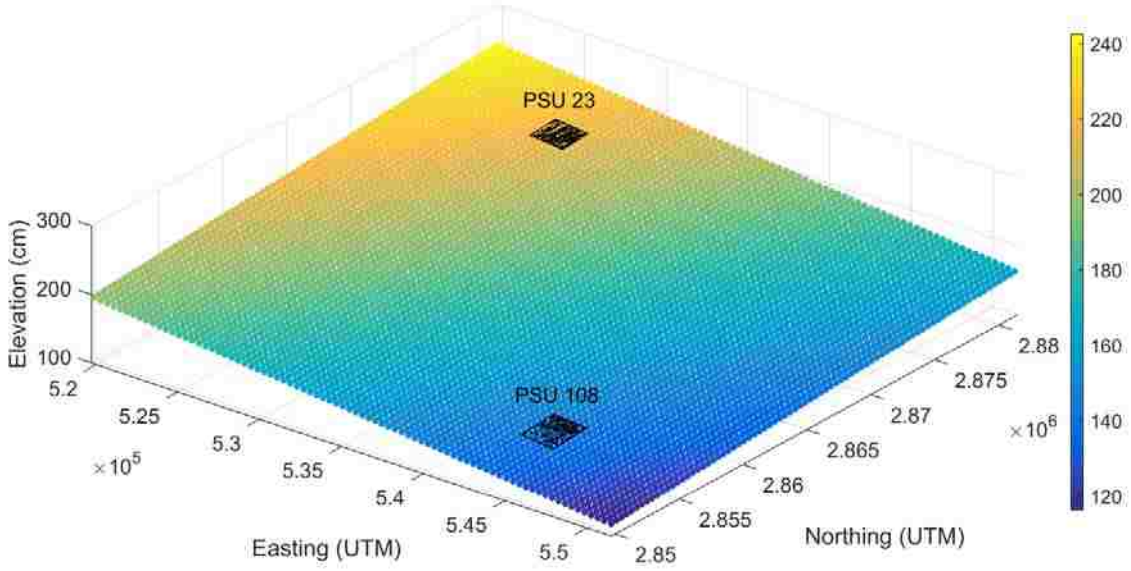

Figure 4.7. Standarized DEM elevations (colored points; NAVD88 cm) created by fitting a plane to selected DEM data in Figure 4.2. These elevations represent the baseline landscapes that were adjusted to have ridge−and−slough structure. PSUs 23 and 108 were rotated clockwise by 0.035 and 0.336 radians, respectively to standardize orientation.

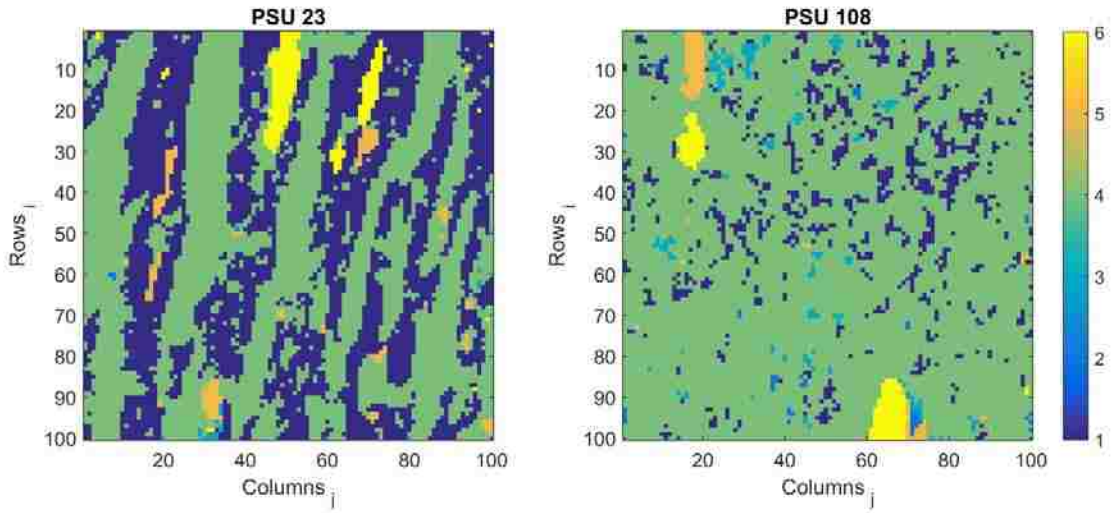

Figure 4.8. FDAL grids (100 x 100 cells) identified by vegetation category, for each PSU. The six categories are (1) flooded slough, (2) emergent slough, (3) slough−ridge, (4) sawgrass, (5) low tree island, and (6) tall tree island. PSU 23 had 4,181 slough cells while PSU 108 had 1,251.

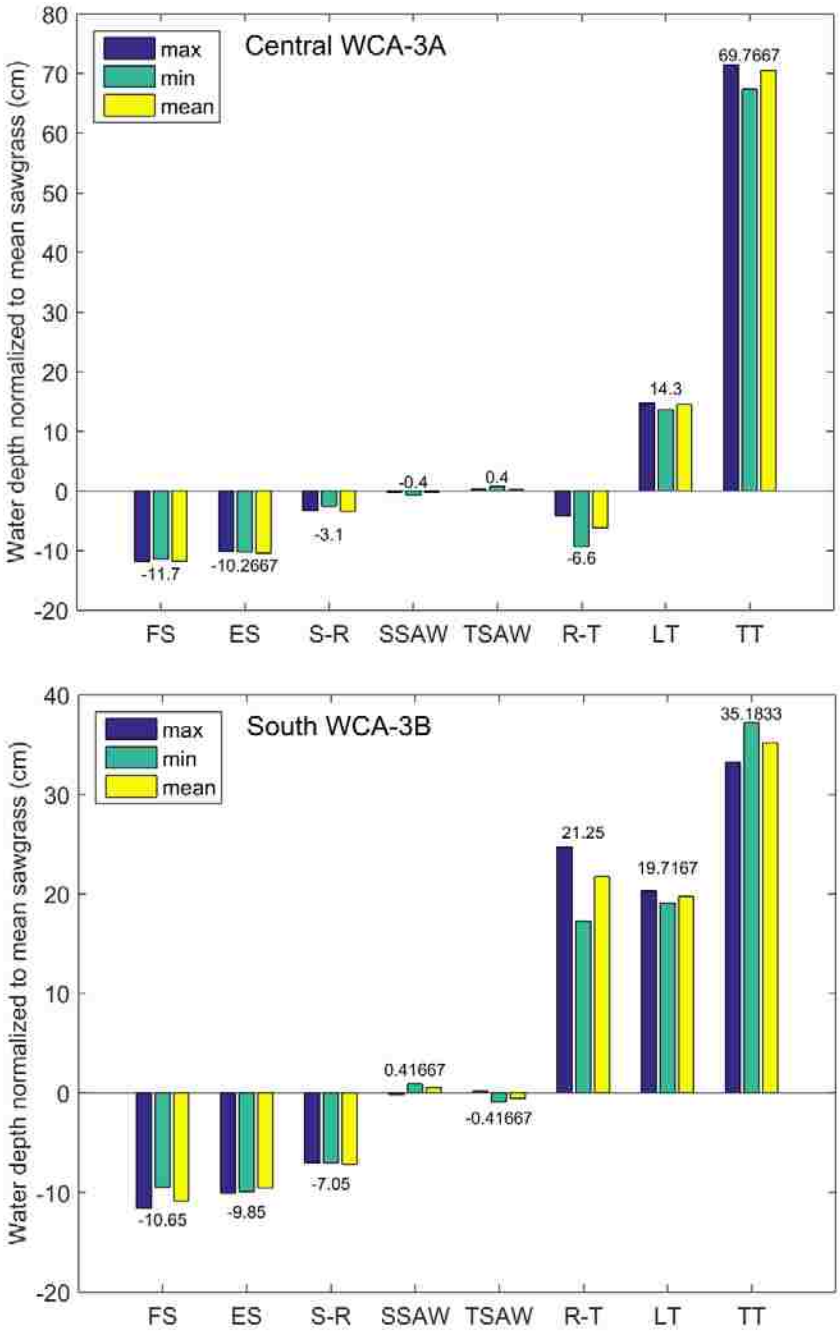

Figure 4.9. Water depths from Givnish et al. (2008) normalized to mean sawgrass depth for two areas of the Everglades near the mapped PSUs. The maximum, minimum, and mean depths from January 2000 to December 2005 are shown. The eight vegetation categories in this study were: flooded slough (FS), emergent slough (ES), sawgrass−ridge (S−R), short sawgrass (SSAW), tall sawgrass (TSAW), ridge−tree island (R−T), low tree

island (LT), and tall tree island (TT). Sites in central WCA−3A were near PSU 23, while sites in south WCA−3B were near PSU 108.

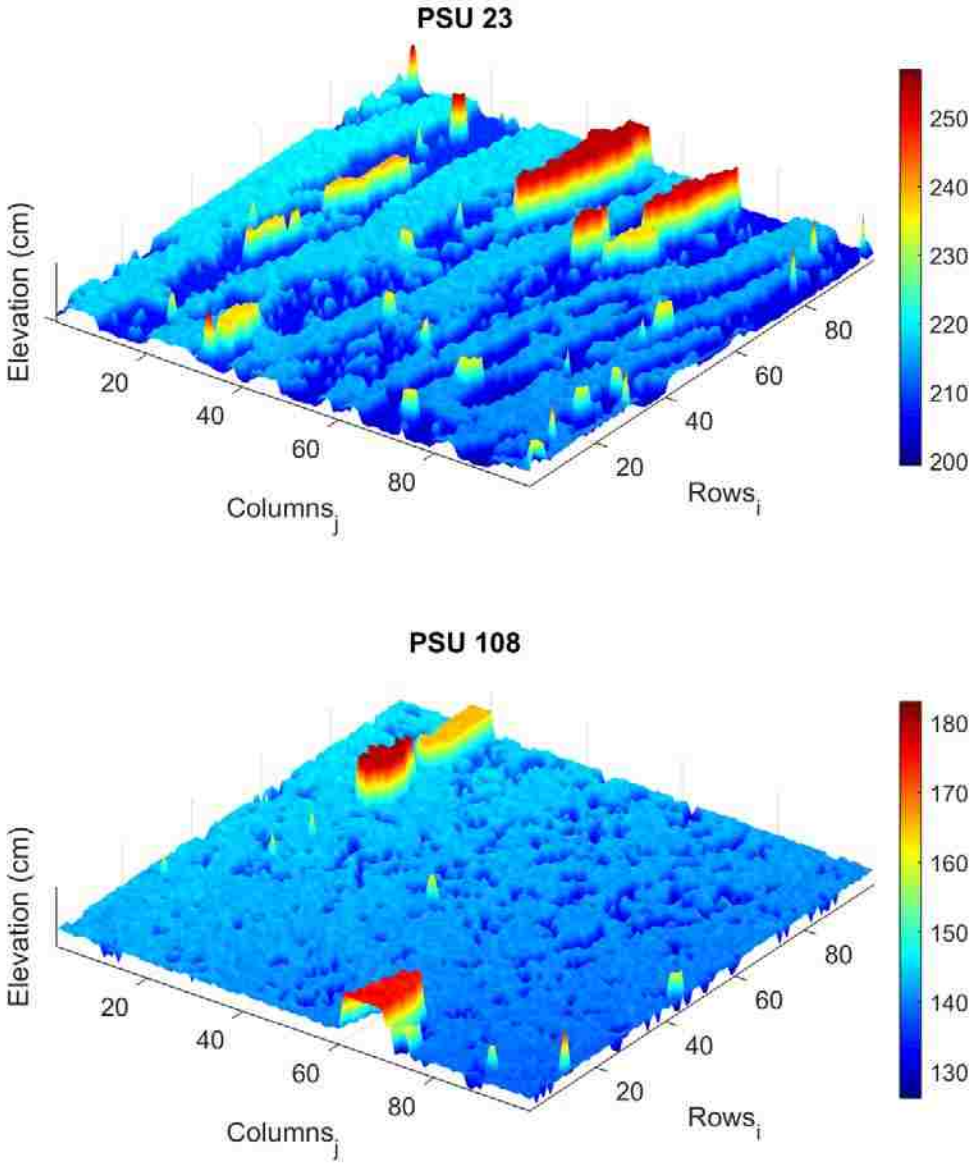

Figure 4.10. Final FDAL topographies for PSUs 23 and 108.

Chapter 5

Fish density responses to hypersalinity and salinity variance at multiple time scales in a seasonally pulsed coastal mangrove ecosystem

Summary

Hypersalinity (> 40 salinity units) is a biologically limiting condition that occurs in many coastal ecosystems, and is likely to increase in frequency, duration, and magnitude under scenarios of climate change and reduced freshwater availability. Predicting population responses and patterns of habitat selection of aquatic biota to frequent hypersalinity is difficult because conditions can be both advantageous and deleterious, depending on severity, and response times can vary through interactions between behavior, population dynamics, and community structure. To evaluate the potential for varying habitat selection patterns in response to hypersalinity in coastal mangrove ecosystems, fish densities were analyzed over different time scales following hypersalinity events along the shoreline of southern Florida, USA. Here, active management of coastal freshwater flows results in prolonged periods of hypersalinity, followed by rapid lowering and high fluctuation of salinity conditions. Quantile regression techniques were used to assess constraining effects of hypersalinity and salinity variance on the upper quantiles of fish densities, over short and long term periods, at the scale of months and years, respectively. Survey data of four common and abundant mangrove fish species were paired with nearby continuous water quality monitoring stations, for a twelve–year time period (2004–2015). For the short term analysis, frequency of hypersalinity and salinity mean and variance were summarized

over 1 and 4 month periods prior to the surveys, and fish densities were regressed on these metrics at each time scale, independently. Seasonal population oscillations were accounted for by including a periodic explanatory variable. For the long term analysis, densities were regressed on measures of time that a survey lagged an event. Densities fluctuated above the ordinary seasonal pattern in the initial phases following an event (1 and 4 months), and the timing varied by species. Densities of *Floridicthys carpio*, a benthic killifish, increased within the first one to two months, while those of small–bodied water column fishes, and larger predatory species, remained low. The trend was reversed in the seven to eleven months post–event. Long term responses showed declines in the densities of all four species over two to three years following events, with approximately four years required for a recovery to pre–event levels. These abrupt shifts could reflect many ecological processes, such as habitat compression, shifts in community and/or predator prey dynamics, and pulsed reproductive or recruitment events, although none of these were explicitly measured. This study provides evidence for variable responses across monthly and annual scales, within and among species, suggesting ecological interactions at the population and community level.

Background

Hypersalinity (> 40 salinity units, Venice System, Anonymous 1959) is a naturally occurring environmental condition in coastal ecosystems. Hypersaline conditions develop when evaporation exceeds freshwater input from precipitation and/or terrestrial inflows, resulting in higher concentrations of solutes than in marine systems (Lohman et al. 2012). Factors that contribute to hypersalinity are high temperatures,

shallow water depths, low atmospheric moisture, reduced or obstructed freshwater flows, and their combinations (de Silva Samarasinghe & Lennon 1987, Savinije & Pages 1992). Hypersaline conditions occur in tropical and subtropical ecosystems during hotter months of the dry season (Kelble et al. 2007), and in other arid ecosystems.

Aquatic biota are differentially adapted to hypersaline conditions (Nordlie 2006), and biological responses to hypersalinity can vary for individuals and populations. Hypersalinity can be advantageous at low levels, for example, by increasing prey mortality (Turner et al. 2014). Some species positively select habitats with hypersalinity, possibly due to exclusion of their competitors or predators (Jerling et al. 2010, Kristensen 1963, Vivier et al. 2010). Alternatively, motile species can avoid hypersalinity through movement. Behavioral avoidance was demonstrated in laboratory experiments by the euryhaline fishes, *Floridichthys carpio* (McManus et al. 2014, Florida, USA), *Mugil liza* (Kristensen 1963, Curaçao), and *Lutjanus griseus* (Serrano et al. 2010, Florida).

Severe and persistent occurrence of hypersalinity can be lethal. Teleost fishes, when taking in hypersaline water, must regulate a four–fold (or greater) increase in salt load across the lumen, and critically, prevent water loss (Gonzalez, 2012), although species have different limits for this ability (Nordlie 2006). Negative responses to hypersalinity can impact population dynamics, for example, by decreasing densities (*Corallinaceae* in Shark Bay, Australia, Harlin et al. 1985), increasing mortality (C*rassostrea gigas* in southern Australia, King 1977), and decreasing reproductive success (*Cynoscion nebulosus* in Matagorda, Texas, USA (Gray et al. 1991; euryhaline fishes, St. Lucia estuary, South Africa, Vivier et al. 2010).

Community dynamics also vary in ecosystems with hypersalinity. In the St. Lucia estuary (above), species abundance and richness were inversely related as hypersalinity increased in areas that were disconnected from inland and marine waters (Jerling et al. 2010). In the Sine Saloum Delta of Senegal, Simier et al. (2004) reported severe limitation on species abundance, richness, and diversity of fishes in hypersaline areas. In the Ria Lagartos lagoon in Mexico, fish densities were higher within the inner, hypersaline areas compared to near the mouth of the system, while species richness, diversity, and biomass were lower (Peralta–Meixueiro & Vega–Cendejas 2011).

Shifts in individual behavior, physiology, reproduction, and overall population size in response to hypersaline events can affect the spatial distribution of species densities, particularly if these occur in combination with compression of suitable habitat. For example, individuals that avoid hypersaline areas through movement behaviors can become concentrated in lower salinity refugia, possibly along the boundary of vacated areas. This phenomenon was documented for *L. xanthurus* and *M. undulates* under limiting conditions of hypoxia in the Neuse River Estuary, North Carolina, USA (Campbell & Rice 2014). Habitat compression can occur temporally as well, by delaying availability of lower salinity habitat, such as is required for foraging and reproduction. Spatially variable and temporally dynamic occurrences of fish concentration are therefore possible through interactions of habitat compression, avoidance behaviors, and pulsed reproductive events. These concentrations can amplify or interfere with ordinary seasonal population cycles, particularly through increases or decreases in reproduction, mortality, prey availability, and predator–prey interactions (Schwartzlose et al. 1999, Turchin 2003).

For these reasons, it is feasible that habitat selection in response to hypersalinity could occur at multiple time scales (Mayor et al. 2009), and would be reflected by changes in fish densities. Responses at three different time scales can be hypothesized: (1) in the initial term following an event (< 1 month), densities are largely determined by foraging and movement behaviors, as fish avoid or utilize hypersaline zones and become concentrated or dispersed, or also leave the system; (2) at the seasonal scale (4 to 6 months), fish densities are impacted by changes in seasonal processes such as reproduction and recruitment, and prey availability; and (3) over the long term following an event (> 1 year), fish densities represent population dynamics that result from combinations of the above factors, and community interactions, such as food web dynamics, which affect annual population cycles. Since it is not feasible to measure all of these ecological parameters empirically (e.g., growth, mortality, reproduction), these hypotheses can be supported, at least through inference, if fish densities are shown to vary with different levels of hypersalinity at each of these time scales.

This study investigated these hypotheses by quantifying density responses of four species of mangrove–associated fishes following hypersalinity events along the southern Florida (USA) coastline, within a twelve–year time period (2004–2015). Since the watershed of this ecosystem is greatly modified, and freshwater flows to the coast are heavily managed, fish may be exposed to a variety of salinity conditions. The first objective of this study was to summarize the salinity regime over the period of record, and the duration of hypersalinity events for each year, to estimate conditions which fish are likely to encounter. The second objective was to test if fish were more or less likely to occur in surveys if hypersalinity had occurred just prior to them, which was tested with

contingency tables. The third objective was to test short term responses, by relating fish densities to metrics of hypersalinity and salinity mean and variance over short term periods of one and four months prior to fish surveys. Finally, long term responses of fish density to hypersalinity, at the scale of years, were quantified using two quantile regression approaches. The fish species in this study have different foraging and life history strategies, and represent two trophic levels of the food web.

Methods

Study area – Nearshore zone of southeast Florida

The focal areas of this study were subtropical, intertidal mangrove shoreline habitats along the southeastern Florida coast (Figure 5.1). These habitats comprise a transition zone from freshwater marshes and upland hammock to subtidal, seagrass habitats. Water depths along the shoreline are generally less than 1m and fluctuate with tides, winds, and freshwater flow. Freshwater input into the nearshore zone is primarily through overland flow, with additional amounts from precipitation and groundwater (Stabenau et al. 2015, Stalker et al. 2009). The nearshore zone is an area of conservation and restoration concern because of its high secondary productivity that supports nearby corals reefs and recreational fishing (Faunce & Serafy 2008, Jones et al. 2010), and because it has been intensively engineered for flood control and water management.

The principal coastal water bodies are, from north to south, Biscayne Bay (BB), Card Sound (CS), and Barnes Sound (BS) (Figure 5.1). These seasonally pulsed lagoons were historically connected to the greater Everglades freshwater wetland, and received consistent overland and groundwater flows, maintaining stable, limnetic and oligohaline

conditions along the coast (Wingard et al., 2004). This hydrologic regime has been altered over the past century through channelization of freshwater flows throughout much of the greater Everglades watershed (see Figure 5.1), resulting in a fluctuating polyhaline system along the coast (Wingard et al. 2004). Within the past 25 years, restoration of flows to coastal wetlands has been mandated (USACE 1999). Currently, freshwater is delivered primarily by five major, actively managed canals.

Flora and fauna of the nearshore habitats represent mangrove and seagrass communities, with some transient reef species. Mangrove tree species are dominated by *Rhizophora mangle* and *Avicennia germinans*, and seagrasses include *Thalassia testudinum*, *Halodule wrightii*, and *Syringodium filiforme*. In many areas, a narrow band (1–2 m wide) of unconsolidated mud or peat bottom separates the mangrove and seagrass habitats along the mangrove fringe, often covered with accumulations (3–15 cm) of macroalgae, leaf litter, and other detritus. Many species of fish, invertebrates, and wading and water birds, as well as the American crocodile and alligator, use the nearshore zone.

Fish study species

Mangrove and seagrass fish communities have been monitored over the past 10 to 15 years through a long–term interagency program. I selected species for this study that are common and abundant in these surveys, and that have well–documented life histories. These included *Lutjanus griseus*, *Sphyraena barracuda*, *Floridichthys carpio*, and a super–species grouping of A*therinidae*, *Clupeidae*, and *Engraulidae*. It was not possible to identify individuals of the latter grouping to species, visually, due to large school sizes. For simplicity, they are referred to here as a single functional group of water column fishes, *Ath–Clup–Eng*. Fishes were surveyed visually along the mangrove fringe,

following a stratified random design (Serafy et al. 2003; 2007). Briefly, a swimming observer using snorkeling gear recorded the number of individuals of all fish species in mangrove prop roots along a 30 × 2 m transect, producing measures of fish density (number of individuals per transect). Salinity was recorded during the survey using a YSI 650 MDS data sonde. Surveys were conducted seasonally, during the wet (August–October) and dry (January–March) seasons. See Serafy et al. (2003) for complete monitoring protocols.

Continuous salinity monitoring

Continuous monitoring of water quality along the shoreline of BB, CS, and BS began in 2004, and continues to the present (Figure 5.1, triangles). These stations were supplemented with additional locations along the coast in 2011. At each station, a YSI Environmental 6600 Series or 600XLM Series sonde is mounted to a platform resting on the substrate, with the sonde positioned ~25 cm above the bottom, and recording salinity every 15 minutes. The array covers shoreline areas with and without canals, and with varying levels of overland flow and salinity conditions. Some gaps in the time series occurred due to equipment malfunction. False data were eliminated through a combination of search algorithms and manual review (BNP 2006).

Analysis of annual salinity conditions across stations

The salinity regime of the study area was summarized as an annual salinity cycle, estimated by a moving average and a periodic function, separately. These analyses were intended for descriptive purposes, and were not used in fish regressions. By comparing the two approaches, regular fluctuations and anomalies can be viewed. The moving average across stations was taken within a one–day sliding time window along the

twelve–year series, along with confidence intervals (CI) of the mean. These were then mapped onto a one–year cycle, and means of the moving average and CIs across years were taken, as well as the variance of the moving average.

The twelve years of salinity data were also modeled as a periodic function representing oscillations in salinity due to seasonal changes in rainfall and freshwater flows to the coast. Since canal discharges were not regular, it was of interest to see if, in addition to the annual fluctuation due to rainfall, there were also fluctuations at smaller time scales of a few months. Salinity values, across stations, were regressed on the time variable, t = 2004–2015 (i.e., 0 to 12 years), by linking them with the trigonometric polynomial model:

$$\Sigma \; a_i \cos \omega_i t + b_i \sin \omega_i t \qquad (1)$$

where a,b were regression coefficients, $\omega = 2\pi i$ radians year^{-1}, and i = 1, 2, 3, 4, representing oscillations with periods of 12, 6, 4, and 3 months, respectively. Each regression term was considered independent and null hypotheses of coefficients $\beta=0$ were tested at $\alpha = 0.05$.

Hypersalinity and salinity variance metrics

Salinity conditions were summarized over periods prior to each fish survey, following methods similar to previous studies (Faunce et al. 2004, Lorenz 1999, Rose & Summers 1992). Salinity data were retrieved from the closest monitoring station to the survey, and if no data were available for that station, the second closest monitoring station, followed by the closest long term station, was used. Station data generally agreed with those taken at the faunal survey sites. The mean difference between station and survey salinity was 2.32 ± 2.65 (S.D.). For each survey, frequency of hypersalinity was

tabulated as the number of single readings (i.e., counts) that exceeded 40 salinity units over two separate time periods prior to the survey, 1 and 4 months, representing the immediate short term and seasonal time scales, respectively. Here, frequency is referred to simply as counts, and not counts per time, since the times were standardized. If data were partially missing over those periods, a criterion of 70% true data was required, otherwise the metric was considered null for that survey. Salinity mean and variance were also tabulated over those intervals, and the length of time between a fish survey and the most recent hypersaline event was taken. These metrics, representing conditions antecedent to the survey, were entered as explanatory variables in fish density regressions below.

Durations of hypersalinity events at each station were also summarized by year, but were not used in regressions. The length of continuous periods above 40 salinity units were tabulated (Table 5.1), with one stipulation – since salinity fluctuates daily with evapotranspiration and temperature, breaks in the hypersaline period of less than one day were not considered interruptions, assuming that these breaks were not sufficient for fish to recover from exposure (Serrano et al. 2011).

Year cycle

Seasonal fluctuations in density and occurrence have been noted for *L. griseus*, *F. carpio*, and *S. barracuda* (Serafy et al. 2003, Serafy et al. 2007). In these studies, both *L. griseus* and *S. barracuda* had higher occurrence, concentration (density when present), and delta–density (a combination of the two) during the wet season, defined as July to September, than during the dry season, January to March. The opposite pattern was found for *F. carpio*; these abundance metrics were higher during the dry season than wet

season. *L. griseus* also demonstrated ontogenetic shifts between seagrass, mangrove, and reef habitats, which may contribute to the observed seasonal patterns of mangrove habitat use (Faunce & Serafy 2003). In the present study, these seasonal dynamics were partitioned from effects due to hypersalinity by including a variable that represented time as a portion of the year cycle, t_{days} = 0 to 365 days, which was similar to the time variable (t) in the periodic regression of salinity (see Equation 1 above).

Analysis of fish occurrence contingency on hypersalinity

To test if fish were more or less likely to select habitats where hypersalinity had recently occurred, fish densities and the antecedent measures of hypersalinity above were converted to binary presence/absence values, and Fisher's exact tests were conducted for each species, at antecedent time scales of one and four months, separately. Contingency tables included tallies of four groups, representing presence (P) and absence (A), of fish (F) and hypersalinity (H), clockwise from top left, FP–HA, FA–HA, FA–HP, FP–HP.

Regression analyses of fish density

Fish densities were regressed in three separate procedures representing responses at the following time scales: (1) immediate short term, within 1 month prior to survey, (2) seasonal, within 4 months prior to survey, and (3) long term, over several years. The procedures for 1 and 2 were the same, except that they were applied at different time scales. In all regressions, fish densities were log–transformed as ln(fish density +1).

The regression models for the short term analyses included the following explanatory variables: frequency metrics of hypersalinity, salinity variance, and mean salinity over defined antecedent periods, the periodic time variable (t_{days}), and a classification variable representing each year, independently. These variables were

included in the same model because hypersalinity, and the management of water flows following it, varied quantitatively each year, resulting in different combinations of the three salinity variables. The year classification variable was included to account for anomalous year effects, such as two years with very cold temperatures (2010, 2011), that were not of interest in this study.

All variables were parameterized as linear or polynomial terms. Since quadratic relationships between fish abundance and salinity conditions are possible (McManus et al. 2014, Vaz et al. 2008), models were run with and without a second–order term of mean salinity, and whichever model version had the most significant quantiles, across variables, was kept. Following Bliss and Blevins (1959), and Batschelet (1970), fish densities were related to the periodic time variable, t_{days}, with the trigonometric polynomial: $a \cos \omega t_{days} + b \sin \omega t_{days}$, where a,b were regression coefficients and $\omega = 2\pi$ year^{-1}.

Following Koenker and Hallock (2001), and Dunham et al. (2002), quantile regression was used to assess limitation at the upper extremes (i.e., quantiles) of fish density by applying the QUANTREG procedure in SAS 9.2 (Chen 2004). This approach focuses on selected quantiles of the density distribution, and includes all data points in the estimation. Briefly, for each iteration of the procedure, residuals are weighted by the quantile value τ and $1-\tau$ according to whether they fall above or below the "predicted" model, respectively, and the sum of absolute residuals is minimized through least squares optimization. The upper quantiles, $\tau = 0.6$ to 0.95, at increments of 0.01, were regressed here. Following Vaz et al. (2008), models were accepted if at least one quantile was significant for all variables.

For the long term analysis, representing annual trends, quantile regression of linear models, and of non–parametric models with spline effects was used. Four linear models were regressed on subsets of the data that comprised the time periods of 1, 2, 3, and 4 years following hypersalinity, respectively. Variables in the model were the time difference between survey and most recent hypersaline event, and the year classification variable. Quantile levels $\tau = 0.6$ to 0.95, at increments of 0.01, were regressed.

Cubic B–spline regression was also applied, following Chock et al. (2000), in the long term analysis as a separate, non–parametric procedure to support and confirm the linear models, since they attempted to estimate an inherently non–linear process, and because positive, negative, and non–correlations are all possible within the same time series analysis (Sugihara et al. 2012, Patten 2014). In this approach, upper quantiles of fish density were particularly informative when they deviated from and/or maintained separate patterns from the median, which represented a central tendency. Spline knots were placed at 1–year intervals along the explanatory axis, and densities were regressed at quantiles $\tau = 0.5, 0.6, 0.7, 0.8, 0.9, 0.95, 0.98$, and 0.99. These levels were chosen because they best describe where parts of the density distribution tended to deviate from each other. This analysis included only the time difference variable.

Results

Physical environment

The period of record of the study was from January 2004 to November 2015, and a total of 416,064 salinity readings were possible for each water quality station. Twelve stations covered the full time series, and all except one were operative from 2011 to

2015. Figure 5.2 shows a timeline of hypersalinity events for each station along the coast, ordered from north to south (top to bottom). Station locations are indicated by triangles in Figure 5.1, and each station has prefix "BISC" not listed in the figure. Continuous hypersaline periods are indicated in red, and missing data in gray. Years 2004, 2011, and 2015 had the overall longest durations of hypersalinity, and occurrence across stations, followed by 2008, 2009, and 2014. Table 5.1 shows the same information quantified as number of events, and mean and maximum duration, at each station and for each year. The longest single hypersaline period was ~80 days at BISC06 in Barnes Sound in 2015. This area of the coast receives no direct canal discharge, and possibly very little groundwater. The timing of hypersaline events within the 12 year series created intervening periods of lower salinity conditions that varied in length, but were as long as ~4 years for most stations, with a maximum of 6.5 years.

The annual salinity cycle for the coast is shown in Figure 5.3 as a moving average (dark blue line) and a periodic function (red line), summarized across stations. These salinity graphs represent shoreline conditions that mangrove fish are most likely to encounter along the area studied. The graphs range from 20–35 salinity units, which span poly– and euhaline zones defined under the Venice system. All eight regression coefficients of the trigonometric polynomial significantly described oscillations in the annual salinity signal (Table 5.2). These results indicate that, in addition to annual cycling of salinity through seasonal rainfall, salinity also oscillates at thirds and quarters of the year, creating shifts in salinity at those time scales. The moving average generally agreed with the periodic function, and also had dynamics at seasonal, third–, and quarter–year scales. The moving average rises to a peak in mid–May, and then declines sharply

through mid–June, rising and falling in two–week intervals through July. Deviations of the moving average from the periodic function are greatest from July to November. Two abrupt declines also occur at the beginning of September and October. This pattern is also reflected in the mean confidence intervals of the moving average (light blue band), and in the salinity variance graph (black line) of Figure 5.3. Salinity variance is lowest from December to January.

Fish occurrence and hypersalinity

Fish occurrence of all four species had nonrandom associations with hypersalinity occurrence, at both times ranges preceding surveys (one and four months), except the *Ath–Clup–Engr* group at one month (Table 5.3). Hypersalinity presence was defined as occurring at least once within the defined time periods preceding a survey, although not necessarily at the time of the survey. A total of 2,333 surveys were tested for the one month range, and 2,369 surveys for the four month range. These totals differed because there were some cases where hypersalinity occurred within two to four months prior to survey, but not within one month. The total number of hypersalinity–absent (A) surveys was 2,172 and 1,839, for one and four month ranges, respectively, and for hypersalinity–present (P), was 161 and 530, respectively. The number and percentage of fish present in hypersaline–absent surveys is shown in rows marked *A* (Table 5.3), and fish present in hypersalinity–present surveys in lines marked *P*. These values were calculated separately for hypersalinity presence and absence. The odds ratios and p–values for each test are also shown in Table 5.3. The odds of *F. carpio* occurring in a survey without hypersalinity were higher than with, which is also supported by the percentages of fish

present. The opposite was true for the other species, and percentages were higher for hypersalinity presence than absence.

Analysis of fish density: Short term

Salinity variance and mean were correlated (not shown) in the short–term regressions (one– and four– month time scales) because they were both impacted by canal discharges, in many areas. However, because discharges were not necessarily uniform, and were not present along the entire coast, it was possible for surveys with similar mean salinity to have varying levels of salinity variance, especially for means within the poly– and euhaline ranges (18–40 salinity units, Venice system). For surveys following hypersalinity events, the mean and variance represented a decrease from hypersalinity to lower levels. Large decreases in salinity were due to canal discharges, such as at BISC14 in 2011 (Figure 5.3), while smaller decreases were likely due to precipitation.

All models for all species had at least one significant quantile, across variables. See Supplement S5 for plots of parameter estimates with confidence intervals of the estimates. The squared term for mean salinity was included in the *S. barracuda* models at both time scales, and in the *F. carpio* model at the one month scale, and was removed from all other models. *F. carpio* densities were generally positively related to hypersalinity frequency at the one month time scale (Figure 5.4a; Supplement S5, Figure S5.1a), and negatively related at the four month scale, at quantiles of ~0.9 and greater (Figure 5.4b; Supplement S5, Figure S5.1b). *L. griseus*, *S. barracuda*, and *Ath–Clup–Eng* were all negatively related to hypersalinity over several quantiles, at both time scales (Figure 5.4c–h), although *L. griseus* at four months (Figure 5.4d, dotted line, $\tau = 0.95$)

was not significant ($p = 0.0548$), but very close to the alpha level. In contrast, quantiles 0.78 and below for this species were positively related to hypersalinity and significant (Figure 5.4 d, solid line; Supplement S5, Figure S5.2b).

All species densities were negatively related to salinity variance, at both time scales, except *S. barracuda*, which was positively related at both scales (Figure 5.4). The linear relationships to mean salinity were: *L. griseus* and *Ath–Clup–Eng* were positively related at both time ranges, and *F. carpio* was negatively related at the four month scale. The quadratic relationships of fish density to mean salinity were: *F. carpio* was related concave down at the one month scale, with a maximum ~22 salinity units. *S. barracuda* was related concave up at both time scales, with minima at ~21 salinity units for both scales.

Annual oscillations in density, described by the variable (t_{days}), were detected for all four species. Densities were linked to this variable with a trigonometric polynomial function. Figure 5.5 shows the mean (black line) and confidence intervals (light blue band), across quantiles, of predicted values of this variable for each species. Estimates are shown for only the one month time scale. Amplitudes of the predicted variables were, on a log scale (fish density +1), approximately 1 for *F. carpio* and *L. griseus*, 0.5 for *S. barracuda*, and 1.5 for *Ath–Clup–Eng*.

Analysis of fish density: Long term

Results of linear regressions of long term periods following hypersalinity events, at the scale of years, are shown in gray boxes in Figure 5.6a–d. Note that these analyses do not account for the amount of hypersalinity preceding a survey, as above, but only the time difference. Subsets of fish densities within four different, increasingly larger, time

ranges were regressed for quantiles $\tau = 0.6$ to 0.95, at increments of 0.01. The upper and lower bounds of the boxes represent upper and lower confidence intervals, across quantiles, of the predicted values of the linear regression model, including intercepts. Negative responses are shown for *L. griseus*, *S. barracuda*, and *Ath–Clup–Eng* over all four years, and positive responses for *F. carpio*, over those periods. The coefficients gradually decrease in absolute value over four years, for all species.

Exploratory spline regressions revealed large increases and decreases in density within six months and one year of the event, for all four species (Figure 5.6a–d). *L. griseus*, *S. barracuda*, and *Ath–Clup–Eng* all increased greatly within two to four months post–event, while *F. carpio* decreased greatly over that period. In contrast, within 7 to 10 months following the event, *F. carpio* increased to higher levels than those immediately after (time difference close to zero). Densities of the other three species fell greatly over that interval. The 0.7 quantiles of these species fell to ~zero, and the 0.9 quantiles fell to lower levels than those just after the event. The 0.7 and 0.9 quantiles of *F. carpio* fell after one year.

This pattern of decline was common for all species in the 2 to 3 years post–event. Spline regression quantiles 0.5 to 0.9 for all species were at the lowest overall levels for a one–year period within one to two years following hypersalinity. Highest overall levels were attained after almost four years had elapsed. Some other species–specific responses occurred within the 1 to 3 years post–event period. The 0.7 quantile of *L. griseus* remained near zero until almost three years had passed, and the median remained at these levels for all surveys. The same pattern occurred for *S. barracuda*; however, the median increased within 1 to 6 months, and after three years post–event. The 0.7 and 0.9

quantiles of *F. carpio* had similar patterns to each other, falling to low levels after one year, and then slowly increasing over the next three. The *Ath–Clup–Eng* group showed the greatest fluctuation in the 0.7 quantile, which fell to near zero after approximately 7 months post–event, and then greatly increased after two years. Interestingly, the upper quantiles (0.9 to 0.99), for all species except *S. barracuda*, were stable and remained at the same approximate levels across the four–year axis.

Figure 7 shows spline regressions of the four species together on one plot, for quantiles $\tau = 0.9$ (top panel), and 0.7 (bottom panel). Note: color labeling does not match Figure 5.6. At both quantile levels, *F. carpio* densities alternate with the other three groups over the first year, then, at the 0.7 quantile, all groups decline after one year. The *Ath–Clup–Eng* group increased greatly over the next year at this quantile, while the other three groups slowly increase.

Discussion

Impacts of hypersalinity and salinity variance on individual densities of three fish species, and one multi–species functional group, were evaluated using data from visual surveys of fishes in nearshore mangrove habitats of the southeastern Florida coastline, for 2004–2015. The annual salinity regime of the study area was summarized as a moving average with confidence intervals and variance, and as a periodic polynomial. These two functions were derived from continuous time series of salinities recorded at 25 automated monitoring stations along the coast. They generally agreed with each other, and represented salinity conditions that were most often present over a year. Fish occurrence was tested for contingency on hypersalinity occurrence, and three of four species were

more likely to be present in habitats with recent hypersalinity than without. Importantly, these habitats were generally not hypersaline at the time that they were surveyed. To further explore this occurrence relationship, the frequency and duration of hypersalinity in these habitats over defined intervals preceding fish surveys were quantified, as well as salinity variance and mean, which were relevant to water flow conditions following hypersalinity. Effects of these variables on fish densities were tested in quantile regressions, together with a periodic variable representing annual population oscillation, and a year classification variable.

In general, densities of all species fluctuated greatly within the first year following a hypersaline event, as demonstrated by positive and negative regression relationships at time scales of one and four months (Figures 5.4a–h), and one year (Figure 5.6a–d). Densities at intermediate quantiles declined after one year, and then recovered over several years, which was reflected in the decreasing absolute values of the linear regression slope coefficients, from time scales of one to four years. Spline analyses supported this pattern (Figure 5.6).

This study is the first in southern Florida to examine effects of hypersalinity on the upper quantiles of fish densities, at monthly, seasonal, and annual time scales, and also accounting for seasonal, periodic oscillation in fish densities in the analysis. Results from this study are relevant to many other studies in Florida that investigated effects of the current coastal salinity regime, and water management strategy, on nearshore flora and fauna. This study showed that the salinity regime for the past 12 years has been largely poly–euhaline, with high salinity variance that negatively impacts fish densities over the long term. Browder et al. (2005) defined ecological targets for the shoreline that

include restoring stable, oligo–mesohaline habitat (Venice System 1959), which was the dominating condition prior to Everglades drainage (Wingard et al. 2004). Lohman et al. (2012) simulated hydrodynamics of Biscayne Bay to determine freshwater budgets required for reducing salinity levels and for preventing hypersalinity. According to my study, mesohaline habitat has not been freely available in these coastal habitats over the past decade, whereas hypersalinity has occurred in several years. For that reason, it is difficult to make predictions on how fish populations would perform under scenarios of increased mesohaline habitat, because the current fish–habitat data cover predominantly poly–euhaline habitat.

The relationships of *S. barracuda* to salinity mean and variance (Figure 5.4e,f) may offer a limited view into dichotomous fish habitat selection patterns for two different salinity scenarios following hypersalinity: (1) low fluctuation in salinity, with mean salinity remaining just below 40, or (2) large deviations that lower the mean salinity to within the mesohaline range. The results suggest a positive relationship to both of these scenarios. Scenario 1 could be explained by increased prey availability (see below). Scenario 2 may be preferred over the poly–euhaline scenario, but it may not occur very often. For example, the minimum value of *S. barracuda*'s concave–up relationship to mean salinity is centered around ~20 salinity units, below which is the mesohaline range. These latter conditions may only be available after a large amount of salinity fluctuation, which could explain the positive relationship with salinity variance. Although, conditions where salinity levels fell from hypersalinity, down through poly–euhaline, to mesohaline, were not all that common.

For this reason, the relationship to salinity variance is likely to be more complex than linear. Large fluctuations in salinity may be difficult conditions to tolerate. For example, at the one month scale, no log–densities of *S. barracuda* greater than 1 occurred for values of salinity variance (center panel) between 60 and 100 units (Figure 5.4e), and these levels are likely to be associated with an intermediate mean salinity level and intermittent canal discharges. It is possible that the positive relationship to salinity variance is pertinent to the mesohaline scenario described above, but may be negative when salinity is lowered only as far as the polyhaline range (20 to 30). Although regressions do not directly support this explanation, the quadratic relationship of *S. barracuda* to mean salinity, which is lowest within the polyhaline range, suggests it is at least possible.

Measures of antecedent environmental conditions have been used in other studies of southern Florida fishes. Faunce et al. (2004) took means and standard deviations of salinity and water level, over ranges of 10 to 360 days, along the limnetic–oligohaline boundary of the Everglades and estuarine dwarf mangrove forest, and related fish collections to them. They found short–term (< 90 days) and long–term (> 240 d) responses to water level, and short–term (> 30 d) responses to salinity, for different taxa. In the same system, Lorenz (1999) analyzed constraints of high salinity, defined as > 5 units, on freshwater community assemblages. The means and standard deviations of salinity, water level, and temperature were calculated over periods of 30–360 days (increments of ~30 days) prior to samples, and fish biomass was negatively related to high salinity. Both of these studies found patterns of short–term changes in fish abundance at monthly time scales that could cumulatively impact long–term population

dynamics. These monthly shifts may prove to be critical in forming and sustaining fish assemblages, as discussed by Lorenz (1999). I found in my study that ~ 4 years was required for fish densities to return to levels comparable to those just prior to the hypersaline event. Similarly, Lorenz and Serafy (2006) found that four years or more were required for fish assemblages in mangrove creek headwaters to return to a freshwater community structure.

Three important questions emerged from this hypersalinity study: (1) Do the short term density fluctuations result from habitat compression, behavior, predator–prey dynamics, or combinations of all of these? (2) Are these fluctuations representative of population–level patterns or just locally isolated events? (3) Are the short term fluctuations mechanistically linked to the longer term population declines? Although these questions can not be fully answered in this study, some tentative inferences can be made, until further modeling work is done to confirm them. Theoretical work by Holt (2008) found that short term pulsed increases in a population correlated with longer term population decline. Results from this hypersalinity study suggest a similar temporal pattern. For example, the regression relationships of *F. carpio* to hypersalinity were inversely positive and negative at one and four month time scales, respectively (Figure 5.4a,b), suggesting that an initial concentration response occurred within one month following hypersalinity, while a reduction in density occurred in later months. This fish is a euryhaline benthic detritivore, and consumes primarily amphipods and detritus (Odum & Heald 1972). McManus et al. (2014) proposed a preference of this fish for meso– or polyhaline conditions, however, it can tolerate extreme salinity conditions of up to 1,450 milliosmoles kg^{-1} (Kaill 1976). One hypothesis to explain the hypersalinity relationships

found in this study, for this fish, is that it uses the boundary of hypersaline areas for foraging, where mortality of its prey, which may have limited dispersal abilities, and accumulation of detritus, are high, and where lower salinity refugia are present nearby. Additionally, behavioral avoidance of rapidly expanding hypersaline habitats may also lead *F. carpio* to become concentrated in refugia. This spatially explicit hypothesis can be tested using simulation modeling of movement behaviors on dynamic hydroscapes (Yurek et al. 2013).

Predators of *F. carpio*, for example *L. griseus* and *S. barracuda* (De Sylva 1963, Starck & Schroeder 1971) may respond to its one month increases in density. These two predator species are known to shift between mangrove, seagrass, and reef habitats (Faunce & Serafy 2007, Jones et al. 2010, Serafy et al. 2007), and may avoid areas of hypersalinity until their prey populations build up and become concentrated, and salinity is lowered. If this is true, the food chain linking detritus, invertebrates, forage fish, and predators may be impacted by successional cascades that stem from hypersalinity. This hypothesis is supported by the higher occurrence of *L. griseus* and *S. barracuda* in habitats with recent hypersalinity (see odds ratios, Table 5.3).

Results from this study were contingent upon a few assumptions. For one, the response quantiles that result from quantile regression were interpreted as constraints applied by the explanatory variables, i.e., environmental conditions, on faunal densities (Cade & Noon 2005), rather than as indicators of an overall response of the full distribution of densities, such as is done with linear mean regression. Deviations between different quantiles of density were used to infer changes in fish populations, based on shifts in the distribution of densities across quantiles. Since these density patterns appear

to be temporally dynamic, and these dynamics are determined by spatiotemporal heterogeneity in water flows to the coast, it may be useful to use computer modeling to simulate these interactions at different spatial and temporal scales, combining movement hypothesized movement behaviors and food web interactions.

A second consideration in this study was that representing population cycles with a periodic function does not necessarily describe mechanistic processes that drive those cycles, such as increases or decreases in reproduction, survivorship, and/or predator–prey interactions. Instead, it provides an approximate measure of some amount that is attributable to those processes and is common among all years of surveys. The periodic time variable, t_{days}, was included in the regression model to explain some variation that was not due to the salinity variables of interest. It is more likely that regular population cycles, which are features of the life history of the fish, are altered through continued exposure of the fish to hypersalinity and salinity variance, resulting in abnormal fluctuations, such as were found in this study.

Hypersalinity is a widespread phenomenon in tropical and subtropical aquatic coastal ecosystems throughout the world. Recently, massive seagrass die–off events occurred in areas of northern Florida Bay where hypersalinity was extreme (> 50). Other examples of effects on benthic ecology of southern Florida can be found in Lee at al. (2006), Kelble et al. (2007), and Lirman et al. (2014). These events signal potential scenarios for coastal ecosystems worldwide. Hypersalinity is likely to increase in frequency, duration, and magnitude under climate change, and can be further complicated by tradeoffs between sea level rise and freshwater resource availability and management (Obeysekera et al. 2011). Areas of high human population density along the coast are

particularly vulnerable, and the footprint of urbanization is currently increasing (McGranahan et al. 2007). As more water is removed from below–ground aquifers for human use, saltwater intrusion can be counter–induced, and salinity conditions in aquifer–dependent estuaries could potentially convert to hypersaline. This human–hydrologic feedback loop was first documented as early as 1967 by Kohout and Kolipinski for Biscayne Bay. More recently, Blanco et al. (2013) estimated an overall 12–17% replacement of freshwater by saltwater in the Biscayne Aquifer over 25 years. Similar cases on a broader scale throughout North America were reviewed by Barlow and Reichard (2010).

Examples from southern Florida, and other well–documented ecosystems (Glantz 2005) can be applied as indicators for potential scenarios of other tropical and subtropical coastal ecosystems. Evidence from my study strongly suggests that reduced freshwater flows negatively affect fish populations at the scale of several years. I strongly urge care in planning and management water resources, particularly in areas where they are already limited, and where humans depend heavily on artisanal fisheries for their food base.

Figures

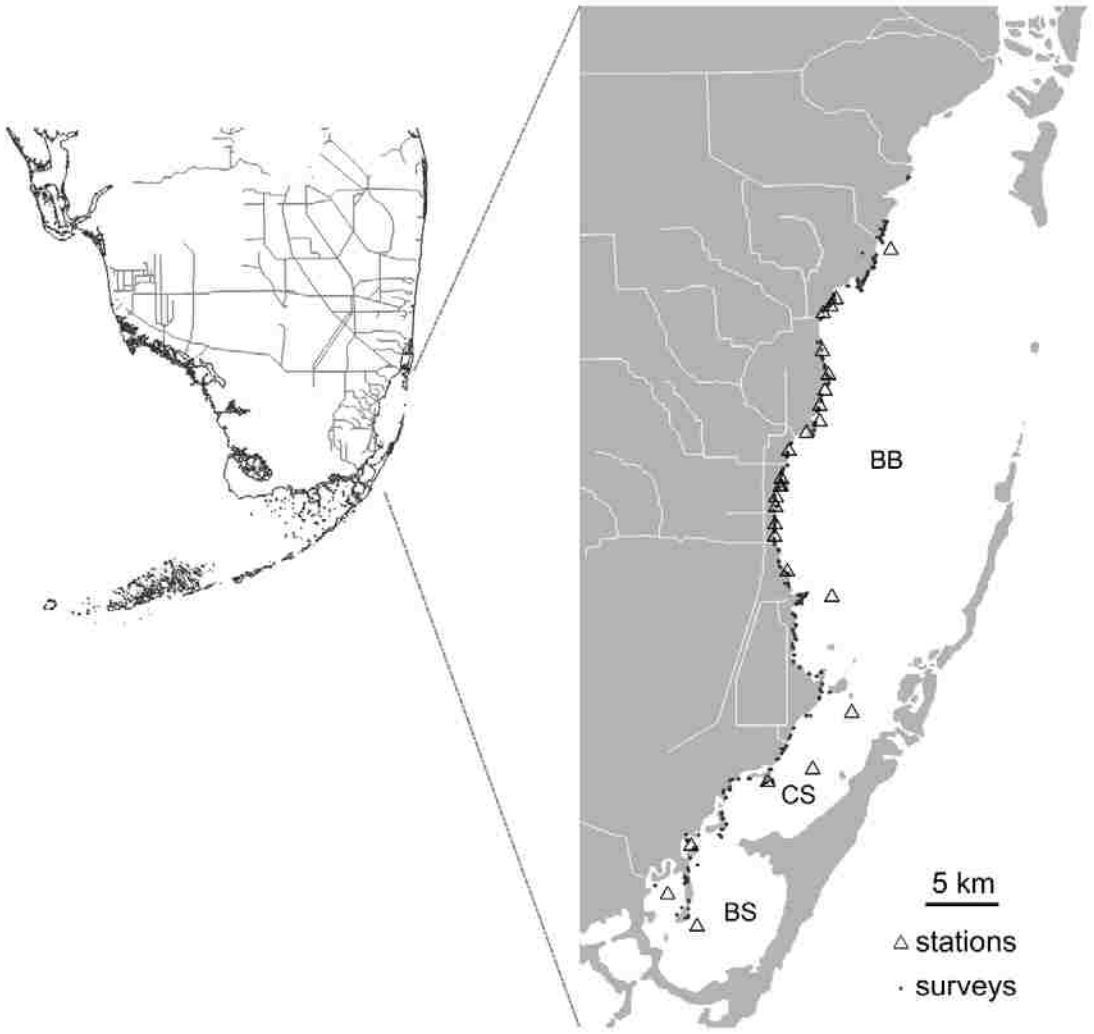

Figure 5.1. Location of study area in southeastern Florida. Left panel shows the Greater Everglades watershed at the regional scale, with shoreline and network of dredged canals indicated by black and gray lines, respectively. Right panel is a zoom of the coastal areas sampled in this study, including Biscayne Bay (BB), Card Sound (CS), and Barnes Sound (BS). Triangles and gray dots indicate locations of water quality monitoring stations and faunal surveys, respectively.

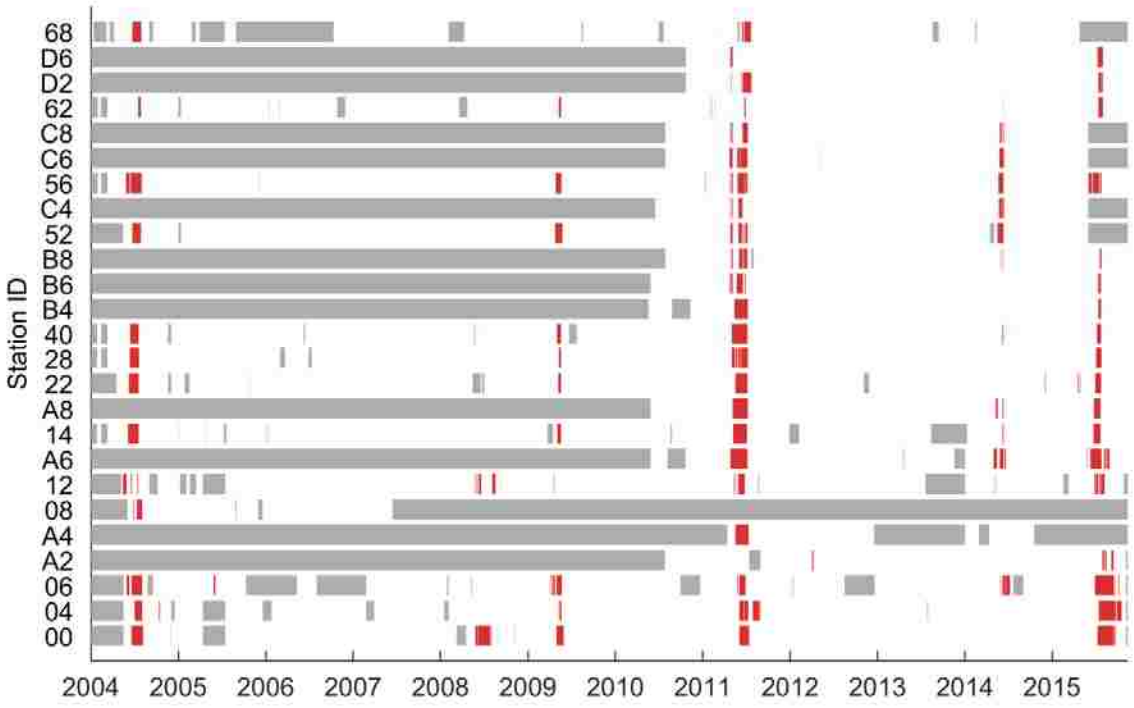

Figure 5.2. Timeline of hypersalinity events for 25 continuous water quality monitoring stations, ordered from north to south (see triangles in Figure 1). Period of record is from January 2004 to November 2015. Red bars indicate continuous hypersaline events. Gray bars indicate missing data. Lettered stations were initiated in 2011.

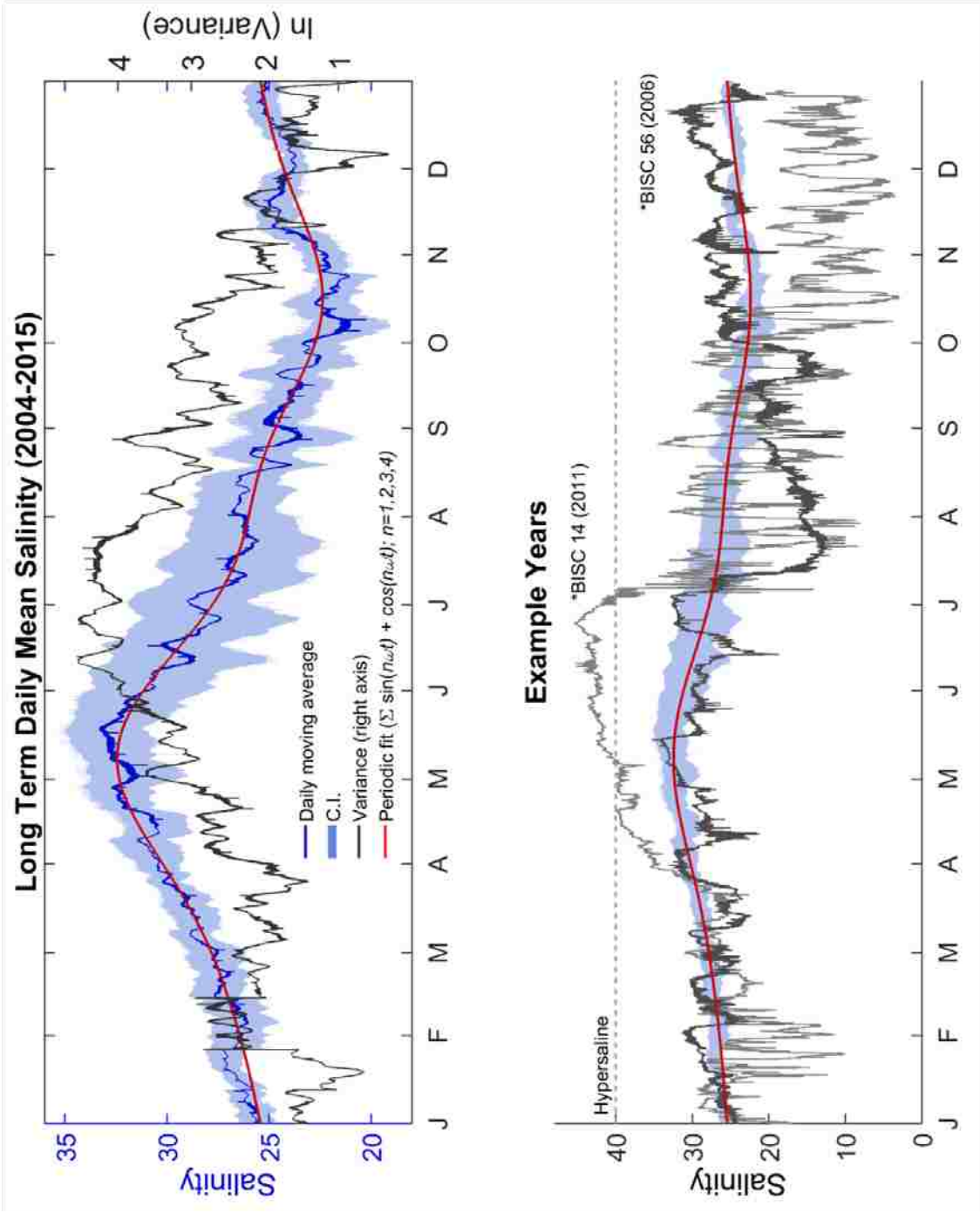
Long Term Daily Mean Salinity (2004-2015)
Salinity
ln (Variance)
Daily moving average
C.I.
Variance (right axis)
Periodic fit (Σ sin(nωt) + cos(nωt); n=1,2,3,4)
J F M A M J J A S O N D
Example Years
*BISC 14 (2011)
*BISC 56 (2006)
Hypersaline

Figure 5.3. Top panel: annual salinity cycle (January to December) summarized as a daily moving average (dark blue line), variance (black line, right axis), and a periodic function (red line) over 25 monitoring stations. Functions were calculated over the twelve–year period of record (2004–2015), and then mapped onto a one–year time axis. The moving average is shown as a mean and variance (across years) of mean salinity (across stations), and similarly, mean of confidence intervals (light blue band). The periodic function had a frequency (ω) of one cycle (2π) year^{-1}, and three additional higher frequency components representing 6–, 4–, and 3– month oscillations. Bottom panel: examples of a hypersaline year (station BISC12 in 2011), and a high variance year (BISC56 in 2006), with periodic function (red) and mean C.I.s of the average (blue).

a)

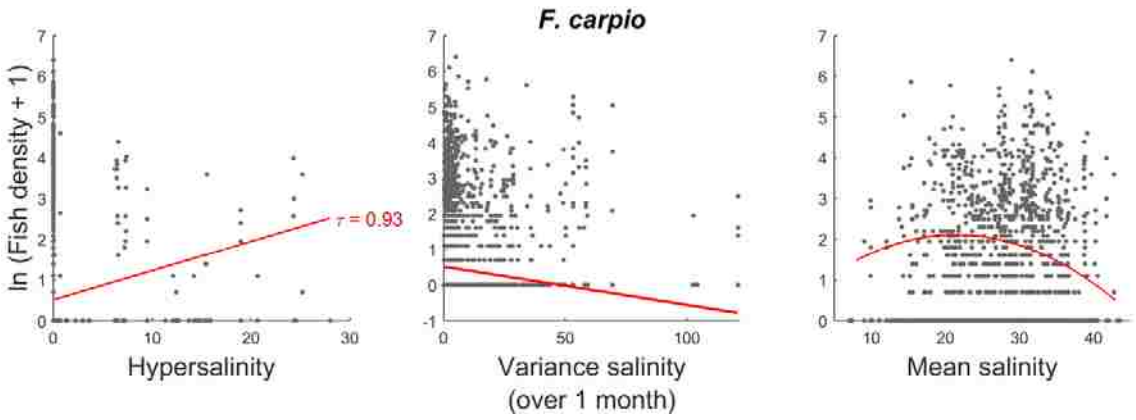

b)

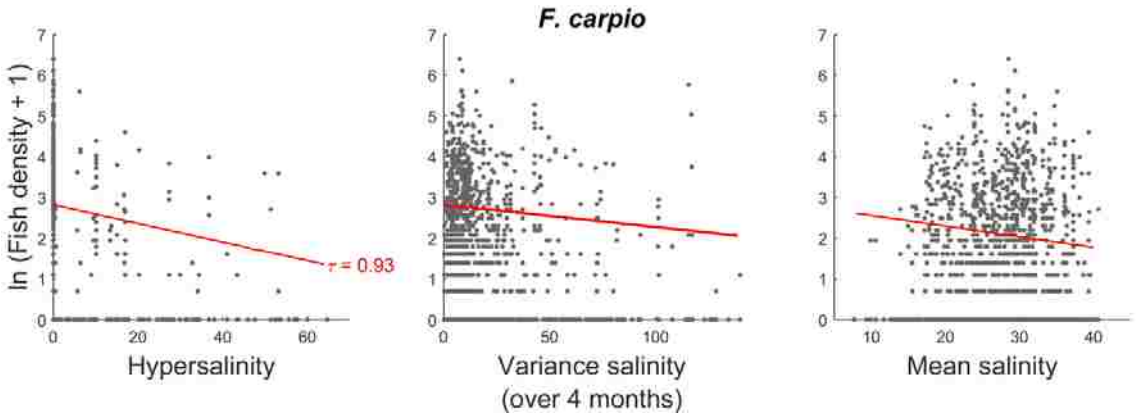

Figure 5.4a,b. Results of quantile regression on salinity metrics that summarized conditions over time ranges antecedent to surveys, representing the immediate short term (one month, top row) and seasonal (bottom row) time scales following hypersaline events. Hypersalinity frequency (left column) is represented simply as counts (days), over one and four month time ranges. Salinity mean and variance (center, right columns) are also represented at both time scales. Quantiles $\tau = 0.6$ to 0.95 were regressed. Black dots indicate log–transformed fish densities, and red lines indicate representative significant relationships with the highest absolute values of parameter estimates.

(c)

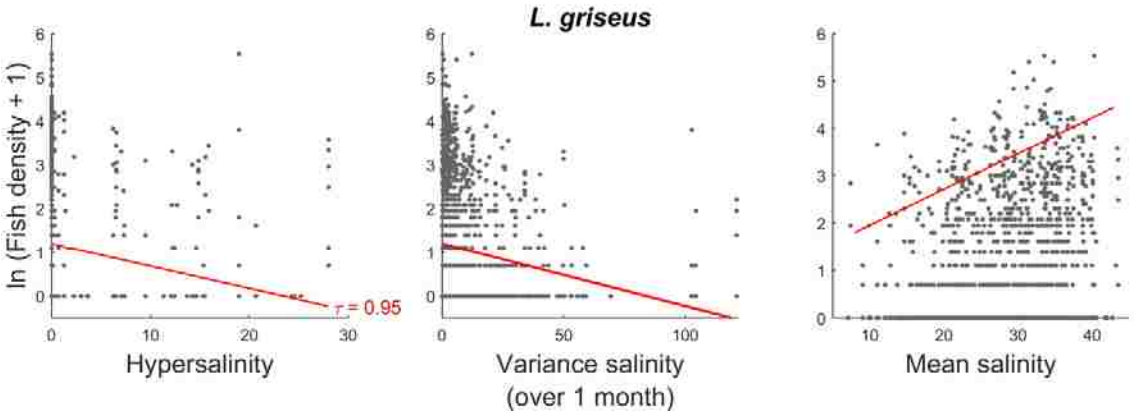

(d)

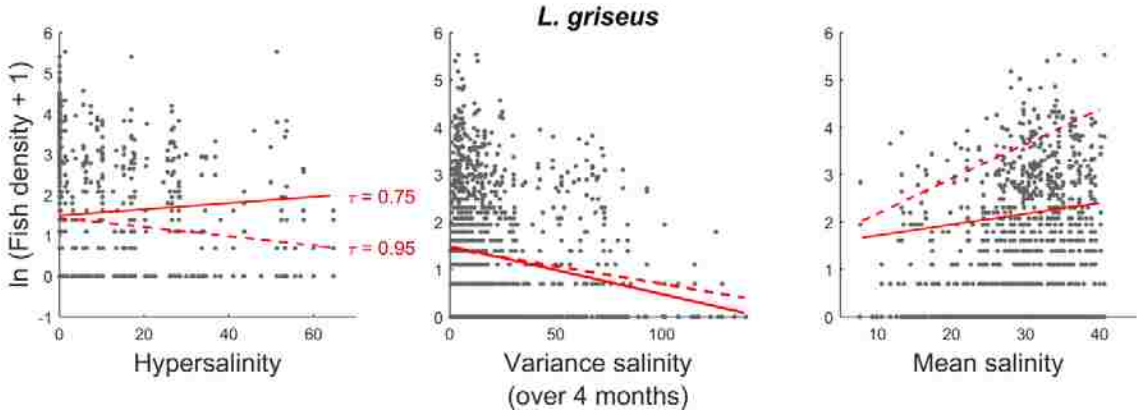

Figure 5.4c,d. Results of short term quantile regression for *L. griseus*. Note, at the four month time scales, densities for this species were positively related to hypersalinity at lower quantiles (0.6 to 0.78), while negatively related at higher quantiles, although the latter was not significant (p = 0.0548).

(e)

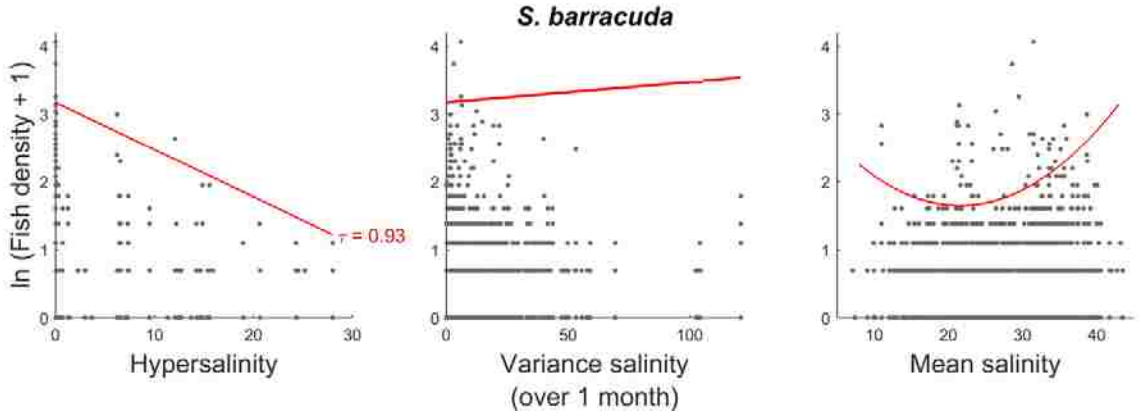

(f)

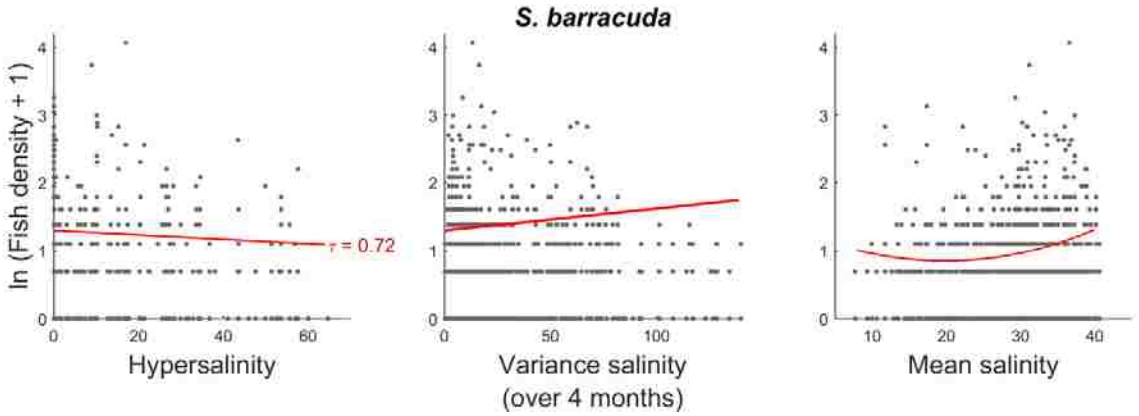

Figure 5.4e,f. Results of short term quantile regression for S. *barracuda*.

(g)

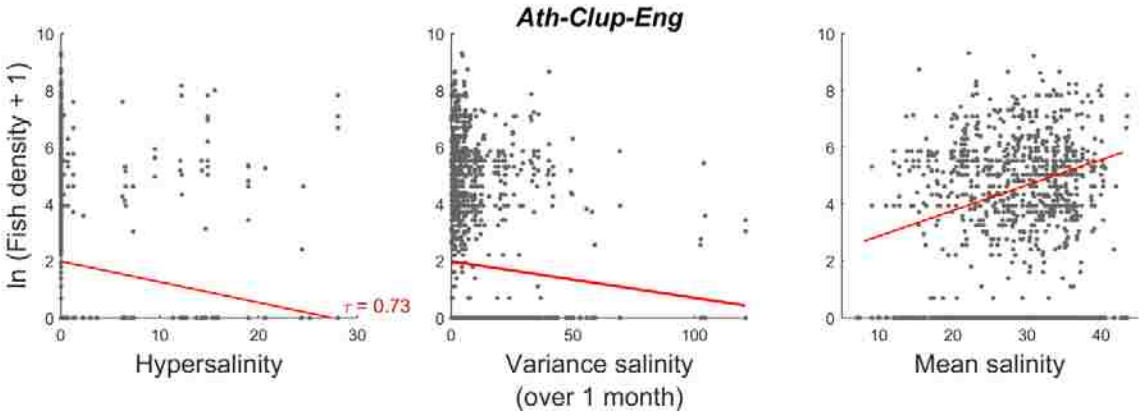

(h)

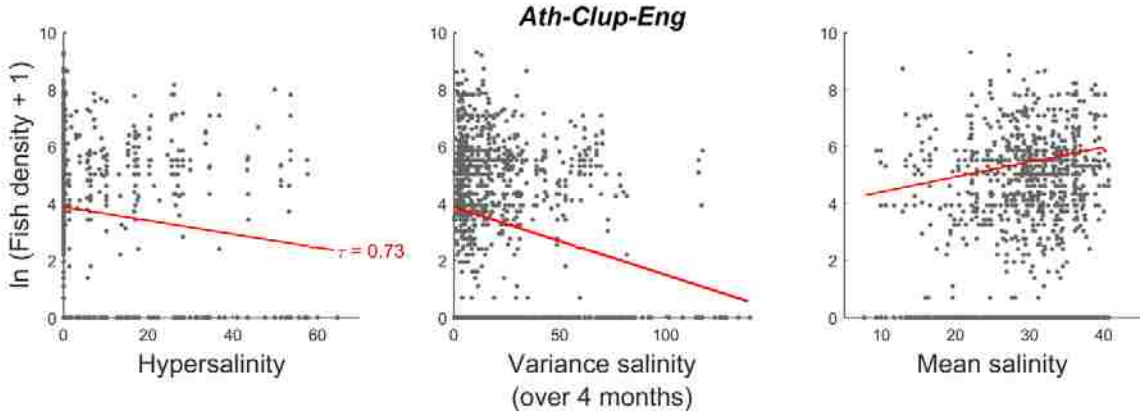

Figure 5.4g,h. Results of short term quantile regression for the super–species group of A*therinidae*, *Clupeidae*, and *Engraulidae*.

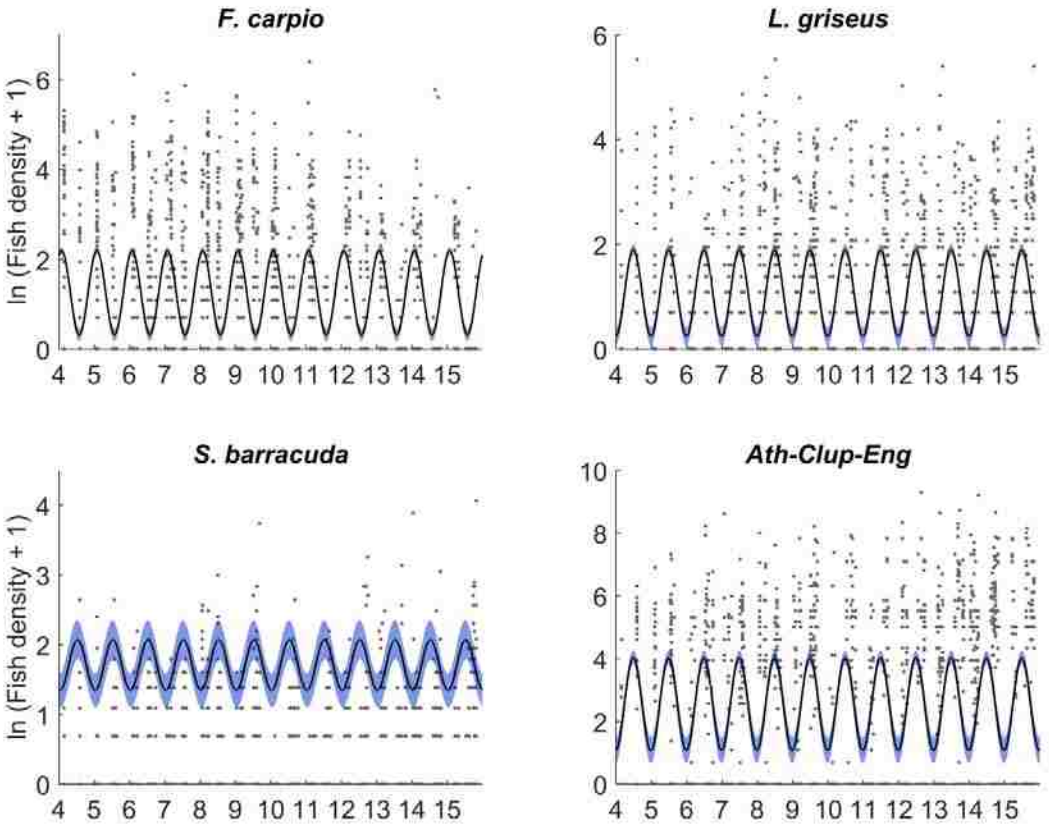

Figure 5.5. Relationship between regression quantiles of fish density and the periodic time variable (t_{days}), from short–term quantile regression models (antecedent period = 1 month). Densities were related to t_{days} with a parameterized trigonometric polynomial link function: cos ωt + sin ωt, where $\omega = 2\pi$ year^{-1}, at quantiles $\tau = 0.6$ to 0.95 (increments of 0.01). The mean (black line) and confidence intervals (light blue band), across quantiles, of the predicted relationship are shown for each species. Years 2004–2015 are indicated by digits 4 to 12.

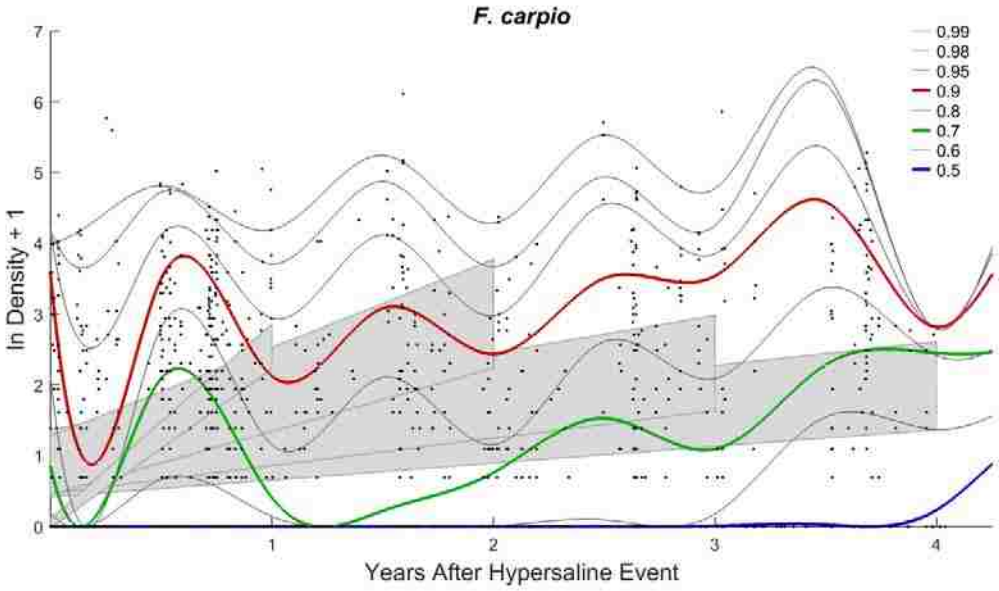

Figure 5.6a–d. Results of long term quantile regression (0–4 years) of log–transformed fish densities (black dots) on length of time following a hypersalinity event. Inter–annual patterns were identified using two qualitatively different models: parametric linear models (gray bars), and non–parametric regression splines (colored and gray lines). Four different linear models were regressed for surveys that fell within 1, 2, 3, and 4 years following an event, respectively, including quantiles 0.6 to 0.95, at 0.01 increments. Gray bars indicate range (lower to upper confidence intervals) of predicted values across quantiles. Selected quantiles (colored lines) were particularly informative when compared to each other. A year classification variable (not shown) was included to account for anomalous shifts in the time series, for example, two successive years that had very low temperatures.

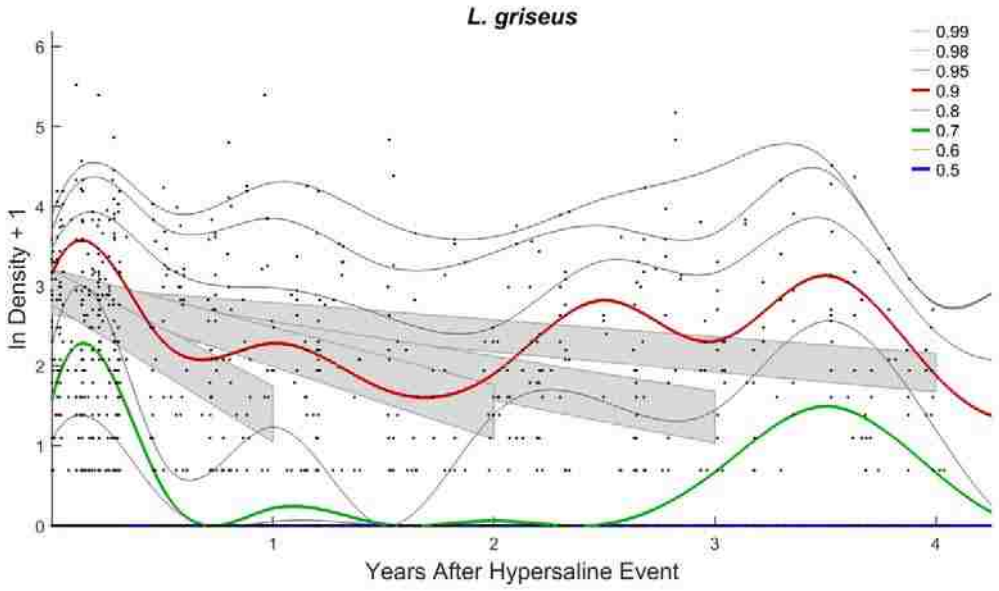

Figure 5.6b.

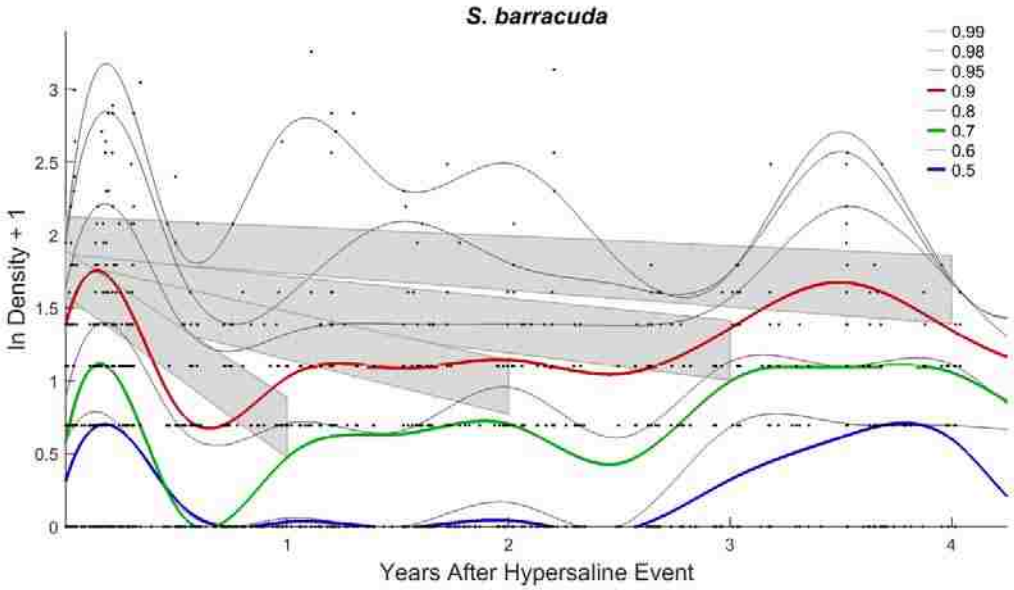

Figure 5.6c.

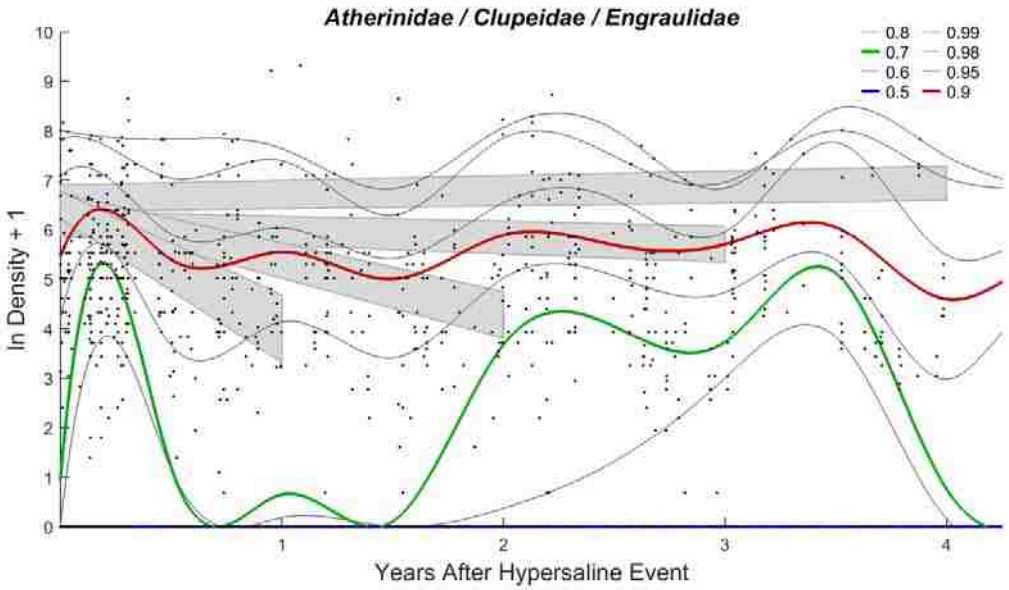
Atherinidae / Clupeidae / Engraulidae
0.8
0.99
0.7
0.98
0.6
0.95
0.5
0.9
ln Density + 1
Years After Hypersaline Event

Figure 5.6d.

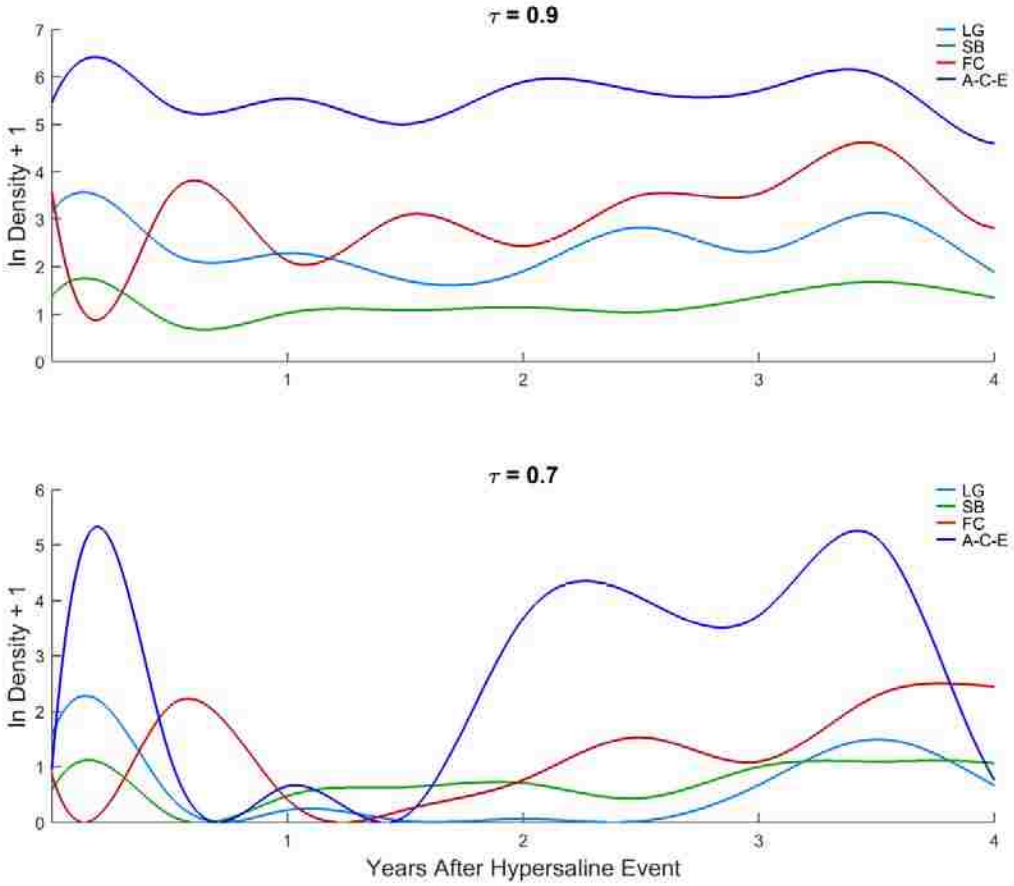

Figure 5.7. Inter–species comparison of selected quantiles from Figure 5.6 (above). Note: color identification not equivalent to Figure 5.6.

Table 5.1. Hypersalinity events for each of 25 continuous water quality monitoring stations (rows), and each year of the time series (columns). Number of events for each year (in parentheses), mean, and maximum duration are listed. See Methods for tabulation of duration.

ID	2004	2005	2006	2007	2008	2009	2010	2011	2012	2013	2014	2015
68	(1) 37.23							(3) 11.49 27.56			(1) 0.01	
D6								(2) 3.55 6.86				(1) 22.03
D2								(9) 4.43 35.25				(2) 8.09 12.89
62	(1) 11.04					(2) 4.74 9.47	(1) 0.63	(4) 1.72 6.60				(1) 17.88
C8								(4) 7.70 22.49			(2) 4.34 6.25	
C6								(3) 18.51 30.49			(2) 9.01 17.45	
56	(3) 20.86 46.93	(1) 0.73				(3) 8.15 23.83		(4) 11.44 29.48			(2) 10.82 21.64	(3) 15.13 27.79
C4								(6) 3.44 15.66			(2) 8.84 11.16	
52	(1) 34.85	(2) 0.33 0.53				(1) 28.63		(6) 6.38 14.93			(1) 24.55	
B8								(4) 9.47 14.95			(4) 0.57 1.14	(1) 6.55

B6						(5) 8.28 26.70		(1) 0.32	(2) 5.57 6.36
B4						(3) 17.76 35.60			(1) 10.27
40	(1) 35.30		(1) 1.32	(1) 16.71		(1) 66.51		(1) 4.07	(1) 15.69
28	(1) 39.33			(1) 10.02		(6) 9.64 29.38			(1) 22.20
22	(2) 19.47 38.30			(1) 10.63		(2) 25.76 51.44			(3) 9.81 24.15
A8						(2) 30.97 61.71		(3) 3.38 6.80	(1) 28.09
14	(1) 44.18			(1) 14.56		(3) 19.73 59.06		(2) 1.50 2.97	(1) 30.38
A6						(5) 14.59 72.26	(1) 0.25	(5) 7.09 16.38	(4) 16.92 47.36
12	(5) 3.91 14.93		(9) 3.20 13.30	(1) 0.54	(2) 0.39 0.73	(8) 4.44 26.66		(1) 1.36	(7) 5.23 11.93
08	(4) 6.84 22.95	(1) 0.05							
A4						(1) 56.64			
A2							(3) 1.92 3.69	(1) 0.80	(7) 2.86 8.75
06	(3)	(2)	(4)	(5)		(3)		(3)	(4)

	18.98	3.69	0.42	6.85	10.61	10.81	21.13
	46.20	7.24	1.03	21.60	27.52	17.00	79.94
04	(3)			(3)	(4)	(1)	(2)
	11.75			2.60	17.02	1.30	46.35
	31.63			7.45	27.45		72.19
00	(1)		(5)	(1)	(1)		(4)
	47.46		12.74	28.95	39.88		18.15
			51.73				68.04

Table 5.2. Results of periodic regression of twelve–year salinity time series (2004–2015) for southeast Florida coastline. A periodic function was regressed on salinity data taken from 25 continuous water quality monitoring stations along the coast, with four component sinusoids: Intercept + $\Sigma\, a_i \cos \omega_i t + b_i \sin \omega_i t$, where $\omega = 2\pi$ year^{-1}, i = 1, 2, 3, 4, and t = 0 to 12 years. Regression coefficient estimates, standard errors of the estimate (S.E.), and t–statistics and p–values for test of H_0: a,b = 0 at $\alpha = 0.05$ are listed.

	Estimate	**S.E.**	**t–stat**	**p–value**
Intercept	26.79	0.0028764	9313.7	0
a_1	-1.8372	0.004078	-450.51	0
b_1	3.7073	0.0040577	913.66	0
a_2	0.040573	0.004068	9.9736	1.9888e–23
b_2	-0.79006	0.0040674	-194.24	0
a_3	0.69894	0.0040701	171.73	0
b_3	-0.047445	0.0040653	-11.671	1.8024e–31
a_4	-0.2733	0.0040674	-67.192	0
b_4	-0.069378	0.004066	-17.063	2.8121e–65

Table 5.3. Results of Fisher's exact test on 2 × 2 contingency tables of presence or absence, of fish in surveys, and of hypersalinity over a time range preceding a survey. Each species was tested separately for two time ranges, one month (2,333 surveys), and four months (2,369 surveys). The number of surveys with hypersalinity preceding it was 161 and 530, at one and four month periods, respectively, and 2172 and 1839 without, respectively. Number of fish and percentages indicate how many surveys had fish present for surveys with hypersalinity present (P), or absent (A), separately. Odds ratios and p–values ($\alpha = 0.05$) from tests are also listed.

Species	Month	Hypersaline present / absent	# of surveys with fish present		% of surveys with fish present	Odds ratio	p–value
F. carpio	1	A	739 (2172)	*	0.34	1.51	0.0301
		P	41 (161)		0.25		
	4	A	717 (1839)	*	0.39	3.3	2.56E–24
		P	86 (530)		0.16		
L. griseus	1	A	675		0.31	0.48	1.06E–05
		P	78	*	0.48		
	4	A	490		0.27	0.35	3.18E–25
		P	271	*	0.51		
S. barracuda	1	A	826		0.38	0.54	1.53E–04
		P	86	*	0.53		
	4	A	637		0.35	0.45	6.06E–16
		P	288	*	0.54		
Ath.	1	A	730		0.34	0.77	0.12
Clup.		P	64		0.4		
Engr.	4	A	566		0.31	0.58	9.44E–08
		P	230	*	0.43		

Supplement S5. Parameter estimates for short term quantile regressions of fish density on hypersalinity, salinity mean and variance, year cycle, and year class. Note: the latter two variables are not shown here. Black lines and blue bands indicate coefficient estimates and 95% confidence intervals, respectively, for each quantile. The squared term for mean salinity was only included in *F. carpio* (one month) and *S. barracuda* (both time scales) models.

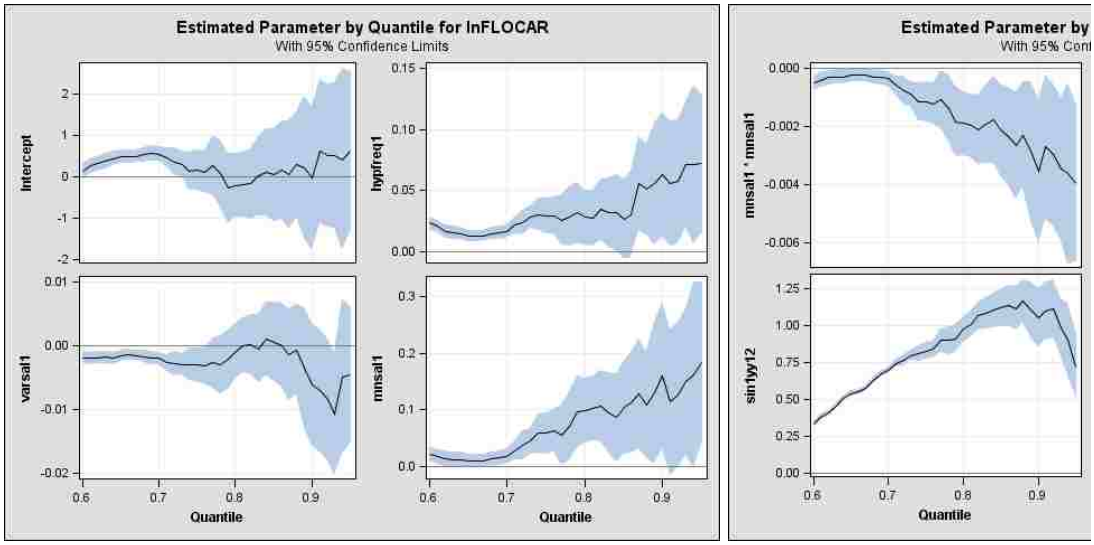

Figure S5.1a. Results of *F. carpio* (1 month range)

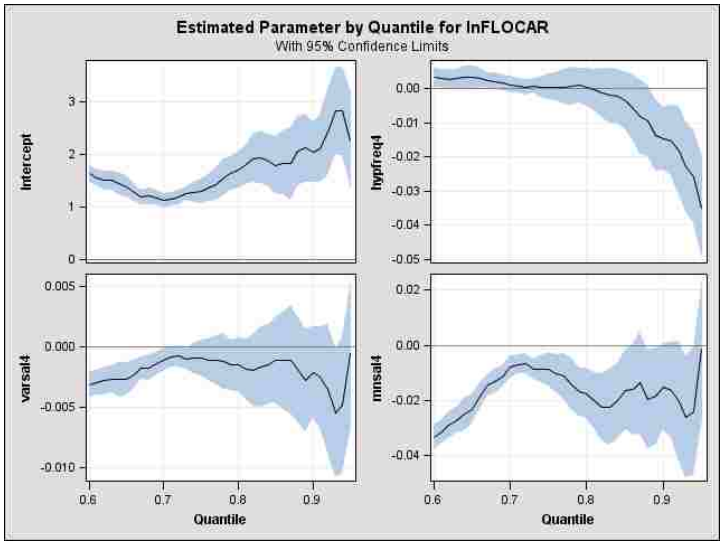

Figure S5.1b. Results of *F. carpio* (4 month range)

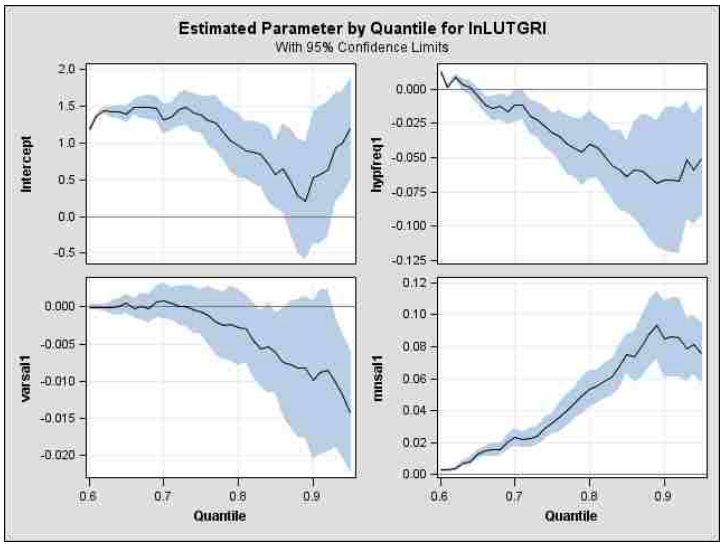

Figure S5.2a. Results of *L. griseus* (1 month range)

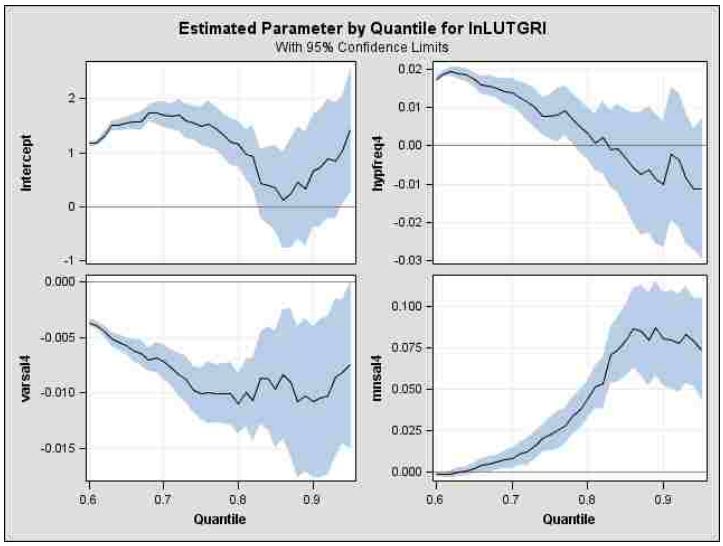

Figure S5.2b. Results of *L. griseus* (4 month range)

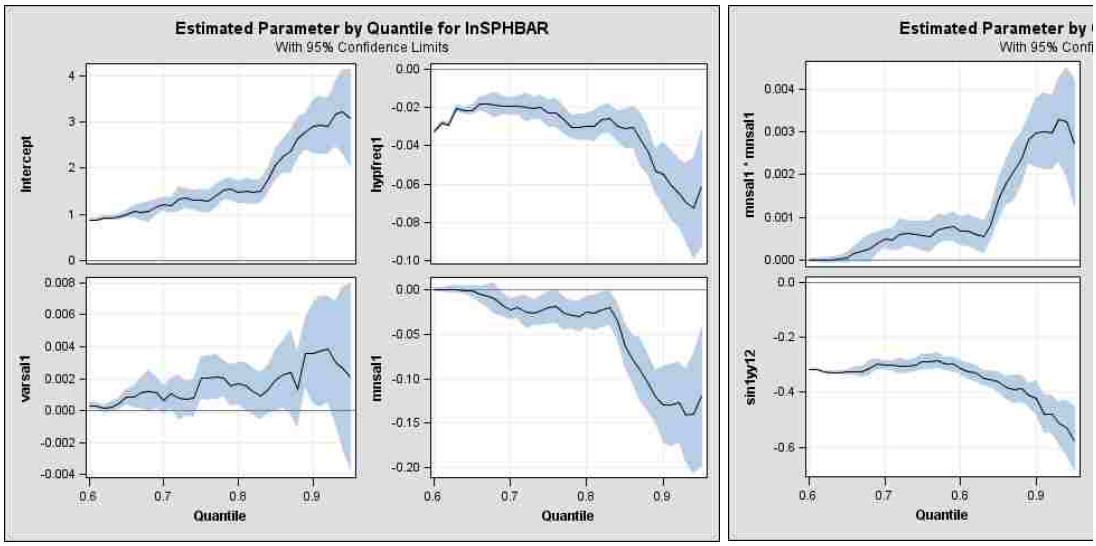

Figure S5.3a. Results of *S. barracuda* (1 month range)

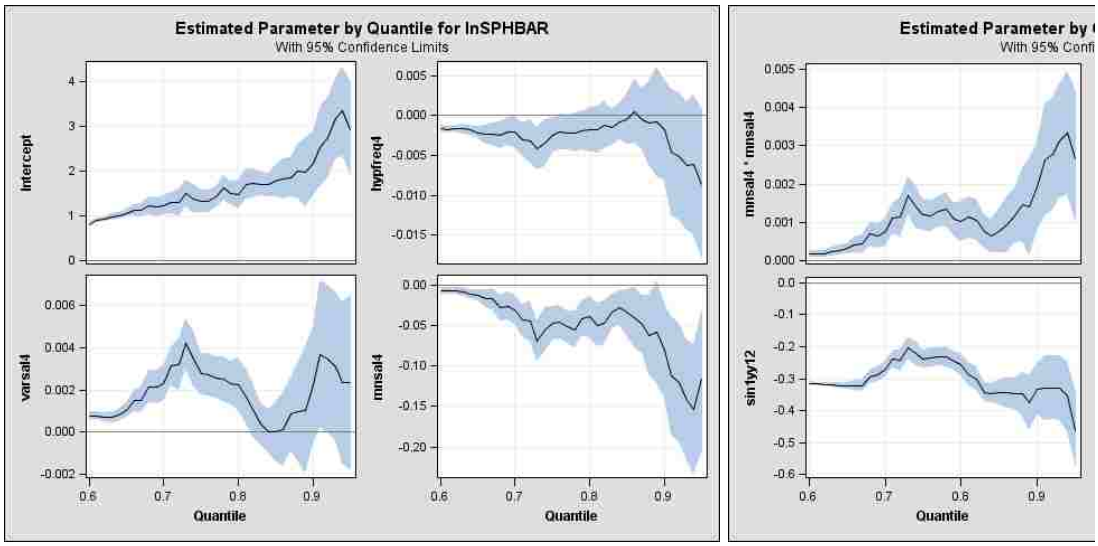

Figure S5.3b. Results of *S. barracuda* (4 month range)

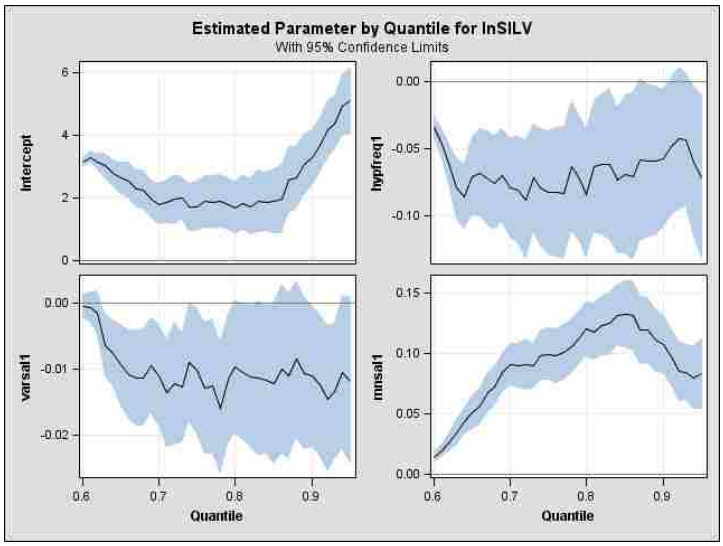

Figure S5.4a. Results of *Atherinidae*, *Clupeidei*, and *Engraulidae* (1 month range)

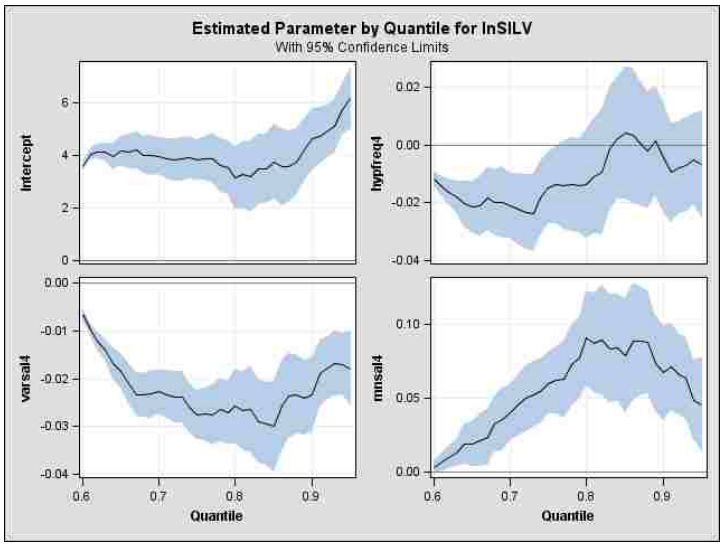

Figure S5.4b. Results of *Atherinidae*, *Clupeidei*, and *Engraulidae* (4 month range)

Chapter 6

Conclusion

Spatiotemporal dynamics of small-bodied (< 8 cm) fish populations in seasonally-pulsed, sub-tropical wetlands were investigated in this dissertation, using computer simulation modeling (Chapters 2 to 4), and statistical analyses of empirical census data (Chapter 5). Computer simulations were of fish communities within the central freshwater Everglades of Florida, and empirical analyses were of mangrove-associated fish species along the southern Florida coastline.

The primary goal of these studies was to determine processes by which these fishes become concentrated in high densities, representing increased prey availability and foraging opportunities for higher level predators. An overarching hypothesis of this dissertation was that interactions between fish population dynamics (e.g., growth, mortality, trophic interactions), movement behaviors, and spatially dynamic environmental conditions result in dynamic and heterogeneous spatial distributions of fish, which form, at times, very high, localized concentrations. These concentrations are thought to be critical for generating sufficient biomass to support food webs in nutrient limited systems.

Various forms of this concentration hypothesis have existed for several decades, but have not been sufficient to explain declining predator populations in Florida wetlands. This dissertation describes a new approach for explaining fish concentration with complementary empirical monitoring and computer modeling, explicitly tracking population dynamics across several relevant spatial and temporal scales. This

multi-scale, spatially explicit approach revealed complexity in fish populations, particularly with regard to landscape connectivity, that has not been previously detected.

The spatially explicit concentration hypothesis of this dissertation was explored by simulating food web interactions and behavioral movement of fishes in response to wetland drying in the freshwater Everglades, and by analyzing fish density responses to hypersalinity events at varying time scales in coastal mangrove habitats. In the Everglades study, trophic dynamics and movement were explicitly tracked on fine spatial and temporal scales (e.g., meters, days). Spatial and temporal predictions of fish biomass accumulations were made, and can be tested, given appropriate empirical data. In the mangrove study, it was not feasible to track food web interactions and movement, although these interactions were assumed to occur, as supported by descriptive literature of fish natural history. Conclusions on these mechanistic processes could not be drawn, but patterns of temporal and successional dynamics of fish densities emerged from the analysis, which at least suggested that foraging and movement are potential factors affecting fish density. This possibility could be further explored through simulation modeling of population dynamics and movement behaviors, similar to the Everglades studies, and spatially explicit predictions of fish density could be made and tested with empirical data.

In this way, this dissertation developed a methodology for using computer simulation modeling to complement empirical monitoring, and vice versa. Through this process, conclusions from one approach can be used to generate hypotheses for the other. The success of this methodology is greatly aided by the fulfillment of two conditions: (1) deficiencies of either approach are mutually revealed and corrected through an exchange

of information, and (2) new hypotheses and theory are generated. This iterative process was described by Box (1976) for mathematical analysis, and by Grimm et al. (2010), Rose et al. (2015), and Werner et al. (2001) for simulation modeling, and stems from the rules for philosophical inquiry laid out by Galilei (1638), Newton (1686), and many others before them. Box (1976) asserts, "it is, of course, the error signal – for example, the discrepancy between what tentative theory suggests should be so and what practice says is so – that can produce learning." This is similar to Newton's fourth rule of inquiry, which can be paraphrased as: propositions inferred from general phenomena are considered true, until new phenomena occur.

This dissertation produced new theory, hypotheses, and conclusions for explaining fish concentrations that disagree with long–standing hypotheses of Everglades and coastal wetlands research. For example, for over 60 years, it has been generally assumed that fish in the Everglades follow a regional scale "drying front" that propagates over large tracts of land, and that they become concentrated along the front, from higher to lower elevations. Following this reasoning, empirical data are typically collected and analyzed over large regional gradients (Chick et al. 2004, Reutz et al. 2005, Trexler et al. 2002). However, investigations of this hypothesis do not tend to include variables that explicitly measure spatial heterogeneity of the landscape at local scales, or dynamic patterns of connectivity of the landscape throughout various flooding and drying phases, which can affect spatial drying patterns and fish movement, although these factors have been acknowledged to be important (Larsen et al. 2007, McVoy et al. 2011, Obeysekera & Rutchey 1997, Ogden 2005). For these reasons, it may be useful to update the concept

of a drying front to incorporate the topographic complexity that can cause concentrations of fish to vary spatiotemporally over broad areas, and not simply along a drying front.

New recommendations could also be made for monitoring strategy, following hypotheses developed through spatially explicit modeling. GEFISH was initially developed to simulate regional scale fish concentration (Chapter 2). However, further development of the model revealed a possibility that changes in connectivity of the anisotropic landscape, namely reductions in dispersal corridors, may act at a local spatial scale to concentrate fish over small areas, and that this process is recursively replicated across the landscape throughout the drying phase. In that case, concentrations within different monitoring sites, which are spread out across the region and relatively far from each other, may be independent in terms of the spatial dynamics that lead to concentration, which are determined primarily by local landscape geomorphology. A new monitoring strategy could be recommended that selects sites within closer proximity, at the scale of local topography, and that is timed ahead of and during the drying processes.

The simulations of fish movement on the intact ridge−and−slough landscape (RSL, Chapter 3) showed only a very small portion of fish biomass propagating in a straight line along the regional northwest-southeast gradient. Instead, much more biomass was routed down into the sloughs, and collected in small embayment sinks, or cul−de−sacs. The topography had a resistance effect on fish movement, reducing fluxes of biomass across the landscape while increasing their local density. However, the pattern was reversed on the degraded RSL, that is, more biomass followed the regional gradient and collected along the southeast boundary because fewer sloughs patches were available for concentration. These results suggest that fish concentration over spatially heterogeneous

landscapes can be theorized to function similarly to capacitance in circuit theory (McRae 2008), where dynamic connectivity acts as a form of resistance. It may therefore be appropriate to apply measures of resistance and capacitance to ecological systems. This study concludes, contrary to other studies, that the regional drying front hypothesis is most appropriate for flat landscapes, such as the Rocky Glades in the Everglades, which does not have RSL structure.

For the landscape to have a great effect on local fish density, it must be spatiotemporally dynamic so that fish habitat becomes channelized or compressed, and fish aggregate in localized areas. For that reason, dynamic heterogeneity of the landscape was considered as an important factor affecting fish ecology. Landscape effects were either simulated, in the Everglades studies, or summarized as temporal variables representing conditions that preceded surveys, in the mangrove study. Habitat compression has been documented in other shallow water aquatic ecosystems, for example in the Neuse River estuary in North Carolina, USA (Campbell & Rice 2014), and it is reasonable to assume that these effects are more widespread than are currently being studied.

The results of this dissertation were achieved by taking a combined landscape and systems ecology approach with a focus on ecosystem constraints, or how biota respond to limitations applied by the physical environment. One important consideration, as summarized by Ulanowicz (2014), is that physical laws can constrain, but never determine, ecological outcomes, because heterogeneity in ecological variables allows for complex recombinations in the system, and effective avoidance of boundary conditions. In this dissertation, constraints were represented as deleterious conditions that are

limiting on some aspect of the life history of the fish, for example, desiccation in the central Everglades, and hypersalinity in coastal wetlands. Although these conditions can negatively impact the fitness of fish if they are exposed, the fish can also avoid the conditions through movement to refugia, which are made available through spatial heterogeneity of the landscape and dynamic hydrology. It is also reasonable to assume some individual variability in fish movement. Here is a tangible example of heterogeneity leading to ecological complexity, through a tractable explanation of fish movement behavior. This explanation was developed through a combination of computer simulations and empirical analysis, and differs from popular approaches that evaluate responses of central tendencies, and for that reason, achieved different results.

The driving variable of this dissertation was dynamic hydrology, represented by overland freshwater flows. Freshwater availability is a growing concern for human populations and ecosystems. Although this resource is seemingly abundant throughout the world, it is becoming limited in local areas where human population density, and therefore freshwater usage, are increasing (Gerten et al. 2011). Demands for freshwater differ greatly between humans and ecosystems, and conflicts arise when humans develop and alter watersheds and wetlands in ways that interfere with processes that support ecosystems. For example, humans have diverted and impounded water flows for storage, recreation, generation of hydroelectric power, flood prevention, and reclamation of flooded and arid lands for agriculture. These anthropogenic activities occur worldwide (Tockner & Stanford 2002). However, many ecosystems require consistent and/or pulsed water flows to sustain ecological processes (Junk et al. 1989, Tockner et al. 2000), and

diversion or reduction in flows can negatively impact aquatic habitat, such as through sedimentation.

As we become aware of these conflicts, through research and communication, development of water resource policy becomes more challenging, particularly if resources are declining (Obeysekera et al. 2011). For these reasons, the future of freshwater availability could be critical. However, work from this dissertation demonstrates that the complex relationships of wetland ecosystems to the water flows that sustain them can be investigated and explained through spatially explicit modeling, and testable predictions can be made to support management decisions for future scenarios.

REFERENCES

Alho CJR (2008). Biodiversity of the Pantanal: Response to seasonal flooding regime and to environmental degradation. Brazilian Journal of Biology, 68:957–966.

Anonymous (1959). Symposium on the classification of brackish waters. Venice 8–14th April 1958. Archivio di Oceanografia e Limnologia, Vol.11,Supplemento (Simposio sulla Classificazione della Acque Salmastre).

Bakun A (2006). Wasp–waist populations and marine ecosystem dynamics: navigating the "predator pit" topographies. Progress in Oceanography, 68:271–288.

Barlow PM, Reichard EG (2010). Saltwater intrusion in coastal regions of North America. Hydrogeology Journal, 18(1):247–260.

Batschelet E (1970).Periodic Functions. In: Krickeberg K, Levin SA (Eds.), Biomathematics, Vol. 2: Introduction to mathematics for life scientists. Springer–Verlag, Berlin.

Bayley PB (1991). The flood pulse advantage and the restoration of river–floodplain systems. Regulated Rivers: Research & Management, 6:75–86.

Beddington JR (1975). Mutual interference between parasites or predators and its effect on searching efficiency. Journal of Animal Ecology, 44:331–430.

Belicka L, Sokol E, Hoch JM, Jaffé R, Trexler J (2012). A molecular and stable isotopic approach to investigate algal and detrital energy pathways in a freshwater marsh. Wetlands, 32:531–542.

Bernhardt CE, Willard DA, Marot M, Holmes CW (2004). Anthropogenic and natural variation in ridge and slough pollen assemblages. Open File Report 2004–1448. U.S. Geological Survey, Washington, D.C., USA.

Bernhardt CE, Willard DA (2009). Response of the Everglades ridge and slough landscape to climate variability and 20th–century water management. Ecological Applications, 19(7):1723–1738.

Biscayne National Park (2006). Report to the United States Army Corps of Engineers for the Monitoring and Assessment Plan of the Comprehensive Everglades Restoration Plan for RECOVER Assessment Team, Southeast Estuary Subteam. URL: http://141.232.10.32/pm/ssr_2009/ssr_pdfs/hc_scs_salinity_bb_pi_report_2005.pdf.

Blanco RI, Naja GM, Rivero RG, Price RM (2013). Spatial and temporal changes in groundwater salinity in South Florida. Applied Geochemistry, 38:48–58.

Bliss CI, Blevins DL (1959). The analysis of seasonal variation in measles. American Journal of Hygiene, 70(3):328–34.

Bornette G, Amoros C, Piegay H, Tachet J, Hein T (1998). Ecological complexity of wetlands within a river landscape. Biological Conservation, 85(1):35–45.

Box GE (1976). Science and statistics. Journal of the American Statistical Association, 71(356):791–799.

Bronmark C, Klosiewski SP, Stein RA (1992). Indirect effects of predation in a fresh–water, benthic food–chain. Ecology, 73:1662–1674.

Browder JA, Gleason PJ, Swift DR (1994). Periphyton in the Everglades: Spatial Variation, Environmental Correlates, and Ecological Implications. In: Davis SM, Ogden JC (Eds.) Everglades, the Ecosystem and Its Restoration. St. Lucie Press, Delray Beach, FL, USA, 379–418.

Browder JA, Alleman R, Markley S, Ortner P, Pitts PA (2005). Biscayne Bay conceptual ecological model. Wetlands, 25(4):854–869.

Burgess OT, Pine WE, Walsh SJ (2013). Importance of floodplain connectivity to fish populations in the Apalachicola River, Florida. River Research and Applications, 29(6):718–733.

Cade BS, Noon BR (2003). A gentle introduction to quantile regression for ecologists. Frontiers in Ecology and the Environment, 1(8), pp.412–420.

Cade BS, Noon BR, Flather CH (2005). Quantile regression reveals hidden bias and uncertainty in habitat models. Ecology, 86(3):786–800.

Calabrese JM, Fagan WF (2004). A comparison–shopper's guide to connectivity metrics. Frontiers in Ecology and the Environment. 2(10):529–536.

Campbell LA, Rice JA (2014). Effects of hypoxia–induced habitat compression on growth of juvenile fish in the Neuse River Estuary, North Carolina, USA. Marine Ecology Progress Series, 497:199–213.

Chapman LJ, Mckenzie DJ (2009). Behavioral responses and ecological consequences. Fish Physiology, 27:25–77.

Chambers LG, Davis SE, Troxler TG (2015). Sea Level Rise in the Everglades: Plant–Soil–Microbial Feedbacks in Response to Changing Physical Conditions. CRC Press: Boca Raton, FL, USA, 89–112.

Chea R, Guo C, Grenouillet G, Lek S (2016). Toward an ecological understanding of a flood–pulse system lake in a tropical ecosystem: Food web structure and ecosystem health. Ecological Modelling, 323:1–11.

Chick JH, Ruetz CR, Trexler JC (2004). Spatial scale and abundance patterns of large fish communities in freshwater marshes of the Florida Everglades. Wetlands, 24: 652–664.

Chick JH, Geddes P, Trexler JC (2008). Periphyton mat structure mediates trophic interactions in a subtropical marsh. Wetlands, 28:378–389.

Chen L (2004). An introduction to quantile regression and the QUANTREG procedure. SAS Institute, Inc. Cary, NC. Paper 213–30.

Chock DP, Winkler SL, Chen C. (2000). A study of the association between daily mortality and ambient air pollutant concentrations in Pittsburgh, Pennsylvania. Journal of the Air & Waste Management Association, 50(8):1481–1500.

Craighead FC (1971). The trees of south Florida: Vol.1. The natural environments and their succession. Miami University Press, Coral Gables.

Cucherousset J, Carpentier A, Paillisson JM (2007). How do fish exploit temporary waters throughout a flooding episode? Fisheries Management and Ecology, 14:269–276.

Cyrus DP, Vivier L, Jerling HL (2010). Effect of hypersaline and low lake conditions on ecological functioning of St Lucia estuarine system, South Africa: An overview 2002–2008. Estuarine, Coastal and Shelf Science, 86(4):535–542.

Dale MR (2000). Spatial pattern analysis in plant ecology. Cambridge University Press.

Daufresne M, Bady P, Fruget JF (2007). Impacts of global changes and extreme hydroclimatic events on macroinvertebrate community structures in the French Rhone River. Oecologia, 151:544–559.

Davis SM, Gunderson LH, Park WA, Richardson J, Mattson J (1994). Landscape dimension, composition, and function in a changing Everglades ecosystem. In: Davis SM, Ogden JC (Eds.) Everglades, the Ecosystem and its Restoration. St. Lucie Press, Delray Beach, FL, USA, 419–444.

de Silva Samarasinghe JR, Lennon GW (1987). Hypersalinity, flushing and transient salt–wedges in a tidal gulf–an inverse estuary. Estuarine, Coastal and Shelf Science, 24(4):483–498.

De Sylva DP (1963). Systematics and life history of the great barracuda, *Sphyraena barracuda* (Walbaum). University of Miami Press, Coral Gables, FL.

DeAngelis DL, Goldstein RA, O'Neill RV (1975). A model for trophic interaction. Ecology, 56:881–892.

DeAngelis DL, Loftus WF, Trexler JC, Ulanowicz RE (1997). Modeling fish dynamics and effects of stress in a hydrologically pulsed ecosystem. Journal of Aquatic Ecosystem Stress and Recovery, 1:1–13.

DeAngelis DL, Gross LJ, Huston MA, Wolff WF, Fleming DM, Comiskey EJ, Sylvester SM (1998). Landscape modeling for Everglades ecosystem restoration. Ecosystems, 1(1):64–75.

DeAngelis DL, Mooij WM (2005). Individual–based modeling of ecological and evolutionary processes. Annual Review of Ecology, Evolution, and Systematics, 147–168.

DeAngelis DL, Trexler JC, Cosner C, Obaza A, Jopp F (2010). Fish population dynamics in a seasonally varying wetland. Ecological Modelling, 221:1131–1137.

DeAngelis DL (2012). Self–organizing processes in landscape pattern and resilience: a review. ISRN Ecology, 2012:274510.

DeAngelis DL, Yurek SY (In revision). Spatially–explicit modeling in ecology: A review. Ecosystems.

Desmond G (2007). High Accuracy Elevation Data Collection Project. U.S. Geological Survey.

Dunham JB, Cade BS, Terrell JW (2002). Influences of spatial and temporal variation on fish–habitat relationships defined by regression quantiles. Transactions of the American Fisheries Society, 131.1:86–98.

Dutterer AC, Mesing C, Cailteux R, Allen MS, Pine WE, Strickland PA (2013). Fish recruitment is influenced by river flows and floodplain inundation at Apalachicola River, Florida. River Research and Applications, 29(9):1110–1118.

Eby LA, Crowder LB (2002). Hypoxia–based habitat compression in the Neuse River Estuary: context–dependent shifts in behavioral avoidance thresholds. Canadian Journal of Fisheries and Aquatic Sciences, 59(6):952–965.

Faunce CH, Serafy JE, Lorenz JJ (2004). Density–habitat relationships of mangrove creek fishes within the southeastern saline Everglades (USA), with reference to managed freshwater releases. Wetlands Ecology and Management, 12(5):377–394.

Faunce CH, Serafy JE (2007). Nearshore habitat use by gray snapper (*Lutjanus griseus*) and bluestriped grunt (*Haemulon sciurus*): environmental gradients and ontogenetic shifts. Bulletin of Marine Science, 80(3):473–495.

Faunce CH, Serafy JE (2008). Growth and secondary production of an eventual reef fish during mangrove residency. Estuarine, Coastal and Shelf Science, 79(1):93–100.

Frederick P, Gawlik DE, Ogden JC, Cook MI, Lusk M (2009). The White Ibis and Wood Stork as indicators for restoration of the everglades ecosystem. Ecological Indicators, 9(6):S83–S95.

Gaff H, DeAngelis DL, Gross LJ, Salinas R, Shorrosh M (2000). A dynamic landscape model for fish in the Everglades and its application to restoration. Ecological Modelling, 127:33–52.

Gaff H, Chick J, Trexler J, DeAngelis D, Gross L, Salinas R (2004). Evaluation of and insights from ALFISH: a spatially explicit landscape–level simulation of fish populations in the Everglades, Hydrobiologia, 520:73–87.

Gaiser E (2009). Periphyton as an indicator of restoration in the Florida Everglades. Ecological Indicators, 9:S37–S45.

Galilei G (1638). Two new sciences, including centers of gravity & force of percussion. Translated: S. Drake. 1947, University of Wisconsin Press, Toronto, Canada.

Gawlik DE (2002). The effects of prey availability on the numerical response of wading birds. Ecological Monographs, 72:329–346.

Gerten D, Heinke J, Hoff H, Biemans H, Fader M, Waha K (2011). Global water availability and requirements for future food production. Journal of Hydrometeorology, 12(5):885–899.

Givnish TJ, Volin JC, Owen VD, Volin VC, Muss JD, Glaser PH (2008). Vegetation differentiation in the patterned landscape of the central Everglades: importance of local and landscape drivers. Global Ecology and Biogeography, 17:384–402.

Glantz MH (2005). Climate variability, climate change and fisheries. Cambridge University Press, New York, NY.

Gleason PJ, Stone P (1994). Age, origin, and landscape evolution of the Everglades peatland. In Davis SM, Ogden JC (Eds.) Everglades, the Ecosystem and its Restoration. St. Lucie Press, Delray Beach, FL, USA. 149–197.

Gonzalez RJ (2012). The physiology of hyper–salinity tolerance in teleost fish: a review. Journal of Comparative Physiology B, 182(3):321–329.

Goodwin BJ, Fahrig L (2002). How does landscape structure influence landscape connectivity? Oikos, 99:552–570.

Goodwin, BJ (2003). Is landscape connectivity a dependent or independent variable? Landscape Ecology, 18(7):687–699.

Goss CW, Loftus WF, Trexler JC (2014). Seasonal fish dispersal in ephemeral wetlands of the Florida Everglades, Wetlands, 34(1):147–157.

Gray JD, King TL, Colura RL (1991). Effect of temperature and hypersalinity on hatching success of spotted seatrout eggs. The Progressive Fish–Culturist, 53(2):81–84.

Grether GF, Kolluru GR (2011). Evolutionary and plastic responses to resource availability. In: Evans JP, Pilastro A, Schlupp I (Eds.), Ecology and Evolution of *Poeciliid* Fishes. The University of Chicago Press, Chicago, IL, 61–71.

Grimm V, Berger U, DeAngelis DL, Polhill JG, Giske J, Railsback SF (2010). The ODD protocol: a review and first update. Ecological Modelling, 221(23):2760–2768.

Gunderson LH, Loftus WF (1993). The Everglades. In: Martin WH, Boyce SG, Echternacht AC (Eds.), Biodiversity of the Southeastern United States: Lowland Terrestrial Communities. John Wiley & Sons, Inc., New York, 199–255.

Harlin MM, Woelkerling WJ, Walker DI (1985). Effects of a hypersalinity gradient on epiphytic *Corallinaceae* (Rhodophyta) in Shark Bay, Western Australia. Phycologia, 24(4):389–402.

Harvey JW, Schaffranek RW, Noe GB, Larsen LG, Nowacki DJ, O'Connor BL (2009). Hydroecological factors governing surface water flow on a low–gradient floodplain. Water Resources Research, 45:W03421.

Hoch JM, Sokol ER, Parker AD, Trexler JC (2015). Migration strategies vary in space, time, and among species in the small–fish metacommunity of the Everglades. Copeia, 103(1):157–169.

Hohausova E, Lavoy RJ, Allen MS (2010). Fish dispersal in a seasonal wetland: influence of anthropogenic structures. Marine and Freshwater Research, 61:682–694.

Holt RD (2008). Theoretical perspectives on resources pulses. Ecology, 89(3):671–681.

Hsieh CH, Glaser SM, Lucas AJ, Sugihara G (2005). Distinguishing random environmental fluctuations from ecological catastrophes for the North Pacific Ocean. Nature, 435(7040):336–340.

Jerling HL, Vivier L, Cyrus DP (2010). Response of the mesozooplankton community of the St. Lucia estuary, South Africa, to a mouth–opening event during an extended drought. Estuarine, Coastal and Shelf Science, 86(4):543–552.

Jones DL, Walter JF, Brooks EN, Serafy JE (2010). Connectivity through ontogeny: fish population linkages among mangrove and coral reef habitats. Marine Ecology Progress Series, 401:245–258.

Jones JW, Desmond GB, Henkle C, Glover R (2012). An approach to regional wetland digital elevation model development using a differential global positioning system and a custom–built helicopter–based surveying system. International journal of remote sensing, 33(2): 450–465.

Jopp F, DeAngelis DL, Trexler JC (2010). Modeling seasonal dynamics of small fish cohorts in fluctuating freshwater marsh landscapes. Landscape Ecology, 25:1041–1054.

Junk WJ, Bayley PB, Sparks RE (1989). The flood pulse concept in river–floodplain systems. Canadian special publication of fisheries and aquatic sciences, 106(1):110–127.

Kahl MP (1962). Bioenergetics of growth in nestling wood storks. The Condor, 64(3):169–183, University of California Press on behalf of the Cooper Ornithological Society, DOI:10.2307/1365200.

Kahl MP (1964). Food ecology of the wood stork (*Mycteria americana*) in Florida. Ecological Monographs, 34(2):98–117.

Kaill WM (1967). Ecology and behavior of the cyprinodontid fishes *Jordanella floridae* (Goode and Bean), *Floridichthys carpio* (Gunther), and *Cyprinodon variegatus* Lacipede. Ph.D. dissertation, Cornell University, Ithaca, NY.

Kelble CR, Johns EM, Nuttle WK, Lee TN, Smith RH, Ortner PB (2007). Salinity patterns of Florida Bay. Estuarine, Coastal and Shelf Science, 71(1):318–334.

King MG (1977). Cultivation of the Pacific oyster (*Crassostrea gigas*) in a non–tidal hypersaline pond. Aquaculture, 11(2):123–136.

King RS, Richardson CJ (2007). Subsidy–stress response of macroinvertebrate community biomass to a phosphorus gradient in an oligotrophic wetland ecosystem. Journal of the North American Benthological Society, 26:491–508.

Koenker R, Hallock KF (2001). Quantile regression. Journal of Economic Perspectives, Fall 2001, 15(4):143–156.

Kobza RM, Trexler JC, Loftus WF, Perry SA (2004). Community structure of fishes inhabiting aquatic refuges in a threatened Karst wetland and its implications for ecosystem management. Biological Conservation, 116:153–165.

Kohout FA, Kolipinski MC (1967). Biological zonation related to groundwater discharge along the shore of Biscayne Bay, Miami, Florida. American Association for the Advancement of Science, Publication No. 83, Washington D.C.

Kristensen I (1963). Hypersaline bays as an environment of young fish. In Annual Proceedings of the Gulf and Caribbean Fisheries Institute, 1963:139–141.

Kushlan JA (1974). Effects of a natural fish kill on water quality, plankton, and fish population of a pond in the Big Cypress Swamp, Florida. Transactions of the American Fisheries Society, 103:235–243.

Kushlan JA (1976a). Wading bird predation in a seasonally fluctuating pond. The Auk, 93(3):464–476.

Kushlan JA (1976b). Environmental stability and fish community diversity. Ecology, 57:821–825.

Kushlan JA (1986). Responses of wading birds to seasonally fluctuating water levels: strategies and their limits. Colonial Waterbirds, 9:155–162.

Lake PS (2011). Drought and aquatic ecosystems: effects and responses. John Wiley & Sons, Oxford, UK.

Lantz SM, Gawlik DE, Cook MI (2011). The effects of water depth and emergent vegetation on foraging success and habitat selection of wading birds in the everglades. Waterbirds, 34:439–447.

Larsen LG, Harvey JW, Crimaldi JP (2007). A delicate balance: ecohydrological feedbacks governing landscape morphology in a lotic peatland. Ecological Monographs, 77(4):591–614.

Larsen LG, Harvey JW (2010). How vegetation and sediment transport feedbacks drive landscape change in the Everglades and wetlands worldwide. The American Naturalist, 176(3):E66–E79.

Larsen LG, Harvey JW, (2011). Modeling of hydroecological feedbacks predicts distinct classes of landscape pattern, process, and restoration potential in shallow aquatic ecosystems. Geomorphology, 126(3):279–296.

Larsen LG, Aumen N, Bernhardt CE, Engel V, Givnish T, Hagerthey S, Harvey JW, Leonard L, McCormick P, McVoy C, Noe G, Nungesser MK, Rutchey K, Sklar F, Troxler T, Volin J, Willard D (2011). Recent and historic drivers of landscape change in the everglades ridge, slough, and tree island mosaic. Critical Reviews in Environmental Science and Technology, 41(S1):344–381, Taylor & Francis Group, LLC. ISSN:1064–3389.

Larsen LG, Choi J, Nungesser MK, Harvey JW (2012). Directional connectivity in hydrology and ecology. Ecological Applications, 22(8):2204–2220.

Lasne E, Lek S, Laffaille P (2007). Patterns in fish assemblages in the Loire floodplain: the role of hydrological connectivity and implications for conservation. Biological Conservation, 139(3):258–268.

Lee TN, Johns E, Melo N, Smith RH, Ortner P, Smith D (2006). On Florida Bay hypersalinity and water exchange. Bulletin of Marine Science,79(2):301–327.

Levin SA (1992). The problem of pattern and scale in ecology: the Robert H. MacArthur award lecture. Ecology, 73(6):1943–1967.

Light SS, Dineen JW (1994). Water control in the Everglades: a historical perspective. In: Davis SM, Ogden JC (Eds.) Everglades, the Ecosystem and its Restoration. St. Lucie Press, Delray Beach, FL, USA. 5:47–84.

Lirman D, Thyberg T, Santos R, Schopmeyer S, Drury C, Collado–Vides L, Bellmund S, Serafy J (2014). SAV Communities of western Biscayne Bay, Miami, Florida, USA: Human and natural drivers of seagrass and macroalgae abundance and distribution along a continuous shoreline. Estuaries and Coasts, 5:1243–1255.

Liston SE, Trexler JC (2005). Spatiotemporal patterns in community structure of macroinvertebrates inhabiting calcareous periphyton mats. Journal of the North American Benthological Society, 24:832–844.

Liston, S.E., (2006). Interactions between nutrient availability and hydroperiod shape macroinvertebrate communities in Florida Everglades marshes. Hydrobiologia, 569:343–357.

Liston SE, Newman S, Trexler JC (2008). Macroinvertebrate community response to eutrophication in an oligotrophic wetland: an in situ mesocosm experiment. Wetlands, 28:686–694.

Liu AJ, Cameron GN (2001). Analysis of landscape patterns in coastal wetlands of Galveston Bay, Texas (USA). Landscape Ecology, 16(7):581–595.

Liu Z, Volin JC, Dianne Owen V, Pearlstine LG, Allen JR, Mazzotti FJ, Higer AL (2009). Validation and ecosystem applications of the EDEN water–surface model for the Florida Everglades. Ecohydrology, 2:182–194.

Lloyd DP, Allen RJ (2015) Competition for space during bacterial colonization of a surface. Journal of The Royal Society Interface, 12(110):20150608.

Loftus WF, Kushlan JA (1987). Freshwater fishes of southern Florida. Bulletin of the Florida State Museum Biological Sciences, 31:147–344.

Loftus WF, Eklund A (1994). Long–Term Dynamics of an Everglades Small–Fish Assemblage. In: Davis SM, Ogden JC (Eds.) Everglades, the Ecosystem and Its Restoration. St. Lucie Press, Delray Beach, FL, USA, 461–485.

Lohman MA, Swain ED, Wang JD, Dixon J (2012). Evaluation of effects of changes in canal management and precipitation patterns on salinity in Biscayne Bay, Florida, using an integrated surface–water/groundwater model. U.S. Department of the Interior, U.S. Geological Survey, Scientific Investigations Report 2012–5099.

Lorenz JJ (1999). The response of fishes to physicochemical changes in the mangroves of northeast Florida Bay. Estuaries, 22(2):500–517.

Lorenz JJ, Serafy JE (2006). Subtropical wetland fish assemblages and changing salinity regimes: Implications for everglades restoration. Hydrobiologia, 569(1):401–422.

Lytle DA, Poff NL (2004). Adaptation to natural flow regimes. Trends in Ecology and Evolution, 19(2):94–100.

Magoulick DD, Kobza RM (2003). The role of refugia for fishes during drought: a review and synthesis. Freshwater Biology, 48:1186–1198.

Martin J, Runge MC, Nichols JD, Lubow BC, Kendall WL (2009). Structured decision making as a conceptual framework to identify thresholds for conservation and management. Ecological Applications, 19(5):1079–1090.

MATLAB and Statistics Toolbox Release (2015a). The MathWorks, Inc., Natick, Massachusetts, United States.

Mayor SJ, Schneider DC, Schaefer JA, Mahoney SP (2009). Habitat selection at multiple scales. Ecoscience, 16(2):238–247.

Mazzotti FJ, Brandt LA (1994). Ecology of the American alligator in a seasonally fluctuating environment. In: Davis SM, Ogden JC (Eds.) Everglades, the Ecosystem and Its Restoration. St. Lucie Press, Delray Beach, FL, USA, 485–505.

McGranahan G, Balk D, Anderson B (2007). The rising tide: assessing the risks of climate change and human settlements in low elevation coastal zones. Environment and Urbanization, 19(1):17–37.

McManus LC, Yurek S, Teare PB, Dolan TE, Serafy JE (2014). Killifish habitat suitability as a measure of coastal restoration performance: Integrating field data, behavioral trials and simulation. Ecological Indicators, 44:173–181.

McRae BH, Dickson BG, Keitt TH, Shah VB (2008). Using circuit theory to model connectivity in ecology, evolution, and conservation. Ecology, 89(10):2712–2724.

McVoy CW, Said WP, Obeysekera J, van Arman J, Dreschel TW (2011). Landscapes and hydrology of the predrainage Everglades. University Press of Florida, Gainesville, Florida, USA.

Mertes LA, Daniel DL, Melack JM, Nelson B, Martinelli LA, Forsberg BR (1995). Spatial patterns of hydrology, geomorphology, and vegetation on the floodplain of the Amazon River in Brazil from a remote sensing perspective. Geomorphology, 13(1):215–232.

Minkowski H (1952). Space and time. The Principle of Relativity. Dover Books on Physics. Dover Publications, Inc., New York, USA, 0486600815, 73–91.

Newton I (1686). The Principia: Mathematical principles of natural philosophy. Translated: F. Cajori, 1934, University of California Press, Berkeley, CA.

Nordlie FG (2000). Patterns of reproduction and development of selected resident teleosts of Florida salt marshes. Hydrobiologia, 434(1–3):165–182.

Nordlie FG (2006). Physicochemical environments and tolerances of cyprinodontoid fishes found in estuaries and salt marshes of eastern North America. Reviews in Fish Biology and Fisheries, 16(1):51–106.

Nungesser M (2011). Reading the landscape: temporal and spatial changes in a patterned peatland. Wetlands Ecology and Management, 19(6):475–493, Springer, Netherlands. ISSN:0923–4861.

Obaza A, DeAngelis DL, Trexler JC (2011). Using data from an encounter sampler to model fish dispersal. Journal of Fish Biology, 78:495–513.

Obeysekera J, Rutchey K (1997). Selection of scale for Everglades landscape models. Landscape Ecology, 12(1):7–18.

Obeysekera J, Irizarry M, Park J, Barnes J, Dessalegne T (2011). Climate change and its implications for water resources management in south Florida. Stochastic Environmental Research and Risk Assessment, 25(4):495–516.

Odum WE, Heald EJ (1972). Trophic analyses of an estuarine mangrove community. Bulletin of Marine Science, 22(3):671–738.

Odum WE, McIvor CC, Smith III TJ (1982). The ecology of the mangroves of south Florida: a community profile. U.S. Fish and Wildlife Service, Office of Biological Services, Washington, D.C., FWS/OBS–81/24.

Odum WE, Odum EP, Odum, HT (1995). Nature's Pulsing Paradigm. Estuaries, 18(4):547–555. Papers from William E. Odum Memorial Symposium (Dec., 1995).

Ogden JC (1994). A Comparison of Wading Bird Nesting Colony Dynamics (1931–1946 and 1974–1989) as an Indication of Ecosystem Conditions in the Southern Everglades. In: Davis SM, Ogden JC (Eds.) Everglades, the Ecosystem and Its Restoration. St. Lucie Press, Delray Beach, FL, USA, 533–570.

Ogden, J. C. (2005). Everglades ridge and slough conceptual ecological model. Wetlands, 25:810–820.

Ovaskainen O, Luoto M, Ikonen I, Rekola H, Meyke E, Kuussaari M (2008). An empirical test of a diffusion model: predicting clouded apollo movements in a novel environment. The American Naturalist, 171(5):610–619.

Palaseanu M, Pearlstine L (2008). Estimation of water surface elevations for the Everglades, Florida. Computers and Geosciences, 34:815–826.

Parker GG, Ferguson GE, Love SK, others. (1955). Water resources of south–eastern Florida, with special reference to the geology and ground water of the Miami area. U.S. Geological Survey, Water–Supply Paper 1255, Washington, D.C.

Parkos JJ, Ruetz CR, Trexler JC (2011). Disturbance regime and limits on benefits of refuge use for fishes in a fluctuating hydroscape. Oikos, 120:1519–1530.

Patten BC (2014). Systems ecology and environmentalism: getting the science right. Part I: Facets for a more holistic nature book of ecology. Ecological Modelling, 293:4–21.

Pease CM, Lande R, Bull JJ (1989). A model of population growth, dispersal and evolution in a changing environment. Ecology, 1657–1664.

Peralta–Meixueiro MA, Vega–Cendejas ME (2011). Spatial and temporal structure of fish assemblages in a hyperhaline coastal system: Ría Lagartos, Mexico. Neotropical Ichthyology, 9(3):673–682.

Pires MN, Banet AI, Pollux BJA, Reznick DN (2011). Variation and evolution of reproductive strategies. In: Evans JP, Pilastro A, Schlupp I (Eds.) Ecology and Evolution of *Poeciliid* Fishes. The University of Chicago Press, Chicago, IL, 28–37.

Poff NL, Allan JD, Bain MB, Karr JR, Prestegaard KL, Richter BD, Sparks RE, Stromberg JC (1997). The natural flow regime. BioScience, 769–784.

Rehage JS, Trexler JC (2006). Assessing the net effect of anthropogenic disturbance on aquatic communities in wetlands: community structure relative to distance from canals. Hydrobiologia, 569:359–373.

Rehage JS, Loftus WF (2007). Seasonal fish community variation in headwater mangrove creeks in the southwestern Everglades: an examination of their role as dry–down refuges. Bulletin of Marine Science, 80(3):625–645.

Reigada C, Schreiber SJ, Altermatt F, Holyoak M (2015). Metapopulation dynamics on ephemeral patches. The American Naturalist, 185(2):183–195.

Robertson WB, Kushlan JA (1974). The southern Florida avifauna. Homestead, FL.

Rose KA, Summers JK (1992). Relationships among long–term fisheries abundances, hydrographic variables, and gross pollution indicators in northeastern U.S. estuaries. Fisheries Oceanography, 1(4):281–293.

Rose KA (2000). Why are quantitative relationships between environmental quality and fish populations so elusive? Ecological Applications, 10(2):367–385.

Rose KA, Sable S, DeAngelis DL, Yurek S, Trexler JC, Graf W, Reed DJ (2015). Proposed best modeling practices for assessing the effects of ecosystem restoration on fish. Ecological Modelling, 300:12–29.

Rosendahl PC, Rose PW (1982). Freshwater flow rates and distribution within the Everglades marsh, Proceedings of the National Symposium on Freshwater Inflow to Estuaries, Coastal Ecosystems Project, (Eds. Cross RD, Williams DL), Washington D.C., U.S. Fish and Wildlife Service, 385–401.

Ruetz CR, Trexler JC, Jordan F, Loftus WF, Perry SA (2005). Population dynamics of wetland fishes: spatio-temporal patterns synchronized by hydrological disturbance? Journal of Animal Ecology, 74(2):322–332.

Rutchey K, Schall T, Coronado C, Nungesser M, Volin J, Owen D, Sklar F (2009). Landscape. In: Sklar F, Dreschel T, Warren K (Eds.) Ecology of the Everglades Protection Area, Chap. 6. South Florida Environmental Report. South Florida Water Management District, West Palm Beach, 6–83–6–87.

SAS Institute Inc. (2008). SAS/STAT® 9.2 User's Guide. SAS Institute Inc., Cary, NC.

Saint–Paul U, Zuanon J, Correa MAV, García M, Fabré NN, Berger U, Junk, WJ (2000). Fish communities in central Amazonian white–and blackwater floodplains. Environmental Biology of Fishes, 57(3), 235–250.

Sargeant BL, Gaiser EE, Trexler JC (2011). Indirect and direct controls of macroinvertebrates and small fish by abiotic factors and trophic interactions in the Florida Everglades. Freshwater Biology, 56:2334–2346.

Savenije HH, Pagès J (1992). Hypersalinity: a dramatic change in the hydrology of Sahelian estuaries. Journal of Hydrology, 135(1):157–174.

Schwartzlose RA, Alheit J, Bakun A, Baumgartner TR, Cloete R, Crawford RJM, Fletcher WJ, Green–Ruiz Y, Hagen E, Kawasaki T, Lluch–Belda D (1999). Worldwide large–scale fluctuations of sardine and anchovy populations. South African Journal of Marine Science, 21(1):289–347.

Serafy JE, Faunce CH, Lorenz JJ (2003). Mangrove shoreline fishes of Biscayne Bay, Florida. Bulletin of Marine Science, 72:161–180.

Serafy JE, Valle M, Faunce, CH, Luo J. (2007). Species–specific patterns of fish size and abundance along a subtropical mangrove shoreline: application of the delta approach. Bulletin of Marine Science, 80(3):609–624.

Serrano X, Grosell M, Serafy JE (2010). Salinity selection and preference of the grey snapper *Lutjanus griseus*: field and laboratory observations. Journal of Fish Biology, 76(7):1592–1608.

Serrano X, Serafy JE, Grosell M. (2011). Osmoregulatory capabilities of the gray snapper, *Lutjanus griseus*: salinity challenges and field observations. Marine and Freshwater Behaviour and Physiology, 44:185–196.

Sheaves M (2005). Nature and consequences of biological connectivity in mangrove systems. Marine Ecology Progress Series, 302:293–305.

Simenstad CA, Hood WG, Thom RM, Levy DA, Bottom DL (2002). Landscape structure and scale constraints on restoring estuarine wetlands for Pacific coast juvenile fishes. In: Weinstein MP, Kreeger DA (Eds.) Concepts and controversies in tidal marsh ecology, Springer Netherlands, 597–630.

Simier M, Blanc L, Aliaume C, Diouf PS, Albaret JJ (2004). Spatial and temporal structure of fish assemblages in an "inverse estuary", the Sine Saloum system (Senegal). Estuarine, Coastal and Shelf Science,59(1):69–86.

Stabenau E, Renshaw A, Luo J, Kearns E, Wang JD (2015). Improved coastal hydrodynamic model offers insight into surface and groundwater flow and restoration objectives in Biscayne Bay, Florida, USA. Bulletin of Marine Science, 91:433–454.

Stalker JC, Price RM, Swart PK (2009). Determining spatial and temporal inputs of freshwater, including submarine groundwater discharge, to a subtropical estuary using geochemical tracers, Biscayne Bay, South Florida. Estuaries and coasts, 32(4):694–708.

Starck II, WA, Schroeder RE (1971). Investigations on the gray snapper, *Lutjanus griseus*. University of Miami Press, Coral Gables, FL.

Sugihara G, May R, Ye H, Hsieh CH, Deyle E, Fogarty M, Munch S (2012). Detecting causality in complex ecosystems. Science, 338(6106):496–500.

Thomas TM (1974). Detailed Analysis of Climatological and Hydrological Records of South Florida With Reference To Man's Influence Upon Ecosystem Evolution: in Environments of South Florida: Present and Past. (tDAR ID:125171).

Tiner RW (2003). Geographically isolated wetlands of the United States. Wetlands, 23(3):494–516.

Tischendorf L, Fahrig L, (2000a). On the usage and measurement of landscape connectivity. Oikos, 90(1):7–19.

Tischendorf L, Fahrig L, (2000b). How should we measure landscape connectivity? Landscape Ecology, 15(7):633–641.

Tockner K, Malard F, Ward JV (2000). An extension of the flood pulse concept. Hydrological Processes, 14(16–17):2861–2883.

Tockner K, Stanford JA (2002). Riverine flood plains: present state and future trends. Environmental Conservation, 29(03):308–330.

Trexler JC, Loftus WF, Jordan F, Chick JH, Kandl KL, McElroy TC, Bass Jr. OL, (2002). Ecological scale and its implications for freshwater fishes in the Florida Everglades. In: Porter JW, Porter KG (Eds.) The Everglades, Florida Bay, and Coral Reefs of the Florida Keys: An Ecosystem Sourcebook. CRC Press, Boca Raton, FL, 53–181.

Turchin P (2003). Complex population dynamics: a theoretical/empirical synthesis, Vol.35. Princeton University Press, Princeton, NJ.

Turner AM, Trexler JC, Jordan CF, Slack SJ, Geddes P, Chick JH, Loftus WF (1999). Targeting ecosystem features for conservation: standing crops in the Florida Everglades. Conservation Biology, 13:898–911.

Turner EL, Bruesewitz DA, Mooney RF, Montagna PA, McClelland JW, Sadovski A, Buskey EJ (2014). Comparing performance of five nutrient phytoplankton zooplankton (NPZ) models in coastal lagoons. Ecological Modelling, 277:13–26.

Ulanowicz RE (2014). Reckoning the nonexistent: Putting the science right. Ecological Modelling, 293:22–30.

U.S. Army Corps of Engineers (1999). In: District J (Ed.), Comprehensive Everglades Restoration Plan: Final Feasibility Report and PEIS. U.S. Army Corps of Engineers, Jacksonville, FL.

U.S. Army Corps of Engineers and U.S. Department of the Interior (2015). Comprehensive Everglades Restoration Plan, Central and Southern Florida Project, 2015 Report to Congress. United States Army Corps of Engineers, Jacksonville, FL, and United States Department of the Interior, Washington, DC.

Vaz S, Martin CS, Eastwood PD, Ernande B, Carpentier A, Meaden GJ, Coppin F (2008). Modelling species distributions using regression quantiles. Journal of Applied Ecology, 45(1):204–217.

Vivier L, Cyrus DP, Jerling HL (2010). Fish community structure of the St Lucia Estuarine System under prolonged drought conditions and its potential for recovery after mouth breaching. Estuarine, Coastal and Shelf Science, 86(4):568–579.

Watts DL, Cohen MJ, Heffernan JB, Osborne TZ (2010). Hydrologic modification and the loss of self–organized patterning in the ridge–slough mosaic of the Everglades. Ecosystems, 13:813–827.

Werner FE, Quinlan JA, Lough RG, Lynch DR, (2001). Spatially–explicit individual based modeling of marine populations: a review of the advances in the 1990s. Sarsia, 86(6):411–421.

Whelan KR, Smith TJ, Cahoon DR, Lynch JC, Anderson GH (2005). Groundwater control of mangrove surface elevation: Shrink and swell varies with soil depth. Estuaries, 28(6):833–843.

Wickham JD, Norton DJ (1994). Mapping and analyzing landscape patterns. Landscape Ecology, 9(1):7–23.

Williams AJ, Trexler JC (2006). A preliminary analysis of the correlation of foodweb characteristics with hydrology and nutrient gradients in the southern Everglades. Hydrobiologia, 569:493–504.

Winemiller KO (1996). Factors driving spatial and temporal variation in aquatic floodplain food webs. In: Polis GP, Winemiller KO (Eds.) Food Webs: Integration of Patterns and Dynamics. Chapman & Hall, New York, 298–312.

Winemiller KO, Jepsen DB (1998). Effects of seasonality and fish movement on tropical river food webs. Journal of Fish Biology, 53:267–296.

Wingard GL, Cronin TM, Holmes CW, Willard DA, Dwyer G, Ishman SE, Orem W, Williams CP, Albietz J, Bernhardt CE, Budet CA (2004). Ecosystem history of southern and central Biscayne Bay: Summary report on sediment core analyses–Year two. U.S. Geological Survey Open File Report, 2004, 1312.

Yang LH, Bastow, JL, Spence KO, Wright AN (2008). What can we learn from resource pulses. Ecology, 89(3):621–634.

Yoder JM, Marschall EA, Swanson, DA (2004). The cost of dispersal: predation as a function of movement and site familiarity in ruffed grouse. Behavioral Ecology, 15:469–476.

Yurek S, DeAngelis DL, Trexler JC, Jopp F, Donalson DD (2013). Simulating mechanisms for dispersal, production and stranding of small forage fish in temporary wetland habitats. Ecological Modelling, 250:391–401.

Yurek S, DeAngelis DL, Trexler JC, Klassen JA, Larsen LG (In revision). Persistence and diversity of directional landscape connectivity improves biomass pulsing in simulations of expanding and contracting wetlands. Ecological Complexity.

Zeug SC, Winemiller KO (2008). Relationships between hydrology, spatial heterogeneity, and fish recruitment dynamics in a temperate floodplain river. River Research and Applications, 24(1):90–102.